

**PHYSICAL AND THERMODYNAMIC PROPERTIES
OF ALUMINOSILICATE MELTS
AS A FUNCTION OF COMPOSITION**

Dissertation
zur Erladung des Doktorgrades
der Mathematisch-Naturwissenschaftlichen Fakultäten
der Georg-August-Universität zu Göttingen

vorgelegt von
Katarzyna Falenty
Diplom-Geologin
aus
Wołomin, Polen

Göttingen, 2007

D 7

Referentin/Referent: Prof. Dr. Sharon Webb
(Georg-August Universität Göttingen)

Koreferentin/Koreferent: Priv. Doz. Dr. Harald Behrens
(Leibniz Universität Hannover)

Tag der mündlichen Prüfung: 7. Dezember 2007

ACKNOWLEDGEMENTS

Several people have been instrumental in allowing this project to be completed.

I would like to thank especially **Prof. Dr. Sharon L. Webb** for choosing the accurate and successful range of composition, for making this study possible, for her encouragement and patience at all stages of my work, for invaluable supervision, for help in producing the experimental results for this thesis, for very productive scientific discussions, for linguistic help. Her constructive criticism and comments from the initial conception to the end of this work are highly appreciated.

I am also very grateful to all members of Mineralogy Department (Uni Göttingen). **Heinz Büttner** is gratefully acknowledged for introducing me into torsion machine technique and CATMAN software, for his help and advice at the start of the project. My appreciation also goes to **Peter Meier** who helped with the glass samples preparation. I am also deeply indebted to **Uschi Köhler** for making wet chemistry and AAS analyses, for a lot of warmth and nice plants :) I would like to thank **Gerrit Raschke** for his help with the sample preparation and viscosity measurements. I am grateful to **Johanna Rahn** for density and viscosity measurements.

My thanks also goes to **Dr. Burkhard Schmidt** and **Prof. Dr. Roland Stalder** for an interest in the project and formal and informal conversations.

I thank to **Dr. Andreas Kronz** for the chemical analyses in the Geochemistry Department (Uni Göttingen). I would like to thank people from the **Institute for Low Temperature Physics** (Uni Göttingen) who willingly lent me their time and equipment to do the ultrasonic measurements and for valuable discussion and comments.

I am very grateful to **Dr. Milada Zimová, Elke Schlechter, Aneta Kiebała** and **Magda Banaszak** who supported me at this time and have found enough time and patient for nice chatting or sometimes to listen my grumbling.

Appreciation continues to **Petra Wolfrath** for the help with formalities; to **D.G. Brouwer, K.H. Klapproth** and **E. Wartala** for technical support.

A very special appreciation is due to my husband, **Andrzej**. Dziękuję Ci za zrozumienie, cierpliwość, codzienne wsparcie i skuteczne dodawanie wiary w siebie.

I am also thankful to my **parents**. Kochani Rodzice - dziękuję Wam za troskę, duchowe wsparcie i stały kontakt.

I thank **Prof. Dr. Sharon L. Webb, Priv. Doz. Dr. Harald Behrens, Prof. Dr. Konrad Samwer, Prof. Dr. Gerhard Wörner, Prof. Dr. Roland Stalder** and **Dr. Burkhard Schmidt** for being the members of the examination committee.

I would like to thank the **DFG** (Deutsche Forschungsgemeinschaft), not only for providing the funding which allowed me to undertake this research, but also for giving me the opportunity to attend conferences and meet so many interesting people. This work was supported by the grants WE1810/3-1 (2004-2006) and WE1810/3-3 (2006-2007).

Finally, I am very grateful to all others, who supported me during this PhD study...

Thank You ! Danke ! Dziękuję ! Děkuju !

ABSTRACT

Viscosity η , heat capacity C_p , density ρ , compressibility K , thermal conductivity λ , thermal expansion α , diffusivity D , surface tension of melts are all controlled by the melt structure. The structure of the melt is a function of composition, temperature and pressure.

Here viscosity η , heat capacity C_p , density ρ and shear modulus G have been determined in melts as a function of composition (with constant SiO_2 content = 66.7 mol%) from peralkaline to peraluminous. All of these physical and thermodynamic parameters show that there is a change in structure close to the subaluminous composition, when there are not enough charge balancers to compensate the negative charge of Al in tetrahedral coordination (i.e. at $\gamma \sim 0.5^1$; γ is $(\text{Na}_2\text{O} + \text{FeO}) / (\text{Na}_2\text{O} + \text{Al}_2\text{O}_3 + \text{FeO} + \text{Fe}_2\text{O}_3)$).

For the first time in a controlled series of composition the configurational heat capacity C_p^{conf} was calculated. C_p^{conf} shows a deep minimum at $\gamma \sim 0.5$. Configurational entropy S^{conf} and B_e parameter also have not been shown before for the melts with composition investigated in this study. The obtained results indicate a change in structure at $\gamma \sim 0.5$. Viscosities were determined in the range of $10^{8.8} - 10^{12.6}$ Pa s using micropenetration technique. These data also indicate that there is a change in melt structure at $\gamma \sim 0.5$.

The lifetimes of bonds within the melt have been determined by mechanical spectroscopy (0.001 Hz – 1 Hz). The Si-O and Al-O bond lifetimes could not be separately resolved from the slow α -relaxation peak in mechanical spectrum, but the short lived Na-O bond lifetimes were obtained from the β -relaxation peak.

The major advance in this study is the fact that the measured structural relaxation time deviates from the calculated Maxwell relaxation time. This is contrary to the accepted theory of silicate melt flow and structural relaxation. However, the present melts contain much more Al_2O_3 (Al/Si=0.6) than all previous investigated melts (Al/Si=0.2) and therefore the effect of the short lived Al-O bonds on viscous flow is seen for the first time.

As the amount of Al increases, a probable structure is produced in which clumps of long-lived Si-O clusters are surrounded by short-lived Al-O matrix. Thus flow occurs in the melt via Al-O bond breaking at a rate faster than the Si-O bond breaking. Flow occurs in a melt in which the Si-O clusters are not structurally relaxed. This is geologically important, as modelling of viscosity at high pressure, diffusion rates in melts, crystallization rates in melts, cooling rates of magma, flow rates of magma, modelling of the effect of crystals on magma viscosity all rely on the Maxwell equation which relates structural relaxation time to all rate processes involving the motion of Si and O atoms in melt. In Al_2O_3 rich melts (e.g. in phonolites) all these rate processes occur at least 10 times faster than models based on standard Maxwell relationship theory would predict.

¹ “~” means “approximately equal to”

ZUSAMMENFASSUNG

Viskosität η , Wärmekapazität C_p , Dichte ρ , Kompressionsmodul K , Wärmeleitfähigkeit λ , Wärmeausdehnung α , Diffusion D und Oberflächenspannung der Schmelzen werden durch die Schmelzstruktur kontrolliert. Die Schmelzstruktur ist wiederum abhängig von der chemischen Zusammensetzung, Temperatur und Druck.

In dieser Arbeit wurden Viskosität η , Wärmekapazität C_p , Dichte ρ und Schermodul G als Funktion des Schmelzchemismus zwischen peralkaliner und peraluminöser Zusammensetzung (mit einem festgelegten SiO_2 -Gehalt von 66.7 mol%) untersucht. Alle oben genannten physikalischen und thermodynamischen Parameter zeigen eine Änderung der Struktur in der Nähe von subaluminöser Zusammensetzung, d.h. wenn nicht genug ladungsausgleichende Kationen vorhanden sind um die negative Ladung der Al-Tetraeder zu neutralisieren (bei $\gamma \sim 0.5$ ¹; γ ist $(\text{Na}_2\text{O} + \text{FeO}) / (\text{Na}_2\text{O} + \text{Al}_2\text{O}_3 + \text{FeO} + \text{Fe}_2\text{O}_3)$).

Zum ersten Mal wurden Konfigurations-Wärmekapazitäten C_p^{conf} in einer systematischen Zusammensetzungsserie ermittelt. C_p^{conf} zeigt ein Minimum bei $\gamma \sim 0.5$. Die Konfigurationsentropie S^{conf} und der B_e Parameter wurden ebenfalls für Proben dieser Zusammensetzungen zum ersten Mal berechnet. Die Ergebnisse weisen auf eine Strukturänderung bei $\gamma \sim 0.5$ hin. Viskositäten wurden im Bereich $10^{8.8} - 10^{12.6}$ Pa s mit der Mikropenetrationstechnik ermittelt. Diese Daten weisen ebenfalls auf Änderungen der Schmelzstruktur bei $\gamma \sim 0.5$ hin.

Die Lebenszeiten der Bindungen in der Schmelze wurden mit mechanischer Spektroskopie ermittelt (1 Hz – 0.001 Hz). Die Lebenszeiten der Bindungen Si-O und Al-O konnten aus dem langsamen α -Relaxionspeak im mechanischen Spektrum nicht getrennt aufgelöst werden, aber die kurzlebigen Na-O Bindungen konnten separat aus dem β -Relaxionspeak ermittelt werden.

Eine wesentliche Neuerung dieser Arbeit ist die Tatsache, dass die gemessene strukturelle Relaxationszeit von der berechneten Maxwell Relaxationszeit abweicht. Dies steht im Widerspruch zur allgemein anerkannten Theorie zum Fließen und Relaxation von Silikatschmelzen. Die hier untersuchten Schmelzen enthielten jedoch viel mehr Al_2O_3 ($\text{Al/Si} = 0.6$) als früher untersuchte Schmelzen ($\text{Al/Si} = 0.2$), wodurch hier zum ersten Mal der Einfluss der kurzlebigen Al-O Bindungen auf das viskose Fließen gesehen werden konnte.

Der relativ hohe Al Gehalt führt zur Bildung von langlebigen Si-O Clustern umgeben von einer weniger langlebigen Al-O Matrix. Daher wird das viskose Fließen durch das Brechen und Neubilden der Al-O Bindungen bestimmt. Die Schmelze fließt, obwohl die Si-O Cluster nicht vollständig relaxiert sind. Dies ist deshalb Bedeutung, da Modellierungen von Schmelzviskosität bei hohen Drücken, Viskositäten von teilkristallisierten Schmelzen, Diffusions- und Kristallisationsraten in Schmelzen, Abkühl- und Fließraten von Magma, alle auf der Maxwell Beziehung beruhen, die die strukturelle Relaxation mit allen Prozessen in Beziehung setzt, die auf der Bewegung von Si und O beruhen.

In Al_2O_3 reichen Schmelzen (z.B. Phonolithe) laufen alle diese Prozesse 10 Mal schneller ab, als die Modelle vorhersagen, die auf der Standard Maxwell Beziehung beruhen.

¹ “~” bedeutet “ungefähr gleich“

TABLE OF CONTENTS

1. Introduction	1
1.1. Viscoelasticity, flow and structural deformation.....	3
2. Structure of Na₂O-Al₂O₃-SiO₂ and Na₂O-Fe₂O₃- Al₂O₃-SiO₂ melts	11
2.1. How to investigate the melt structure?.....	11
2.2. Step by step – theories developed through the years.....	11
2.2.1. Tammann theory.....	11
2.2.2. Goldschmidt theory.....	11
2.2.3. Zachariasen – Warren theory and fundamental groups of ions.....	12
2.2.4. Dietzel theory, field strength and bonds in the structure.....	14
2.3. Structure vs. composition.....	15
2.4. How to describe the melt structure?.....	19
2.5. Triclusters – new structural unit. Do they really exist?.....	22
2.6. Flow mechanisms in aluminosilicates.....	23
2.7. Volcanic Dilemma: “Flow or Blow”.....	24
3. Experimental methods	27
3.1. Sample preparation.....	27
3.2. Microprobe.....	28
3.3. Density.....	29
3.4. Pulse Echo Overlap technique.....	30
3.5. Viscosity η	32
3.5.1. The importance of viscosity.....	32
3.5.2. What is viscosity?.....	33
3.5.3. Machine calibration.....	34
3.5.4. Viscosity measurements.....	36
3.5.5. Viscosity calculation.....	40
3.6. Heat capacity c_p	45
3.6.1. Glass transition range and fictive temperature T_f	45
3.6.2. Description of the machine.....	47
3.6.3. Calibration of the calorimeter.....	48
3.6.4. Measurement and calculation of heat capacity and configurational heat capacity.....	48
3.6.5. Calculation of the fictive temperature.....	51
3.6.6. Dependence of the glass transition on the heating rates of the sample....	51
3.7. Torsion (forced oscillation).....	52
3.7.1. Principle of torsion.....	53
3.7.2. The torsion apparatus.....	55
3.7.3. Stress is applied; strain is measured.....	58
3.7.4. Displacement vs. voltage.....	59
3.7.5. Frequency dependent measurements.....	60
3.7.6. Temperature calibration.....	62
3.7.7. Shear modulus of the torsion rod.....	62
3.7.8. Shear modulus of melts.....	64
3.7.9. Shear modulus as a function of frequency.....	70
4. Results	71
4.1. Composition.....	71
4.2. Density.....	74
4.3. Ultrasonic measurements.....	77
4.4. Viscosity.....	79
4.4.1. Viscosity as a function of temperature.....	79
4.4.2. Activation energy for viscous flow.....	84

4.5. Heat capacity.....	86
4.5.1. Heat capacity data.....	86
4.5.2. Glass transition temperature T_g and fictive temperature T_f	88
4.5.3. 3R parameter.....	89
4.6. Torsion (forced oscillation).....	91
4.6.1. Real and imaginary shear modulus.....	91
4.6.2. Comparison of the shear moduli with literature data.....	106
5. Discussion.....	109
5.1. General.....	109
5.2. Density and partial molar volume at room temperature.....	109
5.3. Heat capacity and configurational heat capacity.....	111
5.4. Configurational entropy $S^{\text{conf}}(T)$ and B_e parameter.....	115
5.5. Viscosity and fragility.....	119
5.5.1. Viscosity η	119
5.5.2. Frequency dependent shear viscosity $\eta^*(\omega)$ (from torsion).....	121
5.5.3. Fragility.....	131
5.6. Shear modulus.....	133
5.6.1. General.....	133
5.6.2. Diffusion.....	135
5.6.3. Attenuation.....	139
5.7. Activation energy from all of the techniques.....	148
5.8. Fast relaxation time in aluminosilicate melts.....	149
6. Conclusions.....	153
7. Outlook.....	157
8. Literature.....	159
Appendices	

1. INTRODUCTION

The mechanical and thermodynamic properties of Si-melts change dramatically with composition. This is because the structure of the melts is determined by composition; and the physical properties of melts depend on structure.

As shown in Figure 1, there is a complex dependence between structure, composition and physical and thermodynamic properties of the melts. Structure is a function of temperature, pressure, composition and time. The measured physical properties also depend on time. If the melt structure is in thermodynamic equilibrium, and also in equilibrium with the perturbation applied in the measurement of a physical property, the melt structure and the physical property are “relaxed”. If the melt structure is in thermodynamic equilibrium but not in equilibrium with the perturbation applied to measurement of physical property, the property is “unrelaxed”. If the melt structure is not in thermodynamic equilibrium, it is also “unrelaxed”. Thus time – especially the time required for equilibrium to be reached – is important in the study of silicate melts.

The relationship between physical properties and structure in the $\text{Na}_2\text{O}-\text{Al}_2\text{O}_3-\text{SiO}_2$ system has been investigated by a number of authors, especially Hunold & Brückner (1980) who measured viscosity as a function of composition (Fig. 2) and temperature. The

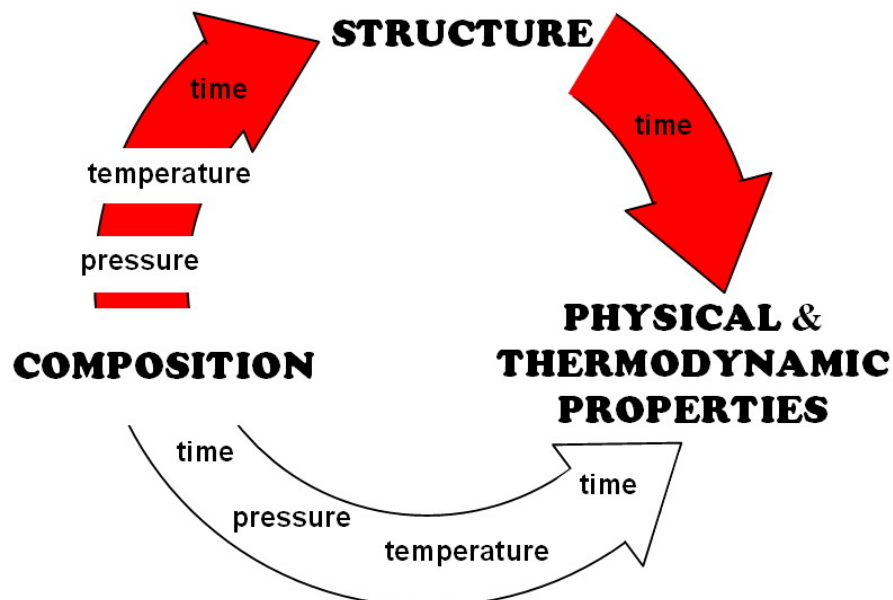


Fig. 1. Complex dependence between structure, composition, temperature, pressure, time and physical and thermodynamic properties of the melts. The red path of investigation has been chosen in this study.

observation was a breaking point in trend at all temperatures as a function of composition at $\text{Na}_2\text{O}/(\text{Na}_2\text{O}+\text{Al}_2\text{O}_3) \sim 0.45$, indicating the presence of a structural change. Interest in this anomalous viscosity trend was awoken by the recent studies of Toplis et al. (1997a, b) and Webb et al. (2004). These studies show the same trend in viscosity as a function of composition as determined by Hunold & Brückner (1980). A similar viscosity trend has been observed in the $\text{LiO}_2\text{-Al}_2\text{O}_3\text{-SiO}_2$ melts by Shelby (1978).

Here the structure of silicate melts is investigated as a function of the changes in their physical and thermodynamic properties with changing composition. It is known that there is a change in structure as a function of Al_2O_3 content in the $\text{Na}_2\text{O-Fe}_2\text{O}_3\text{-Al}_2\text{O}_3\text{-SiO}_2$ system (see Webb, 2005b for a review) but the nature of this structural change is not fully understood. The heat capacity, shear modulus, shear viscosity and structural relaxation rate of a series $\text{Na}_2\text{O-Fe}_2\text{O}_3\text{-Al}_2\text{O}_3\text{-SiO}_2$ melts have been measured; and are presented here together with the calculated structural relaxation time distribution, configurational entropy and configurational heat capacity as a function of composition. The combination of these measurements and calculated parameters has been used to address the question of the structure of these melts.

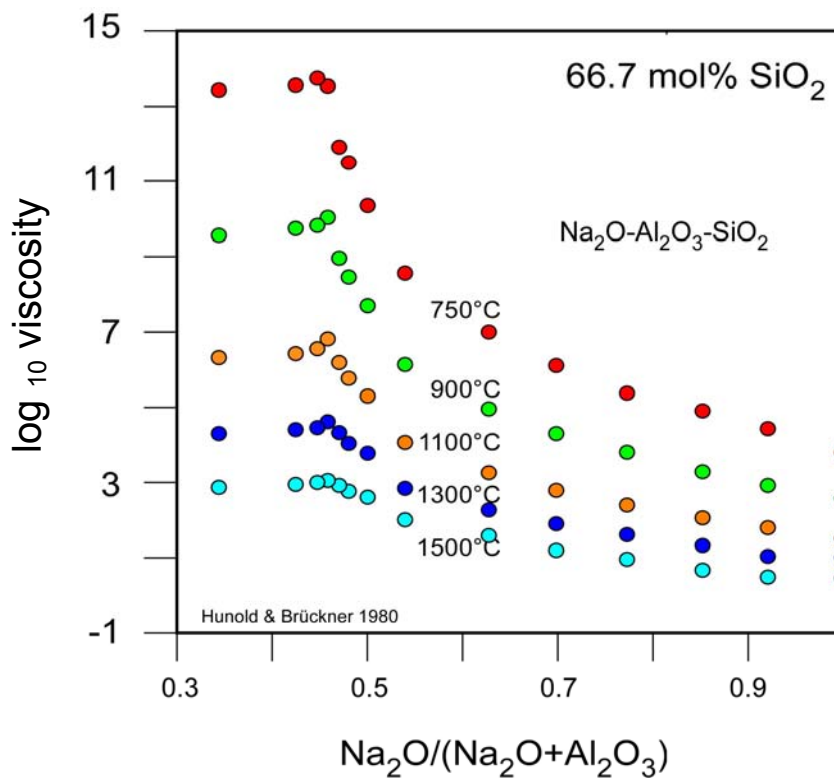


Fig. 2. Log₁₀ viscosity (Pa s) as a function of composition for a series of sodium aluminosilicate melts at different temperatures showing the breaking point at $\text{Na}_2\text{O}/(\text{Na}_2\text{O}+\text{Al}_2\text{O}_3) \sim 0.45$. Redrawn after Hunold & Brückner, 1980.

1.1. Viscoelasticity, flow and structural deformation

The timescale of structural relaxation is traditionally determined by measurement of the viscoelasticity of the melt. Figure 3 illustrates the viscoelastic deformation of a melt due to the application of a step function of stress. First, the instantaneous recoverable elastic deformation occurs. This is followed by the time-dependent recoverable anelastic deformation. Finally, the time-dependent non-recoverable viscous deformation occurs. Thus, the deformation mechanism of the melt changes as a function of time. The structure of the melt is in equilibrium with temperature and pressure; but not in equilibrium with stress σ .

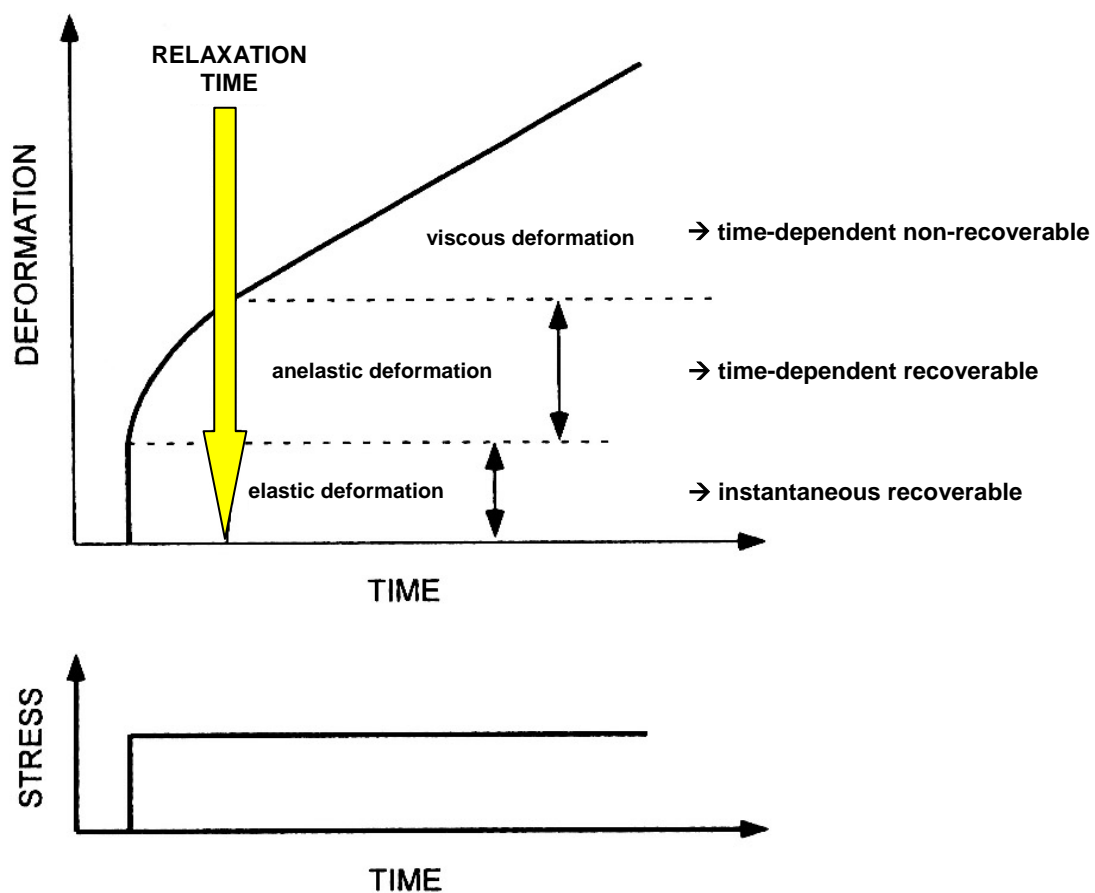


Fig. 3. A step function in stress as a function of time and the resulting time-dependent viscoelastic deformation of the melt. Redrawn after Webb, 2005a.

Such stress – strain measurements result in the calculation of the shear modulus G (stress σ divided by strain ε):

$$G(t) = \frac{\sigma}{\varepsilon(t)} \quad (\text{Eq. 1})$$

and shear viscosity η (stress σ divided by strain rate $\dot{\varepsilon}$):

$$\eta(t) = \frac{\sigma}{\dot{\varepsilon}(t)} \quad (\text{Eq. 2})$$

(see Fig. 4) as a function of time (Jaeger & Cook, 1979). Similarly, a sinusoidal stress wave can be used to determine the shear modulus and viscosity as a function of frequency (Jackson, 1986; Webb, 1992a).

Here, both modulus and viscosity are linear – that is they are independent of the magnitude of the stress and strain. In general the $\varepsilon < 10^{-5}$ is required for linearity of shear modulus (Jackson, 1986).

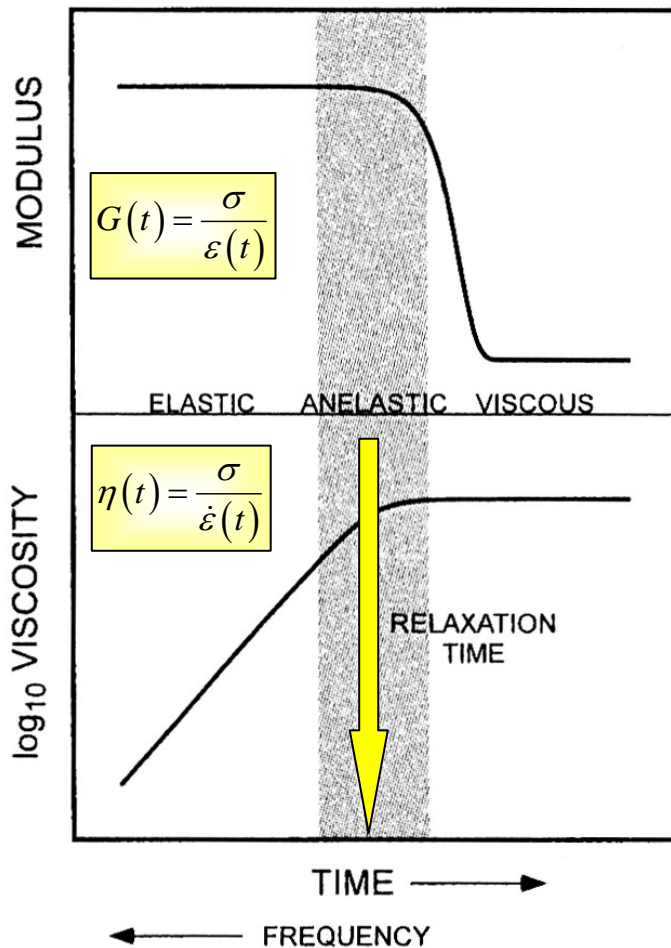


Fig. 4. The time-dependent shear modulus and shear viscosity calculated from the stress-strain plot of Figure 3. The shear modulus and shear viscosity determined by the application of a sinusoidal stress (e.g. torsion or ultrasonic measurements) are dependent upon frequency. Redrawn after Webb, 2005a.

Relaxed liquids deform in the time dependent non-recoverable way what requires a continuous equilibration of the structure during the applying stress. Maxwell (1867) showed the structural relaxation time for a hard-sphere gas is:

$$\tau_M = \frac{\eta_0}{G_\infty}, \quad (\text{Eq. 3})$$

where τ_M is Maxwell relaxation time, η_0 - the long timescale relaxed shear viscosity, G_∞ - the instantaneous elastic shear modulus. The Maxwell relaxation time has been found by number of authors to successfully describe the structural relaxation rate in stress – strain measurements (Herzfeld & Litovitz, 1959; Brawer, 1984; Rivers & Carmichael, 1987; Webb, 1992a; Dingwell & Webb, 1990; Dingwell, 1995; Stebbins, 1995). It has also been shown that the same relaxation time is applicable to perturbations in temperature (Narayanaswamy, 1971; DeBolt et al., 1976; Moynihan et al., 1976; Webb, 1992a,b; Moynihan, 1993).

Figure 5 illustrates the viscosity and calculated Maxwell relaxation time of $\text{Na}_2\text{Si}_2\text{O}_5$ melt as a function of inverse temperature. A number of different techniques with different timescales of measurement (ultrasonic interferometry 1-30ns: Webb, 1992b; torsion 160-0.2s: Webb, 1991; Webb, 1992a; fibre elongation 10^2 - 10^6 s: Webb & Dingwell, 1990) are indicated. In all of these measurements, temperature is held constant and the timescale of measurement is varied. In the calorimetry and dilatometry (30-2s: Webb and Dingwell, 1995) measurements, the sample is heated at a constant rate, and thus the structure of the melt is changing as the experiment is performed.

In all cases, the frequency (or time) dependent behaviour was measured to occur in the vicinity of the calculated Maxwell relaxation time.

The NMR (nuclear magnetic resonance) datum (red point in Fig. 5) is the measured lifetime of Si-O bonds in this melt determined by Liu et al. (1988). This measurement led to the conclusion that the structural relaxation observed in all of these physical property measurements was the lifetime of Si-O bonds. Thus, in the stress – strain measurements at short timescales only the stretching of Si-O bonds is determined; while at timescales longer than the lifetime of Si-O bonds, the measured deformation includes the movement of Si and O atoms.

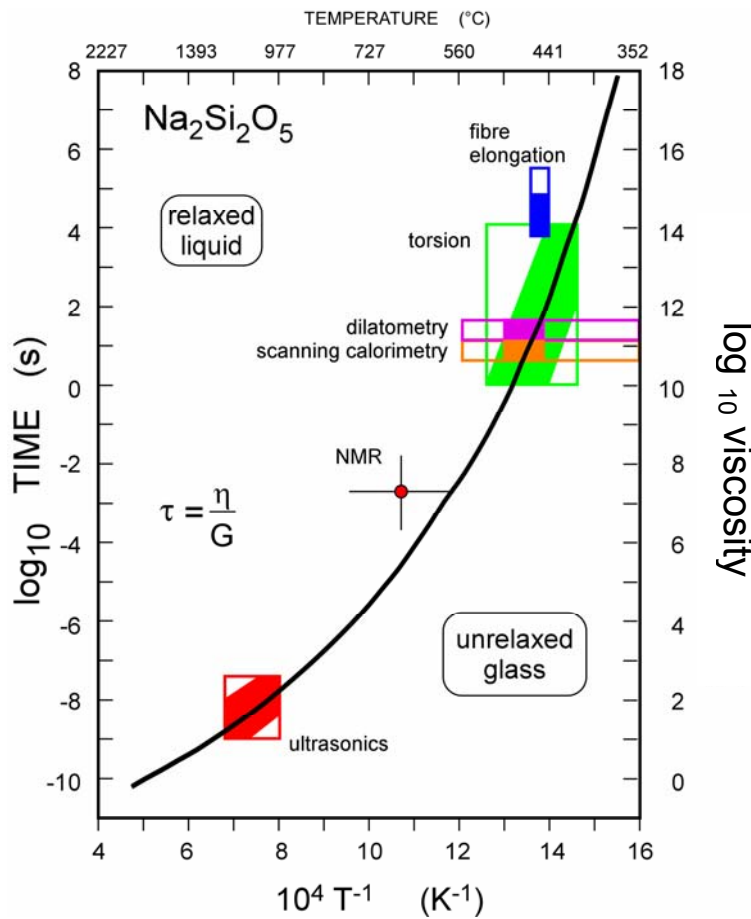


Fig. 5. The curve of relaxation time for $\text{Na}_2\text{Si}_2\text{O}_5$ obtained from Maxwell relationship (1867) (see Eq. 3). Redrawn after Webb, 1992b.

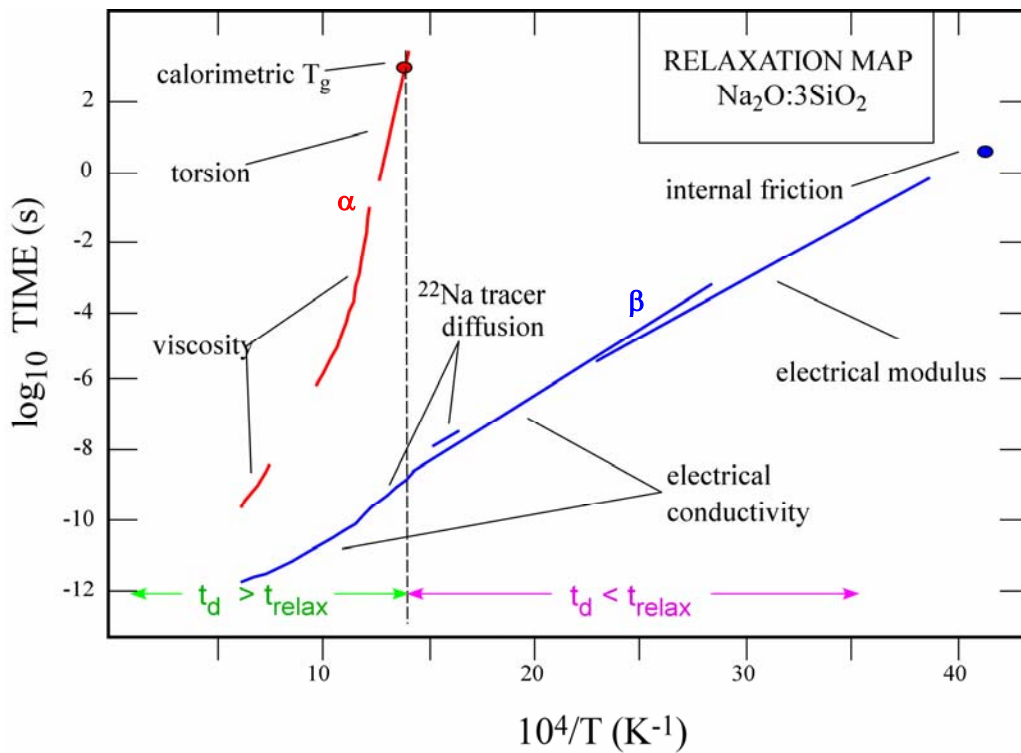


Fig. 6. α -relaxation (slowest, characteristic for Si-O bonds) and β -relaxation (faster, for Na^+ ions) for $\text{Na}_2\text{Si}_3\text{O}_7$ melt. Redrawn after Dingwell, 1990.

The Maxwell relaxation time is the timescale on which the slowest part of the melt structure moves and thus is the glass transition of the melt – as shown in Figure 6. The slowest structural relaxation in a material is called the α -relaxation (Fig. 6). In order to relate melt structure to flow mechanisms and to physical properties, the lifetimes of not only the Si-O but also the Na-O and Al-O bonds need to be measured. It was shown that relaxation process also occurs far away from the glass transition temperature towards lower temperature and it is called β - or secondary relaxation (Zdaniewski et al., 1979; Dingwell & Webb, 1990; Siewert & Rosenhauer, 1997; Meyer et al., 2002). β -relaxation has in general lower activation energy than α and is explained as a diffusion of mono- and divalent ions in the melt. β -relaxation occurs in unrelaxed melt and after this process the melt structure still is not relaxed. α -relaxation is the border between relaxed liquid and unrelaxed glass (see also Fig. 5).

The relationship between the lifetime of Si-O bonds and viscosity in silicate melts has been discussed by a number of authors. The lifetime of the Si-O bonds in a silicate melt; or Na-O, or Al-O bonds can be measured via a range of techniques. These include NMR (e.g. Stebbins, 1991; Stebbins & McMillan, 1993; Stebbins & Xu, 1997; Stebbins et al., 2001); diffusion measurements (e.g. Liu et al., 1988) and mechanical spectroscopy (e.g. Day and Rindone, 1962). The latter is the technique presented here. Mechanical spectroscopy or forced oscillation techniques - involve the determination of energy loss of a stress wave at the frequency at which part of the material structure moves. In the case of metals and ceramics (MacFarlane & Rayne, 1967; Nagel & Balogh, 1999; Carreño-Morelli et al., 2000) this may be the diffusion of atoms (Chakraborty, 1995; Brady, 1975; Freer, 1981; Brady, 1995); in the case of silicate melts it is the frequency (timescale) of motion of Si and O atoms (Bell & Dean, 1970; Gaskell, 1970; Liu et al., 1988; Stebbins, 1991; Stebbins, 1995; Poe et al., 1997) or Na⁺ and K⁺ atoms (Day and Rindone, 1962). Previous forced oscillation measurements on silicate melts have shown the effect of the addition of B, P and F on the frequency dependent energy loss spectrum (Bagdassarov et al., 1993).

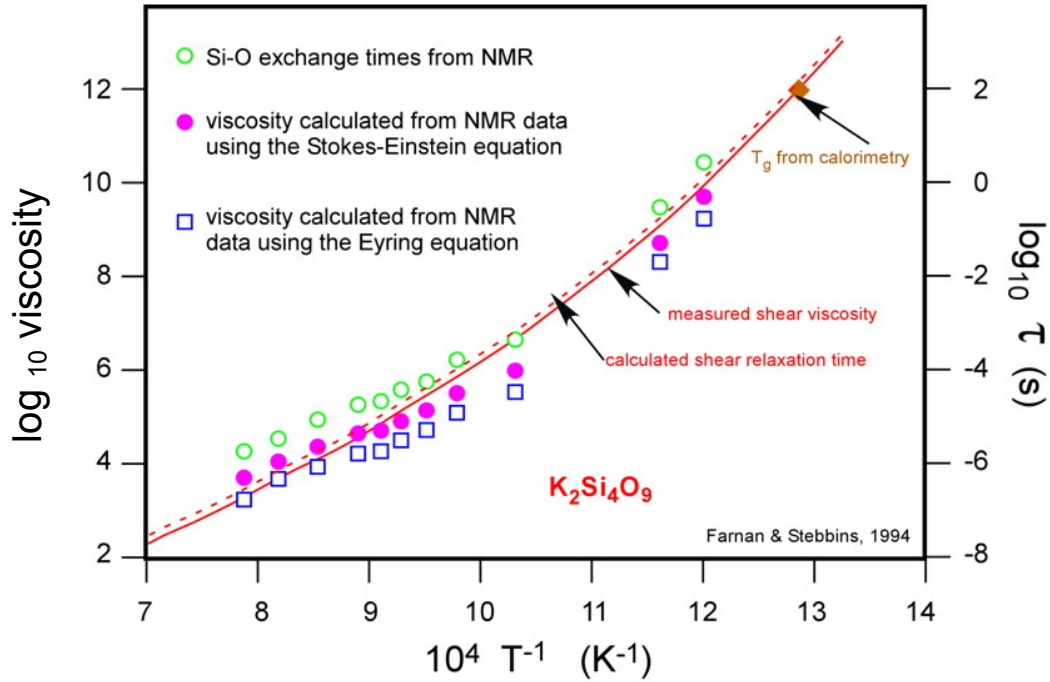


Fig. 7. Plot of the $\log_{10}\eta$ and relaxation time as a function of inverse temperature. Description in the text. Redrawn after Farnan & Stebbins, 1994.

Farnan & Stebbins (1994) showed that there is a close relationship between viscosity, relaxation time and diffusivity of the melts. In Figure 7 the solid curve shows the viscosity of $K_2Si_4O_9$ (Farnan & Stebbins, 1990a,b; Farnan & Stebbins, 1994). The dotted curve is the calculated relaxation time using the Maxwell equation (Eq. 3). The open green circles are the lifetimes of Si-O bonds from ^{29}Si NMR measurements; solid pink circles and open blue squares are the viscosity data calculated from NMR results but with two different equations (η is viscosity in Pa s, k_B is Boltzmann's constant $1.380 \cdot 10^{-23} \text{ J K}^{-1}$, T is temperature in Kelvin, D is self-diffusion coefficient in $\text{m}^2 \text{ s}^{-1}$, λ is translation distance; r is the van der Waals radius of the molecule in meters):

- Eyring equation:

$$\eta = \frac{k_B T}{\lambda D} \quad (\text{Eq. 4})$$

- and Stokes-Einstein equation (Cruickshank Miller, 1924):

$$\eta = \frac{k_B T}{6 \pi r D} \quad (\text{Eq. 5})$$

They discovered that there is no difference between measured and calculated viscosity data and that correlation can be used in the future investigations. This relationship between viscosity, relaxation time and diffusivity is used to determine high pressure viscosity from diffusivity data (Reid et al., 2001; Reid et al., 2003)

In this study we address the changes in lifetimes of the Si-O and Al-O bonds; and the rate at which Na⁺ ions move through Na₂O-Al₂O₃-SiO₂ melts via forced oscillation measurements. As peralkaline and peraluminous melts have different structures, it is to be expected that the distribution of lifetimes of Si-O and Al-O bonds as well as the diffusion rate of Na⁺ is different in the two composition extremes.

2. STRUCTURE OF $\text{Na}_2\text{O-Al}_2\text{O}_3\text{-SiO}_2$ AND $\text{Na}_2\text{O-Fe}_2\text{O}_3\text{-Al}_2\text{O}_3\text{-SiO}_2$ MELTS

2.1. How to investigate the melt structure?

An investigation of the melt structure can be done by a range of methods. Because melts show short range order, medium range and extended medium range order the best methods are spectroscopic (Hawthorne, 1988; Beran & Libowitzky, 2004), e.g. nuclear magnetic resonance (NMR) (Stebbins et al., 1995), infrared (IR), Raman spectroscopy, Mössbauer spectroscopy, X-ray absorption near-edge structure (XANES), extended X-ray absorption fine structure (XAFS), neutron scattering or X-ray diffraction (Meade et al., 1992; Zotov & Delaplane, 2000; Hennes et al., 2005; Matsumura et al., 2007). These techniques allow measurement of the bond angles and distances between atoms, for determination of the coordination number of the central atom and for investigation the nearest and next nearest neighbours in the melt structure. Here changes in physical properties as a function of composition are used to infer possible changes in melt structure.

2.2. Step by step – theories developed through the years

2.2.1. Tammann theory

Many different theories describing the structure of glasses and melts have been developed during the past 100 years. The first theory was proposed by Tammann (Tammann, 1903; Tammann, 1923; Tammann, 1933), who said that glasses have exactly the same structure as the melt. He assumed that structure of liquids is largely retained and it stays intact during the cooling.

2.2.2. Goldschmidt theory

Second hypothesis by Goldschmidt defined a glass structure from his chemical investigations (Goldschmidt, 1926). Goldschmidt assumed that to create the glass there is needed a cation/anion ratio between 0.2 and 0.4 which is exactly in such glass forming compounds as SiO_2 , P_2O_5 or B_2O_3 and even BeF_2 solidifying to a glass.

2.2.3. Zachariasen – Warren theory and fundamental groups of ions

In 1932 Zachariasen (Zachariasen, 1932) proposed a new theory which was confirmed by Warren (1933) with the X-ray diffraction. They discovered that in the vitreous SiO_2 glass the smallest unit is a SiO_4 tetrahedron. The tetrahedra create a disordered three-dimensional network. The new idea was also introducing a “coordination number” term (an average number of nearest neighbours); for example, in the SiO_4 tetrahedron in SiO_2 glass this number equals 4; and for B_2O_3 glass coordination number for planar trigonal BO_3 unit is 3 (Fig. 8).

Zachariasen – Warren theory assumes that oxides are trying to form the polyhedral groups as the smallest units building the structure and such two polyhedra may be linked just to one corner. On the other way, the polyhedron cannot have more than six corners. The anions like O^{2-} or S^{2-} create the bridges between pairs of polyhedra because they cannot be connected to more than two central atoms of polyhedra. Minimum three corners of a polyhedron need to be bonded with the neighbouring polyhedra through anion bridges (in silicate melts: bridging oxygens).

The bridges between polyhedra will be broken, if the large cation appears in the structure (e.g. Na^+ or Mg^{2+}). Then oxygen from the additional oxide will go to a free corner of the separate tetrahedra and the cation will balance the negative charge of the tetrahedra and causes the breaking of the network by reason of its size (Vogel, 1965).

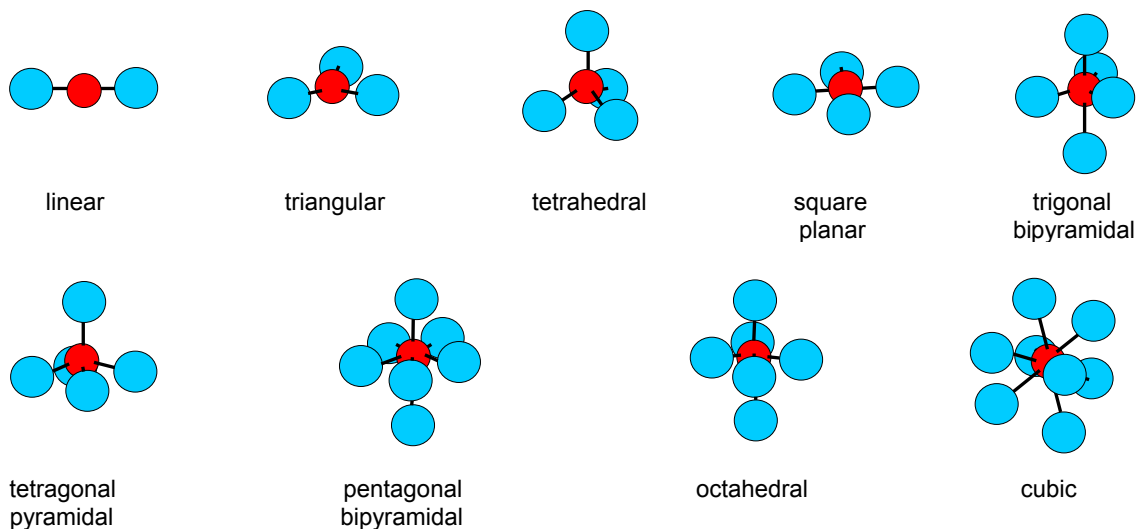


Fig. 8. Coordination number of the atom, congruous with the geometric shape. The number of blue surrounding atoms says about the value of coordination number of the central red atom.

Zachariasen (1932) has classified the ions creating the glass structure into three groups: network formers (e.g. Si, B, P, Ge, As and Be with coordination number 3 or 4), network modifiers (like Na, K, Ca or Ba with coordination number higher than 6) and intermediate oxides (e.g. Al, Mg, Zn, Pb, Be, Nb or Ta with coordination number between 4 and 8). The intermediate oxides can be either the network formers or network modifiers.

With the present stage of knowledge about the glass structure the scientists distinguish more groups (Fig. 9):

- **network formers** (e.g. Si^{4+} , Al^{3+} , Fe^{3+} or Ti^{4+}) arranged in the tetrahedra and creating the network owing to the covalent bonding forces;
- **network modifiers** (alkali or alkaline-earth metal cations) – make with oxygen weaker covalent and metal bonds and they have mostly octahedral coordination. They connect with an oxygen and through that they generate non-bridging oxygens;
- **charge balancers** (alkali or alkaline-earth metal cations) compensating the negatively charged tetrahedrally coordinated units. There is loose exchange between network modifiers and charge balancer depending on the composition of the melt;
- **bridging oxygens (BO)** – oxygen atoms bonding two central atoms of the tetrahedra;
- **non-bridging oxygens (NBO)** – oxygen atoms bonding one central atom of tetrahedra with some other atom (e.g. network modifier).

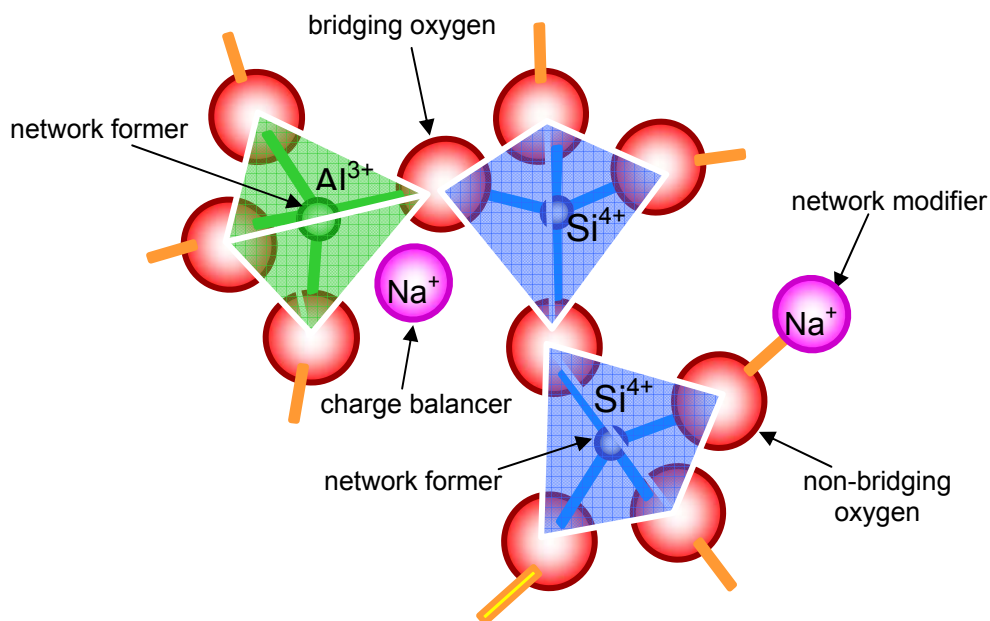


Fig. 9. Fundamental groups of ions in the melt. Description in the text.

2.2.4. Dietzel theory, field strength and bonds in the structure

The next big step in the knowledge about structure of the glasses was made by Dietzel (1942). He developed the Goldschmidt's hypothesis and took into consideration also the field strengths of the ions. During the cooling, the central atoms are trying to keep the surrounding atoms in the closest possible packing. If the central atoms have the same value of field strength, then the homogenisation of the melt can not occur and melt divides into separate phases. In the case of the cations with different field strength, the oxygens will create a closest packing near to the atom with stronger field. The cation with the lowest field strength gets a higher coordination number and is bonded to the tetrahedron with negative charge, e.g. $[\text{SiO}_4]^{4-}$.

Copolymerisation is possible when also separate structural units have similar chemical properties. The difference between donor – acceptor properties of two bonded elements determines the covalence (degree of ionicity) of the chemical bond. The strength of such bond can be described by a term γ_Φ :

$$\gamma_\Phi = \frac{I_n}{r_{orb}^{n+}}, \quad (\text{Eq. 6})$$

where I_n is the ionisation potential of the n^{th} electron and r_{orb}^{n+} is the orbital radius of an ion with a charge n^+ (Godovikov, 1979). In other words, it says about Coulomb forces between the n^{th} electron and the atomic core with charge n^+ (see Table 1).

In vitreous silicate melt only one type of bonds occurs, namely between network forming Si and the oxygens. Because Si^{4+} cations have the strongest γ_Φ parameter with oxygen, the structure of this melt should be very strong and that would explain the slowest (the longest) relaxation time. Smaller ionicity of the bond with oxygen show successively Al^{3+} and Fe^{3+} .

Al^{3+} and Fe^{3+} are network formers in peralkaline melts and build the tetrahedra with one negative charge (Mysen et al., 1985c). Hierarchy of the charge balancer is the same for both: K^+ , Na^+ , Ca^{2+} , Fe^{2+} , Mg^{2+} (Mysen, 1987). To create a stable Al- and Fe-tetrahedra these units need to be charge balanced by cations with smaller γ_Φ value than respectively Al^{3+} and Fe^{3+} . Hess and Wood (1982) also showed that compensation the Al-tetrahedra will first occur by cations with lower field strength and then together with increasing γ_Φ .

Tab. 1. Force characteristics γ_ϕ of cation (Godovikov, 1979).

Cation	γ_ϕ
Si ⁴⁺	225.6
Al ³⁺	128.7
Ti ⁴⁺	94.8
Fe ³⁺	86.3
K ⁺	7.3
Ba ²⁺	11.5
Sr ²⁺	16.4
Na ⁺	18.5
Ca ²⁺	22.1
Li ⁺	28.5
Fe ²⁺	44.4
Mg ²⁺	61.1

The experiments with glasses containing Fe-tetrahedra (Dingwell & Virgo, 1988 a, b) showed that the most stable cation to compensate a negative charge of Fe³⁺ unit is K, then Na, Ba, Sr, Ca and the less stable in this group is Mg.

In the fully polymerized melt (without NBO) the most important bonds are these between oxygen and network formers. The bonds between network former ions are covalent and their average bond valence is above $\frac{3}{4}$ of the valence unit, v.u.) and they are not willing to change the structure. Network modifiers create weak bonds (e.g. Na average bond valences below 0.2 v.u.) (Wispelaere et al., 2004). Na-O and Al-O bonds are longer than Si-O, but Si-O energy bond is at about 20% higher than energy of Al-O bond (Stein & Spera, 1993).

2.3. Structure vs. composition

Structure of the aluminosilicates is strongly dependent on composition, what is shown on the plots as a breaking point in the trends of physical properties as a function of composition (Mysen & Frantz, 1994; Mysen, 1995a). But bulk properties of the melt and glass depend on the presence of different structural units, their concentration and composition (Seifert et al., 1982).

Silicon is tetrahedrally coordinated network former and creates a SiO₄ structural unit. Si is substituted by tetrahedrally coordinated Al³⁺ (Spiering & Seifert, 1985); and tetrahedral Al copolymerizes with silicon (Riebling, 1966; Kushiro, 1976; Dickenson & Hess, 1985).

Aluminium cation can have either a tetrahedral coordination and exists as a network former; or octahedral coordination with respect to oxygen and plays a modifier role (Mysen, 1981; Mysen et al., 1982). [AlO₄]⁻ tetrahedron needs to be compensated by

alkali or alkaline-earth metal cation with a positive charge of one. In peralkaline melts the ratio Al/Na is smaller than one; it means that there is enough sodium to compensate the negative charge of the Al unit. The excess Na ions connect with non-bridging oxygens and play a network modifier role.

If there is enough mono- or divalent alkali or alkaline-earth metals in the melt to compensate negative charge of Al-tetrahedra, Al is tetrahedrally coordinated (Riebling, 1964; Riebling, 1966; Bottinga & Weill, 1972, Mysen et al., 1980b; Wood & Hess, 1980; Stebbins & Farnan, 1992). Mysen et al. (1981a) and McMillan & Piriou (1982) suggested, that when in the melt, there is a lack to charge balance of Al^{3+} , NBO will form what extorts transformation of coordination state of Al^{3+} from tetrahedral to octahedral. MAS NMR measurements of highly peraluminous glasses have found Al in [IV] and [VI] coordination (Risbud et al., 1987; Bunker et al., 1991; Sato et al., 1991a; Sato et al., 1991b; Poe et al., 1992). The intermediate (fivefold) coordinated aluminium, has been also discovered (Poe et al., 1992).

The amount of $^{[VI]}\text{Al}^{3+}$ was however not enough to account for all of the Al without a charge balancer and therefore the current melt structure is based on the idea of triclusters – introduced by Lacy (1963); and discussed by Toplis et al. (1997a, b). This is supported strongly by the viscosity data. Using the simple rules, network formers increase viscosity and polymerization, where network modifiers decrease viscosity and polymerization. One observes that viscosity stays almost constant in Figure 2 in the peraluminous field suggesting there are no new NBOs created upon the addition of Al_2O_3 and therefore Al cannot be octahedral or the amount of octahedral Al is too small to influence any structural change.

Iron plays a significant role in the magmatic systems. Fe is heterovalent and because of that is very important in melting and crystallization, depending on the conditions. However, coordination number of the iron ions can be dominant and has a big influence on the properties of the melt. From the other side, composition, temperature or pressure can control the properties of the iron, like coordination number or oxidation state (Johnston, 1964; Sack et al., 1980; Mysen, 1981; Kilinc et al., 1983; Dyar et al., 1985; Mysen et al., 1985a,b; Paul, 1990; Kress & Carmichael, 1991; Baker & Rutherford, 1996; Burkhard, 2000; Gaillard et al., 2001; Wilke et al., 2002; Botcharnikov et al., 2005; Wilke et al., 2006).

According to the Mössbauer spectroscopy it is known that in the melts iron can exist as Fe^{3+} and Fe^{2+} (Seifert et al., 1979; Virgo et al., 1981). Fe^{3+} may form the tetrahedra but Fe^{2+} can occur as a network modifier and a charge balancer. Then some sort of grouping must occur if a divalent Fe compensates two tetrahedra. One Fe^{2+} ion

replaces two Na^+ ions. The higher field strength of the divalent iron leads to decreasing the free volume through the shortening of the bonds between Fe^{2+} and oxygen.

Fe^{2+} is taken to be octahedrally coordinated and to play a network modifier role (Seifert and Olesch, 1977a,b; Mysen & Virgo, 1978; Nolet et al., 1979; Seifert et al., 1979; Mysen et al., 1980a; Spiering & Seifert, 1985).

Fe^{3+} can be (1) octahedral – when not enough alkali or alkaline-earth metals exist to compensate a negative charge of the anion groups); or (2) tetrahedral – when there is enough alkali or alkaline-earth metals to play network balancer and network modifier roles (investigations of alkali silicate and soda lime silicate glasses by Bamford, 1960; Steele & Douglas, 1965; Kurkjian & Sigety, 1968; Levy et al., 1976; Hirao et al., 1979; DeGrave, 1980; Fenstermacher, 1980; Fox et al., 1982; Calas & Petiau, 1983; Greaves et al., 1984; Brown et al., 1986; Wang & Chen, 1987; Hannover et al., 1992; Wang et al., 1993; Wang et al., 1995). Virgo et al. (1982b) showed that Fe^{3+} tetrahedron does not copolymerize with Si-tetrahedron.

New investigations allow for precise estimation of the ratio between tetrahedrally and octahedrally coordinated cations of Fe^{3+} in melts. Weigel et al. (2006) determined that 95% of Fe^{3+} in the structure of $\text{NaFeSi}_2\text{O}_6$ form tetrahedra. The remaining 5% of iron can be five- or six-coordinated. This 5% of octahedral Fe^{3+} corresponds to ~0.15 mol% of the melt compositions investigated here.

Alkalis and alkaline earths play a role of network modifiers and charge balancers of Al^{3+} in tetrahedral coordination in melts and glasses (Bottinga & Weill, 1972; Mysen et al., 1981a; Secco et al., 1991; Neuville & Mysen, 1996; Mysen, 1997). Sodium ion is very good charge balancer for Fe-tetrahedra (Russel & Wiedenroth, 2004). Stabilization of Fe-tetrahedra with alkali cations increases with decreasing their field strength (Bingham et al., 2007). The effect of alkaline earths on Fe-tetrahedra is the inverse of that of the alkalis.

But what happens exactly in the melts going from peralkaline towards peraluminous composition?

In peralkaline glass or melt, there is enough network modifiers and charge balancers to compensate any negative charge of the structural units. With an increasing number of network modifiers the melt becomes more fluid because silicon-oxygen bonds being the bridges between silicon atoms need to be broken to connect new ion. Decreasing the amount of network modifiers up to their absence induces higher polymerization of the melt and follows that the viscosity increases. The structure gains free volume due to the polymerisation process and the energy needed to break stronger bonds between tetrahedra increases. The increase of the interstices causes that the “doorways” between tetrahedra become larger. That was shown in the experiments with

the diffusion of He in aluminosilicate melts (Roselieb et al., 1992). There is very important dependence between empty and filled interstices because the size of filled interstices strongly depends on the size of empty interstices (Shelby, 1979).

In aluminosilicates with high Al content, the network is controlled by bonds between network formers and oxygen; and the identity of the network modifiers does not play any important role (Shelby, 1989).

Some polymerized units (regions) play an important role in the structure of the melts (Bottinga & Weill, 1972; Burnham, 1975; Mysen, 1988). Lacy (1963) suggested that AlO_6 octahedra are not stable and proposed the new structural unit of AlO_6 tricluster. During formation of AlO_6 tricluster no new NBO are formed. This theory has more or less followers but spectroscopic and diffraction measurements prove an existence of the denser and higher coordinated structural units in the network, which could be triclusters.

Gaskell & Mistry (1979) in the $\text{NaAlO}_2\text{-SiO}_2$ system suggested the presence at least two different types of 3D connected units in aluminosilicate composition. Three dimensional SiO_4 and AlO_4 tetrahedra has been detected with the RDF X-ray technique by Taylor and Brown (1979a), and those results have been confirmed e.g. by Mysen et al. (1980b) with Raman spectroscopy. Dirken et al. (1997) have found clear separate Q3 units (see section 2.4.) with Si-O-Al bridging oxygen and Si-O-Si bridging oxygen in the structure of albite, but no Al-O-Al bridging oxygen or others. Stebbins & Xu (1997) in the investigation of anorthite glass have found Q3 units with the same characteristics, but they have also distinguished NBO in peraluminous composition. That changes a theory that glass with peraluminous composition is fully polymerized. Stebbins & Xu (1997) have also localized other very small feature in the structure of anorthite, what Xue & Kanzaki (1999), using ^{17}O Q3 MAS NMR technique have interpreted as Al-O-Al bridging oxygen and showed that is possible to distinguish triclusters oxygen. However, it is possible to find Si-O-Al BO, but is rather difficult to interpret, whether is it $\text{O}(\text{Si}_2\text{Al})$ or $\text{O}(\text{SiAl}_2)$ triclusters oxygen (Xue & Kanzaki, 1999).

Using a $\{^{17}\text{O}\}^{27}\text{Al}$ Heteronuclear Multiple Quantum Correlation technique Iuga et al. (2005) found a direct proof for the existence of triclusters in $0.50\text{Ca} \cdot 0.50\text{Al}_2\text{O}_3$ glass. The authors have also observed ^{IV}Al in Mg- and Ca-aluminosilicate glasses but this fact still needs better investigations to find full explanation of its influence on the melt structure (see also Toplis et al., 2000; Neuvill et al., 2004; Neuvill et al., 2006). It is quite difficult to precise, whether five-fold coordinated Al is network former or network modifier (Lee et al., 2006; Neuvill et al., 2006).

Al-rich structural units balanced by Al-cations are more stable than these balanced by alkaline earths (Wood & Hess, 1980; Bottinga & Weill, 1972; Mysen et al., 1981a), what would explained high viscosity and activation energy of peraluminous melts.

There is not enough data to fully explain the behaviour of trivalent iron ions in the melts with lack of charge balancer (Mysen et al., 1981b). But it is proved (Mysen et al., 1980a; Mysen et al., 1981a) that Fe^{3+} does not bond with Si-tetrahedra but build own clusters. Goldman (1983) and Mysen et al. (1984) proposed that Fe^{3+} occurs as three-dimensionally interconnected Fe^{3+}O_2 units. Tetrahedrally coordinated Fe^{3+} polymerizes into own structural unit $[\text{FeO}_2]$. Iron plays an important structural role but the importance of its influence depends on the interrelationship between polymerization degree, composition of the melt, amount of iron and its oxidation state (Waff, 1977). Because all the samples were prepared and measured in air conditions (or air-nitrogen conditions) it is obvious that Fe^{3+} can oxidize and change its oxidation state to Fe^{2+} .

There is no clear model of the peraluminous melt structure. Two most popular hypotheses differ in the coordination number of Al ions. The first one assumes a change in Al-coordination from tetrahedral to octahedral, when there is not enough charge balancers. The second one bases on the structure with triclusters of Al- and Si-tetrahedra, where Al stays in tetrahedral coordination (Shelby, 2005). In spite of the considerable progress in experimental techniques the real arrangement of this unique structure still remains undetermined.

In the following discussion it is assumed that in melts with peraluminous composition, the Al and Fe^{3+} are in tetrahedral coordination and both occurs in triclusters. Fe^{3+} in octahedral coordination is negligible and has no large effect on the structure change.

2.4. How to describe the melt structure?

The local structure can be described by the structural units Q^n for SiO_4 tetrahedra and $\text{Q}^n(m\text{Al})$ for Al-tetrahedra, where n is the number of bridging bonds in the tetrahedron and m is the number of aluminium atoms in the second coordination sphere of the silicon atoms (Mysen, 1990). Q species (e.g. Schramm et al., 1984) are commonly used in NMR measurements. It describes the connectivity of tetrahedra (polymerization of the melt).

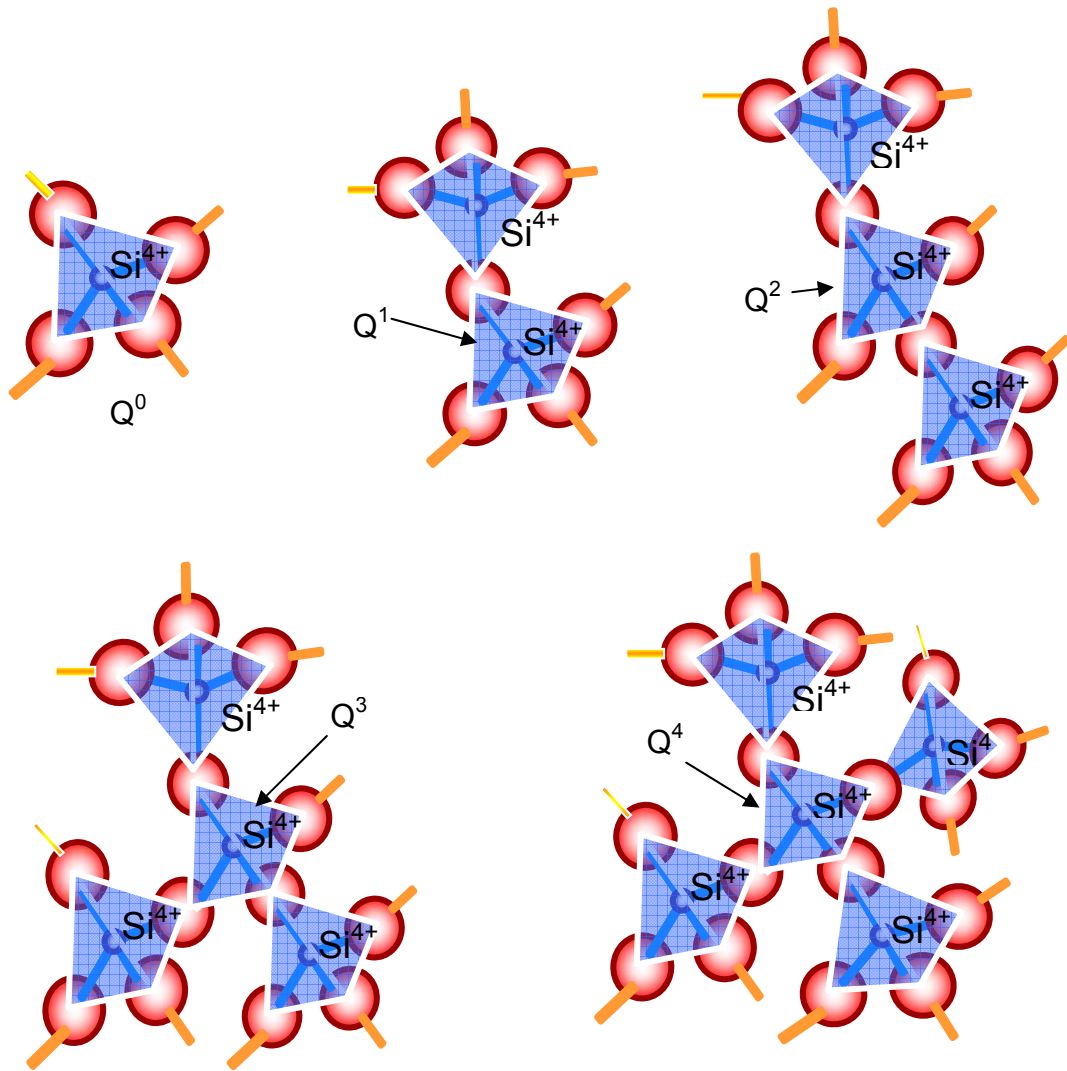


Fig. 10. Q species – distinguished as structural units in silicate melts. Description in the text.

Q^0 is a separate SiO_4 tetrahedron which has no connection with any other tetrahedron in the melt (Fig. 10). Q^1 unit is linked with one other tetrahedron, Q^2 – with two tetrahedra, Q^3 – with three tetrahedra and Q^4 is bonded to 4 other tetrahedra (Stebbins, 1995). The same nomenclature can be used for Al^{3+} tetrahedra (Mysen et al., 2003). Q species show the arrangement of bridging and non-bridging oxygens in the melt structure.

NBO/T parameter describes the number of non-bridging oxygens (NBO) per one tetrahedron (T), e.g.:

$$\frac{NBO}{T} = \frac{2(Na_2O - Al_2O_3)}{2Al_2O_3 + SiO_2} \quad (\text{Eq. 7})$$

(Mysen et al., 1981a; Mysen, 1987). NBO/T is generally used for peralkaline melts; otherwise the value will be negative. This historical problem has been solved by Gwinn & Hess (1989) and more recently by Toplis et al. (1997a,b) using γ .

The **GAMMA** value (γ) is the sum of network modifiers in the form of oxides (X^{n+}) divided by the sum of all oxides in the melt (without SiO_2):

$$\gamma = \frac{\sum n X^{n+}}{\sum n X^{n+} + Al^{3+}}, \quad (\text{Eq. 8})$$

where X^{n+} and Al^{3+} are a number of atoms in one mole of melt (Gwinn & Hess, 1989; Toplis et al., 1997a,b; Webb et al., 2004). Gamma parameter avoids the negative values needed for NBO/T and also ignores silica content. In this work γ is calculated as a ratio of the amounts of oxides (in mole fractions).

For Fe-free samples:

$$\gamma = \frac{Na_2O}{(Na_2O + Al_2O_3)} \quad (\text{Eq. 9})$$

and for Fe-bearing melts:

$$\gamma = \frac{Na_2O + FeO}{(Na_2O + Al_2O_3 + FeO + Fe_2O_3)} \quad (\text{Eq. 10})$$

Using γ parameter, the melts can be described as:

- **peraluminous**, when $0 \leq \gamma < 0.5$;
- **subaluminous**, when $\gamma = 0.5$;
- **peralkaline**, when $0.5 < \gamma \leq 1$.

2.5. Triclusters – new structural unit. Do they really exist?

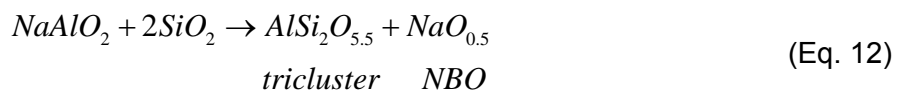
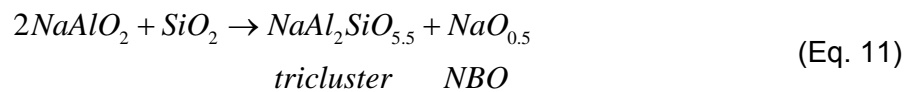
The structure of the melt becomes more homogenous with increasing temperature (Bykov et al., 2003). There is also known that when the structure starts to flow, the anionic units of the network formers are connected in some structural groups with different degree of polymerisation and a short lifetime. In the Raman spectrum, at 1000cm^{-1} vibrations of $\text{Q}^4(\text{mAl})$ (highly polymerised aluminosilicate anions) were observed (Bykov et al., 2003).

Tetrahedrally coordinated cations (such as Si^{4+} , Al^{3+} , Ti^{4+} or Fe^{3+}) create tetrahedra which can be copolymerised or grouped in some special units (Kuryaeva, 2004). In Fe-free melts alumina and silica tetrahedra can group in triclusters. In high peraluminous melts is not ruled out the existing of the triclusters with three Al-tetrahedra. In Fe-bearing melts the tricluster can contain also Fe^{3+} tetrahedra.

When for Fe-free glasses $\gamma=0.5$, the number of Na ions is exactly the same as the number of aluminium ions, and theoretically non-bridging oxygens do not exist. All Na ions compensate the negative charge of the Al-tetrahedra. With a further decrease in Na content there is not enough sodium to charge balance the Al-tetrahedra and a new structure must be formed. The new structure called “tricluster” is created (Isard, 1959; Day & Rindone, 1962; Lacy, 1963; Lacy, 1965; Terai, 1969; Taylor & Rindone, 1970; Shelby, 1978; Hunold & Brückner, 1980; Toplis et al. 1997a; Kuryaeva, 2004).

Lacy (1963) described possible structures based on Zachariasen – Warren theory. His tricluster (Fig. 11) consists two Si-tetrahedra and one Al-tetrahedron (or one Si-tetrahedron and two Al-tetrahedra) sharing one oxygen has been argued for by Toplis et al. (1997a,b).

Formation of such structure can arise according to the equations:



(Kuryaeva, 2004).

In the measurements of the physical properties of aluminosilicate glasses the sharp breaks in their properties are observed at the moment when the composition changes from peralkaline to peraluminous and, as a consequence of that, the triclusters form. The triclusters can also occur in the peralkaline melt, but their sparse presence does not influence significantly on the physical properties of the melt (Toplis et al., 1997a).

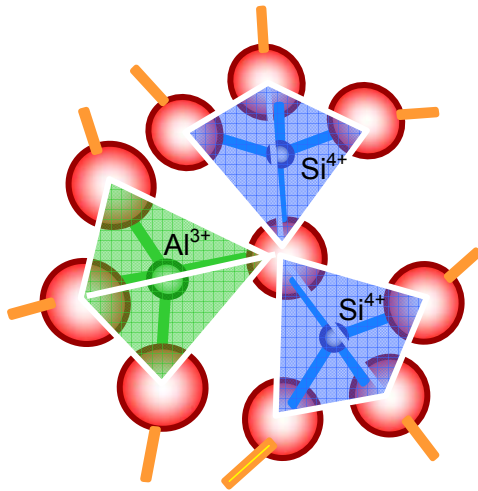


Fig. 11. Scheme of the tricluster – structural unit in the peraluminous melts proposed by Lacy, 1963.

NMR measurements (Kubicki & Toplis, 2002) have not found triclusters, but calculations show the tricluster peak lies under large Si-O-Al and Al-O-Al peaks. While NMR data give us information about the structure of the melt, viscosity studies have shown the effect of structure on physical properties. Toplis et al. (1997a,b) and Webb et al. (2004) have shown that for melts with constant mol% SiO_2 content, the viscosity of peralkaline melts increases as the amount of NBO formed by Na^+ is reduced, and the amount of Al^{3+} increases. In the peraluminous composition range, the viscosity decreases very slowly as the amount of charge-balancing Na^+ is reduced and the number of triclusters increases. This results in a maximum in η at $\gamma \sim 0.5$.

2.6. Flow mechanisms in aluminosilicates

It has long been assumed that the structure of peraluminous $\text{Na}_2\text{O-Al}_2\text{O}_3\text{-SiO}_2$ melts must be different to that of peralkaline melts. NMR studies of peralkaline $\text{Na}_2\text{O-Al}_2\text{O}_3\text{-SiO}_2$ melts have found that Na^+ prefers to form non-bridging oxygens bonded to Si^{4+} ; and also acts as a charge balancer for the tetrahedrally coordinated Al^{3+} (Mysen, 1987; Allwardt et al., 2003). Mysen et al. (2003) concluded from their ^{29}Si NMR and Raman spectroscopic study on peralkaline glasses that the dominant fraction (>70%) of Al^{3+} resides in fully polymerized Q^4 units. Lacy (1963) discussed the various possible structures of peraluminous melts in terms of geometry and energy and concluded that triclusters of two Si^{4+} -tetrahedra and one Al^{3+} -tetrahedron sharing one apical oxygen was the most probable structure for the Al^{3+} tetrahedra without a Na^+ charge balancer. Thus, the mechanism by which peralkaline and peraluminous $\text{Na}_2\text{O-Al}_2\text{O}_3\text{-SiO}_2$ melts flow must be slightly different.

Flow in peralkaline melts probably begins by

- (1) the network modifying Na^+ diffusing away from its Si^{4+} tetrahedron, followed by
- (2) the bonding of the free O to a neighbouring Si to create a $^{\text{VI}}\text{Si}$ (as seen to exist in NMR measurements, Stebbins, 1991; Stebbins & McMillan, 1993),
- (3) the breaking apart of an Si-O-Si bond, and
- (4) the replacement of the Na^+ to the O with only one bond to a Si.

This flow process is that proposed by Farnan & Stebbins (1994), McMillan *et al.* (1994) and Stebbins (1995).

The proposed flow mechanism for peraluminous composition $\text{Na}_2\text{O-Al}_2\text{O}_3\text{-SiO}_2$ melts involves the creation of a tricluster and is

- (1) the charge balancing Na^+ diffuses away from its Al^{3+} tetrahedron and the Al-O bond is broken,
- (2) a $\text{AlSi}_2\text{O}_{5.5}$ tricluster is formed,
- (3) the breaking apart of the Si-O-Si bond, and
- (4) the replacement of the charge balancing Na^+ to the Al^{3+} tetrahedron and the O to the Si^{4+} with only 3 oxygens (Toplis *et al.*, 1997a; Webb *et al.*, 2004; Webb, 2005a).

This change of structure can be observed as a breaking point on the plots of viscosity, T_g , density or shear modulus. The base structure of Fe-free and Fe-bearing glasses appears to be similar. In peralkaline melts the major role is played by the modifying ions because they decide about the connectivity in the structure. In peraluminous melts the Si-O-Al bonds are more important.

Isostructural with aluminosilicate structure appears to be a galliosilicate structure, where the same behaviour of the trends was observed (Lapp & Shelby, 1986; Piguet & Shelby, 1985; Piguet *et al.*, 1985).

2.7. Volcanic Dilemma: “Flow or Blow”

The volcanic explosions can look differently depending on the composition of the magma. More interesting is that even magma with the same composition can behave in different ways, what is caused by its various thermodynamic properties. Numerous experiments and computer modelling contributed to increase the significance of glass transition in volcanic processes and to prove that crossing the glass transition can be a reason for brittle failure (Dingwell, 1996).

The base of this hypothesis is enough high strain rate of the magma deformation to change the melt into a pseudo-plastic (shear thinning) liquid, which finishes in a brittle

failure. But the present observations exclude such high strain rate of the magma in the conduits, where glass transition zone with brittle failure can not be reached.

The laboratory investigations showed that fragmentation of the sample being at temperature and pressure of volcanic eruption is easy when the fast decompression is used. In the condition of prompt decompression, high bubble density or high temperature are not required (Dingwell, 1996), what changes the present scientific point of view on the volcanic eruption.

One needs to discuss the aspect of hydration and dehydration of magma. Formation of the bubbles leads to depleting the magma of the water. Migrating upwards bubbles supply the sharp vertical volume, pressure and viscosity gradient. Ascending magma, crossing such a low pressure region, is suddenly decompressed, reaches the conditions of the glass transition region with brittle failure and explodes (Fig. 12).

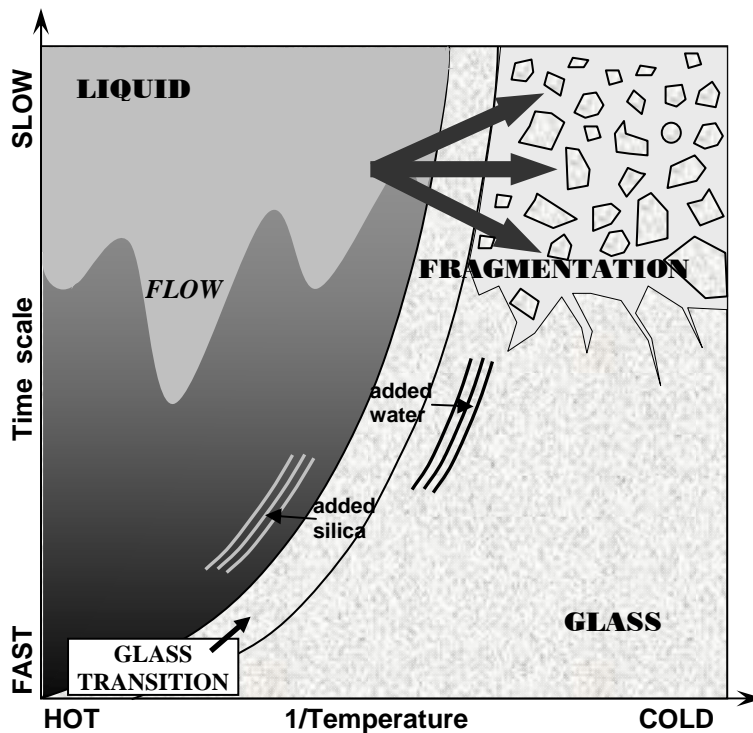


Fig. 12. The glass transition as a function of time and inverse temperature. Redrawn after Dingwell, 1996.

3. EXPERIMENTAL METHODS

3.1. Sample preparation

Fourteen sodium-aluminosilicate samples with constant value of 66.7 mol% SiO₂ and one sodium-silicate melt were investigated. Melts G9-G14 had 3 mol% Al₂O₃ replaced by Fe₂O₃ (sample G8 has only 1 mol% Fe₂O₃, otherwise it will crystallize). The batch composition is presented in the Table 2. The compositions of the final melts were determined by microprobe analysis (see Tables 8 and 9 – section 4.1.).

The ratio between Al and Na determines whether the melt is peralkaline or peraluminous. In this study the γ value for the most peralkaline melt is 1.00 and for the most peraluminous is 0.40. More peraluminous melts in this series crystallise upon cooling to a glass and thus cannot be investigated using the techniques presented here.

The oxides SiO₂ (99.9%), Al₂O₃ (99.997%), Fe₂O₃ (99.99%) and the carbonate Na₂CO₃ (99.5%) were used to make the samples. The chemicals were dried overnight before weighing. Weighing was done with the accuracy of ± 3 mg. These chemicals were shaken together in a plastic bottle to homogenise the powders before further preparation. The mixture was decarbonised at 800°C (at a heating rate of 300°C/h for 12 hours) in a Nabertherm LHT 04/17 furnace. This process allows escaping CO₂ from the carbonate and avoids the creation of CO₂ bubbles in the final melt.

Tab. 2. Nominal compositions (in mol%) of the investigated 15 samples.

	SiO ₂ mol %	Na ₂ O mol %	Al ₂ O ₃ mol %	Fe ₂ O ₃ mol %	GAMMA (Eq. 9&10)	Temperature of melting	Time of melting
G0	66.7	33.3	-	-	1.00	1200 °C	3 hours
G1	66.7	13.3	20.0	-	0.40	1650 °C	42 hours
G2	66.7	15.0	18.3	-	0.45	1650 °C	30 hours
G3	66.7	15.6	17.7	-	0.47	1650 °C	12 hours
G4	66.7	16.7	16.7	-	0.50	1650 °C	13 hours
G5	66.7	17.7	15.6	-	0.53	1650 °C	5 hours
G6	66.7	18.3	15.0	-	0.55	1600 °C	6 hours
G7	66.7	20.0	13.3	-	0.60	1550 °C	4 hours
G8	66.7	13.3	19.0	1.0	0.40	1650 °C	20 hours
G9	66.7	15.0	15.3	3.0	0.45	1650 °C	13 hours
G10	66.7	15.6	14.7	3.0	0.47	1600 °C	10 hours
G11	66.7	16.7	13.7	3.0	0.50	1315 °C	8 hours
G12	66.7	17.7	12.6	3.0	0.53	1300 °C	5 hours
G13	66.7	18.3	12.0	3.0	0.55	1350 °C	3 hours
G14	66.7	20.0	10.3	3.0	0.60	1380 °C	6 hours

Melting the final composition of three (for Fe-free glasses) or four oxides (for Fe-bearing glasses) took place in thin walled platinum crucible in the MoSi₂ Nabertherm furnace. Heating rate was 600°C/h. The melting temperature depended on the composition of the samples (see Table 2) but the technical limitation of the furnace does not allow exceeding 1650°C. However, at higher temperature, platinum from the crucibles (PtRh₁₀) could start to contaminate the melts. The Nabertherm Company guarantees the resistance of the insulation and heating elements up to 1870°C but the melting temperature of platinum is 1768°C (2041 K).

Peralkaline samples needed lower melting temperature and shorter time of melting than the peraluminous samples. Some melts had to be mechanical stirred (up to 12 hours) to accelerate a homogenization and to remove the bubbles. Attention was also paid to the time and temperature of the melting, because too long at too high temperature causes the escape of sodium from the melt.

Cooling rate from the highest temperature to 700°C was always 600°C/h but between 700°C and 500°C was much slower (only 60°C/h) to reduce the creation of internal stress upon cooling through the glass transition. If the sample is not well annealed, later, during drilling out with a diamond drill from the high crucible and polishing, the samples will break.

There were two kinds of samples (with plane parallel surfaces) prepared: (1) for viscosity measurements (discs, ~8mm in diameter, 3-4mm thick) used also to determine the composition, density and ultrasonic shear modulus; and (2) for torsion measurements (cylinders, ~8mm in diameter, 25-30 mm long). Long cylinders did not need the polishing but faces of the small discs were polished with 1 µm jewellers' rouge.

3.2. Microprobe

The ratio between oxides building the structure plays an important role in glass properties. Therefore, a precise measurement of the samples' composition was necessary.

Samples were analyzed by microprobe JEOL JXA 8900 RL in the Geochemistry Department Georg-August University Göttingen using a 15 kV voltage, with a defocused 10 µm beam diameter and with 12 nA current. Results, presented further in the text (see Tables 8 and 9), are an average of 10 analyses of each glass. Errors are 1σ values.

Polished samples, with a diameter ~8 mm were (directly or fixed in the epoxy tablets) mounted on a gold coated holder. In order to avoid unwanted charging samples have been coated in a high vacuum chamber with a carbon film with a standard 25nm thickness. Contact between coated sample and gold holder was assured by a silver based paint. Samples were measured in WDS (Wavelength-Dispersive Spectrometers) mode. To quantify the precisely the amount of each oxide (SiO_2 , Al_2O_3 , Na_2O), two standards were used, namely albite and anorthite crystals. Consequently Fe_2O_3 , for iron bearing samples, was calibrated with hematite. Characteristically for microprobe analyses where only cations are analysed, the amount of oxygen was stoichiometrically calculated for each oxide.

3.3. Density

Definition of density ρ is expressed as follows:

$$\rho = \frac{m}{V}, \quad (\text{Eq. 13})$$

where m is the mass of the sample and V is its volume. The densities of the glasses at room temperature were determined using the Archimedean technique in ethanol (Fig. 13). Samples were weighed in air as well as in the ethanol. The immersion of the glass into the ethanol causes that the force of buoyancy works on the sample. Buoyancy is the weight of the ethanol displaced by the volume of the sample; in other words, the tendency of the sample to float in the liquid. The density ρ of the sample was calculated from measured values:

$$\rho = \frac{w_a \cdot \rho_l}{w_a - w_l}, \quad (\text{Eq. 14})$$

where ρ is density of the sample, ρ_l is density of the liquid (in this case – of ethanol), w_a is the weight of the sample in air, w_l is the weight of the sample in liquid (ethanol). Density of ethanol at the temperature of measurement was taken from the table of Sartorius (Sartorius, 2004).

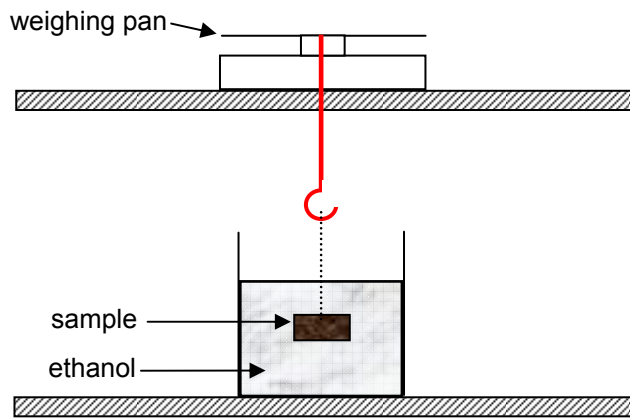


Fig. 13. Scheme of the buoyancy method to measure density of the sample.

Density of the glass is dependent on its thermal history. All the samples were quenched with the same cooling rate (between melting temperature and 700°C with the rate 600°C/h and between 700°C and 500°C: only 60°C/h to remove of the internal stress).

3.4. Pulse Echo Overlap technique

The shear modulus of the glasses was measured at room temperature using the ultrasonic Pulse Echo Overlap method (in the Institute for Low Temperature Physics, Georg-August-University Göttingen) (Fig. 14) (May, 1958; McSkimin, 1961; McSkimin & Aadreatch, 1962; Papadakis, 1966; Truell et al., 1969; King & Stephens, 1975; Papadakis, 1976). A pulse of high frequency waves (here $f=5\text{MHz}$) was sent into the sample via a 5 mm diameter Y-cut quartz piezoelectric transducer which was glued to the sample using a very thin layer of honey. The echo pattern of the multiple reflected pulses was recorded (Fig. 15). After each travel through the sample reflections became weaker as the energy carried by the wave is gradually used for atom vibration motions.

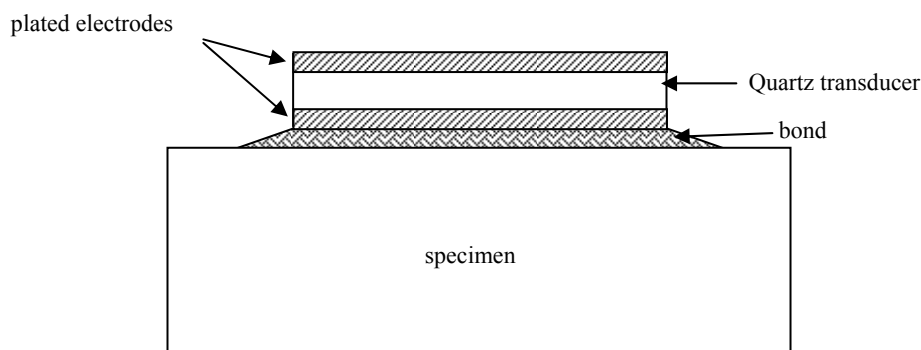


Fig. 14. Schema of specimen, bond and transducers with plated electrodes, use in the Pulse Echo Overlap technique (redrawn after Truell et al., 1969).

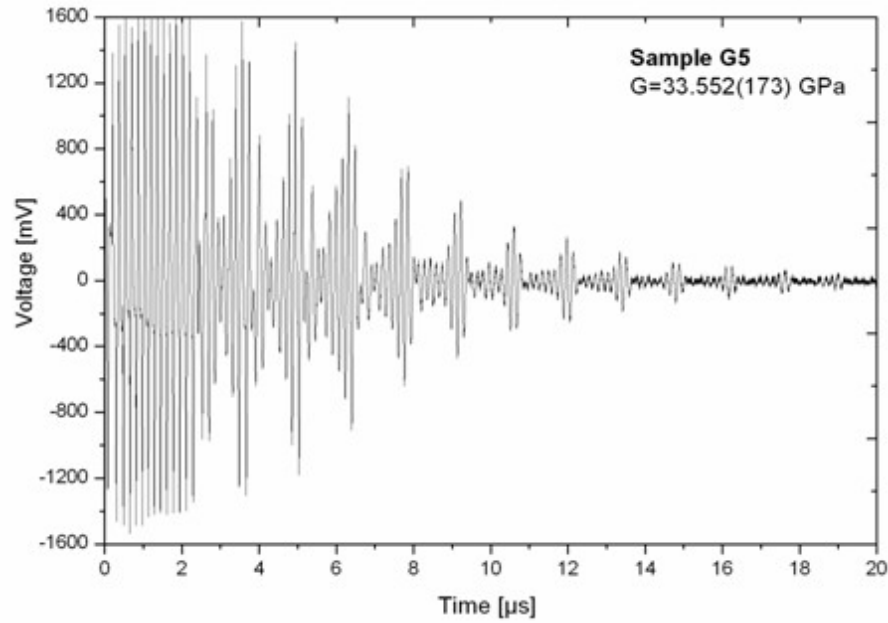


Fig. 15. Typical pulse echo pattern. Here for sample G5.

To determine the wave speed V_s , one has to measure two parameters: (1) thickness of the sample d , which multiplied by $2n$ gives the total distance that the wave travels from the initial point of the measurement and back (where n is the order of reflection) and (2) time delay t between sending a signal and receiving its reflection from a distant surface:

$$V_s = \frac{d}{t}. \quad (\text{Eq. 15})$$

Wave speed V_s for each echo pulse was determined from linear relationship between Δd and Δt (Fig. 16).

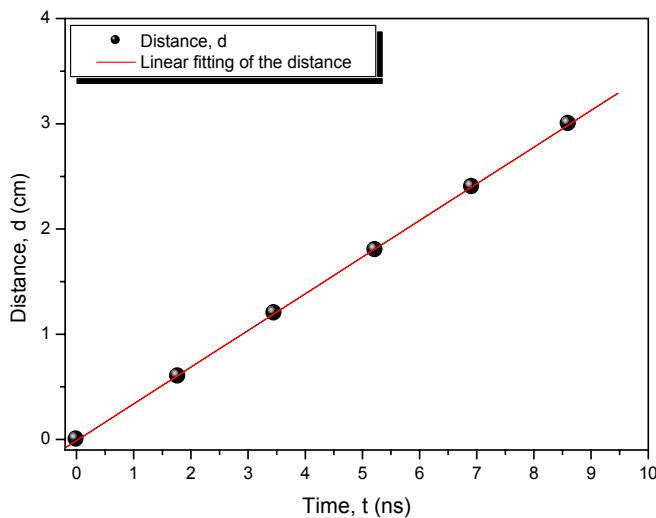


Fig. 16. Linear relationship of the echo pulses travelling through the sample as a function of time.

With known density and wave speed, the shear modulus G of the sample is calculated:

$$G = \rho V_s^2. \quad (\text{Eq. 16})$$

Shear modulus G can be determined from linear relationship between V_s and ρ (Fig. 17).

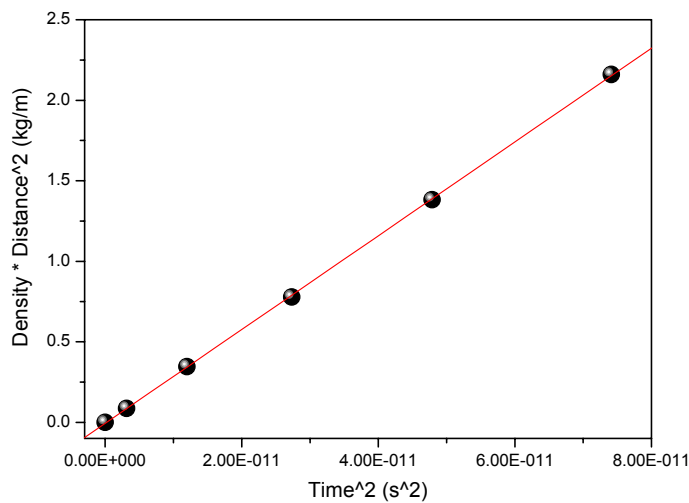


Fig. 17. Linear relationship between ultrasonic wave speed V_s and density of the sample ρ .

The error associated with choosing the correct part of the pulsed signal is at most ± 0.6 GPa. The lengths of the samples were between 2.10 ± 0.01 and 3.70 ± 0.01 mm. The sample thickness was measured with a micrometer.

3.5. Viscosity η

3.5.1. The importance of viscosity

Viscosity is a very important parameter in the glass industry, as well as in geology. It gives information about structural changes and different flow mechanisms in the melt as a function of composition, temperature and pressure. This intrinsic property indicates the resistance of the melt to flow; to change in form.

Temperature effects on viscosity. If one adds some energy to the system (for example: in the form of heat) viscosity decreases – the melt becomes more fluid. Viscosity is inversely related to temperature: with decreasing temperature the viscosity increases.

Viscosity controls the dynamics of the melt in geological settings. On this parameter many reactions depend, like crystallization and differentiation of the magma, diffusion within the melt or magma eruptions. Viscosity, therefore, has a huge importance in volcanology. Highly viscous lavas erupt very explosively. These eruptions occur less frequently because greater pressure is required to push magma outside of the volcano. When magma has low viscosity, the volcanoes are more likely to erupt. In these cases even a little force pushes magma to the surface.

Viscosity measurements play an important role in geology but determination of the viscosity value in very extreme conditions (like in the mantle) is technically difficult. On the contrary, laboratory measurements exclude the possibility to measure an influence of all the factors working in the nature simultaneously (e.g. time, temperature, pressure or volatiles). However, all the measurements can be used to investigate the dynamics of the internal melt structure.

3.5.2. What is viscosity?

Viscosity η of the melt is the ratio of applied shear stress σ to the shear strain rate $\dot{\epsilon}$ (see Fig. 18):

$$\eta = \frac{\sigma}{dv/dt} = \frac{\sigma}{\dot{\epsilon}}, \quad (\text{Eq. 17})$$

where η is viscosity in Pa s, σ is shear stress and $\dot{\epsilon}$ is strain rate. The applied stress σ is directly proportional to the strain rate $\dot{\epsilon}$, what means that with increasing stress, glass deforms faster.

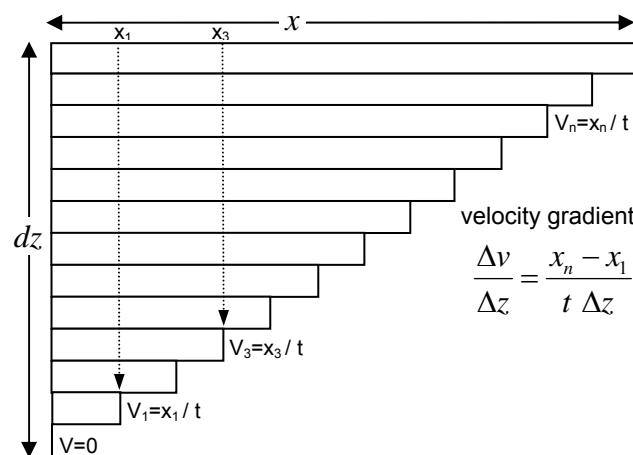


Fig. 18. Diagram for viscosity measurement. Viscosity is the ratio between stress σ and shear strain rate $\dot{\epsilon}$.

Liquids, which obey the linear relationship between stress and strain rate with intercept zero, are known as Newtonian (Fig. 19); that is, the viscosity is independent of the magnitude of σ and $\dot{\varepsilon}$ (see Fig. 26). Non-Newtonian and Bingham liquids behave differently. A Bingham liquid is a material which under low stresses is as a rigid body; only when high stress is applied, the material starts to flow. Non-Newtonian liquids do not have linear relationship between shear stress and strain rate and can be pseudo-plastic or dilatant (Fig. 19). In pseudo-plastic liquids (also called shear thinning fluids) the viscosity decreases with the strain rate. The opposite liquids are dilatant (shear thickening fluids) – their viscosity increases with the higher strain rate.

Newtonian, non-Newtonian and Bingham flow behaviours of glasses and melts have been well explained by Yue & Brückner (1994).

This classification of viscosity types does not include the basic ideas of viscoelastic materials, where the time dependence of physical properties needs to be taken into account. So that the definition of a Newtonian liquid is extended to include time dependence – that is that at high $\dot{\varepsilon}$, σ decreases – but that there is a linear relationship between σ and $\dot{\varepsilon}$ – that is the same η is determined for different magnitudes of σ and $\dot{\varepsilon}$, but is dependent upon $\dot{\varepsilon}$.

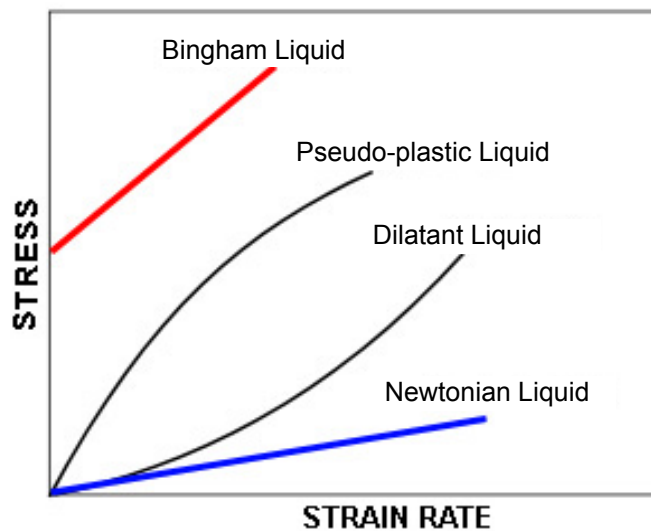


Fig. 19. Classification of the liquids behaviour as a function of dependence between stress and strain rate.

3.5.3. Machine calibration

Viscosity here was measured using the micropenetration technique in a NETZSCH Dilatometer TMA 402. The NETZSCH Dilatometer was calibrated with respect to both temperature and deformation distance. The melting temperatures of three elements were

Tab. 3. Melting temperatures of the three elements used to calibration the NETZSCH Dilatometer, given by NETZSCH Company and measured in the calibration.

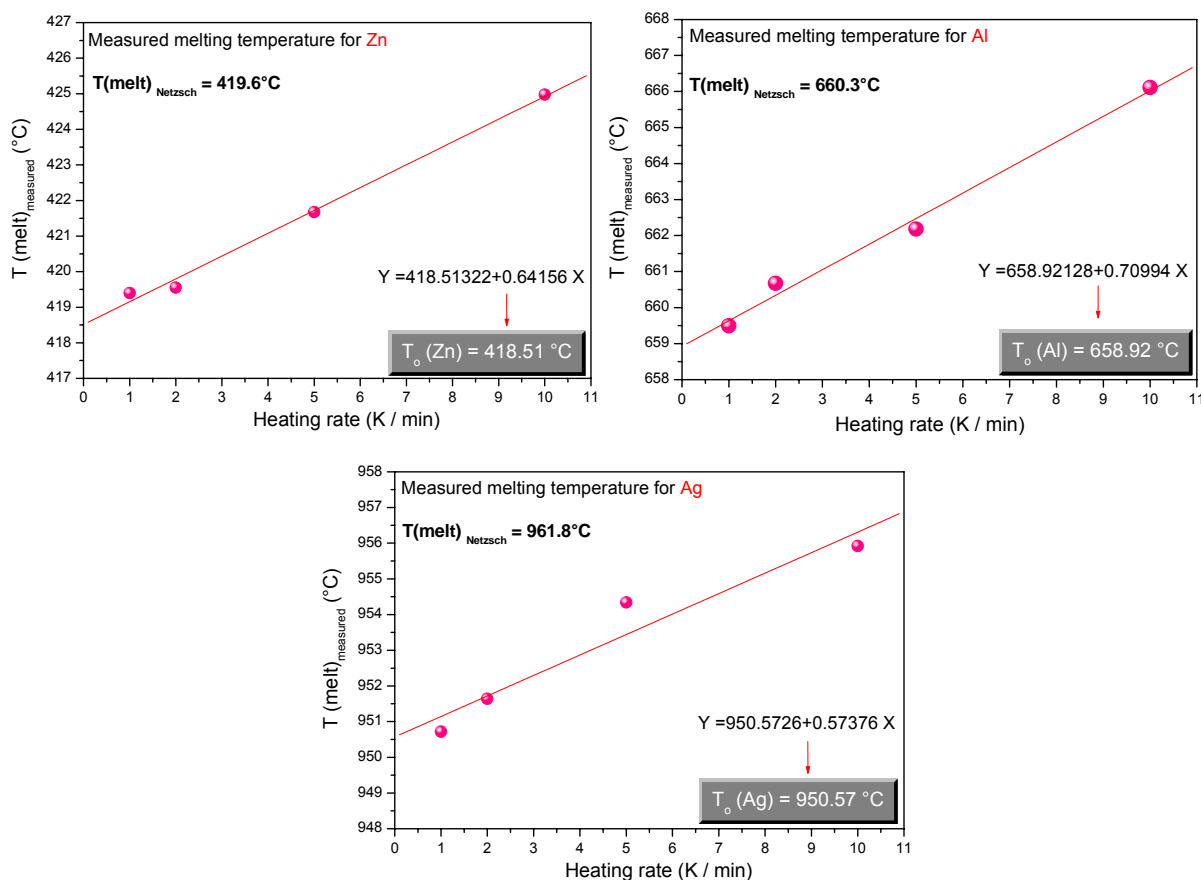
	Melting point (Firma NETZSCH) (°C)	Measured melting point (°C)
Zn	419.6	418.51
Al	660.3	658.92
Ag	961.8	950.51

obtained, namely Ag, Al and Zn. The melting temperatures of these elements have been measured electrically and are shown in the Table 3.

The calibration experiments were done for different heating rates: 1 K min⁻¹, 2 K min⁻¹, 5 K min⁻¹ and 10 K min⁻¹. For all of the elements the melting temperature points at 4 defined heating rates were used to fit a straight line. The intercept of this line and the Y axis gives a temperature T_0 used for the further steps of calibration (Fig. 20).

Three T_0 temperatures created a straight line which is the temperature calibration equation (Fig. 21):

$$T_{calibr} = 1.01677 \cdot T_{measured} - 7.25686 \quad (\text{Eq. 18})$$

**Fig. 20.** Estimating a melting temperature T_0 for Zn, Ag and Al used to calibrate a NETZSCH Dilatometer.

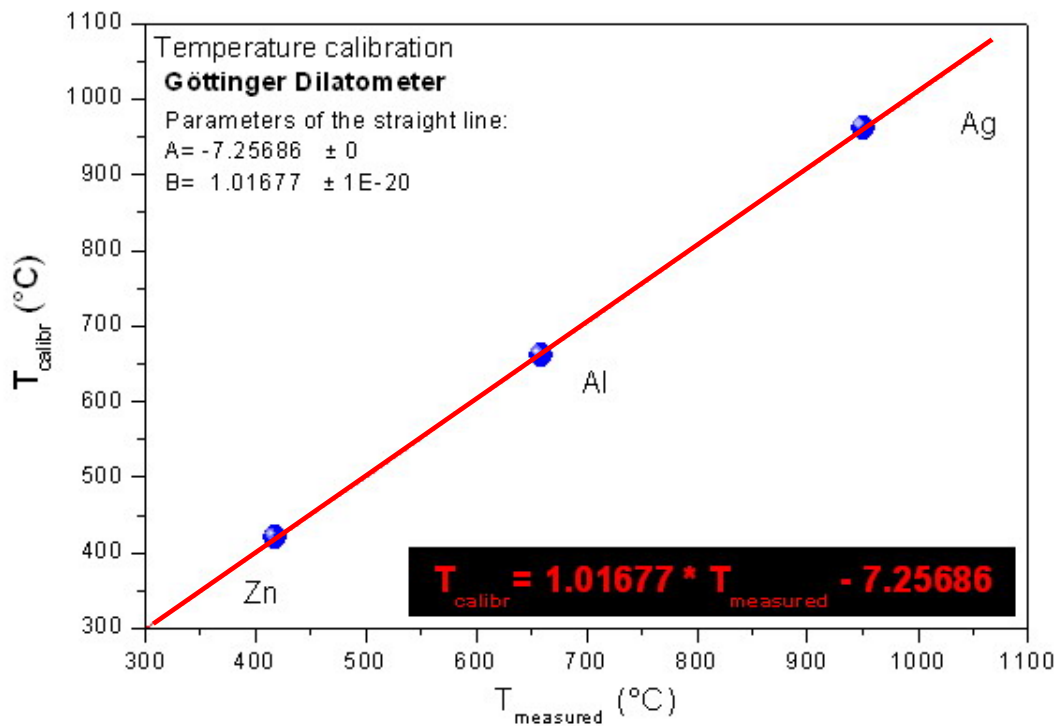


Fig. 21. Plot presenting a calibration equation for NETZSCH Dilatometer.

Viscosity of standard DGG1 (Deutsche Glastechnische Gesellschaft) was measured to check the electronic calibration of displacement measurement. At all temperatures the measured viscosity was within $\pm 0.6 \log \text{ Pa s}$ of the standard viscosity. The error assumed in all of the following viscosity measurements is $\pm 0.6 \log \text{ Pa s}$.

3.5.4. Viscosity measurements

Viscosity measurements were done for all of the samples given in the Table 2. The viscosities of the melts were measured by the micropenetration technique with a NETZSCH TMA 402 Dilatometer (Fig. 22).

The samples were 8 mm cylinders of melt, 3-4 mm thick. The faces of the cylinders were ground parallel to each other and the face which was used for the viscosity measurements was polished with 1 μm jewellers' rouge. The samples were checked with the microscope to exclude the presence of bubbles and crystals.

Viscosity η was determined from the rate at which a single crystal sphere made of sapphire (with diameter between 2006 and 2009 μm) was pushed into the surface of the melt using a force F (Fig. 22b);

$$\eta = \frac{0.1875 F t}{r^{0.5} l^{1.5}}, \quad (\text{Eq. 19})$$

where r is radius of the sphere (μm), t - time (s), l - indent distance, 0.1875 value is a geometric factor (Pocklington, 1940; Douglas et al., 1965; Brückner & Demharter, 1974; Dingwell et al., 1992). The applied force was induced by different masses between 8.253 and 1175.6 g under the acceleration of gravity (9.81 m s^{-2}). Force was applied to the top of the weight pan and through the long ceramic rod (Fig. 22b) the sphere is pushed into the melt. The upper part of the ceramic rod has a ferromagnetic insert which sits in a linear voltage displacement transducer (LVDT). Moving this ferromagnetic rod in the LVDT induces a change in voltage, electronically converted into a displacement of the rod and a change in indent distance.

The indent distance must be less than $200 \mu\text{m}$ as the truncation of the viscosity equation assumes that $l < r$. Measurements have shown that the viscosity equation does not fit the indent data as a function of time for $l > 350 \mu\text{m}$.

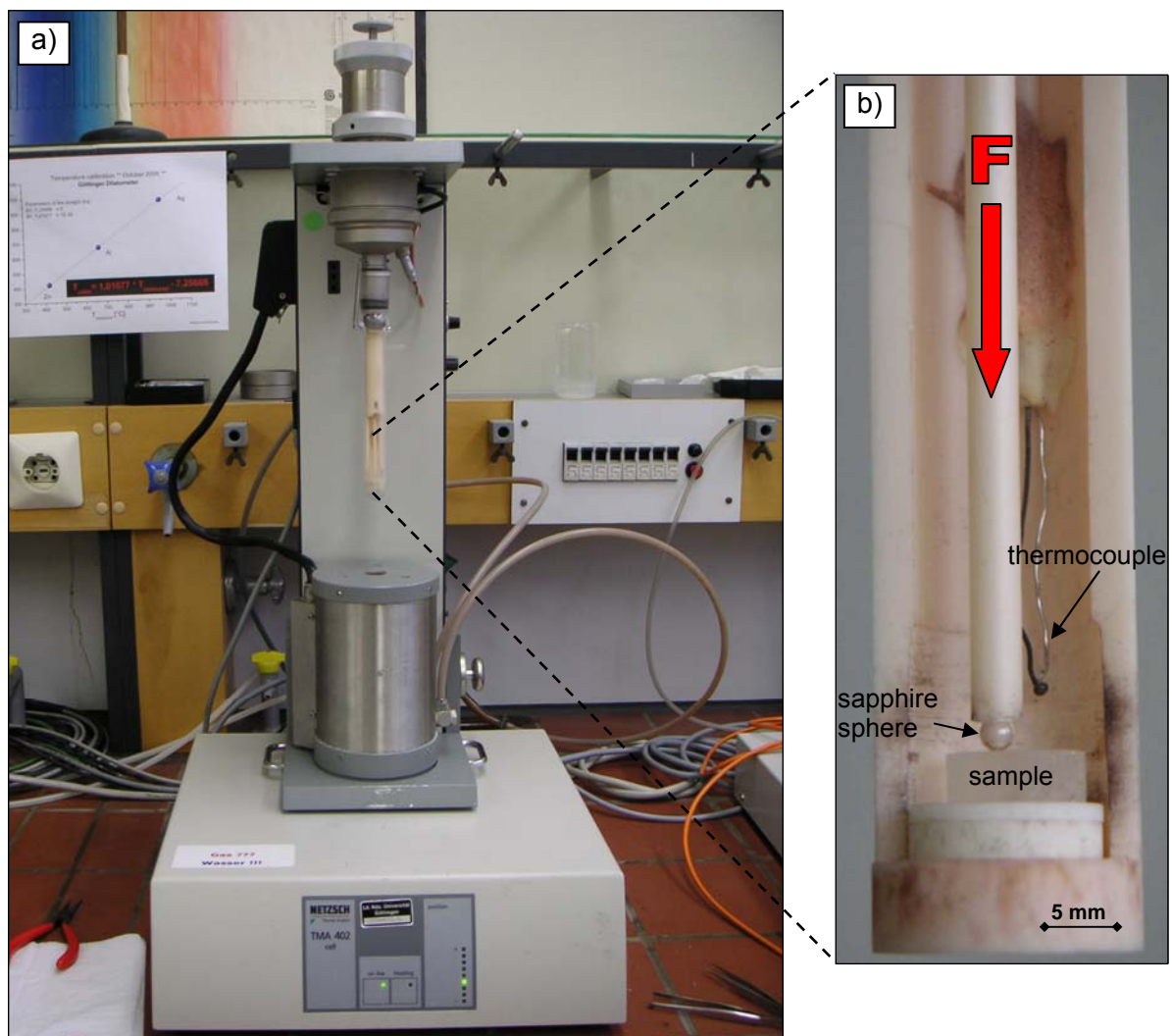


Fig. 22. NETZSCH TMA 402 Dilatometer in the Mineralogy Department, University of Göttingen; used to measure viscosity of the investigated samples.

Controlling the heating and cooling rate and collecting the data was possible with a NETZSCH computer programme. The measurement has been consisted of five segments.

In the **first segment** the sample was heated from the room temperature up to the needed temperature with a constant rate of $10^{\circ}\text{C min}^{-1}$.

The length of the **second segment** (pink line in Figure 23) was dependent on the structural relaxation time τ_M of the sample. At high viscosity conditions (e.g. $10^{11.2}$ Pa s), the sample was held at constant temperature for at least 1 hour in order to allow the melt structure to equilibrate with respect to the applied temperature, before the force is applied. The timescale of structural equilibration is calculated from the Maxwell equation (Eq. 3):

$$\tau_M = \eta_0 / G_{\infty}.$$

G_{∞} is the infinite frequency shear modulus (assuming that $G_{\infty} \sim 10$ GPa from Dingwell & Webb, 1990); and that at least $100 \tau_M$ are required for structural relaxation to be achieved (Dingwell & Webb, 1989). The indent rate of the sapphire sphere is measured in a melt structure that has not relaxed with respect to the applied stress for $100 \tau_M$. This is taken into account in the data analysis and the unrelaxed data are not included in the calculation of viscosity. For viscosities higher than 10^{13} Pa s the relaxation time needs to be very long (over 27 hours) and for this reason such measurements were not done.

Because τ_M is directly proportional to the viscosity it was possible to compute the value of relaxation time from a roughly approximated viscosity (see Table 4). Equilibration time less than 15 minutes was not used.

Tab. 4. Maxwell relaxation times τ_M calculated for each viscosity from the Eq. 3 and equilibration time used in the experiments.

Viscosity $\log_{10} \eta$ (Pa s)	τ_M calculated (s)	$\tau_M * 100$ (s)	Equilibration time used during the measurement
8.0	0.01	1	15 min
8.5	0.03	3	15 min
9.0	0.1	10	15 min
9.5	0.32	320	15 min
10.0	1	100	15 min
10.5	3.16	316	15 min
11.0	10	1000	30 min
11.5	31.62	3162	1.5 h
12.0	100	10000	3 h
12.5	316.23	31623	9h

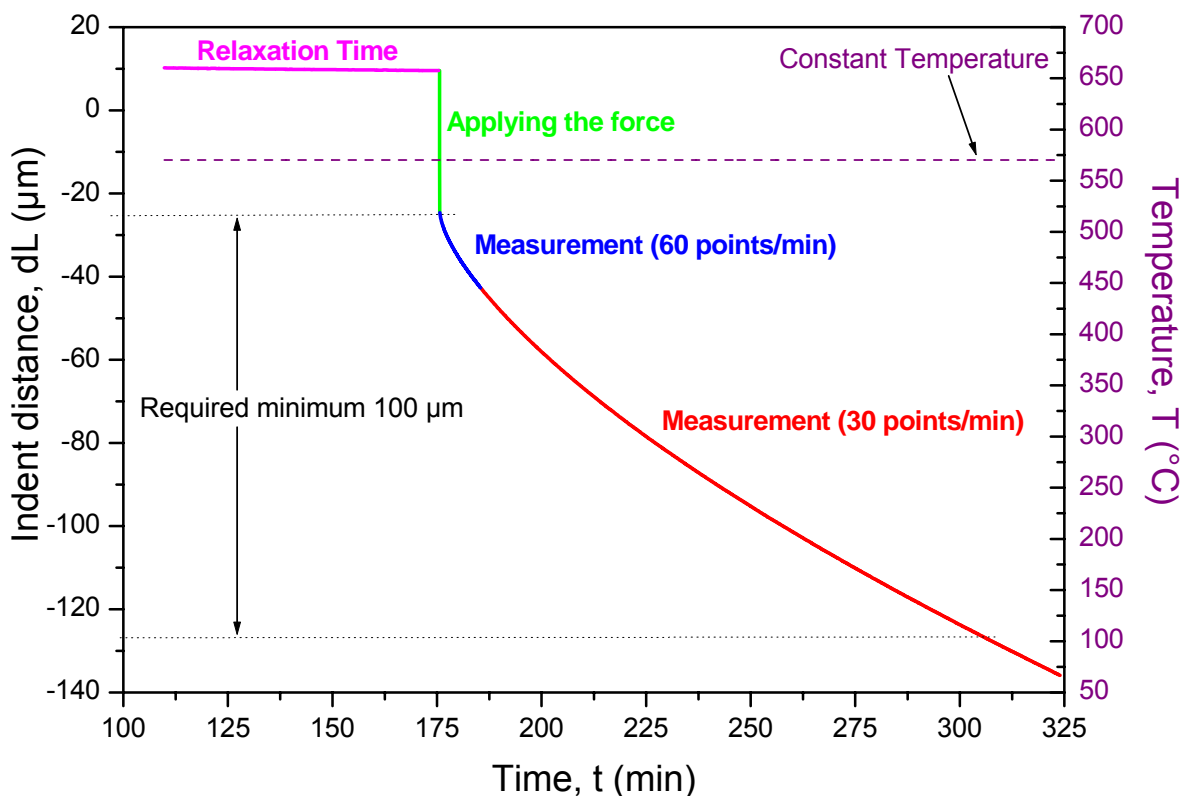


Fig. 23. Schematic view of the viscosity measurement. Description in the text.

Third segment of the experiment is a proper viscosity measurement at a certain temperature and occurs at the same temperature as the second segment. In this part the force is applied (see green line in Figure 23); it means the mass is placed on the top of the weight pan. The mass forces the sapphire sphere into the melt. At the first moment after applying force F , the sapphire sphere comes into intimate contact with the sample.

It is easy to observe that viscosity line in the first stage has larger curvature and with deeper indent distance of sapphire sphere the curvature decreases. In the first 10 minutes of this segment the computer programme has counting 60 measuring points per minute to increase the accuracy of the fitting in the calculation (blue part of line in Figure 23).

The **fourth segment** starts with decreasing the counting rate to 30 points per minute (red part of line in Figure 23). The length of this segment depends on the viscosity of the sample and used weight. The main rule was that the indent distance has to exceed 100 μm for precise calculation of viscosity. For viscosity $10^{8.76}$ Pa s (sample G0) and used weight 18.06 g the measurement time was 11 minutes. On the contrary, for high viscosity ($10^{12.19}$ Pa s for sample G13) and used the maximum weight 1175.6 g the measurement was done over 7.5 hours. The average measurement time was 1.5-2 hours and with the indent distance between 80 and 300 μm .

During the last **fifth segment** the furnace was cooled down. This process was started automatically (after earlier programming) or manually (after reaching required at least 100 μm of the indent distance).

3.5.5. Viscosity calculation

During the experiment with NETZSCH Dilatometer the computer programme saves three different parameters: (1) temperature T ($^{\circ}\text{C}$) measured with a thermocouple inside the furnace (4 mm far away from the sample); (2) the increasing indent distance dL (μm) caused by the sapphire sphere forced into the glass; and (3) time t (s) of the measurement. From the obtained data three plots were prepared.

First plot presents an indent distance dL (μm) as a function of time (Fig. 24). To this characteristic curve a new curve with known parameters was fitted in the ORIGIN Microcal programme, according to the equation

$$y = (k \cdot x)^n, \quad (\text{Eq. 20})$$

where y is the indent distance dL (μm), x is time (s), k is the factor of the fitting and n is an exponent fixed as 0.6667. This fitting equation is based on the formula of Douglas et al. (1965):

$$l = \left(\frac{9 F}{32 \sqrt{2R} \eta} \right)^n \cdot t^n, \quad (\text{Eq. 21})$$

where l is the indent distance dL (μm), F is used force ($F = m \cdot g$), R is the radius of the sapphire sphere (μm), η is viscosity (Pa s) and t - time (s), and $n = 1/1.5 = 0.667$.

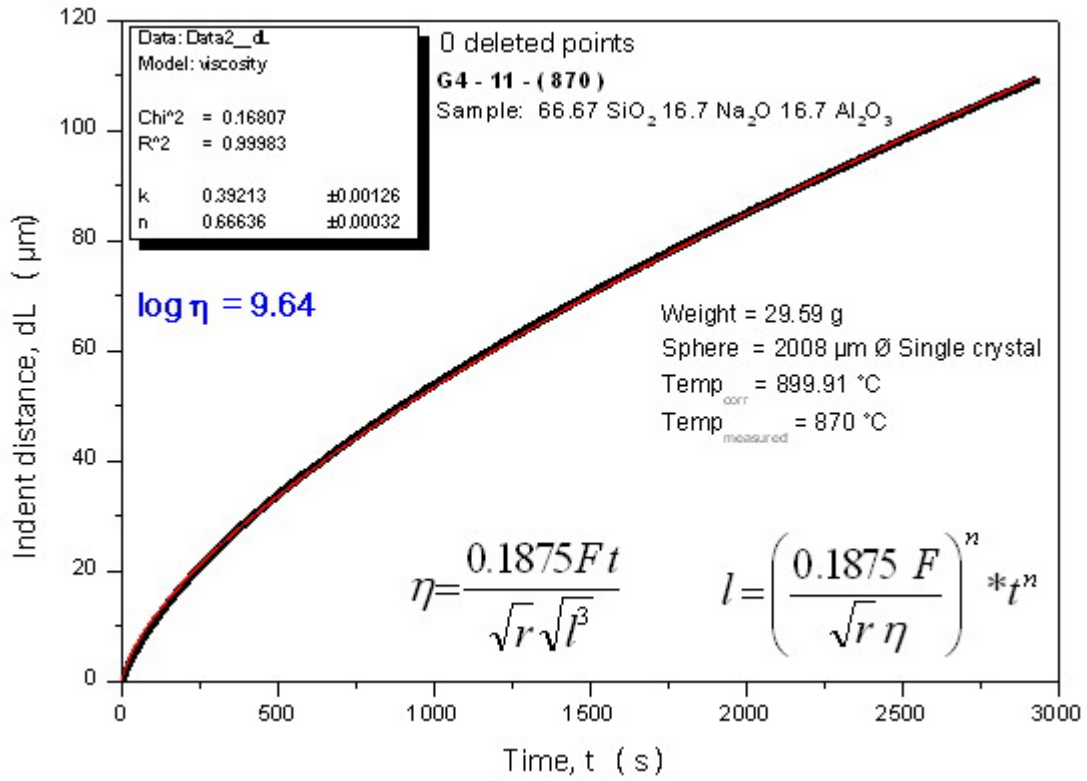


Fig. 24. Plot of the indent distance dL (in μm) as a function of time (in s). Red line is the fit to the data (black line) using Eq. 20. The viscosity is calculated from not linear red curve.

Because the viscosity value must be calculated from the viscous part of the deformation plot, the first points of the plot (with lowest dL and the earliest in the time) need to be deleted. These points represent the unrelaxed part of the melt deformation. Removing them allows getting better estimation of n parameter. Once $n \sim 0.667$ the parameter k is automatically calculated.

With the known k value, viscosity η will be calculated:

$$\eta = \frac{9 F}{32 \sqrt{2R}} \cdot \frac{1}{k} \quad (\text{Eq. 22})$$

(Douglas et al., 1965). The correct temperature for this viscosity needs to be calculated, according to the calibration (Eq. 18).

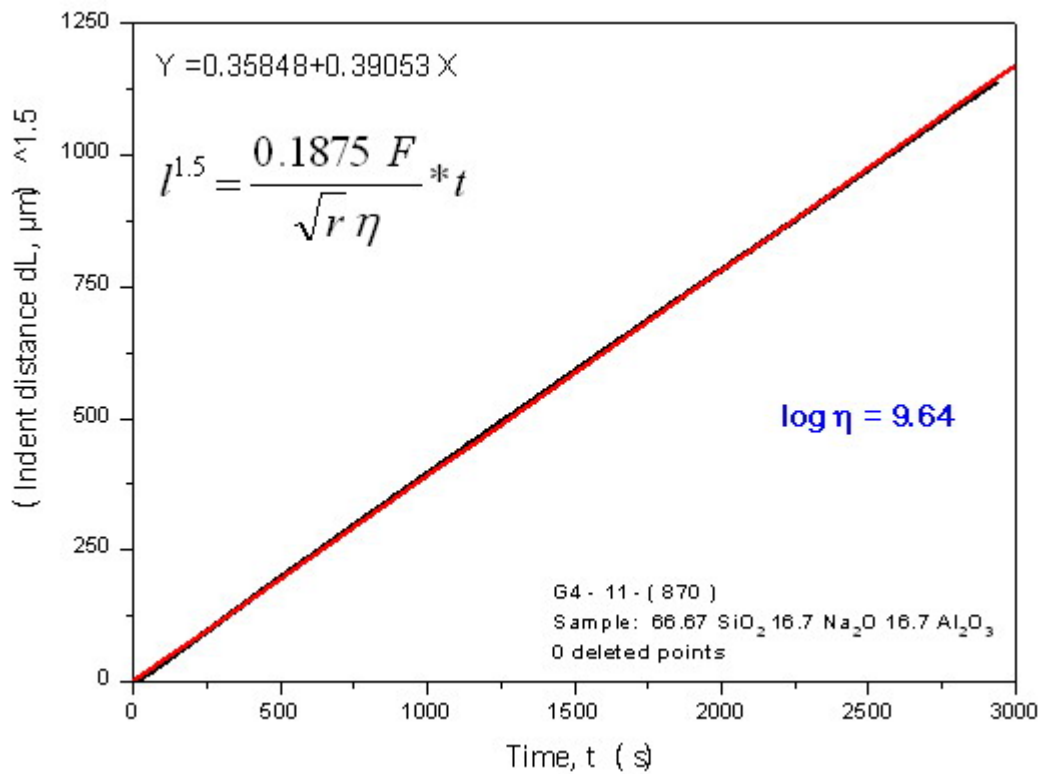


Fig. 25. Plot of the indent distance to the 1.5 ($dL^{1.5}$) as a function of time. Viscosity is calculated from a straight line.

A **second plot**, $dL^{1.5}$ as a function of time is created to compare and to confirm the viscosity calculated from the first plot. Figure 25 shows the linear relationship between $dL^{1.5}$ and time. The line is described with an equation:

$$y = a + k \cdot x. \quad (\text{Eq. 23})$$

Parameter k is used again to calculate viscosity.

A **third plot** shows the relationship of already calculated viscosity η as a function of time (Fig. 26). The vertical initial part of the curve shows the viscosity of still unrelaxed glass. Because the investigated samples are Newtonian, after applying a constant stress, the viscosity of fully relaxed structure is constant and time independent. This behaviour is also used to indicate the absence of the sample crystallisation during the experiment.

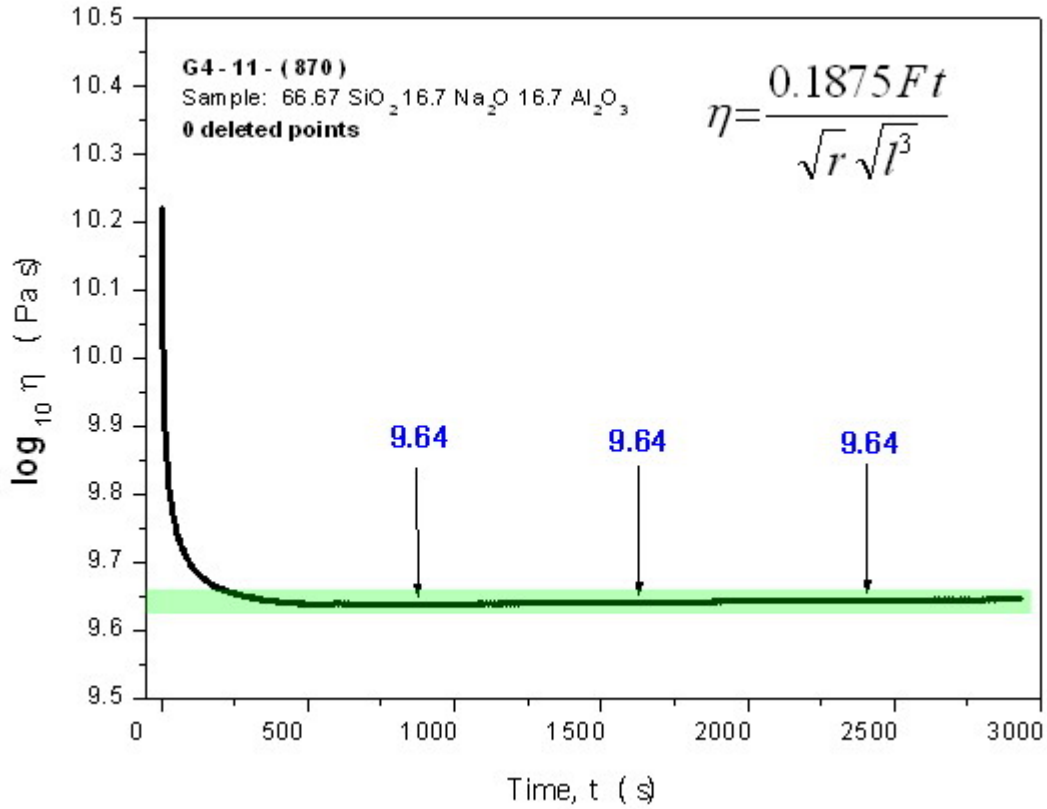


Fig. 26. Plot of the \log_{10} viscosity as a function of time. Viscosity is independent of time.

Viscosities for all samples were measured in the range between 10^8 and 10^{13} Pa s. For each sample 10-13 measurements were done at different temperatures with steps of 10 or 15°C. In Figure 27 data are presented as a function of inverse temperature $10^4/T$ (K^{-1}). A two-parameter Arrhenian equation:

$$y = A + B \cdot x \quad (\text{Eq. 24})$$

was fit to the data; as:

$$\eta = \eta_0 \exp\left(\frac{E_a}{RT}\right) \Rightarrow \log_{10} \eta = A_0 + \frac{E}{RT \ln 10} = A + \frac{B}{T}, \quad (\text{Eq. 25})$$

(Richet & Bottinga, 1995; Webb, 2005a), where R is the gas constant ($8.314474 \text{ J K}^{-1} \text{ mol}^{-1}$), A_0 is the adjustable pre-exponential factor ($A_0 = \log_{10} \eta_0$), E_a is activation energy (energy required to start the flow mechanism of the melt, Glasstone et al., 1941).

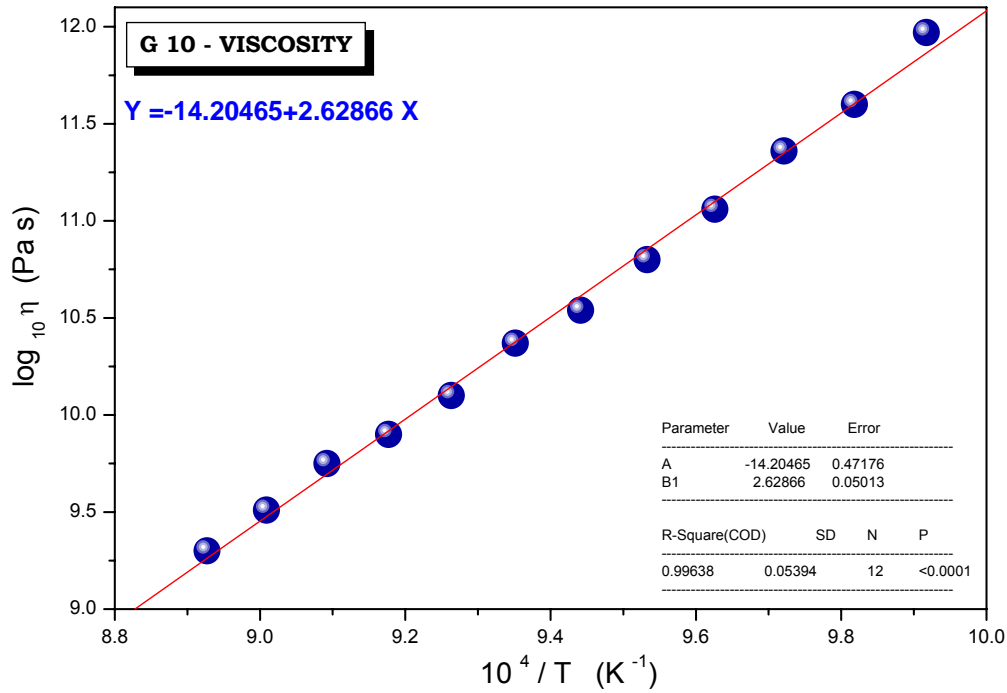


Fig. 27. \log_{10} viscosity (here as an example: sample G10) as a function of inverse temperature.

The Arrhenian equation is exponential. If the temperature range of measurement is less than $\sim 500^\circ\text{C}$ an Arrhenian line is required to describe the η data. If the temperature range is large, the curvature in $\log_{10} \eta$ as a function of inverse temperature becomes large enough to the Vogel-Fulcher-Tamman (VFT) equation is used:

$$\eta = \eta_0 \exp\left(\frac{E_a}{R[T-T_0]}\right) \Rightarrow \log_{10} \eta = A_{VFT} + \frac{E}{R[T-T_0] \ln 10} = A_{VFT} + \frac{B_{VFT}}{T-C} \quad (\text{Eq. 26})$$

(Fulcher, 1925; Tamman and Hesse, 1926; Angell, 1991a; Richet and Bottinga, 1995; Hess and Dingwell, 1996; Webb, 2005a), where A_{VFT} is the constant value of viscosity at infinite temperature, B_{VFT} is pseudo-activation energy and C is VFT temperature. T is absolute temperature (K). Russel et al. (2003) estimated value A_{VFT} of -4.31 ± 0.74 , Giordano et al. (2006) respectively for large data sets as -4.07 ± 1 , Toplis (1998) calculated that as -2.6 ± 1 .

Using B parameter from Eq. 24, it is possible to calculate activation energy E_a :

$$E_a = B \cdot R \cdot \ln 10. \quad (\text{Eq. 27})$$

Here, the Arrhenian equation was used to fit all data.

At the end, viscosity data were presented as a function of the composition (γ value) to illustrate the dependence of the viscosity on peraluminosity or peralkalinity of the melt.

3.6. Heat capacity c_p

The calorimetric techniques base on the measurement of heat. Heat capacity is the energy required to increase the temperature of the sample. In the case of the melts there are two heat capacities as a function of temperature: (1) that of the glass in which flow does not occur, and (2) that of the melt in which energy is also used for flow. The difference between the two c_p values is the configurational heat capacity c_p^{conf} .

The configurational properties of melts can have a large influence on the thermal and volume properties. The configurational heat capacity has a great importance in thermodynamic calculations involving silicate melts and can (through the configurational entropy S_{conf}) be related to viscosity (Richet & Bottinga, 1985; Richet & Neuville, 1992). Changes in the melt structure can be explained by variation of the configurational entropy S_{conf} as a function of composition. Calorimetry is an excellent method to observe the change in enthalpy of the sample as a function of temperature.

3.6.1. Glass transition range and fictive temperature T_f

Differential scanning calorimetry (DSC) is ideal to observe a glass transition from glass to liquid and to calculate the fictive temperature of the melt – the characteristic parameters for each glass composition.

The glass transition occurs across a range of temperature, not at one strictly fixed temperature. It is a change in behaviour between liquid and glass. The width of glass transition region depends on the relaxation time of the glass and the heating rate. The

kinetic nature of the glass transition is strongly connected with heating / cooling rate and is traditionally explained on the enthalpy or volume versus temperature plots.

As pointed out by Narayanaswamy (1971), if the structure of a melt determines the physical properties, the change in physical properties with temperature through the glass transition will follow the same curve as structure does; and thus all physical properties should show the same trend through glass transition. As shown by Webb (1992b) this is the case for enthalpy and volume.

At high temperature the melt structure is fully relaxed. With decreasing temperature the melt needs more time (longer relaxation time) to stay in equilibrium with the new temperature (Fig. 28). The viscosity also increases and with further cooling at some stage the structural units can no longer rearrange to the equilibrated structure because relaxation time is too short. Structure becomes “frozen”, constant and it does not change with further decrease in temperature. Enthalpy of new structure is higher than would be in the equilibrium state and the curve has a decreasing slope, up to the state when could become fully temperature independent. This supercooled liquid with “frozen” structure is called a glass. The temperature region between the high temperature at which structure of the supercooled liquid is still in equilibrium and the temperature at which structure does not change anymore, is called glass transition (Brawer, 1985; Scherer, 1986; Goldstein & Simha, 1976; O’Reilly & Goldstein, 1981; Angell & Goldstein, 1986).

Glass transition region depends on heating / cooling rate. With slower temperature changes, the structure has more time to follow the equilibrium line towards lower temperature and the glass transition will appear at lower temperatures. Such glass will have lower enthalpy than the glass with faster cooling rate.

Crystallization, upon cooling, results in a large drop in enthalpy and the creation of a long range order in the crystal. If the melt is cooled fast enough, the crystalline state does not occur and the change in enthalpy goes slowly then the liquid becomes supercooled. If the lines of the glass and supercooled liquid will be extrapolated, they will cross at the point indicating fictive temperature T_f of the glass. T_f characterises the last equilibrium state of the supercooled liquid.

Because glass transition occurs over a range of temperature, for simplifying this very important parameter (especially in the industry), T_g was defined as the temperature, at which the shear viscosity equals 10^{12} Pa s. By $\log_{10} \eta = 10^{12}$ Pa s the relaxation time of the melt last 100 seconds (Scherer, 1990). The value of T_g is in general, for normal laboratory quench rates comparable with T_f .

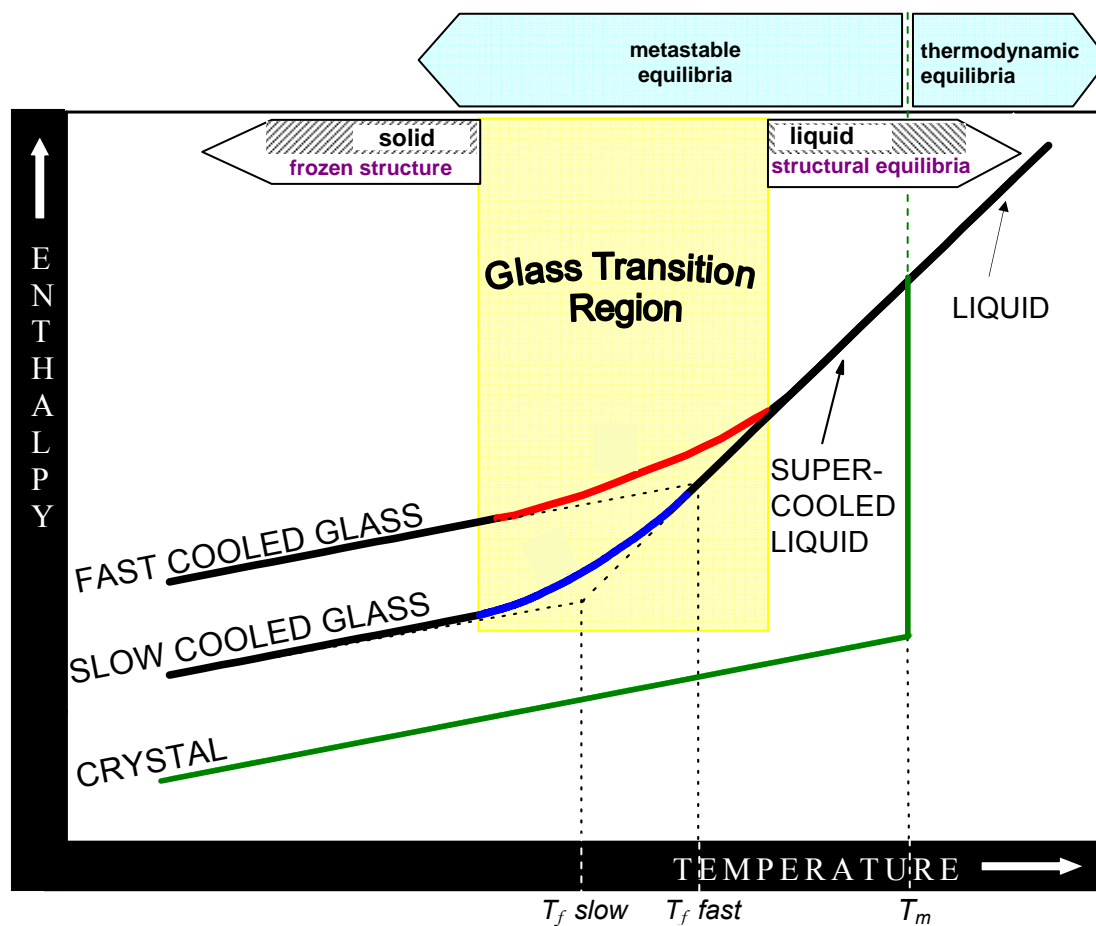


Fig. 28. Effect of temperature on the enthalpy of a glass forming melt for fast and slow cooled glasses and for crystalline material. Red part of the line indicate the glass transition region for fast cooled glass; blue line – glass transition region for slow cooled glass. Other descriptions in the text.

3.6.2. Description of the machine

The DSC measures the heat capacity c_p of the sample against an empty crucible. In this project the heat flux DSC was used (Fig. 29).

The operating conditions for the Netzsch DSC 404C calorimeter are from room temperature up to 1000°C. The heat flow is measured with Pt/Rh thermocouples. Two crucibles composed of platinum are placed on the raised platform in the Pt10%Rh head designed to be used at high temperature and that all is surrounded by the furnace. All the measurements were done in the atmosphere of argon gas to keep the sample dry and to remove superfluous volatiles. The reference crucible remains empty. Sample is placed in the second crucible. The computer programme measures the difference in voltage between the sample and reference thermocouple. Then voltage value is compared with the known equivalent of heat capacity. The result is a plot of differential heat capacity between sample and reference as a function of temperature.

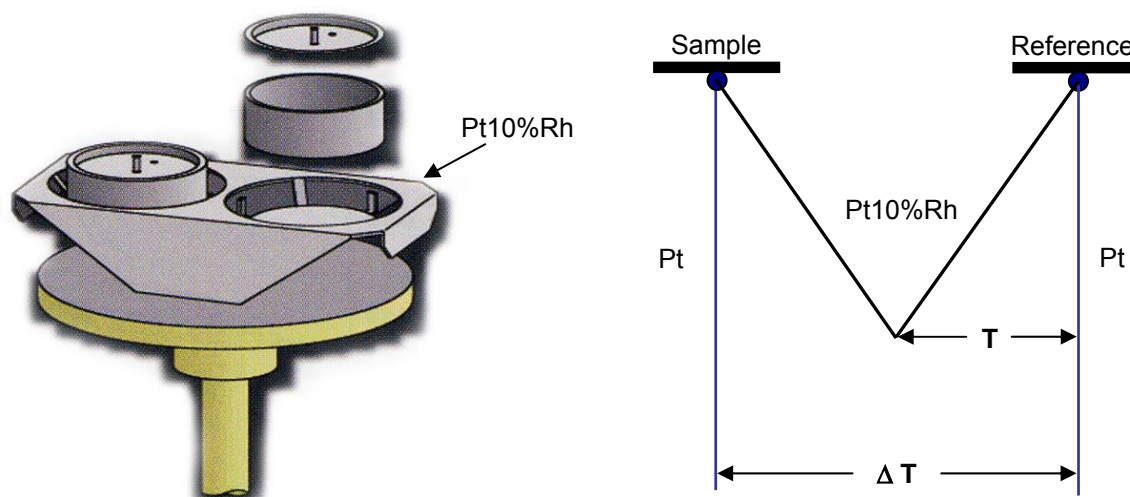


Fig. 29. Schematic presentation of the differential scanning calorimeter (DSC). Description in the text.

3.6.3. Calibration of the calorimeter

Calibration consists on two measurements: (1) when both crucibles are empty and (2) when reference crucible is empty and sample crucible contains a standard. The standard used to calibrate the machine is polycrystalline Al_2O_3 disk (6 mm diameter, ~1 mm thick) with the weight of 55.56 mg. The μV reading from two empty crucibles is subtracted from that with one empty + one crucible with the Al_2O_3 standard in order to remove the effect of the crucible containing the standard. The resulting μV values as a function of temperature are compared with the heat capacity of Al_2O_3 given by Robie et al. (1978). Data of Robie et al. (1978) are in excellent agreement with those of Krupka et al. (1979). The sensitivity curve needed to convert $\mu\text{V g}^{-1}$ to $\text{J g}^{-1} \text{K}^{-1}$ is then used in the subsequent measurements of the heat capacity of the melts.

3.6.4. Measurement and calculation of heat capacity and configurational heat capacity

The sample is prepared as a coarse-grained powder (~0.2-0.3 mm in diameter) and in the crucible is placed about 55 mg the material. Sample and reference are heated up with the same heating rate as the last cooling rate. Only first measurement is worthless because last cooling rate of the sample is unknown.

Fig. 30 shows a typical curve obtained from heat capacity measurement. Marked black part of the heat capacity data was used to fit a curve described by Maier-Kelley equation:

$$C_p = a + b \cdot T + c \cdot T^{-2} \quad (\text{Eq. 28})$$

(Maier & Kelley, 1932; Scherer, 1990) being an extrapolation of heat capacity of the glass, where a , b and c are parameters of the line; and T is temperature in K. Small values of the parameter b describe the simple melts which can be expressed by harmonic oscillation theory.

Range of temperature chosen to this fitting was between 200°C (to exclude all disturbance of the lower temperature) and the temperature at which the glass transition starts (strong bend of the curve).

In the glass transition range the heat capacity curve goes up to reach the maximum at the temperature of structural relaxation of the melt. Melt becomes a supercooled liquid. When the curve becomes temperature independent (horizontal), the measurement needs to be broken off to prevent complete melting of the sample. End of the curve indicates a heat capacity of the melt.

Difference between heat capacity of the melt c_{pl} and heat capacity of the glass c_{pg} at the glass transition (measured at the same temperature) is the configurational heat capacity c_p^{conf} and is the energy difference – integrated over all atoms – between the minima of the potential energy wells explored when flow begins (Richet et al., 1986; Richet & Toplis, 2001):

$$c_p^{conf} = c_{pl} - c_{pg} \quad (\text{Eq. 29})$$

To a first approximation, the c_{pg} can be calculated from a linear summation of the heat capacities of the oxide components. Similarly, if there are no anomalous changes in melt structure upon heating through the glass transition, the c_{pl} will be a linear sum of the contributions of the component oxides (e.g. Richet & Bottinga, 1985). Determination of c_{pl} as a function of composition illustrates the presence of such anomalous structures (see section 4.5.).

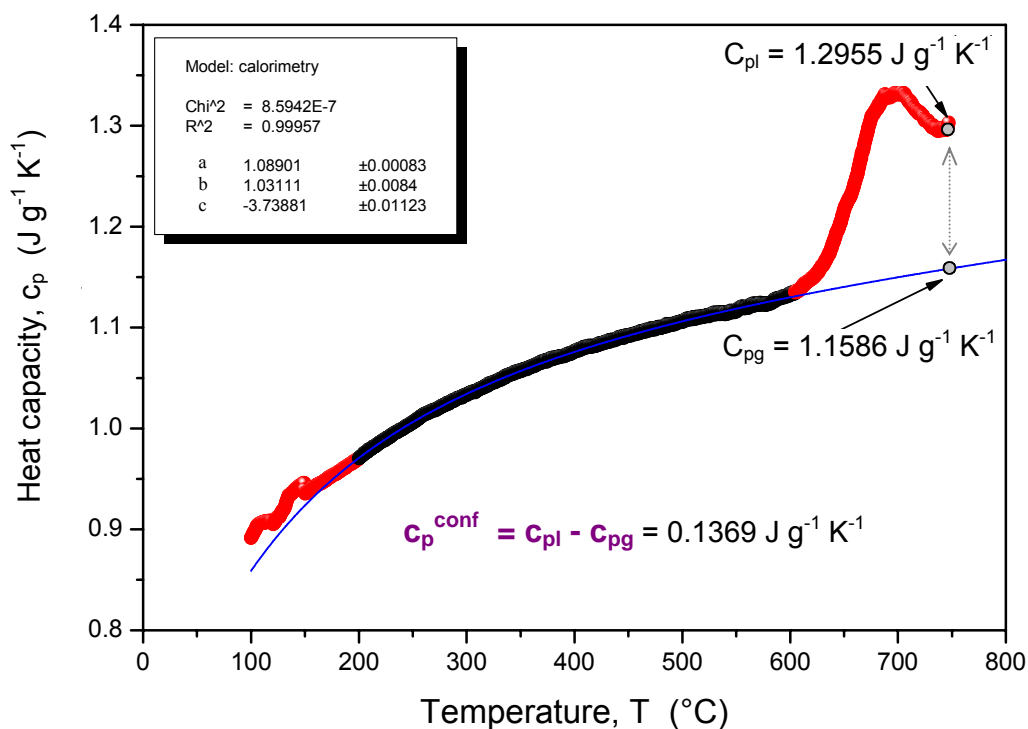


Fig. 30. Heat capacity c_p ($\text{J g}^{-1} \text{ K}^{-1}$) as a function of temperature ($^{\circ}\text{C}$). Blue line is a fit to the three parameter Maier – Kelley equation (Eq. 28). Description in the text.

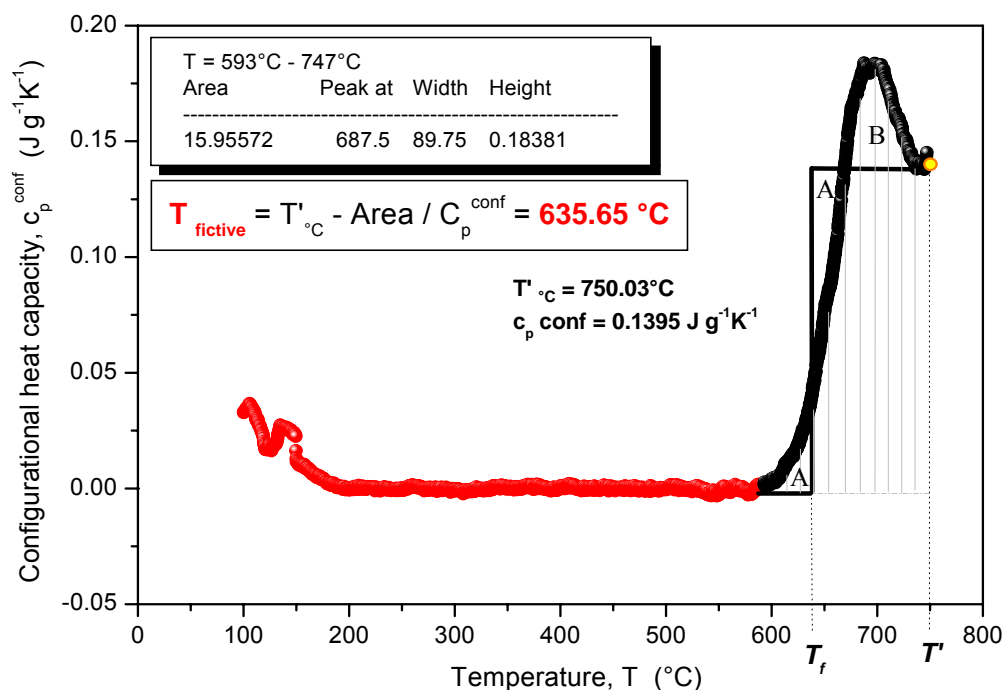


Fig. 31. Configurational heat capacity c_p^{conf} ($\text{J g}^{-1} \text{ K}^{-1}$) as a function of temperature ($^{\circ}\text{C}$). Description in the text.

3.6.5. Calculation of the fictive temperature

Next step of calculation is determination of the fictive temperature of the melt.

Fictive temperature describes the temperature at which the melt structure would be in equilibrium and decreases for decreasing cooling rate (see Fig. 32). Using the options of ORIGIN programme, points of fitted line are subtracted from heat capacity data and a plot of configurational heat capacity is obtained (Fig. 31). Area below the peak (marked as grey vertical lines) is calculated and used to determine fictive temperature according to the equation:

$$T_f = T'_{(^\circ\text{C})} - \frac{\text{area}}{C_p^{\text{conf}}} . \quad (\text{Eq. 30})$$

The areas A and B in Figure 31 are related to the equation:

$$\int_{T \gg T_g}^{T_f'} (c_{pe} - c_{pg}) dT = \int_{T \gg T_g}^{T \ll T_g} (c_p - c_{pg}) dT , \quad (\text{Eq. 31})$$

where c_{pe} is the equilibrium heat capacity of the glass, c_{pg} is the heat capacity of the glass (Moynihan, 1995). Area A matches up to the left side of the equation (Eq. 31), and area B corresponds to the right side. Areas A and B should be equal.

3.6.6. Dependence of the glass transition on the heating rates of the sample

Sample is heated up at different heating rates: 5°C/min, 10°C/min, 15°C/min, 20°C/min and 25°C/min. With reference to the kinetic of the melt and structural relaxation time, different heating rates contribute to change the position of the peak's maximum as a function of temperature (Fig. 32): at lower temperature when heating rate is slow and at higher temperature for faster heating rate.

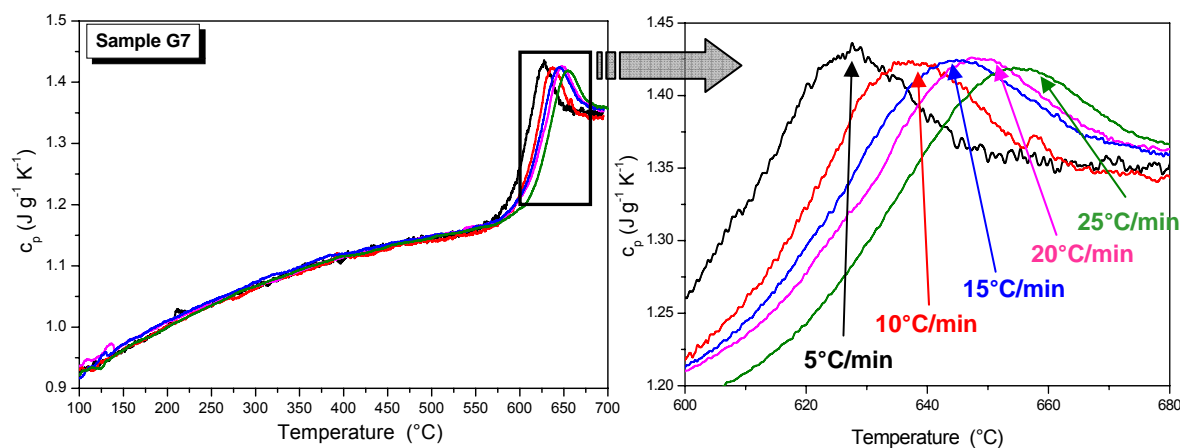


Fig. 32. Different heating rate of the sample causes shift of the peak's position. Description in the text.

3.7. Torsion (forced oscillation)

There are few studies of the frequency – dependence of the shear modulus and viscosity of silicate melts. This technique was first developed for crystalline materials, and is also used for molten samples. The studies on melts have shown:

- (1) the melt structure cannot be described by a single flow mechanism with a single timescale of bond exchange. This is to be expected based upon the statistical nature of the melt structure;
- (2) it is possible to resolve the creation of new structures involved in the flow process. The data of Bagdassarov et al. (1993) show that there is an effect on flow due to the presence of boron and fluorine, but it is only in the case of phosphorus that a second peak in the structural relaxation (flow) spectrum is seen. These data were obtained on single melt compositions and so it was not possible to determine the actual effect due to the added components.

Day & Rindone (1962) have performed forced oscillation measurements on $\text{Na}_2\text{O}-\text{Al}_2\text{O}_3-\text{SiO}_2$ melts, but were interested in the movement of Na atoms and therefore worked between -50 and 0°C .

The determination of the shear modulus and the imaginary part of the shear modulus in the present study will be used to interpret the changes in bond strength and flow units in the melt.

3.7.1. Principle of torsion

Forced oscillation shear deformation is based on the principle of torsion of a fixed cylindrical rod. Here a torque is applied and the resulting deformation (angle of twist, φ) of the rod is measured as a function of frequency.

Torsion measurements have been performed on the samples G0-G14 (see Table 2). In these measurements, the stress σ , and strain ε are determined as a function of frequency from 1 mHz to 1 Hz, and the real $G'(\omega)$ and imaginary $G''(\omega)$ components of the shear modulus are calculated from these measurements.

The relationship between applied stress σ and measured strain ε gives shear modulus G :

$$G = \frac{\sigma}{\varepsilon} . \quad (\text{Eq. 32})$$

The cylinder in Figure 33 is held fixed at surface A and the angle of twist φ (in radians) is measured at surface B ;

$$\varphi = \frac{BB'}{r} , \quad (\text{Eq. 33})$$

where r is the distance from the centre of the cylinder. The shear strain ε_r at a distance r from the centre of the rod is given by φ ; and for small values of ε_r

$$\varepsilon_r = \tan \varepsilon_r = \frac{\varphi r}{L} , \quad (\text{Eq. 34})$$

for L - the length of the rod (Riley et al. 1999). At the centre of the rod $\varepsilon_0 = 0$. The shear stress σ is calculated from the applied torque τ_φ :

$$\sigma_r = \frac{\tau_\varphi r}{J} , \quad (\text{Eq. 35})$$

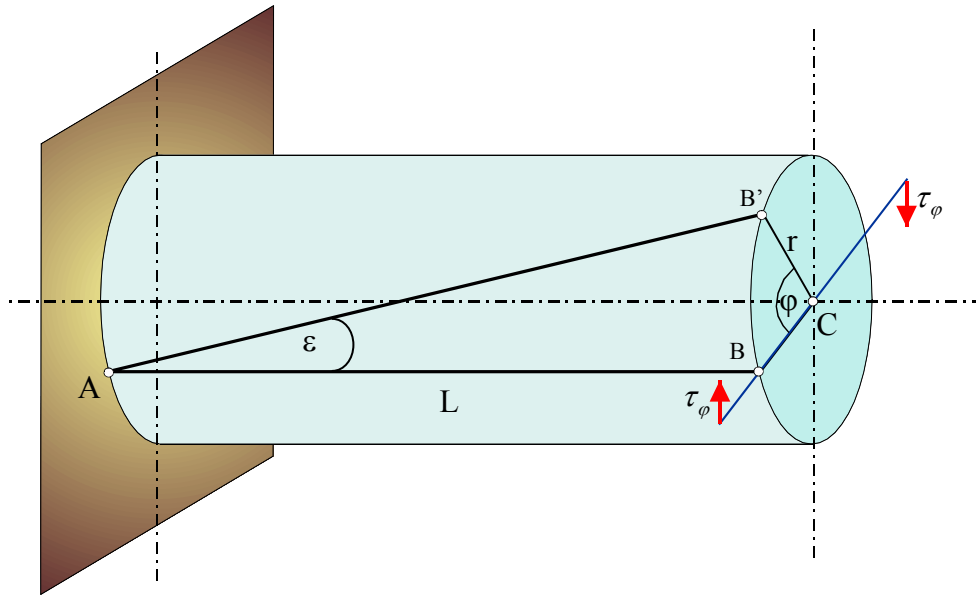


Fig. 33. Schematic diagram of the torsion experiment with characteristic quantities described in the text.

for J - the polar second moment of area which is:

$$J = \frac{\pi r^4}{2} \quad (\text{Eq. 36})$$

(Sass et al., 1966). The shear modulus of the cylinder can then be calculated as a function of frequency:

$$G^*(\omega) = \frac{\sigma}{\varepsilon} = \frac{2 \tau_\phi L}{\pi r^4 \phi}. \quad (\text{Eq. 37})$$

The real component of modulus is the elastic deformation, while the imaginary component is a measure of the energy loss in the melt. A peak in the loss modulus indicates the motion of part of the melt structure.

The shear viscosity can be also calculated as a function of frequency:

$$\eta^*(\omega) = \frac{\sigma}{\dot{\varepsilon}} = \frac{2 \tau_\phi L}{\pi r^4 \dot{\phi}}. \quad (\text{Eq. 38})$$

As the shear modulus and shear viscosity are both frequency dependent and are a function of stress, strain and strain rate:

$$\eta^*(\omega) = \frac{\sigma}{\dot{\epsilon}} = \frac{G^*(\omega)}{i\omega} = \frac{G'(\omega)}{i\omega} + \frac{iG''(\omega)}{i\omega} = \eta'(\omega) + i\eta''(\omega) \quad (\text{Eq. 39})$$

(Webb, 1991). Thus the real component of viscosity is the frequency independent (Newtonian) viscosity and the real component of shear modulus is the frequency independent elastic modulus. Torsional deformation can be used to determine G and η of a material, both in the time domain – for a constant applied torque, and in the frequency domain – for a sinusoidally oscillating torque.

3.7.2. The torsion apparatus

The torsion apparatus was calibrated by measuring the shear modulus of a long rod of polycrystalline Al_2O_3 (Al23 Degussit®). This rod is 8 mm in diameter and fixed at one end (see Fig. 34). The shear modulus of the alumina rod is determined by static measurements in which the torque τ_φ is created by a force F applied to the rod:

$$\tau_\varphi = F \cdot a, \quad (\text{Eq. 40})$$

where a is the distance from the centre of the rod to the applied force (Fig. 35). The force was created by applying different masses. In the successive measurements one pair of the weights were hung on threads which went from the end of the arm of length $a_{av}=100.85$ mm to a pulley at the edge of the top plate. The resulting twist in the alumina rod was determined by the inductive transducers at channels 1 & 2. There are aluminium rods fixed to the alumina rod at the points: channel 1 and channel 2. These rods end in iron plates which sit within pairs of inductive transducers. As the Al_2O_3 rod twists, the angle of twist is magnified by the length of the aluminium rod and the motion of the iron plate results in a voltage change at the inductive transducers.

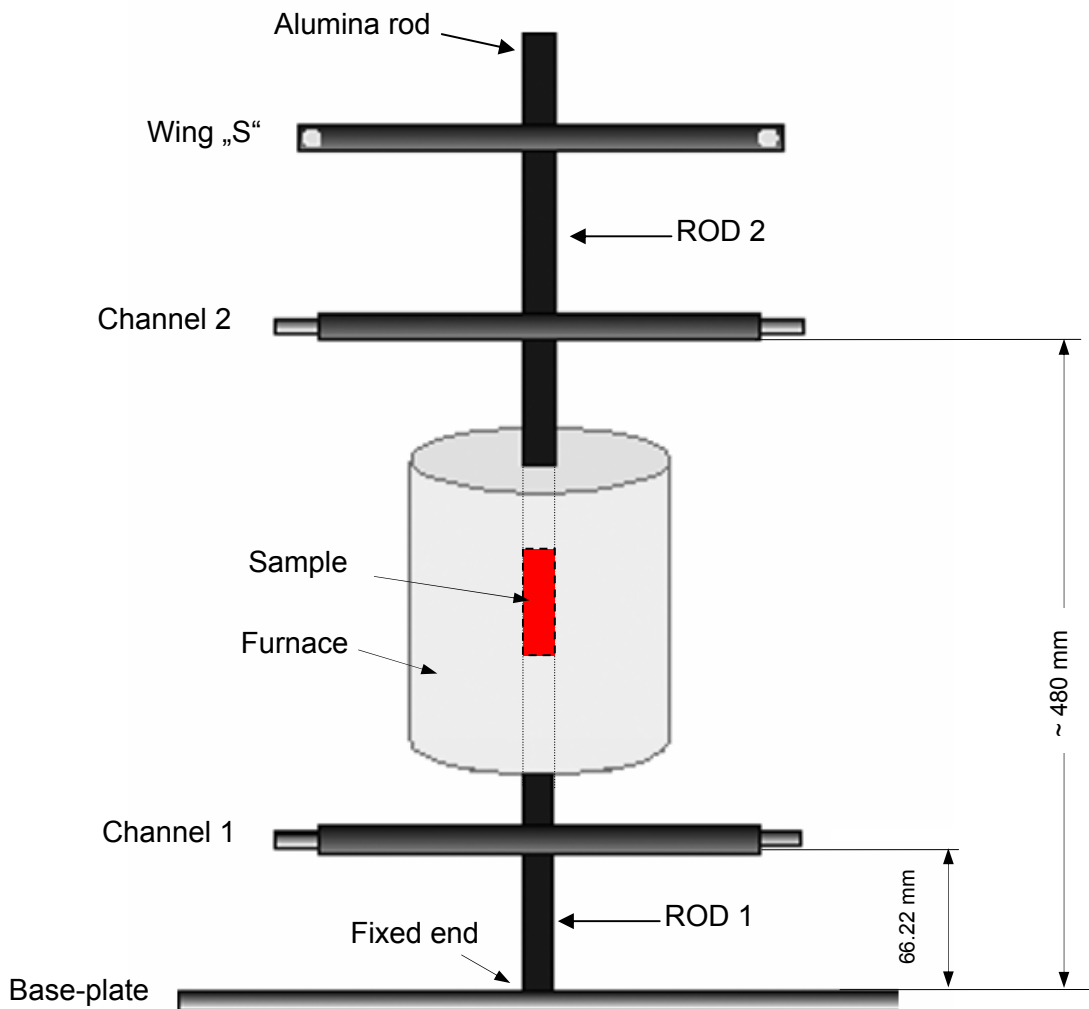


Fig. 34. Scheme of the torsion machine and furnace. The angles of twist are measured at channels 1 and 2; and the torque is applied at “wing S”. The equipment is calibrated using a rod of polycrystalline Al_2O_3 . The sample assembly with a cylinder of melt between two Al_2O_3 rods is shown here.

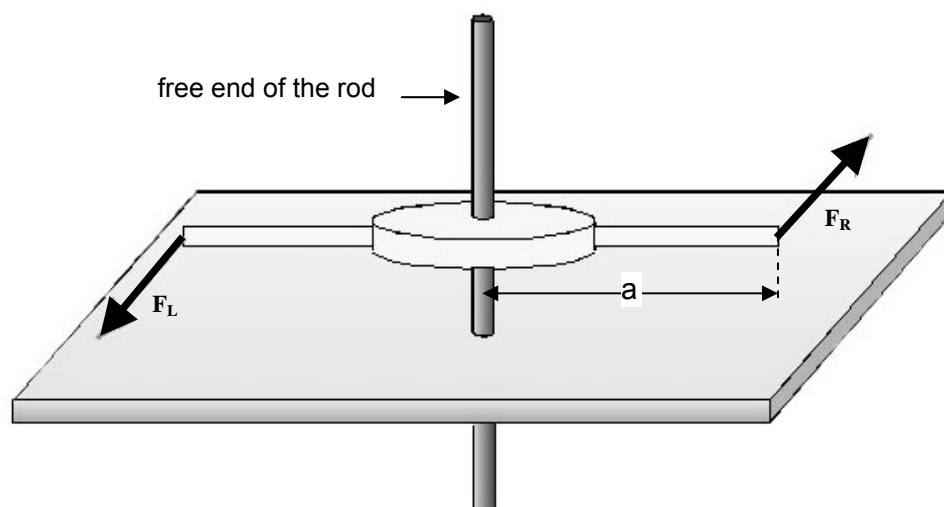


Fig. 35. Scheme of the wing on the top of alumina rod used to determine the shear modulus of the rod. F_L – force applied to the left side of the arm; F_R – force applied to the right side of the arm; a – the distance from the centre of the rod to the applied force (left arm: 100.75 mm; right arm: 100.95 mm).

Tab. 5. Table used to calculation of the torque (here: for Al_2O_3 in 600°C). Description – in the text.

Successive measurements	THE LEFT ARM		THE RIGHT ARM		TORQUE τ_φ	$\text{Al}_2\text{O}_3 - 600^\circ\text{C}$	
	Applied weight	(2) multiplied by length of the left arm	Applied weight	(4) multiplied by length of the right arm		Σ (3)+(5)	VOLTAGE
		[g]		[g · mm]	[g]		[g · mm]
	(1)	(2)	(3)	(4)	(5)	(6)	(7)
1	0	0	0	0	0	5.00E-04	4.00E-04
2	1.747	176.051	1.750	176.642	0.0035	0.0117	0.0452
3	3.512	353.784	3.508	354.173	0.0071	0.0235	0.0895
4	5.256	529.572	5.231	528.019	0.0106	0.038	0.1387
5	6.957	700.877	7.125	719.289	0.0142	0.0531	0.1899
6	8.690	875.518	8.912	899.636	0.0178	0.0647	0.2375
7	10.598	1067.738	10.598	1069.888	0.0214	0.0806	0.2886
8	12.329	1242.167	12.338	1245.561	0.0249	0.0934	0.3358
9	14.110	1421.552	14.077	1421.083	0.0284	0.1064	0.3846
10	15.823	1594.208	15.882	1603.288	0.0320	0.1225	0.4333
11	17.593	1772.515	17.589	1775.640	0.0355	0.1345	0.4848
12	19.507	1965.310	19.548	1973.320	0.0394	0.1496	0.5381

The calculations of torque are shown in the Table 5. In columns (2) and (4) the weight is summed up that each sum is larger by only one next weight. Columns (3) and (5) shows the sum of the weights multiplied suitable by left (100.75 mm) and right (100.95 mm) length of arm of the force, what gives the torque of left and right side. The sum of these partial τ_φ gives the total torque (column 6). The measurements of the voltages on channels 1 & 2 are in columns (7) and (8) respectively. The voltage from channel 1 and channel 2 as a function of torque (see Tab. 5) are shown in Fig. 36. There is a linear relationship between voltage (measured twist of the Al_2O_3 rod) and torque. The parameters f_m1 and f_m2 which are needed in the following calculations were determined from straight line fits to the data.

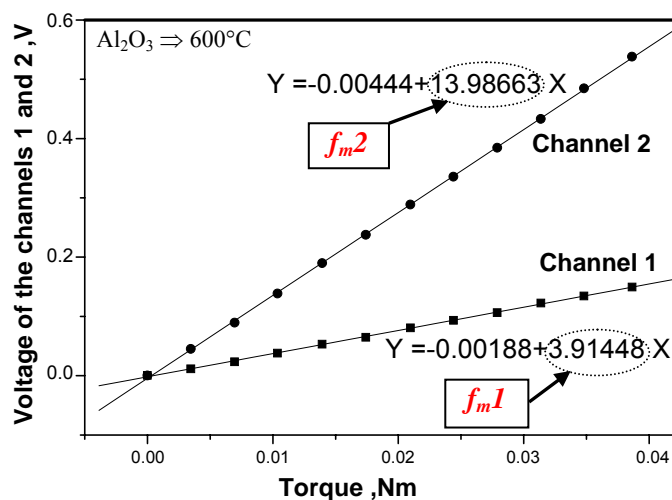


Fig. 36. Plot of the relationship between calculated torque and measured voltage – both parameters come from the weight analysis. f_m1 – factor for the channel 1; f_m2 – factor for the channel 2.

3.7.3. Stress is applied; strain is measured

A torque is applied to the rod by an electromagnetic system (“wing S” in Fig. 34; see also Fig. 37). The angle of twist of the rod is measured from the motion of 10 cm long aluminium arms attached to the rod 66.22 mm and ~480 mm above the fixed end. Fe-plates are attached to these Al arms and move between pairs of inductive transducers (see Fig. 38). The circuits connecting the pairs of inductive transducers delete sway in the rod and only measure twist of the rod. The pick-ups which were used are inductive transducers of Tr 10D type (Fig. 39). They are waterproof front and made of hardened steel. Each pick-up has one coil. The transducers are connected to the half-bridge and work under the alternating current.

Movement of the Fe-plate between the inductive plates reduces the air-gap and results in a change in voltage output of the transducer circuit. The motion of the Fe-plate was also determined manually using a micrometer. For the 2 mm and 4 mm air-gaps, respectively at channel 1 and 2, there is a linear relationship between transducer voltage and angle of twist.

The sensitivity of the inductive transducers depends on the distance between two pick-ups and on the distance between pick-ups and metal plate. When ΔL (distance between pick-ups) is too large, then dependence between ΔL and an outgoing signal is not linear.

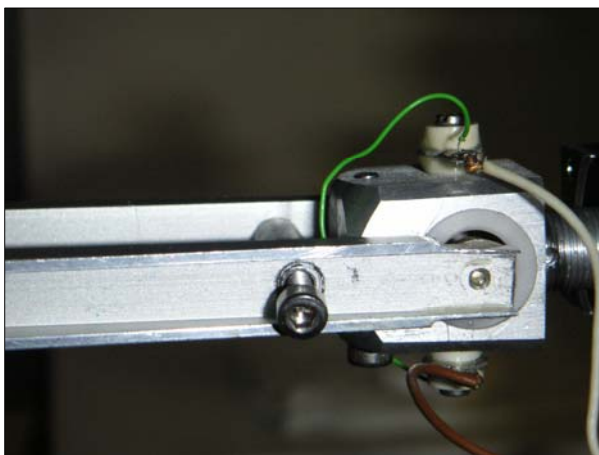


Fig. 37. Electromagnetic system of torsion machine which applied stress to the rod.

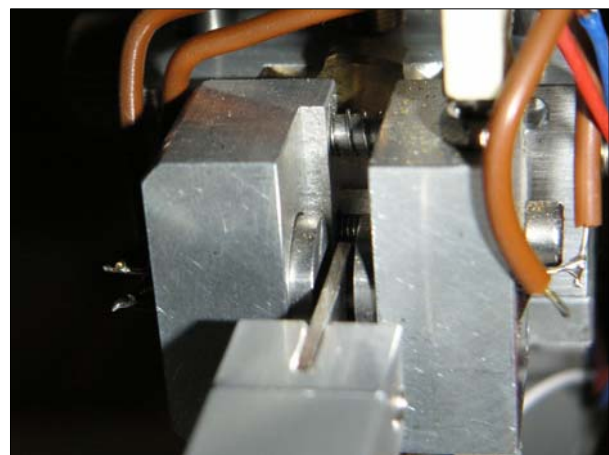


Fig. 38. Pair of inductive transducers with a iron plate between.

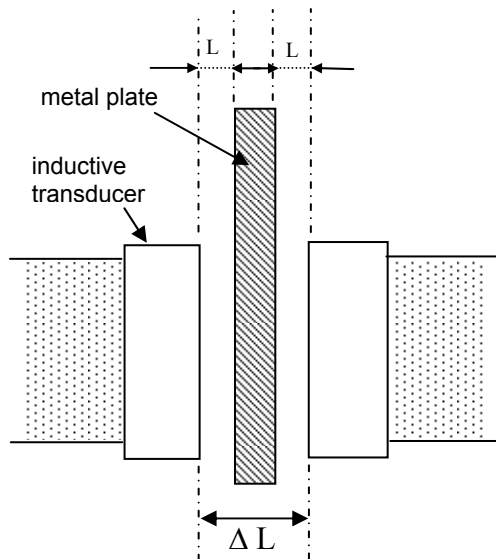


Fig. 39. Scheme of the linear voltage displacement transducer with the metal plate. L – distance between metal plate and pick-ups changes; ΔL – distance between pick-ups: different but constant for the both wings.

3.7.4. Displacement vs. voltage

In order to determine the angle of twist φ (Eq. 33), the relationship between displacement and voltage at channel 1 and channel 2 needs to be measured. As seen in Fig. 40, there is a linear relationship between displacement and the measured voltage for both channels (1&2), described by the two factors: f_{d1} (channel 1) and f_{d2} (channel 2). These are used to calculate BB'_1 (for channel 1) and BB'_2 (for channel 2) according to equation:

$$BB'_i = \frac{V_i \cdot r}{f_{di} \cdot R}, \quad (\text{Eq. 41})$$

where: V_i is voltage of the channel 1 or 2 (see Fig. 42), f_{di} – factor of the channel 1 or 2 from the displacement analysis (see Fig. 40), r – radius of the rod and R – length of the alumina wings.

The displacements BB' need to be used to calculate the angles of twist φ for both channels following equations (33) and (41).

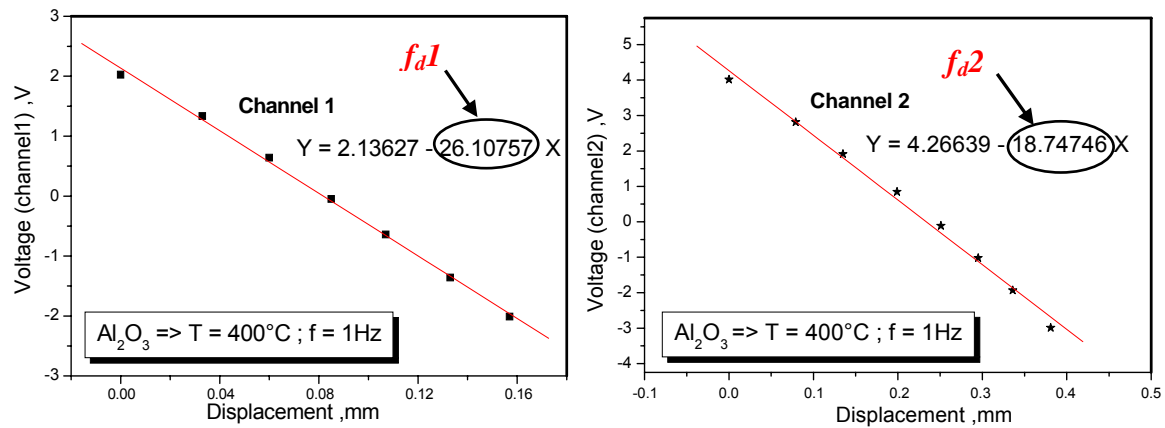


Fig. 40. Plot of the relationship between measured displacement and measured voltage – both parameters come from the displacement analysis. f_d1 – factor for the channel 1; f_d2 – factor for the channel 2.

3.7.5. Frequency dependent measurements

Once the static calibration has been performed the frequency dependence of shear modulus can be determined by applying a sinusoidal torque to the “S” wing. Magnets glued to the ends of the wing sit within loud speaker coils which are attached to the rigid frame near the ends of this wing. A sinusoidal electrical signal is sent to the electromagnetic coils. This signal attracts and repels the magnets attached to wing S which is attached to the free end of the torsion rod – thus producing a sinusoidal torque. This torque is described by:

$$y = a + b t + c \sin(\omega t + \delta), \quad (\text{Eq. 42})$$

for: a, b – drift parameters, c – amplitude of the sinusoid (in V), δ – shift of the sinusoid from starting time (in radians), t – time (in s), ω – angular frequency ($\omega = 2\pi f$).

Comparing the voltages from the channels 1 and 2 and the voltage of the spool, there were calculated the factors of the voltage marked as f_v1 and f_v2 (see Fig. 41) and used in the next calculations.

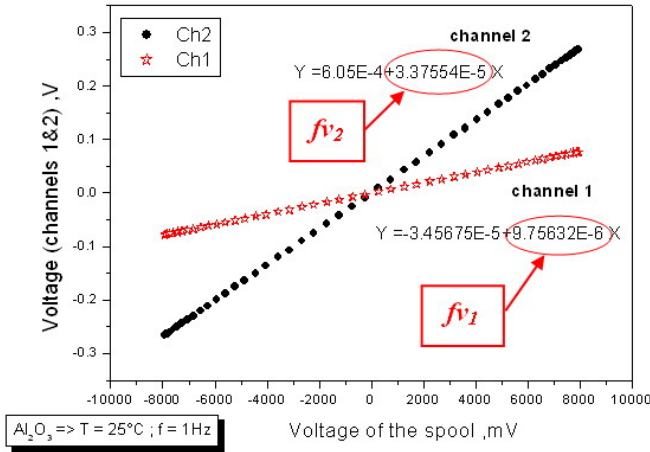


Fig. 41. Plot of the relationship of the voltages from the channels 1 and 2 and voltage of the spool. f_v1 – factor for the channel 1; f_v2 – factor for the channel 2.

The final operation of the whole investigation is to calculate the shear modulus G for the alumina rod using all parameters defined above what means that G is equal:

$$G = \frac{f_v \cdot V_s \cdot l}{f_m \cdot \varphi \cdot J}, \tag{Eq. 43}$$

where G is in GPa, l is the length of the rod from the place of fixing in the base-plate of torsion machine to the channels 1 or 2, remaining symbols were explained in text.

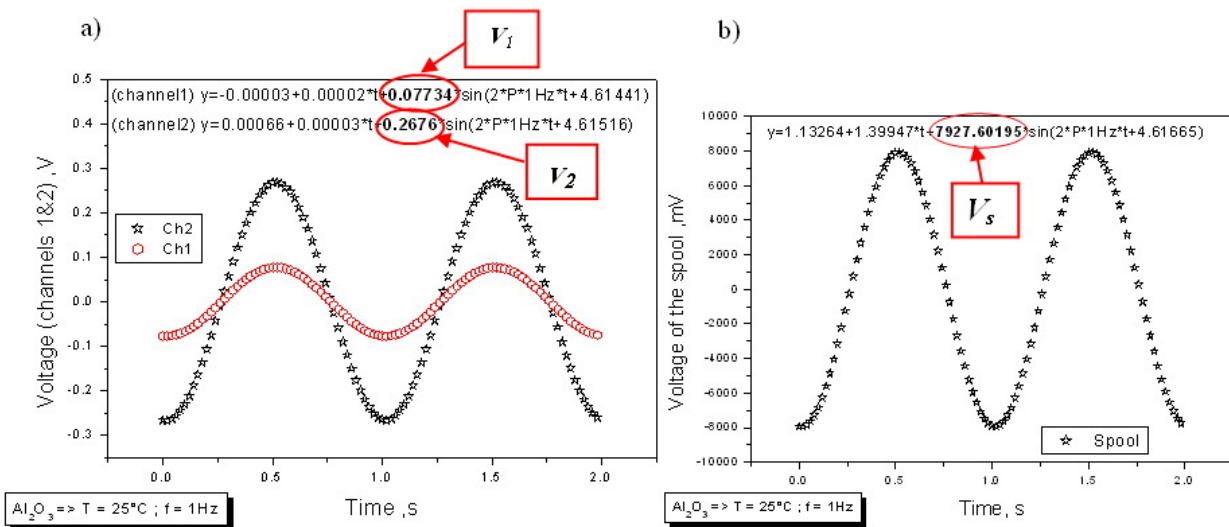


Fig. 42. Plots of the relationship: voltage vs. time. **a)** Sinusoidal signal measured from the channels 1 and 2, where V_1 and V_2 correspond with the voltage of these channels; **b)** Sinusoidal signal of the spool, where V_s corresponds with the voltage of the spool.

3.7.6. Temperature calibration

The angle of twist together and the applied torque are used to calculate shear modulus, as a function of temperature (see in Fig. 43).

The alumina wing of channel 1 (lower) measures only the deformation of rod at room temperature (22-25°C), because the rod from the base-plate to the channel 1 (66.22 mm) is not heated. The alumina wing of channel 2 (upper) measures not only the angular deformation of rod in room temperature, but also deformation this part of rod which is exposed to the high temperature inside the furnace. The deformation measurements at channel 1 are that of an Al₂O₃ rod at room temperature. There is small influence of the high temperature of furnace and therefore the shear modulus appears to be temperature dependent (Fig. 43). The alumina wing of channel 2 measures the deformation of the rod which sits in a temperature gradient from the temperature of interest in the centre of the furnace to room temperature.

3.7.7. Shear modulus of the torsion rod

At 1000°C the time delay δ is the same for both channels; showing that the alumina rod displays elastic behaviour over the entire the temperature range. The effective shear modulus of the alumina rod can then be calculated as a function of frequency from:

$$G = \frac{\text{stress calculated from angle of twist at Channel 1}}{\text{strain calculated from angle of twist at Channel 2}}. \quad (\text{Eq. 44})$$

The forced oscillation technique was tested by measuring the shear modulus of different materials:

- borosilicate glass rod with the composition given in the Table 6 and with $\rho = 2.224 \pm 0.003 \text{ g cm}^{-3}$. The shear modulus of the borosilicate glass at room temperature was found to be $26.04 \pm 1.64 \text{ GPa}$; with an ultrasonic value of $26.37 \pm 0.25 \text{ GPa}$;
- nickel with the result $77.54 \pm 0.05 \text{ GPa}$ (and literature data is 76 GPa);
- shear modulus of brass was measured as $40.05 \pm 0.17 \text{ GPa}$ (where literature data is 40 GPa);
- and also the frequency-dependent deformation of a $0.33\text{Na}_2\text{O}-0.67\text{SiO}_2$ melt (sample G0 – NS2).

Borosilicate Glass	wt%	mol%
SiO ₂	81.060	83.650
Al ₂ O ₃	2.010	1.222
Fe ₂ O ₃	0.051	0.020
B ₂ O ₃	12.730	11.338
CaO	0.016	0.018
Na ₂ O	3.010	3.011
K ₂ O	1.125	0.741

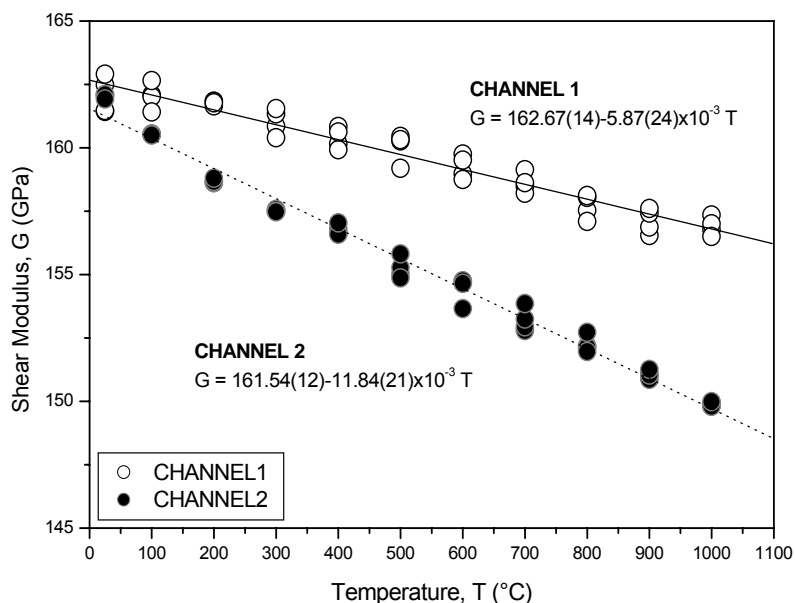
Tab. 6. Composition (in wt% and mol%) of the borosilicate glass used to test of the torsion machine determined by microprobe (JEOL JXA 8900 RL) .

The shear modulus of the Al₂O₃ rod determined at room temperature from channel 1 is 162.07±0.74 GPa and 162.04±0.08 GPa from channel 2. Straight line fits to the temperature dependent shear modulus data give apparent dG/dT values of -5.87(24) MPa K⁻¹ and -11.84(21) MPa K⁻¹ for channels 1 and 2 respectively.

The room temperature shear modulus measured here is in good agreement with the literature data for the shear modulus of polycrystalline Al₂O₃ calculated from single crystal data which is 162.5-163.2 GPa (Ahrens, 1995; see also Ohno et al., 1976). Goto et al. (1989) measured the shear modulus of single crystal Al₂O₃ from room temperature to 1000°C and found $dG/dT = -24$ MPa K⁻¹. The channel 1 shear modulus changes with furnace temperature despite it being outside the furnace. This is because the lower part of the rod heats up from 38°C to 51°C, with furnace temperature changing from 400°C to 1000°C. The shear modulus obtained at channel 2 is for a rod that is outside the furnace at the top and bottom, and sits within a temperature gradient within the furnace.

As most of the torsion measurements were conducted in the temperature range 450 - 800°C, we have chosen to use a temperature independent value of $G_{\text{Al}_2\text{O}_3} = 160$ GPa in our measurements. As the melts have a much lower shear modulus $G_{\text{melt}} \sim 30$ GPa, than the alumina rods, this assumption introduces an error ±1GPa in the calculated melt shear modulus.

	Channel 1 G Al ₂ O ₃ (GPa)	Channel 2 G Al ₂ O ₃ (GPa)
25°C	161.98	162.04
100°C	161.58	159.83
200°C	161.78	157.79
300°C	160.97	155.81
400°C	160.23	154.13
500°C	160.26	152.00
600°C	160.20	150.34
700°C	159.86	149.33
800°C	159.86	148.15
900°C	159.57	147.31
1000°C	159.38	145.83



Tab. 7. Table of measured shear modulus of the alumina rod from room temperature to 1000°C.

Figure 43. Measured shear modulus of the alumina rod from room temperature to 1000°C. The $G_{\text{Al}_2\text{O}_3}$ used in calculation of shear modulus of the melt was set to be 160 GPa.

3.7.8. Shear modulus of melts

The shear modulus of the silicate melts was determined with a set: ~30mm long, 8 mm diameter glass cylinder glued to an upper and lower Al₂O₃ torsion rod. The lower rod is ~295mm long and the upper rod is ~155±20mm long (depending on the length of the sample). Preliminary experiments found it difficult to achieve a good physical connection between the melt cylinder and the alumina torsion rod. First attempts were done with a platinum tube (the method of Bagdassarov et al., 1993). This uses a Pt-foil wrapped around the melt cylinder and alumina rods to hold everything together at high temperature. The result was only bubble filled interfaces between the rods and the melt sample (see Fig. 44). Thus we reverted to the simpler method (Webb, 1992a) of wrapping the glass cylinder and alumina rods in paper to hold the assembly together at high temperature.

It was also necessary to use a glue to bond the rods to the melt. This glue is a Si-rich Fe-bearing melt (composition of obsidian from Little Glass Butte, Oregon), which has a viscosity slightly higher than the most peraluminous melts used. After initial attempts in which the alumina rod melted into the rhyolite melt; a recipe for temperature and duration of contact between rhyolite melt and alumina rod was found; and we now successfully (85%) glue the rods to the glass sample in the first attempt.

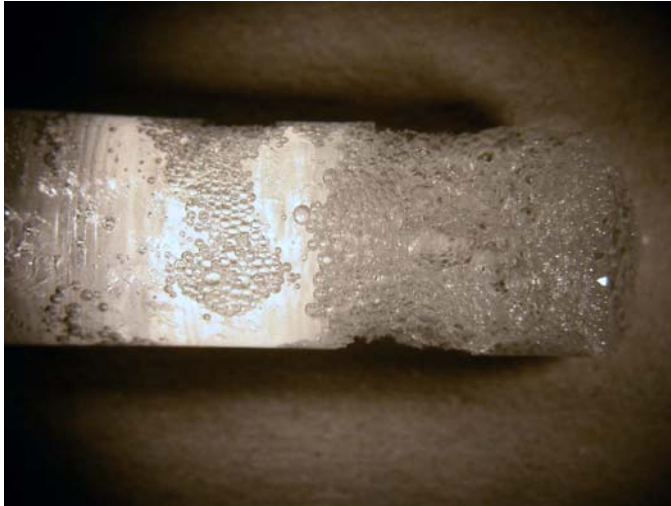


Fig. 44. Bubble filled sample produced by wrapping both glass and Al_2O_3 torsion rod in Pt-foil and going to high temperature.

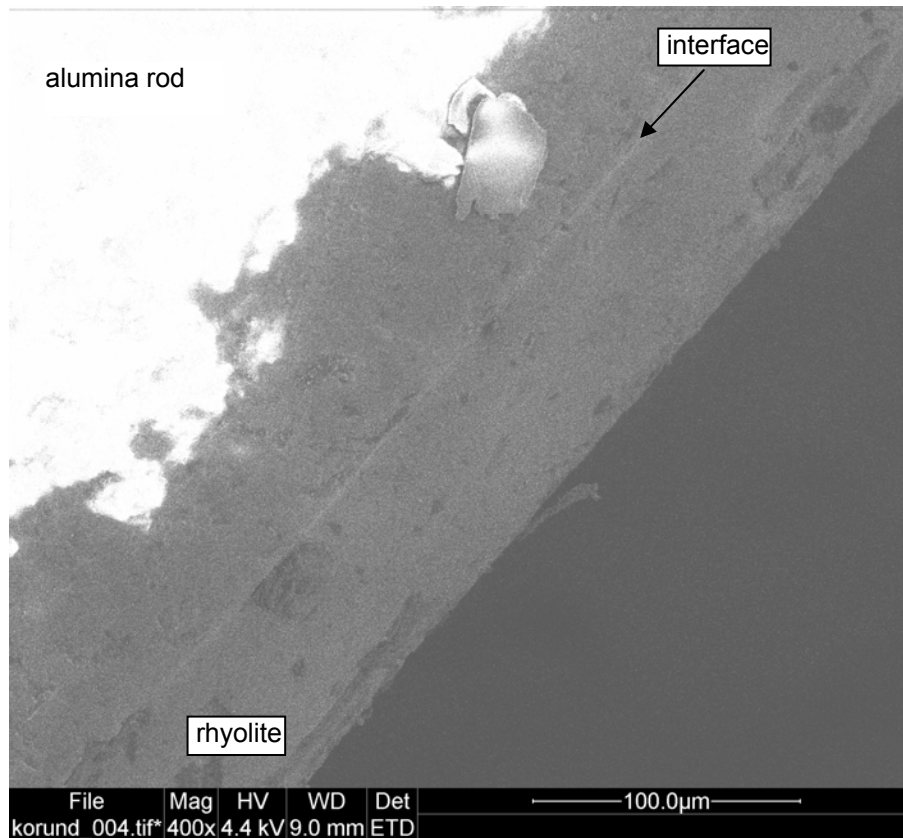


Fig. 45. Rhyolite infiltration $\sim 50 \mu\text{m}$ into the alumina torsion rod measured with Quanta 200F FE-SEM (Crystallography Department, Georg-August-University Göttingen).

A thin film of this rhyolite melt is allowed to react with the Al_2O_3 rod (Fig. 45). The sample is then melted onto the rhyolite at the ends of the two torsion rods to produce a good contact between the $\text{Na}_2\text{O}-\text{Al}_2\text{O}_3-\text{SiO}_2$ melt and the torque rod (Webb, 1991). The

presence of this thin film of highly viscous melt will introduce an error of ~ 1 GPa into the calculated shear modulus of the melt. Thus the measured shear moduli have an error of ± 1.5 GPa due to the use of a temperature independent shear modulus for the torsion rods, and the use of a glue between the sample and the torsion rods.

The temperature inside the furnace has been measured with a type S thermocouple, and it was found to be constant $\pm 3^\circ\text{C}$ across the 40 mm where the melt sample stands (Fig. 46). Therefore, only 10 mm of the alumina rod is at temperature of the measurement, ~ 66 mm are at \sim room temperature (lower part) and the remaining length is in a thermal gradient from room temperature to the temperature of interest. The upper part of the rod is partially at high temperature (up to the upper channel) and then is in a thermal gradient to the room temperature.

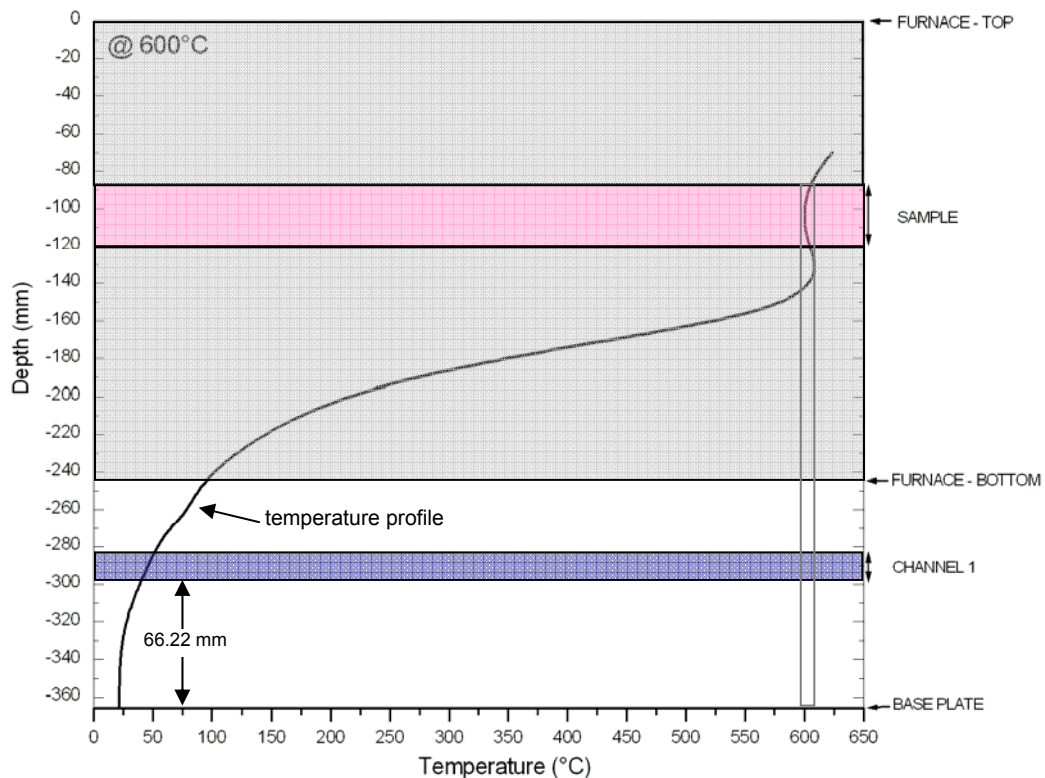


Fig. 46. Temperature profile in the torsion machine. Location of the furnace, sample and the channel 1 and base plate has been marked.

The deformation analysis for the compound torsion rod ($\text{Al}_2\text{O}_3 + \text{melt} + \text{Al}_2\text{O}_3$) as a function of frequency is made in the same manner as for the simple alumina rod but the calculation is slightly different. For the measurement of the frequency dependent deformation of the melt, the torque is created by the application of a sinusoidal signal to a pair of loudspeaker coils. The angle of twist at channel 2, together with the time lag between applied stress σ and resulting strain ε are due to the elastic deformation of the

two alumina rods plus the viscoelastic deformation of the melt. Voltage signals coming from the wing “S” and both channels were also calculated the same way as in previous case. As a result one obtains a sinusoidal angle of twist for channels as a function of time for given frequency (see Fig. 47).

Based upon the earlier calibrations, the voltage from the transducers at channel 1 gives the applied stress, and the voltage at channel 2 gives the deformation of the compound torsion rod. The time delay – $\Delta\delta$ between the applied stress and the resulting strain is also calculated;

$$\Delta\delta = |\delta_1 - \delta_2|. \quad (\text{Eq. 45})$$

With known voltages of the channels V_1 and V_2 as well as time delay $\Delta\delta$ it is possible to calculate the angle of twist φ for both channels:

$$\varphi_1 = \frac{V_1}{f_{d1} (R+r)} \quad \text{and} \quad \varphi_2 = \frac{V_2}{f_{d2} (R+r)}, \quad (\text{Eq. 46 a-b})$$

where R is the length of the wings (in mm) and r – radius of the rod (in mm).

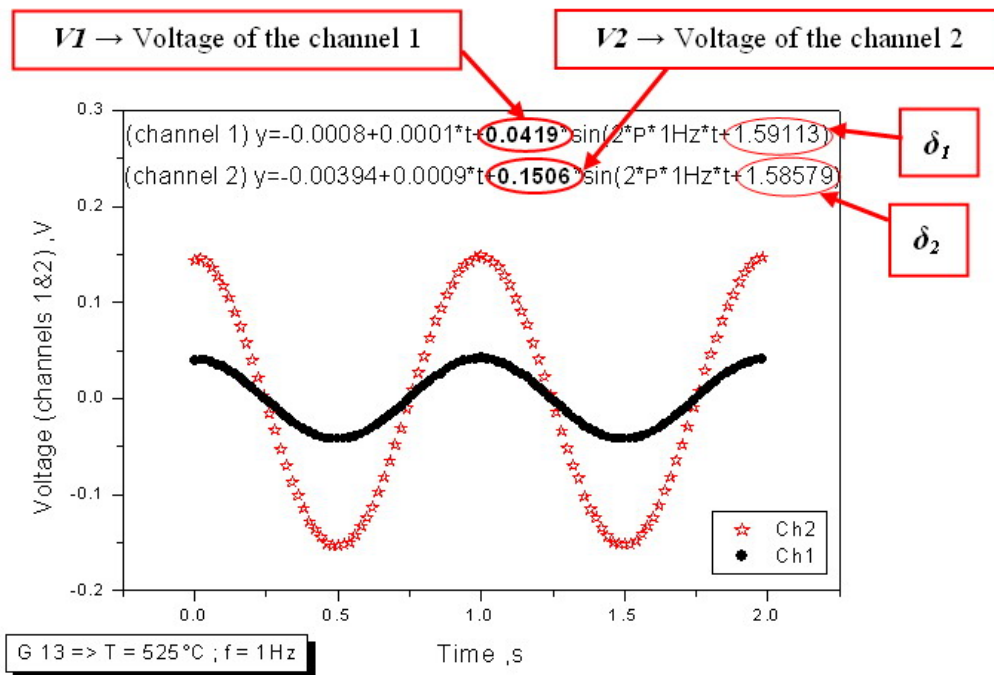


Fig. 47. Plot of the relationship voltage vs. time showed as a sinusoidal signal (measured from the channels 1 and 2), where V_1 and V_2 correspond with the voltage of these channels; δ_1 and δ_2 describe the shift of the sinusoids.

Here it was unnecessary to do a weight analysis because the torque τ is calculated using the angle of twist of the channel 1 φ_1 :

$$\tau_{from \varphi_1} = \frac{\varphi_1 G_{Al_2O_3} \pi r^4}{2 l_{rod1}}, \quad (\text{Eq. 47})$$

where $G_{Al_2O_3}$ is the shear modulus of the alumina rod (160 GPa), r – radius of the rod (in mm) and l_{rod1} – length of the rod from the base-plate to the first channel (in mm).

The angle of twist φ_2 of the compound rod must be separated into the components due to the twist of the lower alumina rod – φ_{rod1} , the melt – φ_{melt} and the upper alumina rod – φ_{rod2} . This is shown graphically in Figure 48. Here, the measured parameters are δ – the delay between the applied stress and the resulting strain of the compound rod; and φ_2 – the deformation measured at channel 2. This must now be separated into the contribution from the elastic twist of rod 1 and rod 2:

$$\varphi_{rod1} = \frac{\tau 2 l_{rod1}}{G_{Al_2O_3} \pi r^4} \quad \text{and} \quad \varphi_{rod2} = \frac{\tau 2 l_{rod2 (ch2)}}{G_{Al_2O_3} \pi r^4} \quad (\text{Eq. 48 a-b})$$

for $l_{rod2 (ch2)}$ – length of the upper Al_2O_3 rod from the melt to the channel 2 (in mm), where τ is calculated from Eq. 47. The complex shear modulus of the melt is:

$$G^*(\omega)_{melt} = \frac{\tau 2 l_{melt}}{\pi r^4 \varphi_{melt}} \quad (\text{Eq. 49})$$

for l_{melt} – the length of the melt (in mm), where φ_{melt} is:

$$\varphi_{melt} = \sqrt{\left[(\varphi_2 \sin \delta)^2 + (\varphi_2 \cos \delta - \varphi_{rod1})^2 \right]} - \varphi_{rod2} \quad (\text{Eq. 50})$$

The complex shear modulus can be separated into the real and imaginary components by:

$$G(\omega)_{im} = G(\omega)_{melt} \sin \gamma = G''(\omega) \quad (\text{Eq. 51})$$

$$G(\omega)_{real} = G(\omega)_{melt} \cos \gamma = G'(\omega), \quad (\text{Eq. 52})$$

where

$$\gamma = \tan \gamma = \frac{\varphi_2 \sin \delta}{\varphi_2 \cos \delta - \varphi_{rod1}}. \quad (\text{Eq. 53})$$

Finally, the shear modulus of the melt can be described by:

$$G(\omega)_{melt} = \sqrt{G''(\omega)^2 + G'(\omega)^2}. \quad (\text{Eq. 54})$$

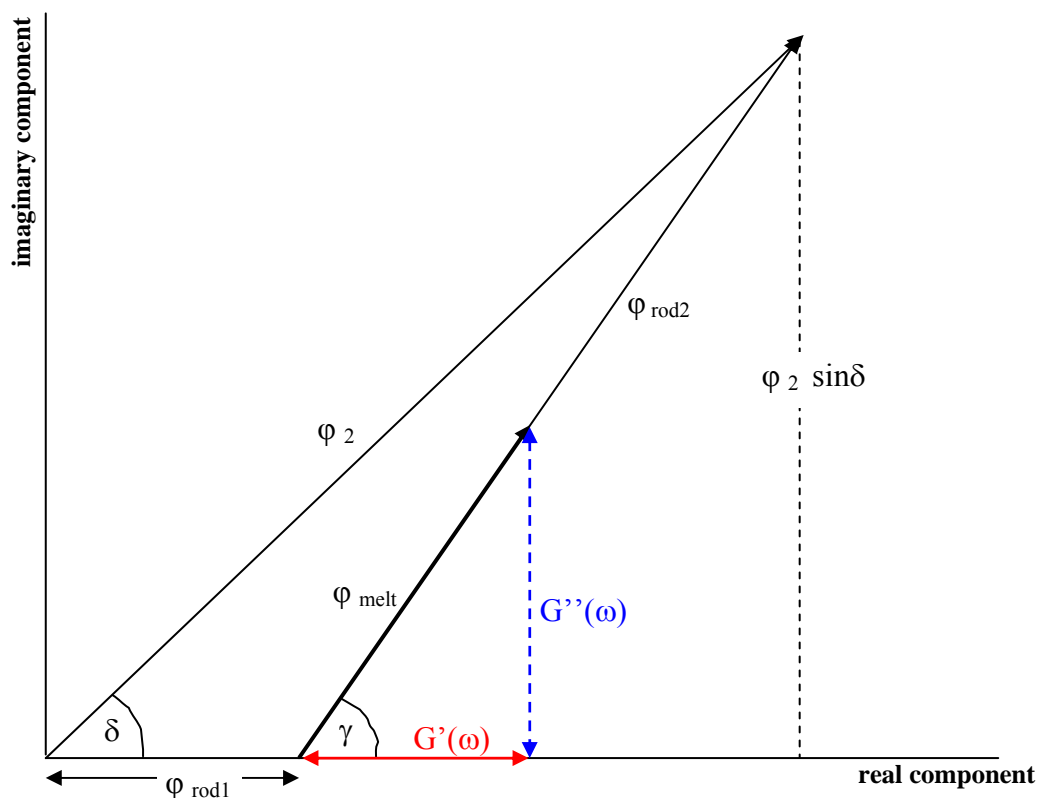


Fig. 48. Plot of trigonometrical relationships for the deformation of the compound torsion rod.

3.7.9. Shear modulus as a function of frequency

This viscoelastic deformation is presented as the real and imaginary components of the shear modulus as a function of frequency. A maximum in imaginary part of the shear modulus (energy loss) appears at the frequency at which part of the melt structure moves. This maximum is accompanied by an increase in the real (storage) part of the modulus. One expects 3 peaks to occur in sodium aluminosilicate melts (Fig. 49). Based on a simplistic model of the rates of motion of the different atoms in the melt there should be the slowest motion of Si-O (with the longest bond lifetime); the fast motion of Na⁺ atoms (based upon diffusion data Na-O bonds are assumed to have the shortest lifetime) and at frequencies between these two there should be a peak for the lifetime of Al-O bonds.

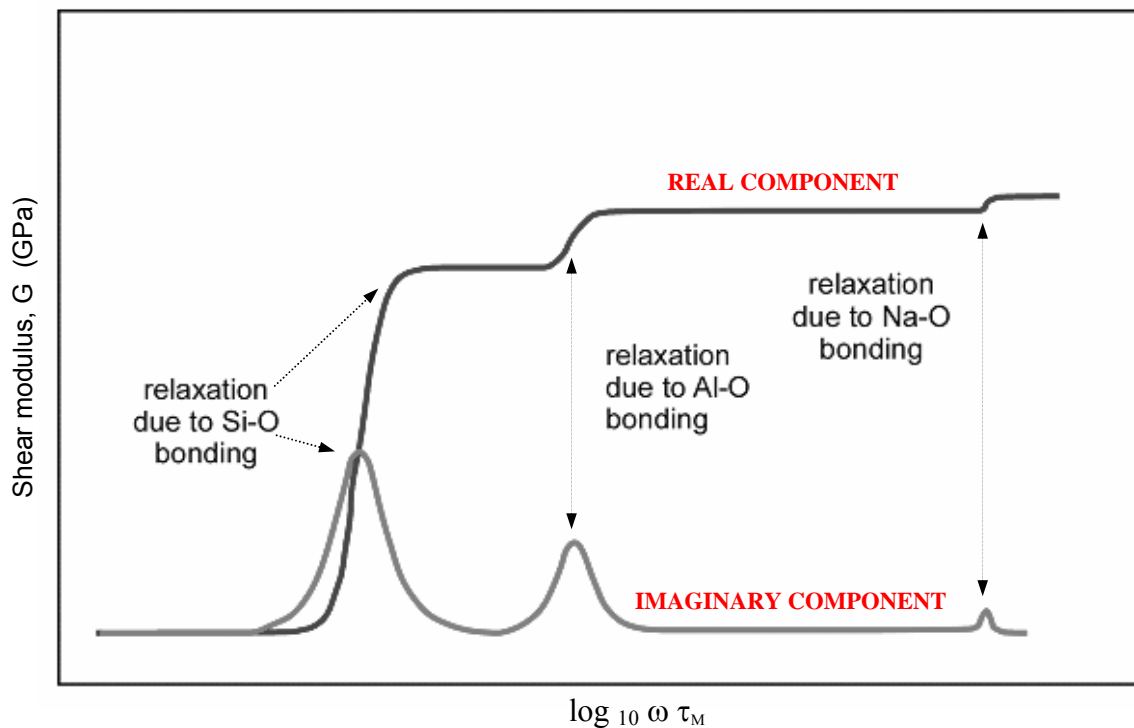


Fig. 49. The known change in modulus with $\log_{10} \omega \tau_M$ for the motion of Si and O atoms in silicate melts together with theoretically expected loss modulus associated with the motion of Al³⁺ and Na⁺ atoms in the present melts.

4. RESULTS

4.1. Composition

The compositions of investigated samples were determined by microprobe and are presented in the Table 8. Fe^{2+} was measured with the $KMnO_4$ titration method (Heinrichs & Herrmann, 1998; Herrmann, 1975). Fe_2O_{3total} was determined by spectral photometry and did not differ from microprobe data.

Tab. 8. Measured glass compositions in wt%. The compositions were determined by microprobe (JEOL JXA 8900 RL): 15 kV voltage, 10 μm beam diameter, 12 nA current. Data are the average of 10 analyses of each glass. Errors are 1σ values. Anorthite, albite and hematite were used as standards.

melt number	wt %			
	SiO ₂	Na ₂ O	Al ₂ O ₃	Fe ₂ O ₃ total
G0	65.9±0.3	34.1±0.2	-	-
G1	58.1±0.2	12.9±0.2	29.8±0.2	-
G2	61.2±0.2	12.8±0.2	26.0±0.2	-
G3	59.4±0.2	14.2±0.1	26.6±0.2	-
G4	58.2±0.3	14.9±0.2	26.5±0.1	-
G5	60.1±0.2	15.5±0.4	24.1±0.2	-
G6	59.1±0.5	16.6±0.3	24.1±0.2	-
G7	59.4±0.5	18.5±0.1	21.8±0.2	-
G8	56.3±0.3	12.2±0.1	28.5±0.1	2.54±0.05
G9	56.9±0.8	12.9±0.2	23.5±0.5	7.12±0.24
G10	59.1±0.5	13.0±0.2	20.8±0.3	6.86±0.16
G11	58.7±1.5	14.0±0.4	20.0±1.0	7.08±0.32
G12	59.2±1.2	15.1±0.2	18.2±0.8	7.49±0.33
G13	59.1±0.5	16.0±0.2	17.7±0.3	7.20±0.12
G14	60.5±0.3	17.5±0.1	14.7±0.1	6.98±0.10

Tab. 9. Calculated glass compositions in mol%. The compositions of SiO₂, Na₂O and Al₂O₃ were determined by microprobe (Tab. 8); FeO was measured with a titration method, Fe₂O₃ was measured by microprobe and confirmed by spectral photometry (data are the average of 10 analyses of each glass). Errors are 1σ values. Anorthite, albite and hematite were used as standards. NBO/T value was determined follow the Eq. 7; and γ from the Eqs. 9&10. $\Sigma atoms/mol$ presents the number of atoms (times Avogadro's Number) in one mol of melt. Fe^{2+}/Fe_{total} is an atomic ratio between Fe^{2+} and the total amount of iron in the sample.

melt number	mol %					NBO/T	γ	$\frac{\Sigma atoms}{mol}$	$\frac{Fe^{2+}}{Fe_{total}}$
	SiO ₂	Na ₂ O	Al ₂ O ₃	FeO	Fe ₂ O ₃				
G0	66.6±0.3	33.4±0.3	-	-	-	0.502	1.00	3.000	-
G1	65.9±0.2	14.2±0.1	19.9±0.1	-	-	-0.108	0.42	3.398	-
G2	68.8±0.2	14.0±0.2	17.2±0.1	-	-	-0.062	0.45	3.344	-
G3	66.9±0.2	15.5±0.1	17.7±0.1	-	-	-0.043	0.47	3.357	-
G4	65.9±0.2	16.4±0.2	17.7±0.1	-	-	-0.026	0.48	3.354	-
G5	67.3±0.3	16.8±0.4	15.9±0.2	-	-	0.018	0.51	3.318	-
G6	66.1±0.3	18.0±0.3	15.9±0.2	-	-	0.043	0.53	3.318	-
G7	65.8±0.3	20.0±0.2	14.2±0.1	-	-	0.123	0.58	3.284	-
G8	65.5±0.1	13.8±0.1	19.6±0.1	0.188±0.015	0.96±0.02	-0.105	0.41	3.411	0.098
G9	66.0±0.8	14.6±0.3	16.2±0.4	0.845±0.011	2.99±0.12	-0.014	0.46	3.394	0.141
G10	68.3±0.5	14.6±0.2	14.1±0.2	0.458±0.025	2.97±0.08	-0.039	0.47	3.350	0.077
G11	67.7±1.3	15.7±0.5	13.6±0.8	0.256±0.016	3.00±0.15	-0.013	0.49	3.337	0.043
G12	67.8±1.0	16.8±0.3	12.3±0.6	0.137±0.012	2.93±0.16	0.035	0.53	3.302	0.023
G13	67.4±0.4	17.6±0.2	11.9±0.2	0.331±0.008	2.98±0.05	0.063	0.55	3.301	0.056
G14	68.2±0.1	19.1±0.1	9.75±0.1	0.111±0.007	2.92±0.04	0.140	0.60	3.255	0.019

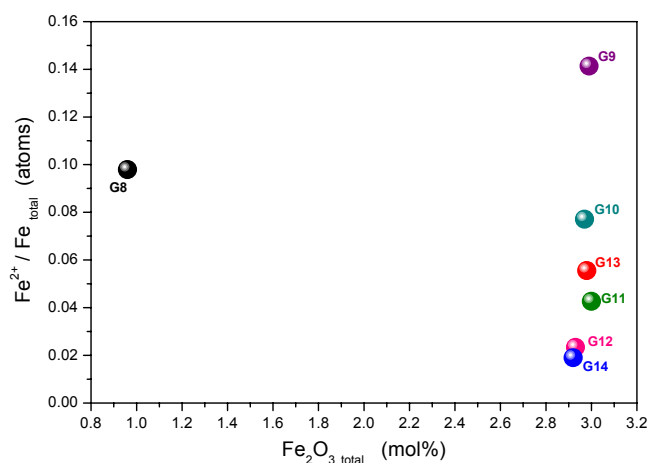


Fig. 50. Plot of the atomic ratio between the number of Fe^{2+} and Fe_{total} as a function of $Fe_2O_3_{total}$ (in mol%).

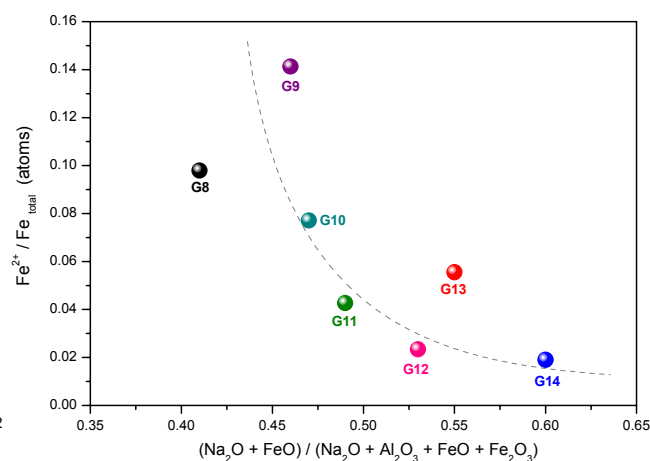


Fig. 51. Plot of the atomic ratio between the number of Fe^{2+} and Fe_{total} as a function of the composition. The trend-line is a guide to the eye.

Peraluminous sample G8 has only 1 mol% of Fe_2O_3 , otherwise it will crystallize. From the reason of composition and Fe_2O_3 content, properties of these melts differ sometimes from the others and the points can lie out of the drawn trends (especially G8).

Figure 50 shows the atomic ratio between the number of Fe^{2+} and total amount of atomic Fe as a function of $Fe_2O_3_{total}$ (in mol%). Peralkaline Fe-bearing samples have lower Fe^{2+}/Fe_{total} (atoms) ratio than peraluminous melts. Fe^{2+}/Fe_{total} (atoms) ratio does not depend on the $Fe_2O_3_{total}$ (Fig. 50), but there is a relationship between this ratio and composition of the melt (Fig. 51). Webb (2005b) suggested that this behaviour is connected with the difference in charge balancing between peraluminous and peralkaline melts. In peraluminous melts, when there is not enough Na^+ to compensate negative charge of Al^{3+} - and Fe^{3+} -tetrahedra, the role of charge balancer is played by Fe^{2+} .

The very characteristic breaking point in all of the physical properties trends indicates minimal number of non-bridging oxygens occurring in the melt and that is in the moment, when peralkaline melt changes into peraluminous (see Table 9). This is shown in Figure 52 (glass transition temperature at $\log_{10}\eta=12$ as a function of NBO/T). As there is dependence between structure, composition and physical and thermodynamic properties of the melts, this behaviour will appear also in the visualisation of other data.

The maximum in T_g^{12} occurs slightly on the peraluminous side of the melt composition; and not exactly at NBO/T=0. In the investigated melts there is no sample which has NBO/T equals zero. The localization of the breaking point has been marked out between samples G3 and G4 in Fe-free melts and between samples G9 and G10 in Fe-bearing melts.

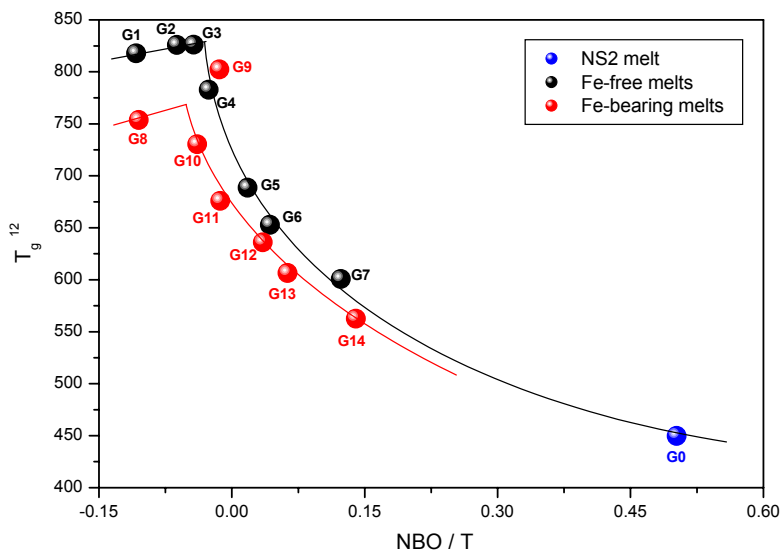


Fig. 52. Glass transition temperature at $\log_{10}\eta=12$ as a function of the parameter NBO/T .

Between NBO/T values and γ for both the Fe-free and Fe-bearing melts there is a linear relationship described by an equation $NBO/T = -0.65 + 1.31 \gamma$ with $R^2 = 0.976$ (Fig. 53). Sodium silicate sample G0 is not described by this correlation. To connect samples G1-G7 and G8-G14 with NS2 melt a curve needs to be drawn (Fig. 53).

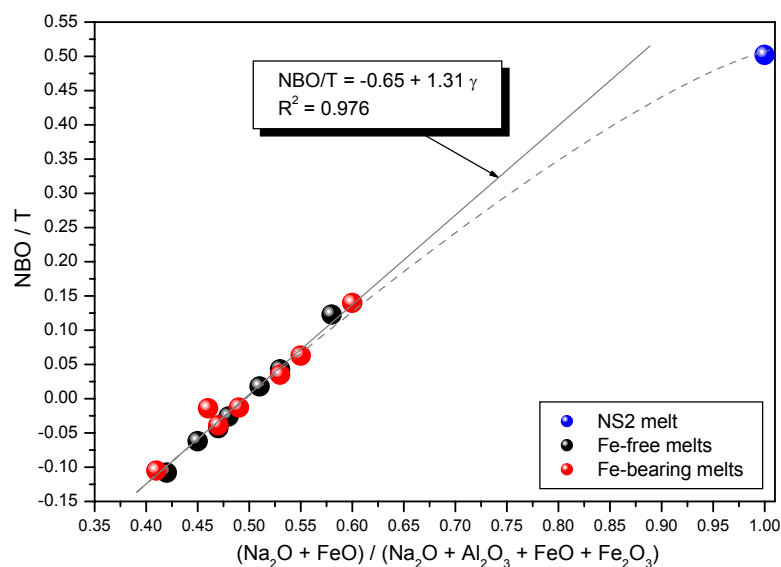


Fig. 53. Parameter NBO/T for all of the samples as a function of their composition. The linear relationship between Fe-free (G1-G7) and Fe-bearing samples (G8-G14) is indicated by a solid grey straight line. Dashed grey curve connects Fe-free and Fe-bearing melts with NS2 melt.

The oxidation state of Fe in melts G8-G14 is controlled by: (1) composition of the melt, (2) temperature and (3) oxygen fugacity (Jeoung et al., 2001; Berry et al., 2003) (the samples were made in air and measured in air-nitrogen atmosphere).

Neither microscopic observation nor microprobe analyses indicated the presence of crystals in Fe-free and Fe-bearing melts. The only one problem was with samples G8 and G9. During viscosity measurements the surface oxidized very fast, what required a polishing the surface before every new measurement.

4.2. Density

The densities of the glasses (see Table 10) as a function of composition together with their standard deviations from 10 measurements are shown in Figure 54. Density decreases as network-modifying Na^+ is removed from the peralkaline glass; and begins to increase as charge-balancing Na^+ is removed from the peraluminous glass. The same situation occurs in Fe-free as well in the Fe-bearing glasses. Fe-bearing glasses are denser and the trend-line is steeper. The characteristic minimum on the density plot is marked by samples G4 for Fe-free glasses and G11 for Fe-bearing glasses.

Figure 55 shows density data of the glasses from the system $\text{Na}_2\text{O}-\text{Al}_2\text{O}_3-\text{SiO}_2$ containing 67 mol% SiO_2 and 75 mol% SiO_2 . The presented data of Hunold & Brückner (1980), Webb et al. (2007) and Fe-free samples from this study (G1-G7) create trends of the same shape. The dashed line drawn through the present data is simply a guide for the eye. A minimum in density is observed in all of these studies at $\gamma \sim 0.5$.

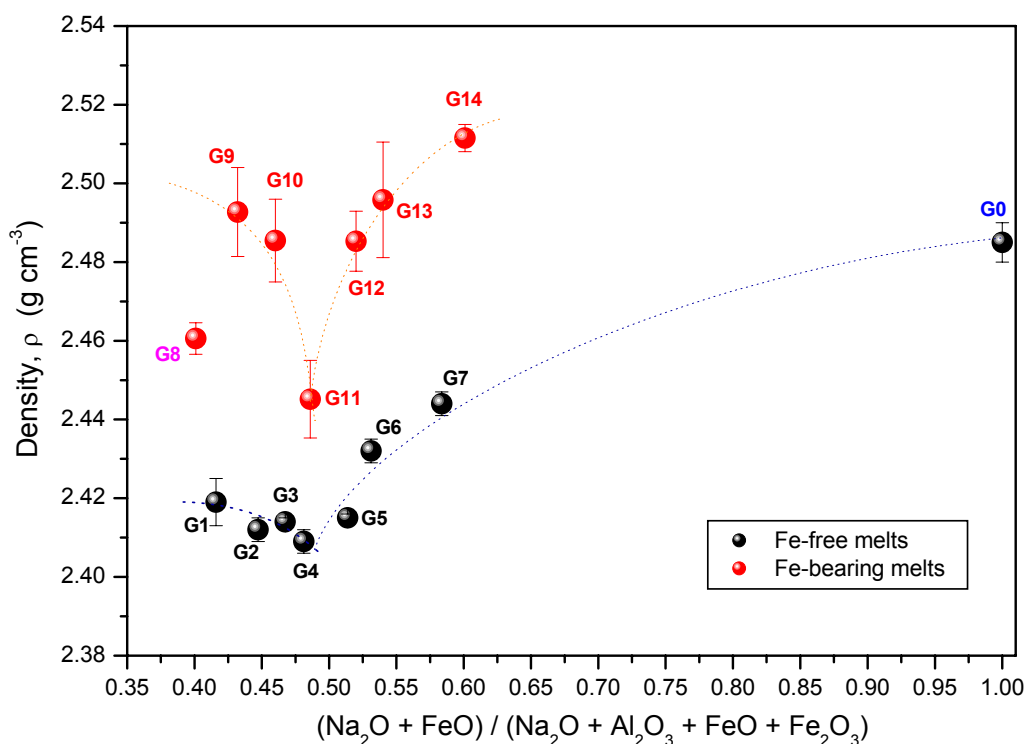
The data of Day & Rindone (1962) show a similar minimum for 75 mol% SiO_2 glasses. The $\pm 0.01 \text{ g cm}^{-3}$ difference between the densities of the 67 mol% SiO_2 glasses may be due to small differences in SiO_2 content; or to differences in cooling rate. The present glasses were cooled down in three stages process:

- between 1650-700°C at $10^\circ\text{C min}^{-1}$;
- between 700-550°C at 1°C min^{-1} ;
- between 550-25°C at $10^\circ\text{C min}^{-1}$;

while those of Webb et al. (2007) were cooled at 5 and $10^\circ\text{C min}^{-1}$. Thus the glasses do not have the same fictive temperatures, but a change in density vs. composition trend is seen as the melt changes from peralkaline to peraluminous, and there is no longer enough Na^+ to charge-balance all of the Al^{3+} in tetrahedral coordination.

Tab. 10. Densities, molar mass and molar volume of the glasses G0-G14 at room temperature. The standard deviations are calculated from 10 measurements.

melt number	density @25°C g cm ⁻³	molar mass g mol ⁻¹	molar volume cm ³ mol ⁻¹
G0	2.485±0.005	60.650±0.078	24.407±0.051
G1	2.419±0.006	68.658±0.076	28.383±0.051
G2	2.412±0.003	67.524±0.129	27.995±0.083
G3	2.414±0.001	67.819±0.075	28.094±0.048
G4	2.409±0.003	67.774±0.113	28.134±0.073
G5	2.415±0.001	67.027±0.223	27.755±0.144
G6	2.432±0.003	67.048±0.175	27.569±0.112
G7	2.444±0.003	66.370±0.106	27.156±0.068
G8	2.460±0.004	69.638±0.077	28.301±0.050
G9	2.493±0.011	70.701±0.410	28.363±0.261
G10	2.485±0.010	69.193±0.284	27.839±0.181
G11	2.445±0.010	69.146±0.707	28.278±0.453
G12	2.485±0.008	68.755±0.608	27.665±0.386
G13	2.496±0.015	68.438±0.220	27.421±0.143
G14	2.512±0.003	67.496±0.146	26.874±0.092

**Fig. 54.** Measured densities of the glasses as a function of their compositions. Sample G8 has less Fe³⁺ than other Fe-bearing samples.

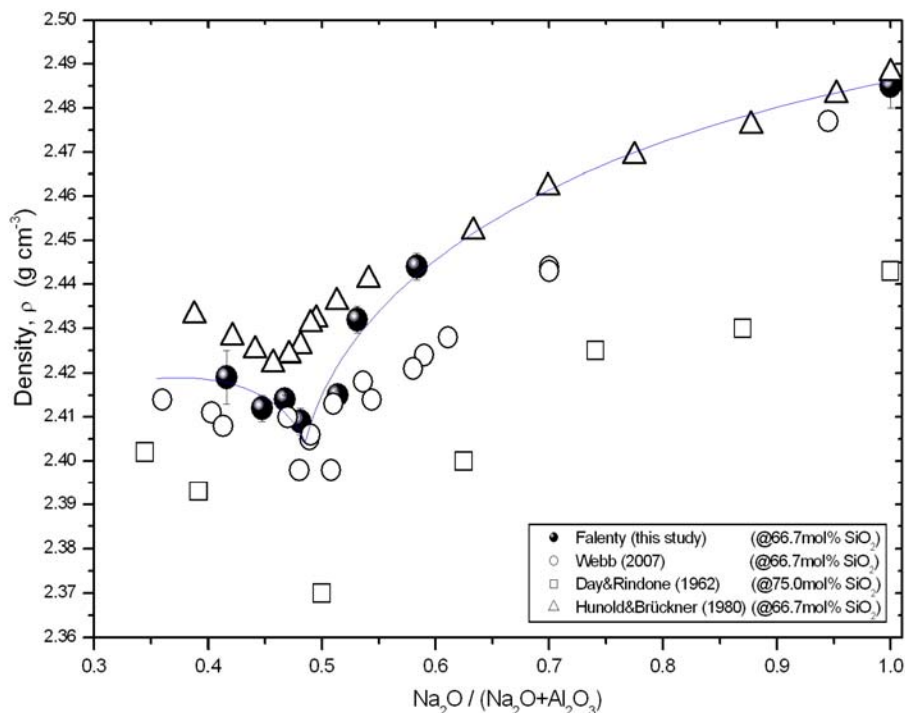


Fig. 55. Measured densities of the Fe-free sodium aluminosilicate glasses as a function of their compositions. Four sets of data have been used: black points – Falenty (samples G1-G7 – from this study); open circles – Webb (2007); open squares – Day & Rindone (1962); open triangles – Hunold & Brückner (1980). The trend-line is a guide to the eye.

Figure 56 shows molar volume of the NS2 glass (blue point), Fe-free (black points) and Fe-bearing (red points) glasses as a function of composition. Here the effect of changing structure is not as clear as in the density plot. Data show that the structural units take up different volumes of space in peraluminous and peralkaline melts; the trend-line is similar to that in Figure 52.

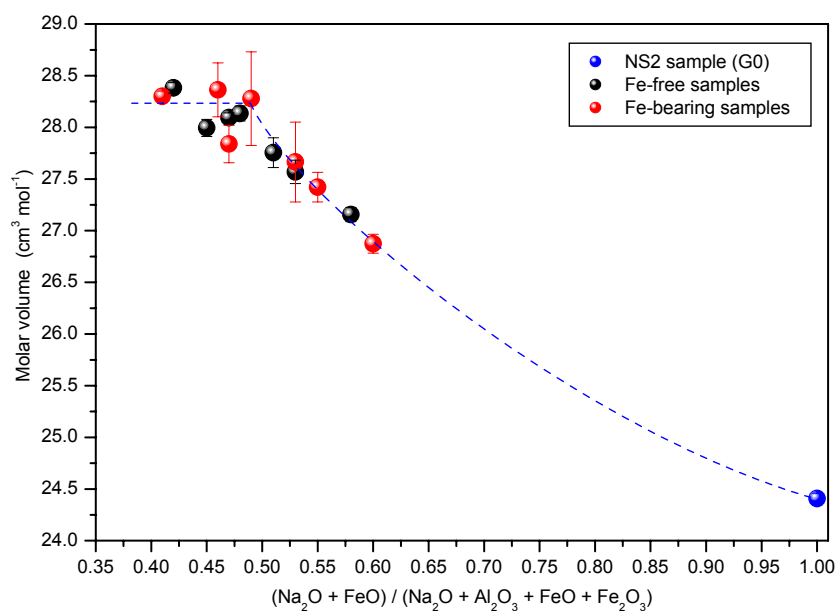


Fig. 56. Molar volume of the glasses as a function of composition.

4.3 Ultrasonic measurements

Shear modulus G and sound speed V_s determined from the pulse echo overlap technique are presented in the Table 11. The shear moduli measured by ultrasonic methods at room temperature are ~ 3.5 GPa higher for Fe-free samples (Fig. 57a) and ~ 1.8 GPa higher for Fe-bearing samples (Fig. 57b) than the moduli determined by torsion methods. As there is, in general, a 500°C temperature difference between the ultrasonic and torsion data, an average temperature dependence of the shear modulus of ~ -6.9 MPa K^{-1} for Fe-free and ~ -3.5 MPa K^{-1} for Fe-bearing glasses is calculated. The temperature dependence of the shear modulus of $\text{Na}_2\text{O}-\text{Al}_2\text{O}_3-\text{SiO}_2$ glasses in the compilation by Ahrens (1995) is between -3 and -10 MPa K^{-1} .

Tab. 11. Shear modulus G and sound speed V_s determined from the pulse echo overlap technique for all of the samples investigated in this study.

melt number	Sound speed, v_s m s^{-1}	Shear modulus, G GPa
G0	3471.60 ± 20.51	29.89 ± 0.23
G1	3918.85 ± 75.84	37.39 ± 0.75
G2	3491.90 ± 160.14	37.84 ± 1.09
G3	3953.50 ± 26.28	38.04 ± 0.15
G4	3973.37 ± 53.20	38.07 ± 0.62
G5	3919.16 ± 19.18	37.12 ± 0.16
G6	3981.36 ± 21.17	36.65 ± 0.19
G7	3754.51 ± 22.73	34.28 ± 0.20
G8	3738.78 ± 20.50	34.23 ± 0.29
G9	3682.87 ± 31.03	34.09 ± 0.13
G10	3631.93 ± 83.16	33.56 ± 0.51
G11	3714.70 ± 35.61	33.54 ± 0.36
G12	3582.22 ± 31.54	32.23 ± 0.27
G13	3524.93 ± 24.36	31.26 ± 0.25
G14	3500.48 ± 29.70	30.94 ± 0.19

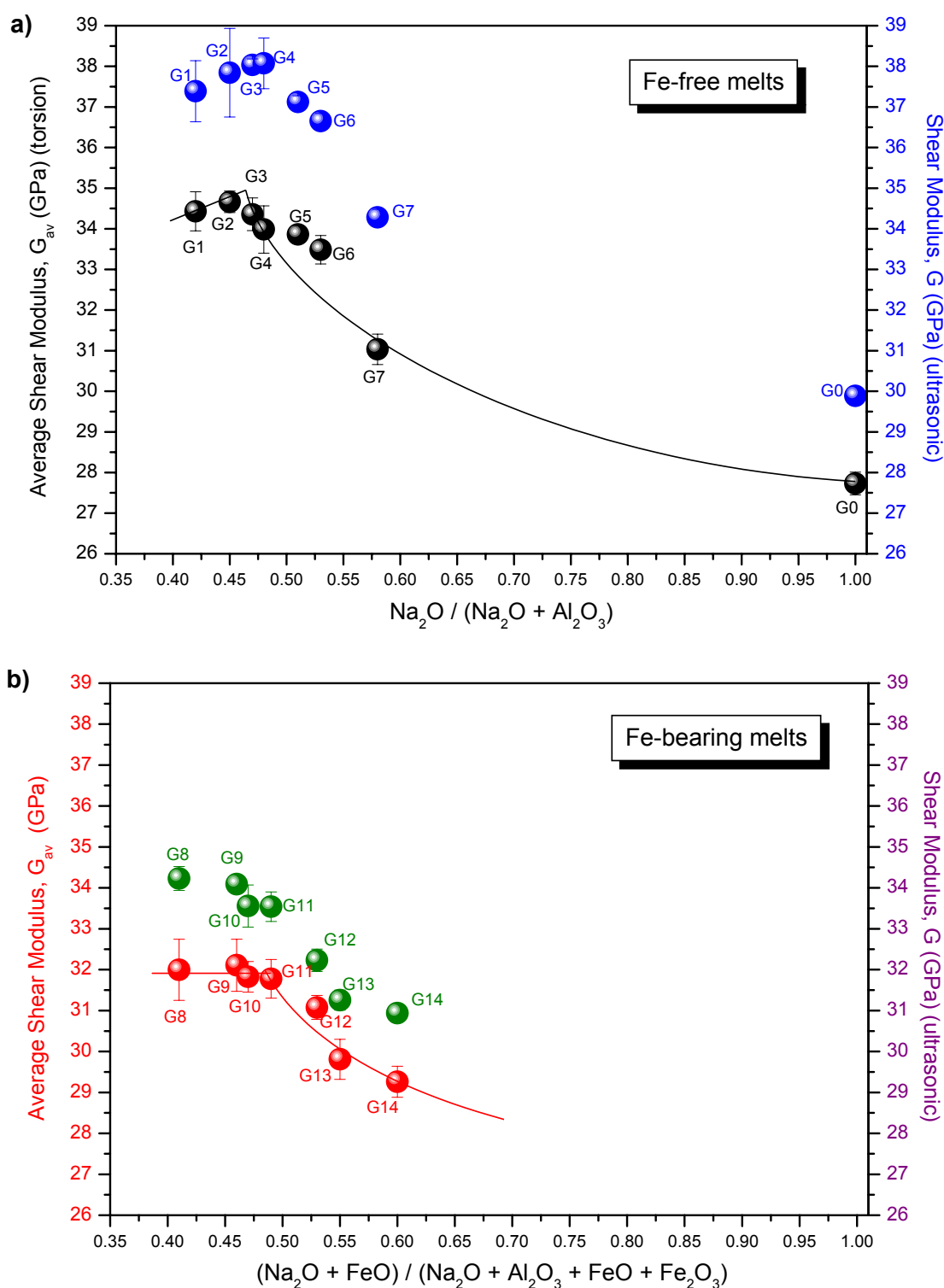


Fig. 57a, b. Shear modulus G determined by pulse echo overlap technique (right axis) and average shear modulus G_{av} from torsion apparatus (left axis) as a function of compositional parameter $\gamma = (\text{Na}_2\text{O} + \text{FeO}) / (\text{Na}_2\text{O} + \text{Al}_2\text{O}_3 + \text{FeO} + \text{Fe}_2\text{O}_3)$. **a)** for NS2 (G0) and Fe-free samples (G1-G7); **b)** for Fe-bearing samples (G8-G14). The trend-lines are a guides to the eye.

Figure 58 presents data of sound speed in the samples; determined by the ultrasonic method. Sound speed V_s depends on the composition of the samples and is slower in Fe-bearing;

$$V_s = \sqrt{\frac{G}{\rho}}, \quad (\text{Eq. 55})$$

where G is shear modulus of the sample and ρ is density.

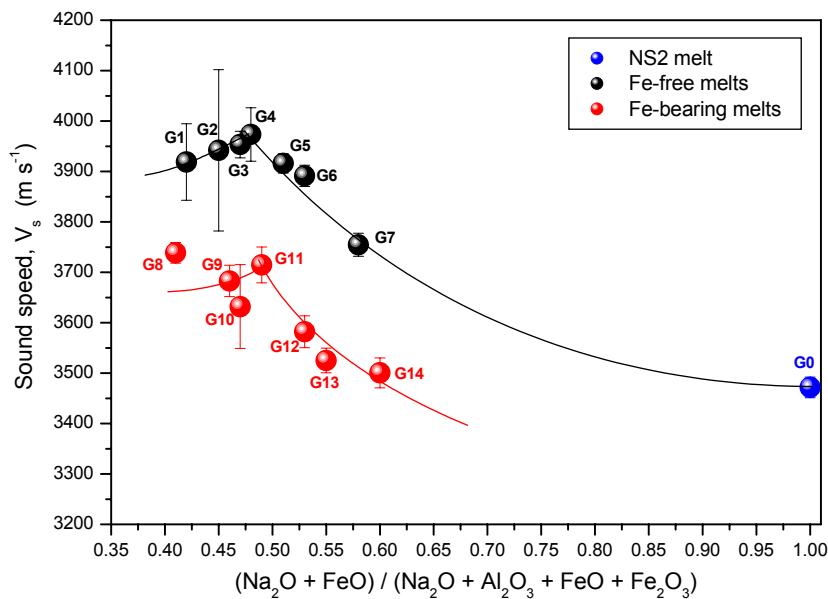


Fig. 58. Sound speed data for all of the samples as a function of compositional parameter $\gamma = (\text{Na}_2\text{O} + \text{FeO}) / (\text{Na}_2\text{O} + \text{Al}_2\text{O}_3 + \text{FeO} + \text{Fe}_2\text{O}_3)$. Sample G8 has less Fe^{3+} than other samples. Trend-lines are the guides to the eye.

4.4. Viscosity

4.4.1. Viscosity as a function of temperature

Viscosity as a function of temperature is presented in Figure 59a, b; and data are gathered in the Table 12. The viscosity data has been fit by an Arrhenian curve, and the A and B parameters (with standard deviation) of the Arrhenian equation are given in the Table 13. The error of viscosity measurements is $\pm 0.06 \log_{10}$ Pa s, and of temperature ± 0.5 °C.

Tab. 12. Viscosity data for NS2 melt (G0), Fe-free melts (G1-G7) and Fe-bearing melts (G8-G14) as a function of temperature.

G0		G1		G2		G3		G4	
T °C	η log ₁₀ Pa s	T °C	η log ₁₀ Pa s	T °C	η log ₁₀ Pa s	T °C	η log ₁₀ Pa s	T °C	η log ₁₀ Pa s
521.79	8.76	938.54	9.26	948.71	9.34	806.16	9.10	928.37	9.62
511.65	9.12	928.37	9.52	938.54	9.54	795.99	9.30	918.21	9.80
501.50	9.53	908.04	9.87	928.37	9.69	775.66	9.70	908.04	10.08
491.35	9.90	897.87	10.04	918.21	9.85	765.49	9.94	897.87	10.31
481.20	10.37	887.70	10.29	908.04	10.12	755.32	10.16	887.70	10.51
471.06	10.79	877.54	10.56	897.87	10.30	745.15	10.43	877.54	10.72
460.91	11.41	867.37	10.75	887.70	10.56	734.98	10.73	867.37	10.97
450.76	11.96	857.20	11.02	877.54	10.74	724.82	11.00	857.20	11.22
440.61	12.62	847.03	11.29	867.37	11.01	714.65	11.20	847.03	11.50
		836.86	11.58	857.20	11.27	704.48	11.58		
				847.03	11.48	694.31	11.95		
				836.87	11.78				

G5		G6		G7		G8		G9	
T °C	η log ₁₀ Pa s	T °C	η log ₁₀ Pa s	T °C	η log ₁₀ Pa s	T °C	η log ₁₀ Pa s	T °C	η log ₁₀ Pa s
918.21	9.04	765.49	9.10	704.48	9.01	887.14	9.10	876.99	10.22
908.04	9.30	755.32	9.32	694.31	9.22	876.99	9.20	866.84	10.38
897.87	9.50	745.15	9.60	684.15	9.48	866.84	9.44	856.69	10.61
887.70	9.70	734.98	9.81	673.98	9.78	856.69	9.56	846.54	10.84
877.54	9.85	724.82	10.02	663.81	10.05	846.54	9.91	836.39	11.02
867.37	10.05	714.65	10.32	653.64	10.35	836.39	10.08	826.25	11.47
857.20	10.30	704.48	10.60	643.48	10.64	826.25	10.22	816.10	11.55
847.03	10.46	694.31	10.85	623.14	11.22	816.10	10.44	805.95	11.83
836.86	10.71	684.15	11.11	612.97	11.60	805.95	10.84	795.80	12.28
826.70	11.01	673.98	11.40	602.80	12.02	795.80	10.94		
816.53	11.28					785.65	11.27		

G10		G11		G12		G13		G14	
T °C	η log ₁₀ Pa s	T °C	η log ₁₀ Pa s	T °C	η log ₁₀ Pa s	T °C	η log ₁₀ Pa s	T °C	η log ₁₀ Pa s
847.03	9.30	816.53	8.87	735.19	9.26	694.52	9.37	664.01	8.83
836.86	9.51	806.36	9.05	725.02	9.53	684.35	9.58	653.85	9.06
826.70	9.75	796.19	9.26	714.85	9.81	674.18	9.80	643.68	9.31
816.53	9.90	786.03	9.55	704.68	10.10	664.01	10.11	633.51	9.64
806.36	10.10	775.86	9.65	694.52	10.38	653.85	10.39	623.34	9.89
796.19	10.37	765.69	9.98	684.35	10.59	643.68	10.73	613.18	10.23
786.03	10.54	755.52	10.02	664.01	11.24	633.51	11.10	603.01	10.56
775.86	10.80	745.36	10.36	653.85	11.48	623.34	11.40	592.84	10.94
765.69	11.06	735.19	10.45	643.68	11.70	613.18	11.79	582.67	11.34
755.52	11.36	725.02	10.89			603.01	12.19	572.50	11.71
745.36	11.60	714.85	11.06						
735.19	11.97								

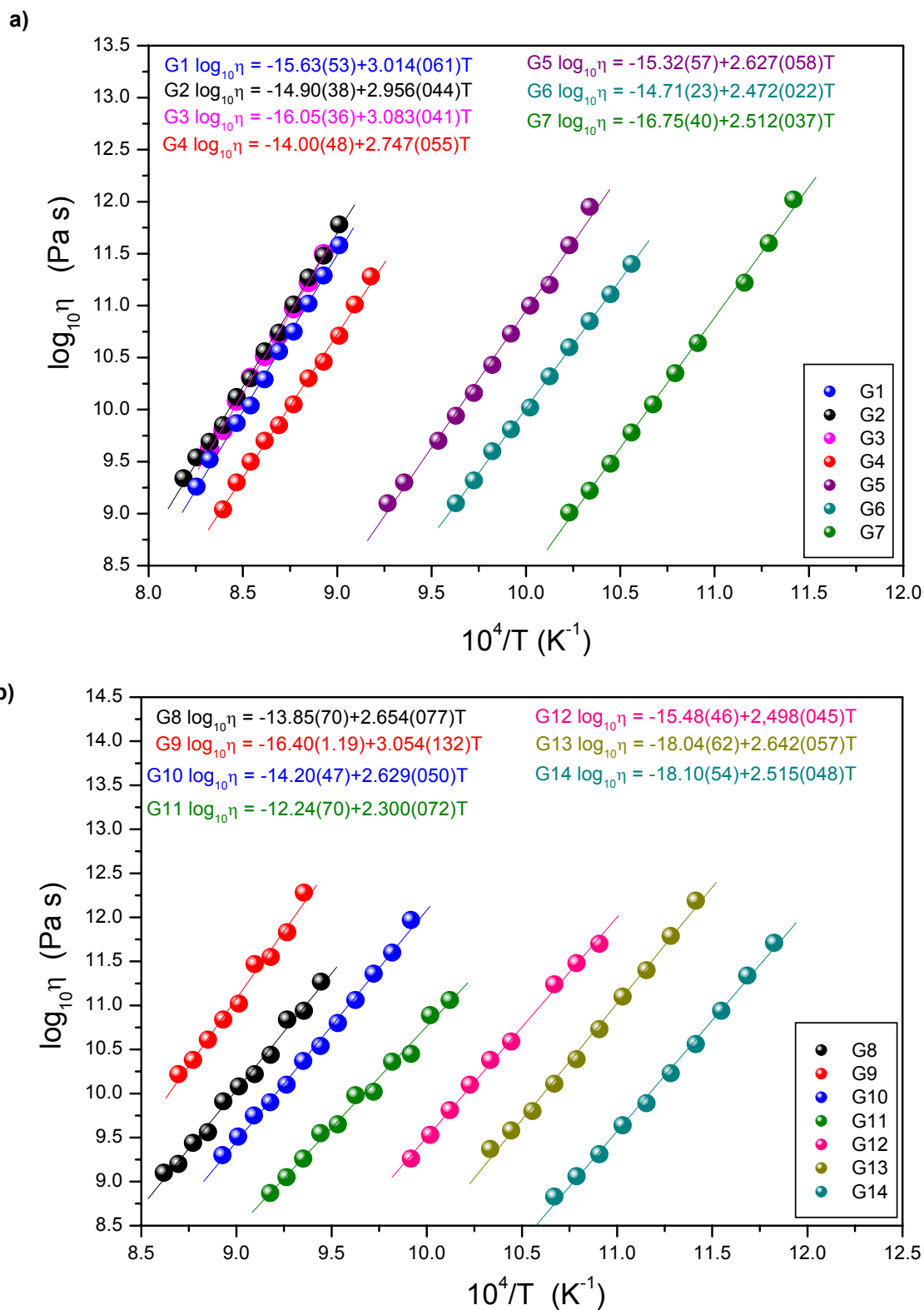


Fig. 59. Melt viscosity as a function of inverse temperature determined by the micropenetration method. The straight lines are the Arrhenian fits to the data (equations for Arrhenian fits above the data points). **a)** for Fe-free melts (G1-G7); **b)** for Fe-bearing melts (G8-G14).

Table 13. Fits to the Arrhenian equation (Eq. 24) for the viscosity data of melts G0-G14. The activation energy E_a calculated with using the Eq. 27; $\gamma = (\text{Na}_2\text{O}+\text{FeO})/(\text{Na}_2\text{O}+\text{Al}_2\text{O}_3+\text{FeO}+\text{Fe}_2\text{O}_3)$; \log_{10} viscosity was determined for temperature 750°C.

Melt number	A (\log_{10} Pa s)	B (K)	Activation Energy, E_a (kJ mol^{-1})	γ	$\log_{10}\eta$ @750°C (Pa s)
G0	-24.98±0.99	2.673±0.074	511.75±14.23	1.00	1.145
G1	-15.63±0.53	3.014±0.061	577.10±11.68	0.42	13.828
G2	-14.90±0.38	2.956±0.044	565.99± 8.42	0.45	13.991
G3	-16.05±0.36	3.083±0.041	590.31± 7.85	0.47	14.082
G4	-14.00±0.48	2.747±0.055	525.97±10.53	0.48	12.848
G5	-15.32±0.57	2.627±0.058	503.00±11.11	0.51	10.356
G6	-14.71±0.23	2.472±0.022	473.32± 4.21	0.53	9.451
G7	-16.75±0.40	2.512±0.037	480.98± 7.08	0.58	7.802
G8	-13.85±0.70	2.654±0.077	508.16±14.74	0.41	12.090
G9	-16.40±1.19	3.054±0.132	584.75±25.27	0.46	13.449
G10	-14.20±0.47	2.629±0.050	503.38± 9.57	0.47	11.495
G11	-12.24±0.70	2.300±0.072	440.38±13.79	0.49	10.240
G12	-15.48±0.46	2.498±0.045	478.34± 8.62	0.53	8.935
G13	-18.04±0.62	2.642±0.057	505.87±10.91	0.55	7.782
G14	-18.10±0.54	2.515±0.048	481.63± 9.19	0.60	6.481

Viscosity of peralkaline samples (with and without iron) increases together with increasing Al_2O_3 content. When the composition becomes peraluminous, viscosity does not change, just the opposite, stays constant.

The clearer change one observes in the plot of viscosity as a function of compositional parameter γ at one chosen temperature. In Figure 60 the extrapolated \log_{10} viscosity data are presented for 750°C (see also Tab. 13). Not all of the melts were analysed at 750°C. Because of that the viscosity data for some melts need to be extrapolated beyond the investigated temperature range. Viscosity data as a function of $(\text{Na}_2\text{O}+\text{FeO})/(\text{Na}_2\text{O}+\text{Al}_2\text{O}_3+\text{FeO}+\text{Fe}_2\text{O}_3)$ create a trend increasing from more to less peralkaline samples and then changes into a plateau in range of peraluminous composition. There can be also observed a weak maximum at 0.47, i.e. in the peraluminous range.

The addition of iron to the sodium aluminosilicate melts decreases viscosity. As can be observed in Figure 60, the difference between viscosity of peralkaline Fe-free and Fe-bearing melts is smaller than the difference between viscosity of Fe-free and Fe-bearing peraluminous melts. The same effect of the influence of Fe on the viscosity was confirmed by Cukierman & Uhlmann, 1974; Mysen & Virgo, 1985; Dingwell & Virgo, 1988a,b or Webb, 2005b.

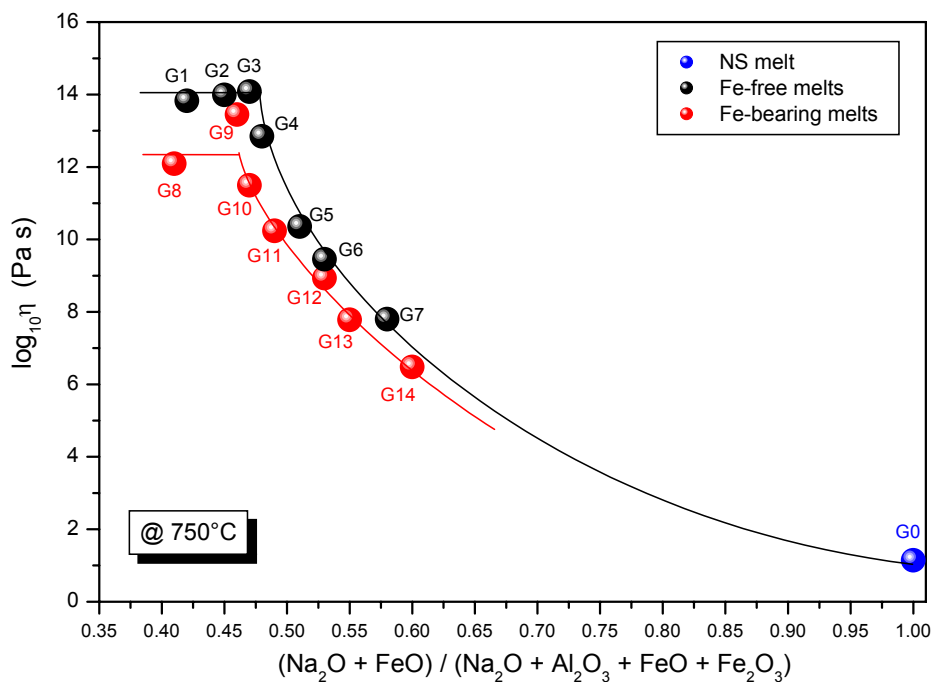


Fig. 60. \log_{10} viscosity as a function of composition. Blue point is for NS2 melt (G0); black points are for Fe-free melts (G1-G7); red points are for Fe-bearing melts (G8-G14). The trend-lines are a guides to the eye.

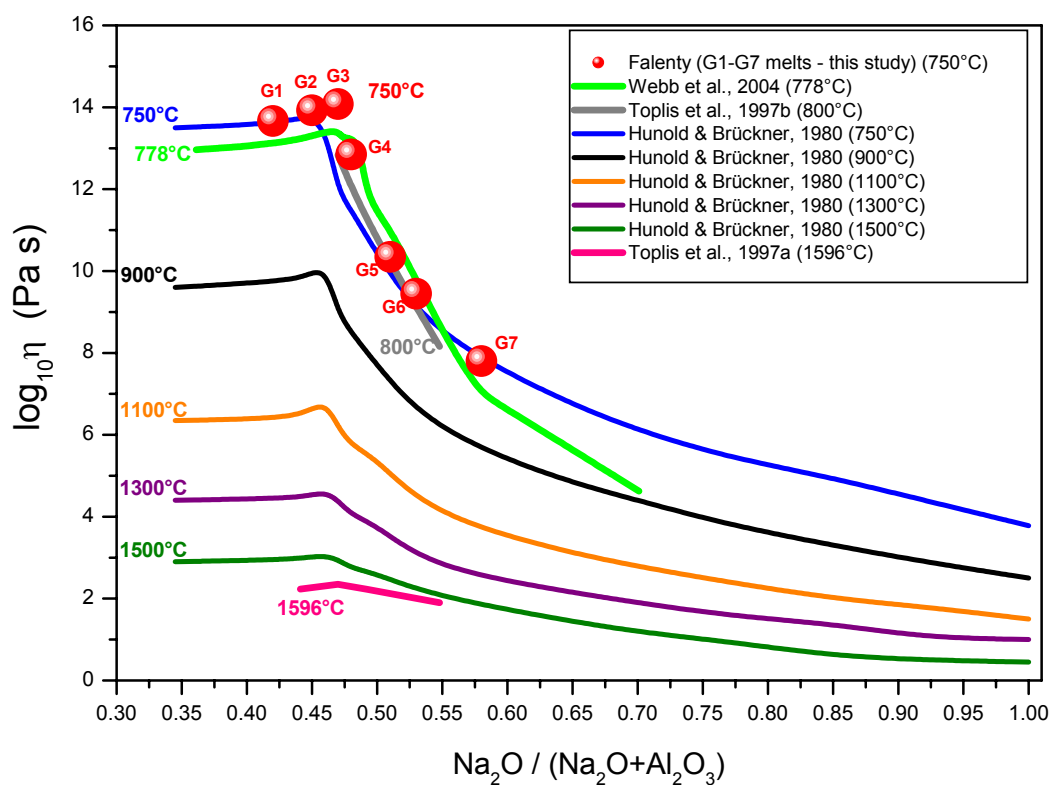


Fig. 61. \log_{10} viscosity for sodium aluminosilicate melts at different temperatures as a function of composition. Coloured lines belong to the data of other authors (see legend); red points are for Fe-free melts from this study (G1-G7).

As has been mentioned before, the viscosity depends on the temperature. Viscosity decreases with increasing temperature. Figure 61 shows viscosity data of Fe-free melts (G1-G7) at 750°C compared to viscosity data of sodium aluminosilicate measured by Hunold & Brückner (1980), Toplis et al. (1997a, b) and Webb et al. (2004) at different temperatures. There is small divergence between data of G1-G7 melts at 750°C and data of Hunold & Brückner (1980) at the same temperature, however, Webb (2005b) assumed that the extrapolation of viscosity data beyond the investigation temperature range (using A and B parameters of the Arrhenian equation) can create an error in calculated viscosity up to $\sim 1 \log_{10} \text{Pa s}$.

4.4.2. Activation energy for viscous flow

Activation energy E_a for NS2, Fe-free and Fe-bearing melts obtained from micropenetration measurements has been presented in Figure 62 as a function of compositional parameter γ and in the Table 13. In Figure 62 data from this study are compared to other data of Fe-free melts (Webb et al., 2004; Toplis et al., 1997a, b) and Fe-bearing melts (Webb, 2005b). Because error bars are large, it is difficult to support a clear trend. Activation energy is the energy needed to trigger the flow mechanism in the melt. A related property is measured in heat capacity investigations, where heat needed to start flow is determined. From this reason the trend (being a guide to the eye in Figure 62) is similar to this one in Figure 76.

Activation energy of Fe-free peralkaline melts appears to be similar to the activation energy of Fe-bearing peralkaline melts. Starting from NS2 melt E_a slowly decreases together with increasing the amount Al_2O_3 in the melts. The breaking point is close to $\gamma=0.53$. Fe-free and Fe-bearing peraluminous melts differ from each other. The activation of Fe-free peraluminous melts is higher than for Fe-bearing peraluminous melts and both of them are slightly higher than peralkaline melts.

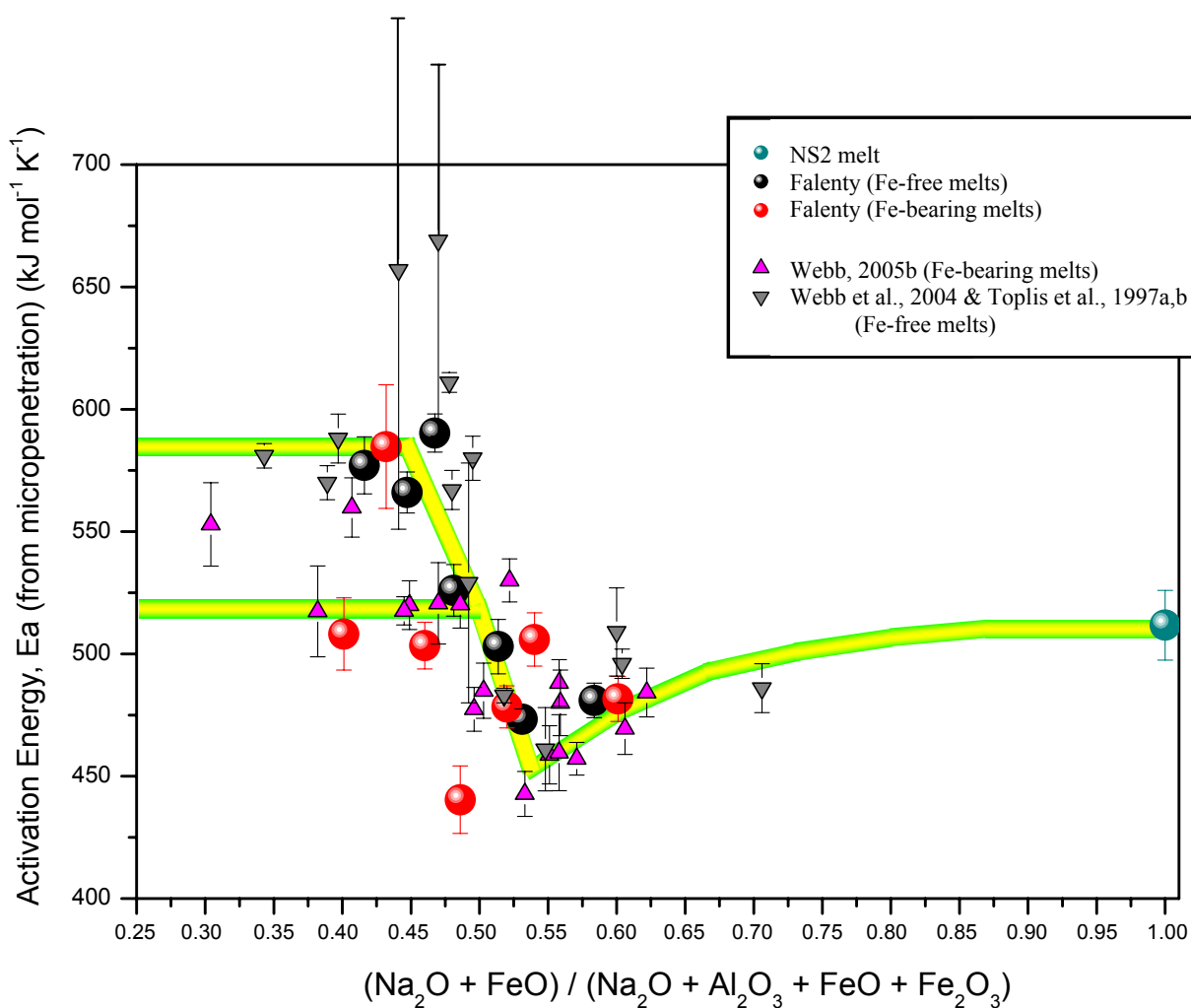


Fig. 62. Activation energy for NS2 (cyan point), Fe-free (black points) and Fe-bearing (red points) melts calculated from micropenetration measurements as a function of compositional parameter γ . Other plotted data come from Webb et al., 2004 and Toplis et al., 1997a, b (Fe-free melts – grey inverted triangles); and Webb, 2005b (Fe-bearing melts – pink triangles).

4.5. Heat capacity

4.5.1. Heat capacity data

Typical results of heat capacity measurements (in $\text{J g}^{-1} \text{K}^{-1}$) for the glasses and liquids in the temperature range between 100 and 925°C with step of temperature of 5°C (heating/cooling rate: $20^\circ\text{C min}^{-1}$) for all of the samples investigated in this study are gathered in Appendix 1.

Heat capacity data are normally presented as a function of temperature (curves in Figure 66) or as a function of composition (Fig. 63) according to the models suggested by Stebbins et al. (1984), Richet (1984) and Richet (1987). The assumption of these models is that composition has no influence on the partial molar heat capacity; and the temperature dependence is expressed by Maier – Kelley equation (Eq. 28). However, in Figure 67 one observes a small compositional dependence for the peralkaline melts.

Heat capacity c_p (in $\text{J g}^{-1} \text{K}^{-1}$) of the glass and of the liquid for all of the samples has been presented in Figure 63a and in the Table 14. Data come from measurements of heat capacity with the heating rate of $20^\circ\text{C min}^{-1}$. Not all of the points in Figure 63a sit on the trend lines (samples G7, G8 and G14); as there is occasionally difficulty in obtaining a stable calibration in a non-temperature controlled laboratory and base line shift can occur. Absolute values can be slightly erroneous, but relative values (configurational heat capacities – see section 5.3.) are correct. However, it is easy to observe, that c_p data of the liquid are higher than c_p data of the glass and additionally within these two category (liquid and glass) Fe-free samples have higher heat capacity values than Fe-bearing samples. Additional remark is that c_p of the peraluminous melts does not change and stays constant with composition. For peralkaline melts from composition where $\gamma \sim 0.48$ towards lower Al_2O_3 content the heat capacity slightly decreases.

Figure 63b shows the same points of heat capacity but in $\text{J mol}^{-1} \text{K}^{-1}$. The models of Richet (1987) and Richet & Bottinga (1985) have been used to fit the trends. These models have been created to calculate the heat capacity of the melts and glasses as a function of chemical composition and temperature. One observes that models work very well for heat capacity of the glasses and do not work for heat capacity of the liquids.

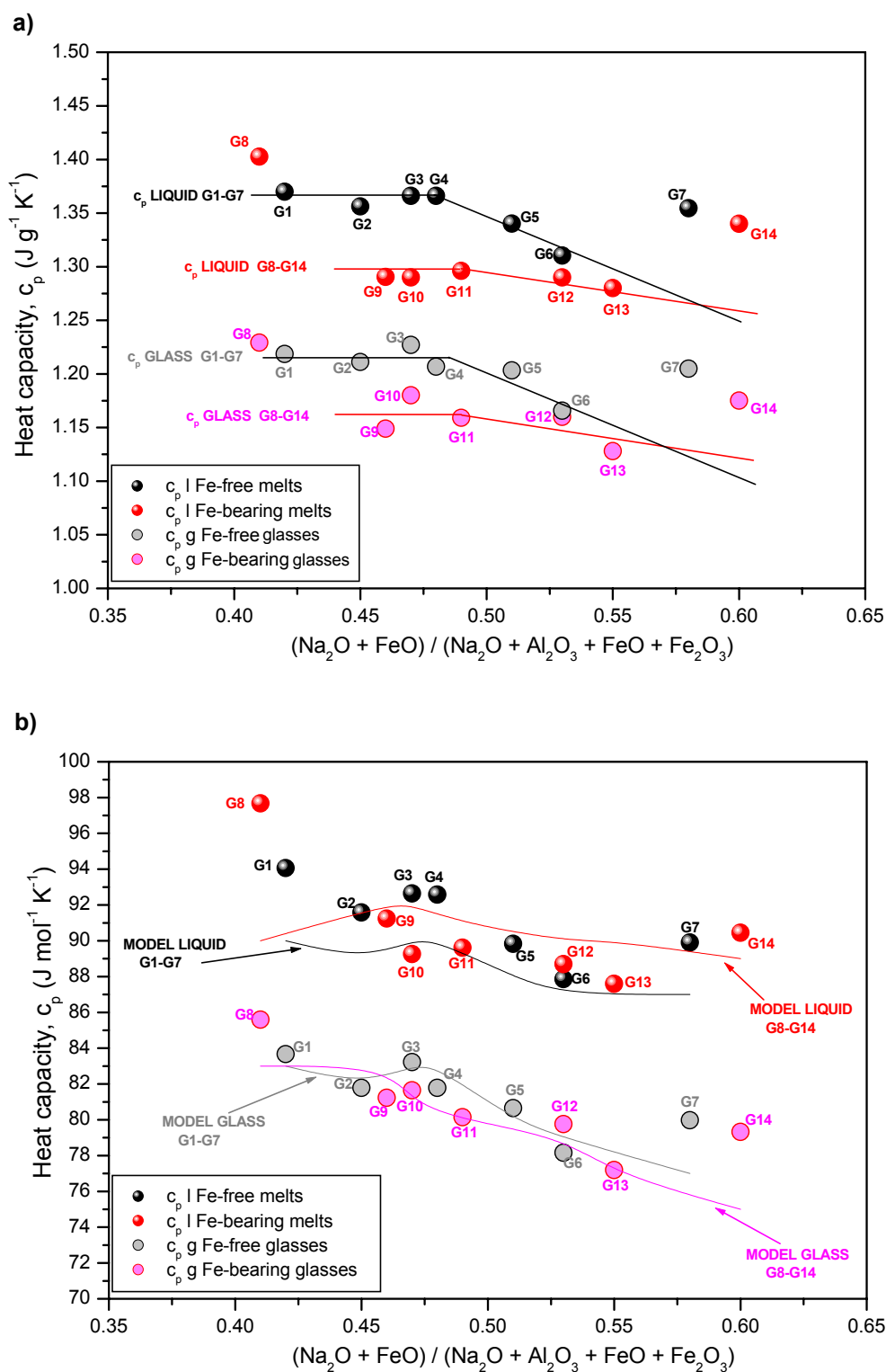


Fig. 63. Heat capacity of the glass c_{pg} and heat capacity of the liquid c_{pl} for peralkaline and peraluminous Fe-free and Fe-bearing samples as a function of compositional parameter $\gamma = (\text{Na}_2\text{O} + \text{FeO}) / (\text{Na}_2\text{O} + \text{Al}_2\text{O}_3 + \text{FeO} + \text{Fe}_2\text{O}_3)$; **a)** in $\text{J g}^{-1} \text{K}^{-1}$; the trends are the guides to the eye; **b)** in $\text{J mol}^{-1} \text{K}^{-1}$; the lines are derived from the models of Richet (1987) and Richet & Bottinga (1985).

Melt number	γ	c_{pg} (J g ⁻¹ K ⁻¹)	c_{pg} (J mol ⁻¹ K ⁻¹)	c_{pl} (J g ⁻¹ K ⁻¹)	c_{pl} (J mol ⁻¹ K ⁻¹)
G0	1.00	1.250	75.812	1.450	90.368
G1	0.42	1.219	83.667	1.370	94.061
G2	0.45	1.211	81.785	1.356	91.583
G3	0.47	1.227	83.221	1.366	92.641
G4	0.48	1.207	81.790	1.366	92.579
G5	0.51	1.203	80.654	1.340	89.830
G6	0.53	1.166	78.164	1.310	87.860
G7	0.58	1.205	79.969	1.355	89.905
G8	0.41	1.229	85.599	1.403	97.681
G9	0.46	1.149	81.228	1.290	91.240
G10	0.47	1.180	81.648	1.290	89.259
G11	0.49	1.159	80.147	1.296	89.620
G12	0.53	1.160	79.756	1.290	88.694
G13	0.55	1.128	77.198	1.280	87.601
G14	0.60	1.175	79.321	1.340	90.445

Tab. 14. Table for all of the samples with compositional parameter γ ; heat capacity of the glass c_{pg} and liquid c_{pl} (in J g⁻¹ K⁻¹ and in J mol⁻¹ K⁻¹).

4.5.2. Glass transition temperature T_g and fictive temperature T_f

The glass transition temperatures (based on viscosity data) T_g^{12} (temperature at which $\eta=10^{12}$ Pas) are shown as a function of composition in Figure 64. The T_g^{12} values for Fe-free and Fe-bearing melts show a change in trends on the peraluminous side of the composition range ($\gamma\sim 0.475$). This change in trend as a function of Na/Al has been discussed previously by Toplis et al. (1997a, b) and Webb et al. (2004) in terms of the structural changes and the presence of triclusters in the melts with changing composition and also in terms of the changes in flow mechanism accompanying such changes in melt structure.

Because Fe ions have relatively low mobility than sodium, its high-field strength leads to much stronger bonds between Fe²⁺ as a network modifier and a surrounding structure. This influence of Fe on the structure can be observed in the glass transition (T_g) plot. The similar situation exists in Ca-bearing melts. Increased field strength of Ca leads to disappearing the breaking point on the plot of T_g (Shelby, 1985; Webb, 2007).

Fictive temperature T_f is calculated from Eq. 30 for heating rate 20°C min⁻¹ and has been shown in the Table 15. It has been also observed that there is a linear relationship between fictive temperature T_f measured for each sample for heating rate 20°C min⁻¹ and T_g^{12} (see Fig. 65).

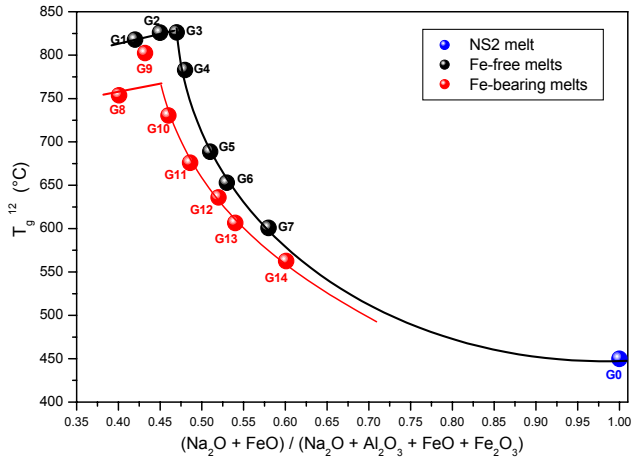


Fig. 64. A plot of T_g^{12} as a function of compositional parameter γ .

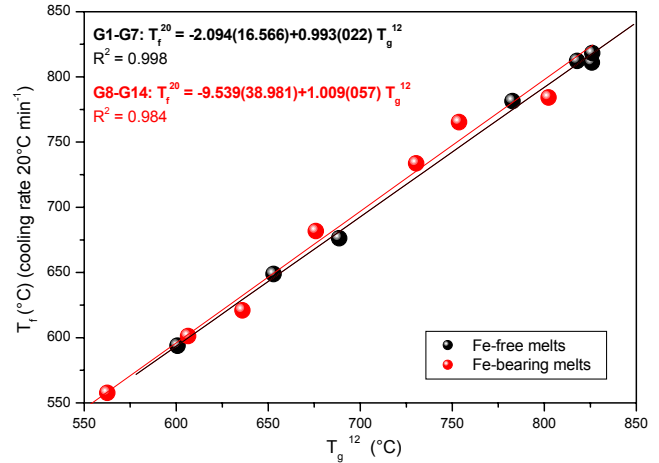


Fig. 65. A plot of T_g^{12} as a function of fictive temperature T_f (for heating/cooling rate of $20^\circ\text{C min}^{-1}$)

Melt number	γ	T_g^{12} (°C)	T_f^{20} (°C)
G0	1.00	449.82	460.36
G1	0.42	817.84	812.19
G2	0.45	825.88	810.97
G3	0.47	826.11	818.26
G4	0.48	782.77	781.44
G5	0.51	688.57	676.28
G6	0.53	652.90	648.80
G7	0.58	600.74	593.81
G8	0.41	753.69	765.31
G9	0.46	802.35	784.18
G10	0.47	730.44	733.70
G11	0.49	675.84	681.75
G12	0.53	636.02	620.94
G13	0.55	606.49	601.29
G14	0.60	562.55	557.72

Tab. 15. Glass transition temperature T_g^{12} at $\log_{10}\eta=12$; fictive temperature T_f (for heating rate of $20^\circ\text{C min}^{-1}$).

4.5.3. 3R parameter

$3R$ ($24.9 \text{ J mol}^{-1} \text{ K}^{-1}$) is a classical limiting value of heat capacity determined empirically from the Dulong – Petit law of atomic heat. $3R$ is valid only for small b parameter of the Maier-Kelley equation (Eq. 28), that is for small atomic oscillation or for high temperatures. $3R$ value, where R is ideal gas constant ($8.314570(70) \text{ J mol}^{-1} \text{ K}^{-1}$) and is equal:

$$3R = k_B \cdot N_A \quad (\text{Eq. 56})$$

where k_B is a Boltzmann's constant ($1.3806504 \cdot 10^{-23} \text{ J K}^{-1}$) and N_A is Avogadro's number ($6.02214179 \cdot 10^{23} \text{ mol}^{-1}$). The Dulong – Petit limit of $3R$ is calculated per mole of atoms, not molecules.

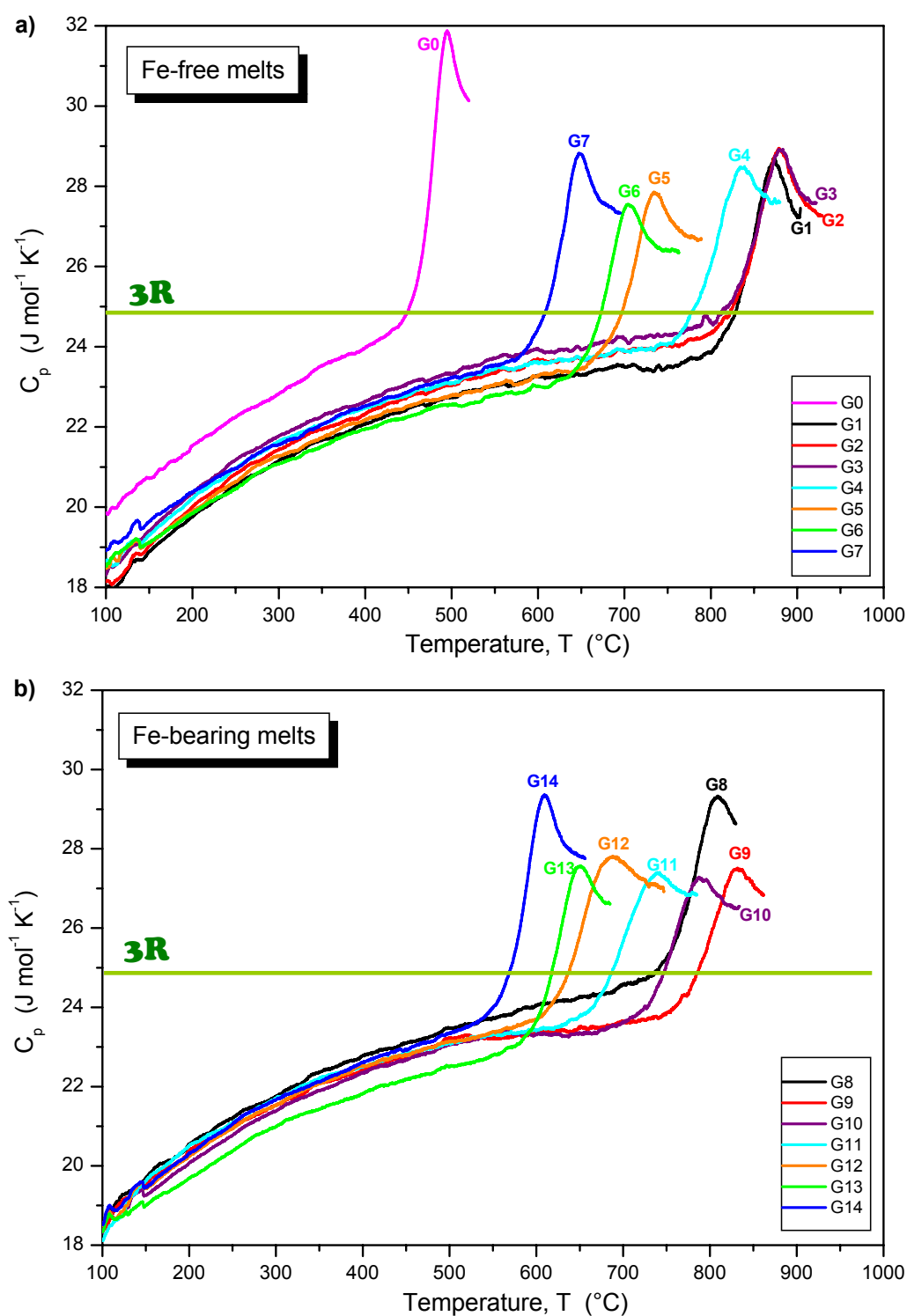


Fig. 66. Plots of classical limiting value $3R$ for heat capacity calculated in mole per atoms. The horizontal line determine a $3R$ value for solids: $24.9 \text{ J mol}^{-1} \text{K}^{-1}$. **a)** data for NS2 (G0) and Fe-free melts (G1-G7); **b)** data for Fe-bearing melts (G8-G14).

4.6. Torsion (forced oscillation)

4.6.1. Real and imaginary shear modulus

The frequency dependent deformation data were obtained from 300-1000°C. The maximum temperature is that at which it is no longer possible to measure the elastic (instantaneous) component of deformation; this occurs at viscosity of $\sim 10^9$ Pa s. The minimum temperature is defined by the point at which the melt breaks away from the alumina torsion rod due to differences in thermal expansion of the two materials.

Figure 67 shows the variation in real and imaginary shear modulus as a function of angular frequency ($\omega = 2\pi f$) times Maxwell relaxation time (τ_M). Data of real and imaginary shear modulus are presented in Appendix 2. The relaxation time is calculated from the Maxwell equation $\tau_M(T) = \eta_N(T) / G_\infty$ for Newtonian viscosity η_N - determined from the micropenetration measurements, and elastic (infinite frequency) shear modulus G_∞ , which is taken to be the shear modulus at 1 Hz at the lowest temperature of measurement (see Tab. 16). The relaxation times for all of the melts are presented in Appendix 3. The studies of Rivers and Carmichael (1987), Webb (1992b) and Farnan and Stebbins (1994) (as well as many others) show that the Maxwell relationship successfully calculates the structural relaxation time of silicate melts. Plotting data from different temperatures on the same curve uses the principle of "thermorheological simplicity" which assumes that the structure and mechanism of flow in these melts does not change over the temperature interval of the measurements (e.g. Narayanaswamy, 1988).

Herzfeld & Litovitz (1959) developed a general equation to describe the frequency dependence of the shear modulus of a material independent of its structure;

$$G^*(\omega) = \frac{G_\infty \omega^2 \tau^2}{1 + \omega^2 \tau^2} + i \frac{G_\infty \omega \tau}{1 + \omega^2 \tau^2} \quad (\text{Eq. 57})$$

where G_∞ is infinite frequency elastic shear modulus, τ is the structural relaxation time and ω is angular frequency (see also Nowick & Berry, 1972; Webb, 1991). The dotted lines in Figure 67 are the real and imaginary shear modulus expected from the theory of Herzfeld & Litovitz (1959). As can be seen in Figure 67, none of the present data is adequately described by this equation. The solid lines are fits to the data (see also Figures 68 and 69) based on the assumption that there is a distribution of relaxation times. Data of the lines are given in Appendix 4a,b (for samples G0 and G1-G7) and in Appendix 4c,d (for samples G8-G14).

Fig. 67. Real and imaginary components of the shear modulus of the present melts as a function of $\log_{10} \omega\tau_M$. Open circles are for real shear modulus; solid circles are for imaginary shear modulus; the dotted line are the model of Herzfeld & Litovitz (1959) for a single structure melt; solid line of the fitting of the data points; grey line is fitting of the imaginary parameters to the real shear modulus of the sample. Not all the data has been shown; for some of the samples the plot has been cut at $\log_{10} \omega\tau_M = 10$.

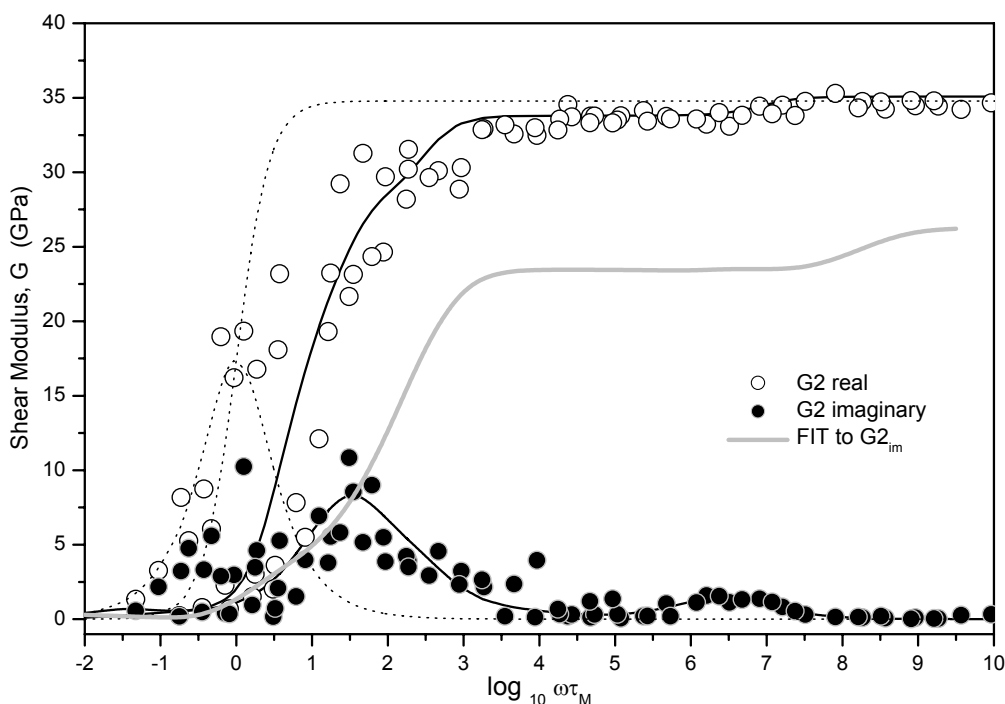
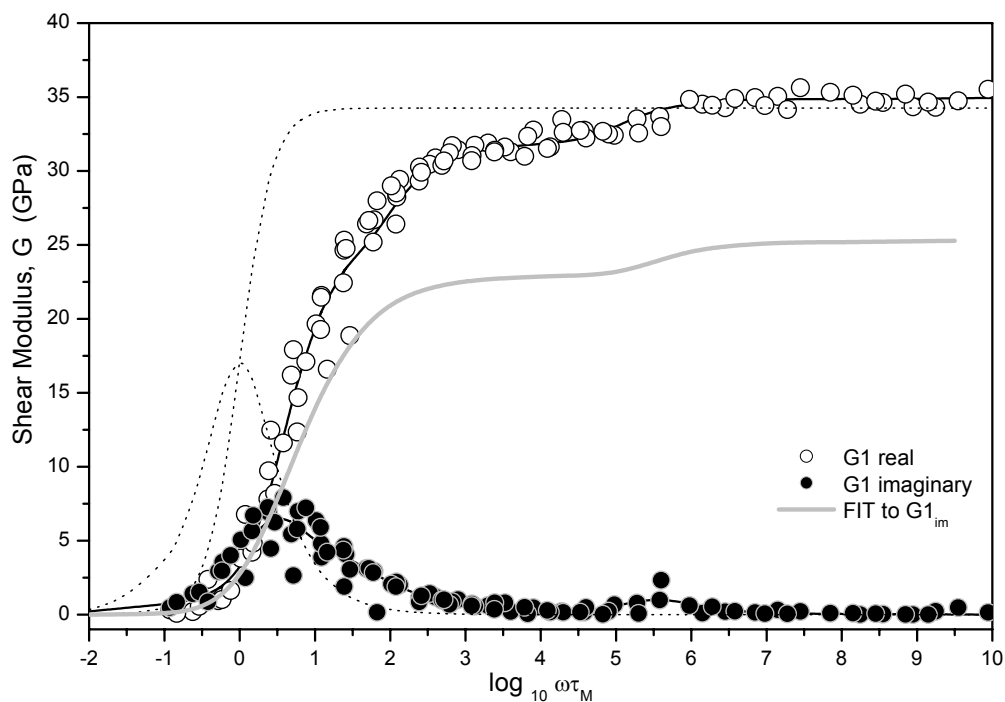


Fig. 67. continuation...

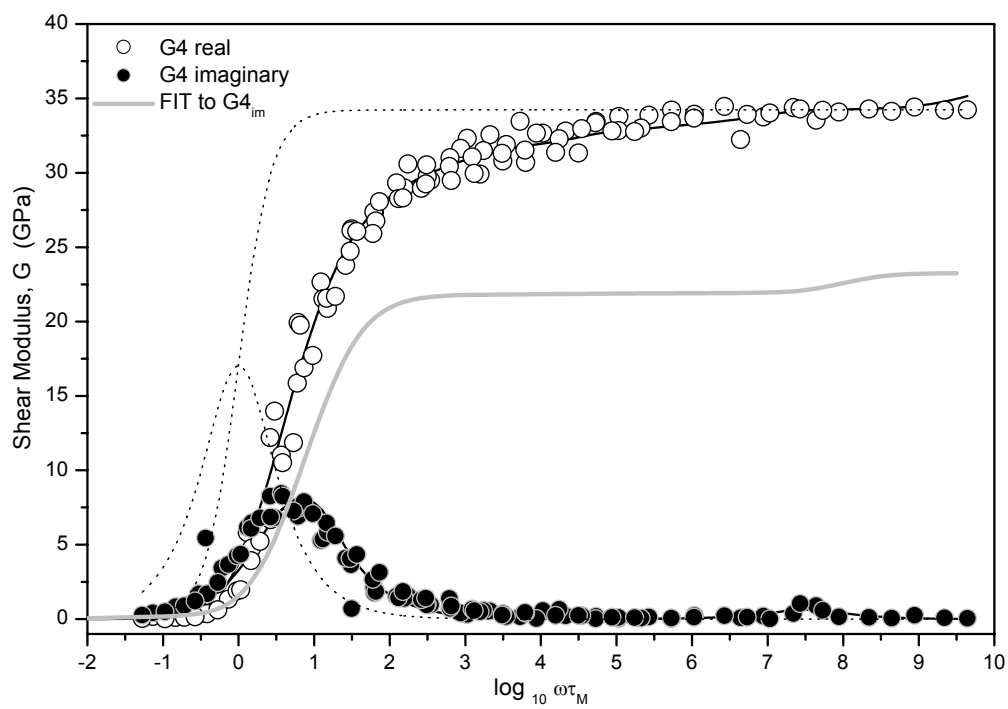
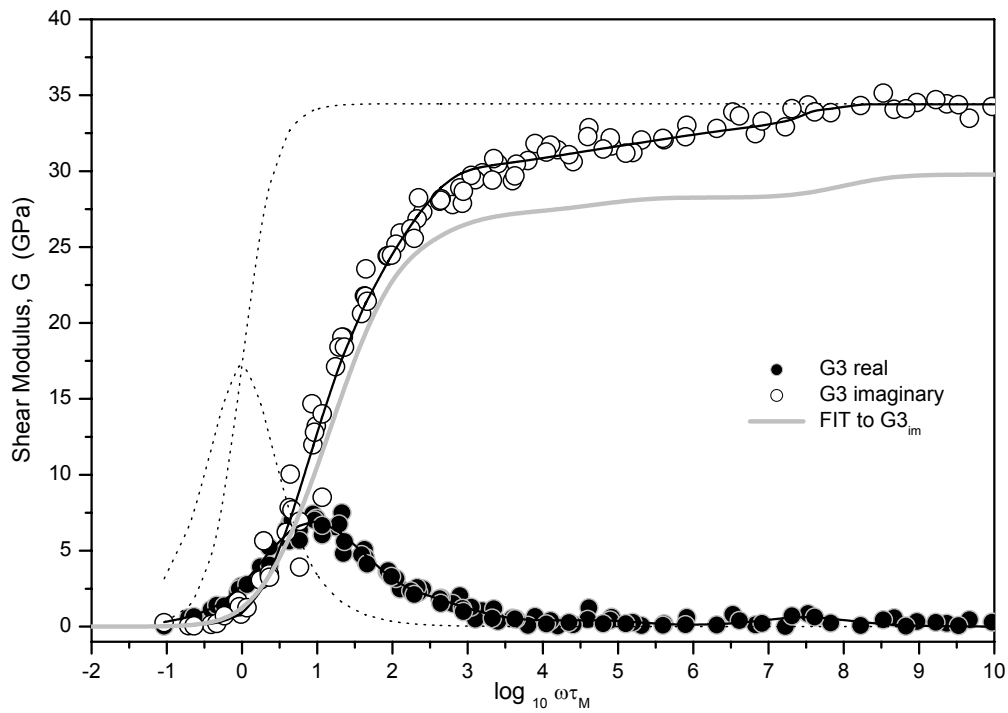


Fig. 67. continuation...

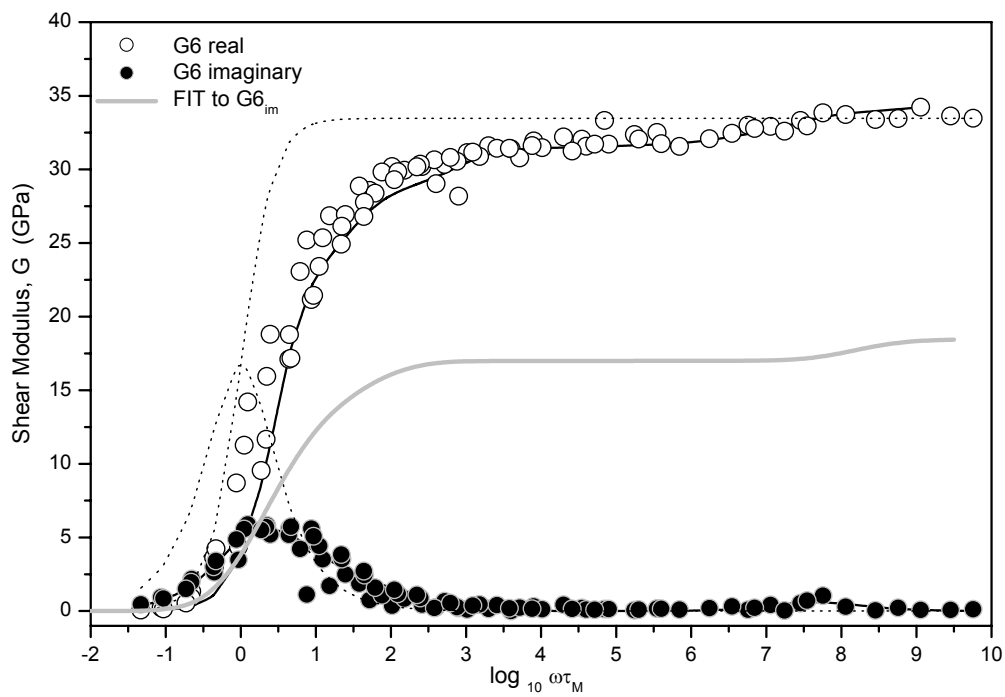
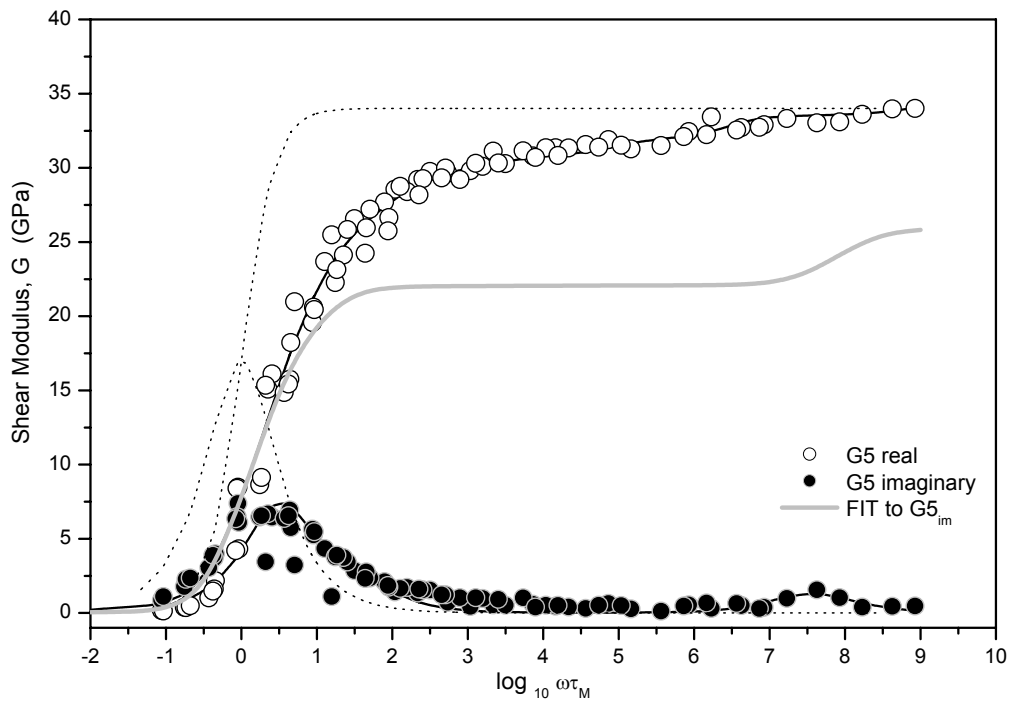


Fig. 67. continuation...

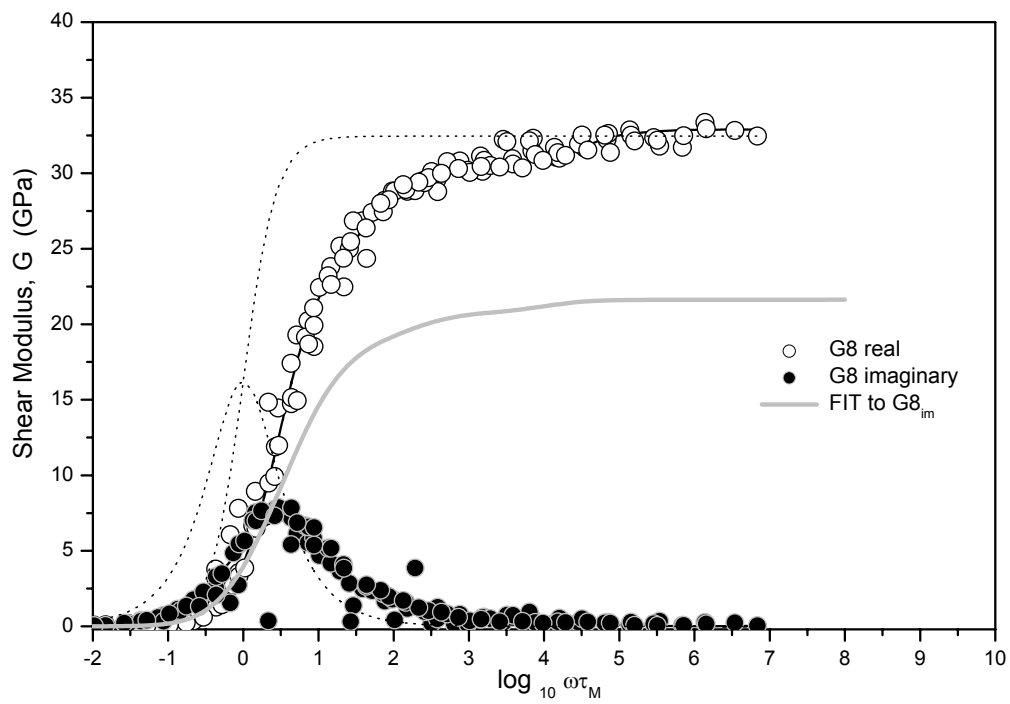
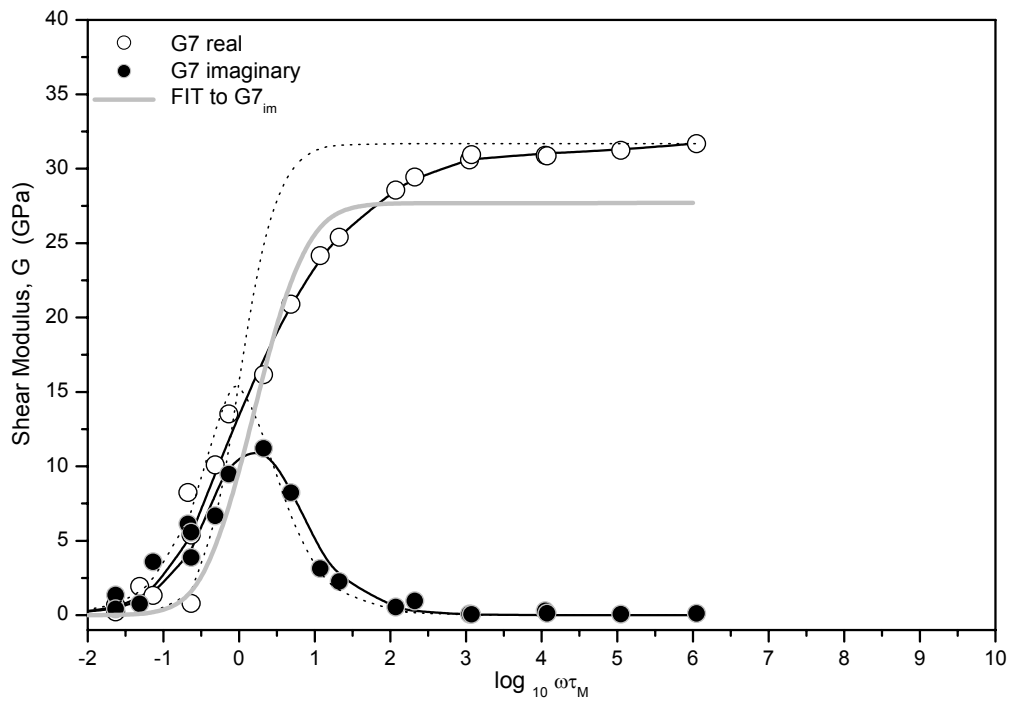


Fig. 67. continuation...

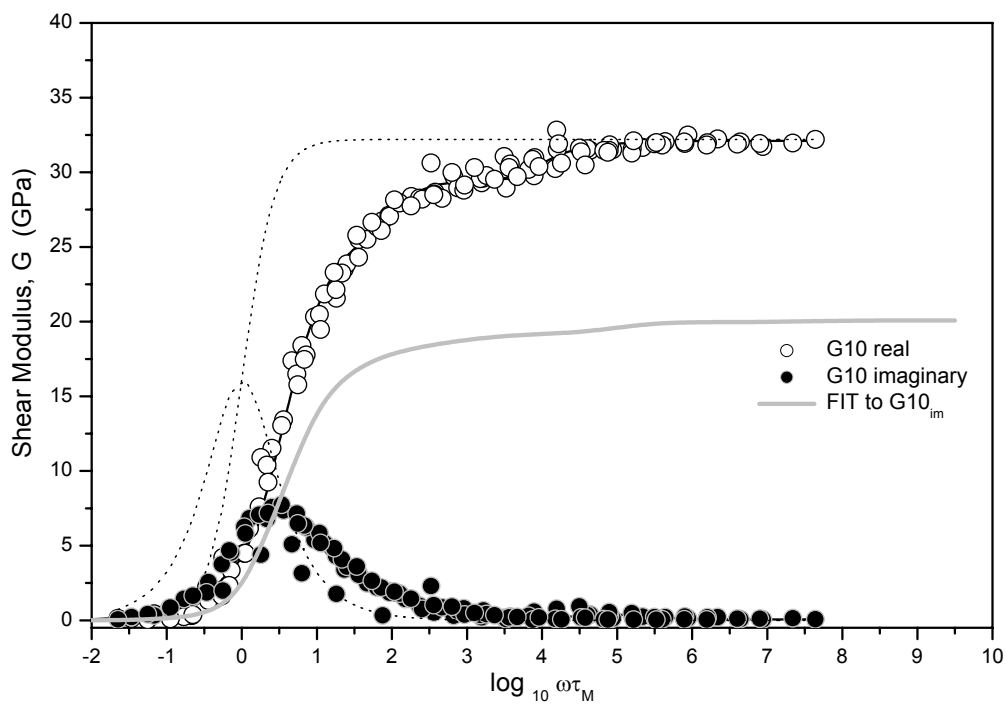
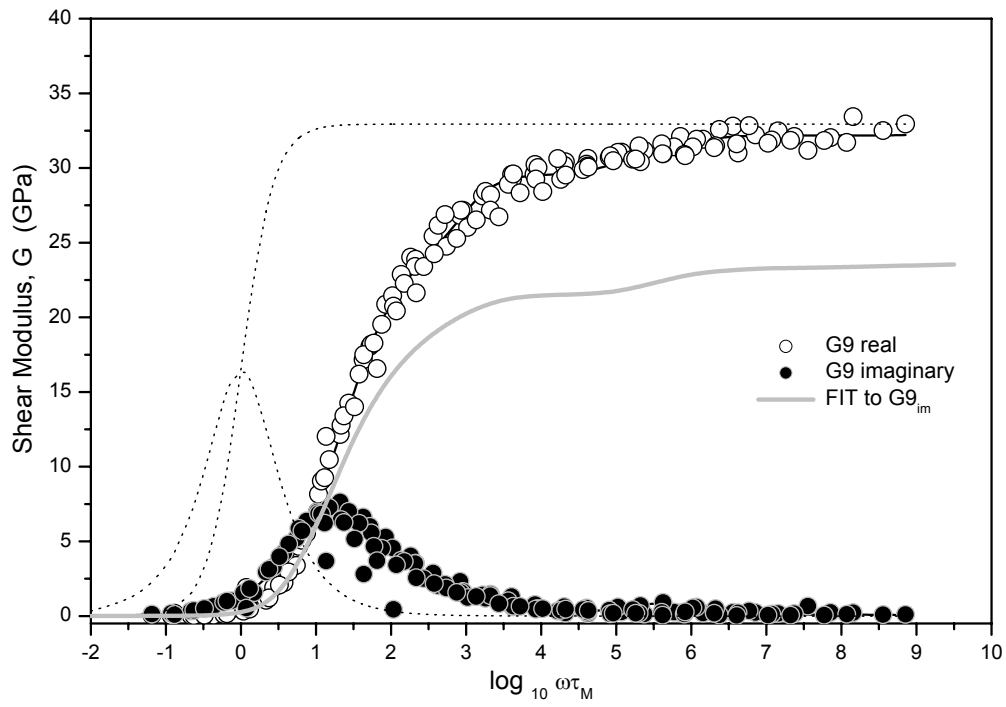


Fig. 67. continuation...

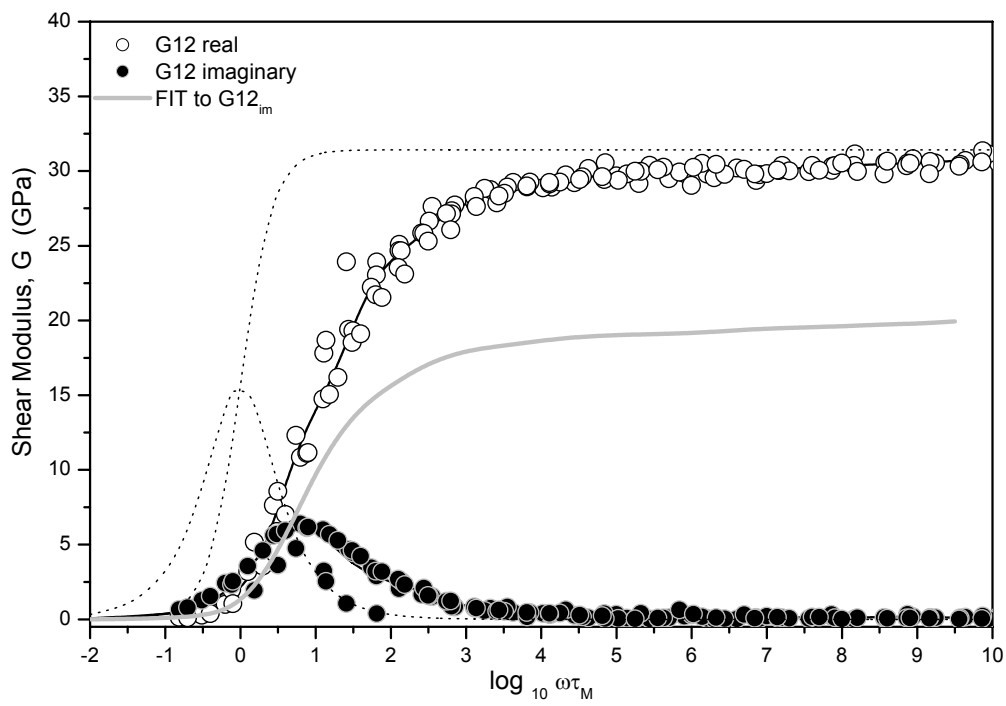
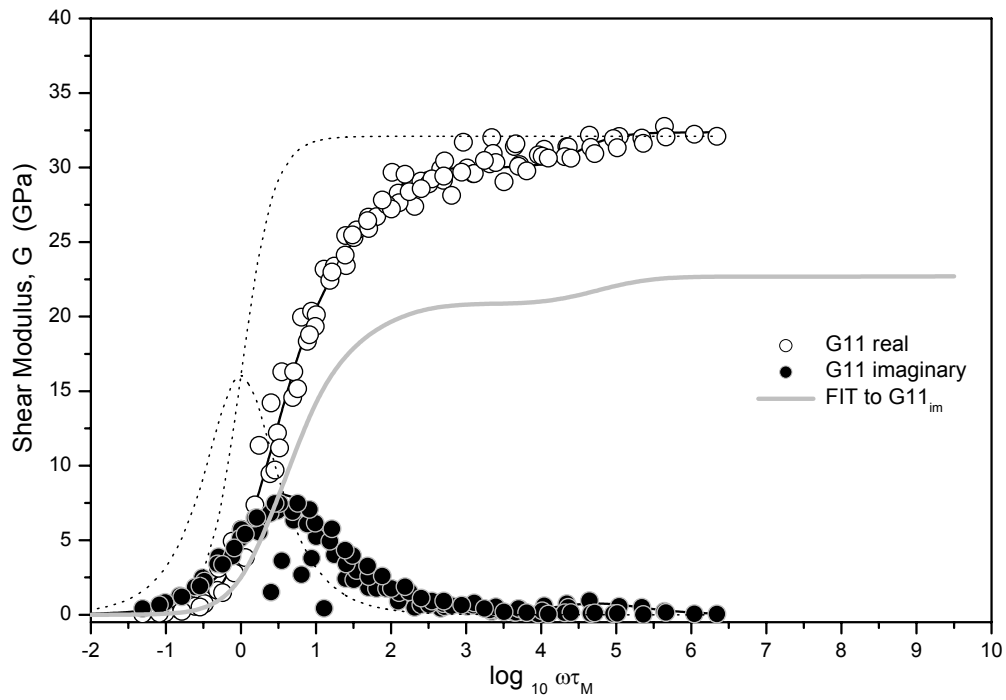
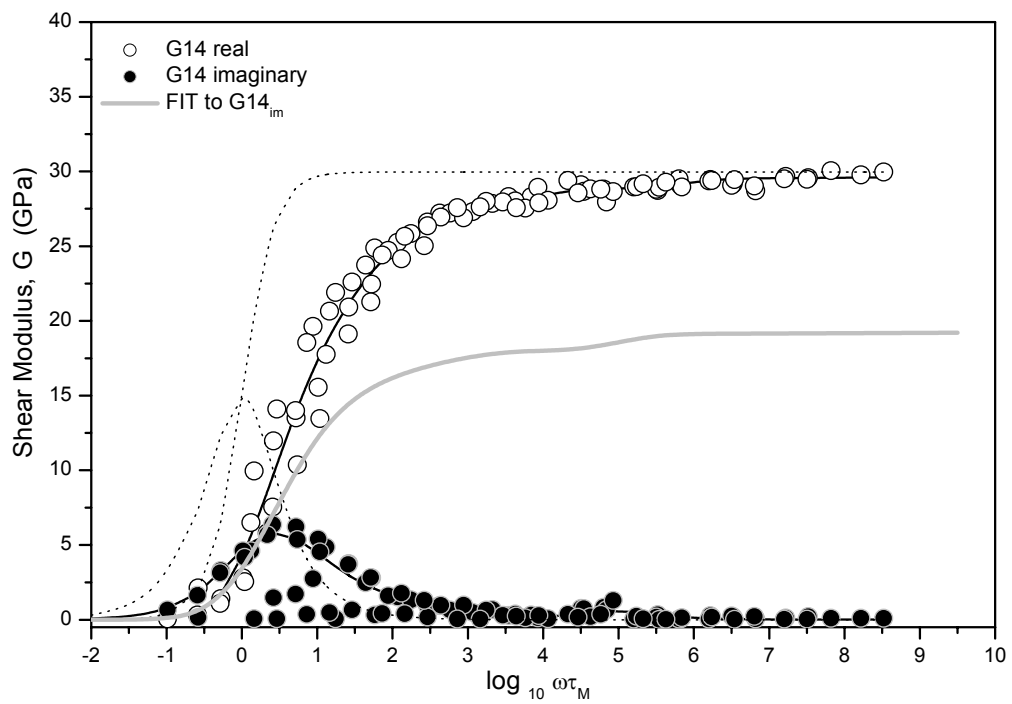
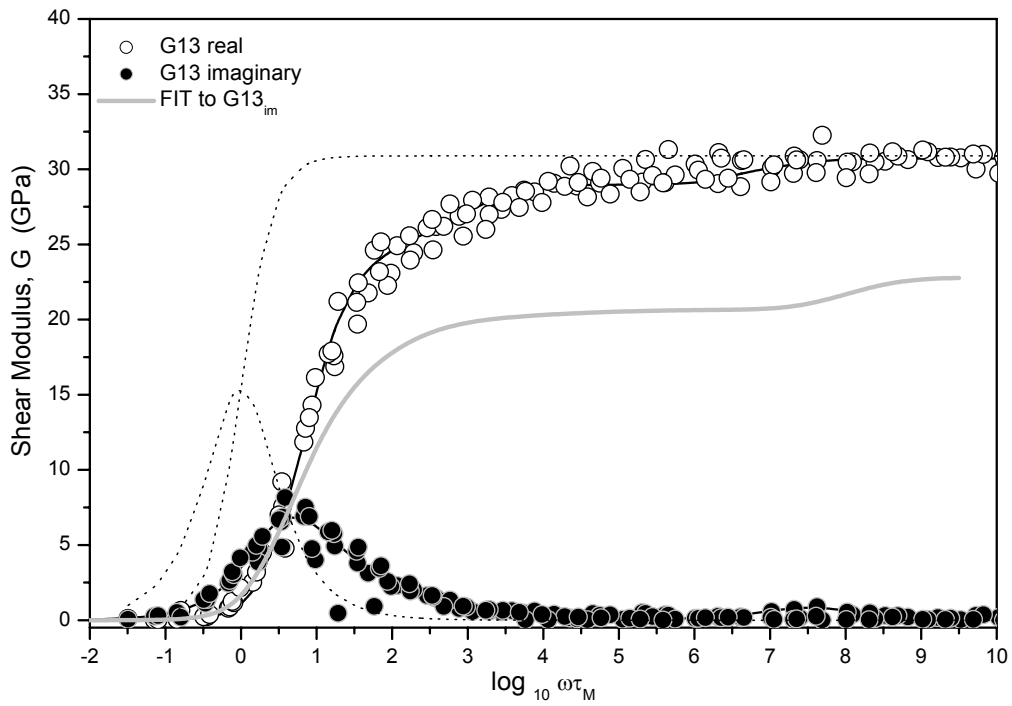


Fig. 67. continuation...



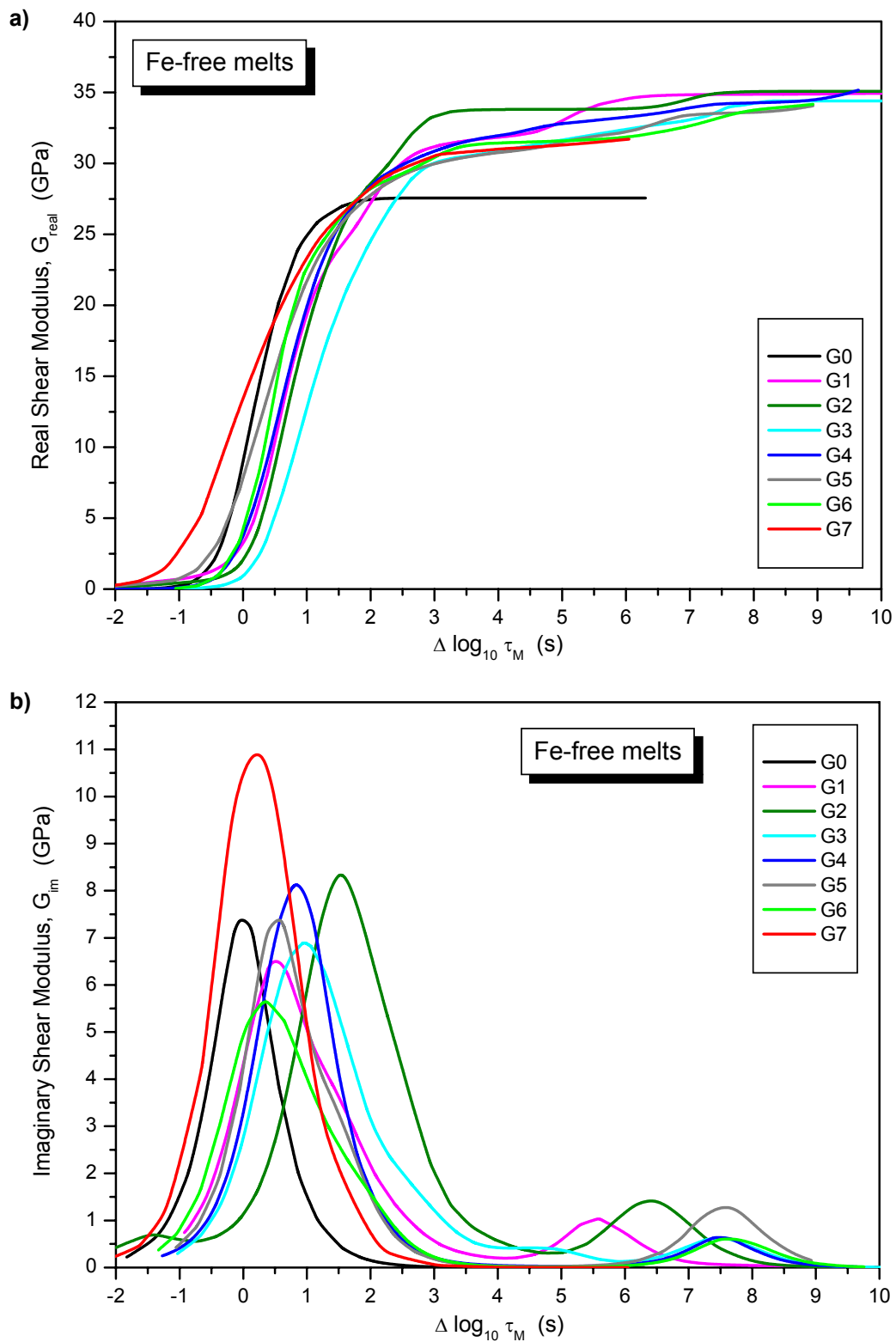


Fig. 68. The fits to the shear modulus data for NS2 (G0) and Fe-free melts (G1-G7), using Eq. 57. **a)** fitted lines for real shear modulus data; **b)** fitted lines for imaginary shear modulus data. See also Appendix 4a,b.

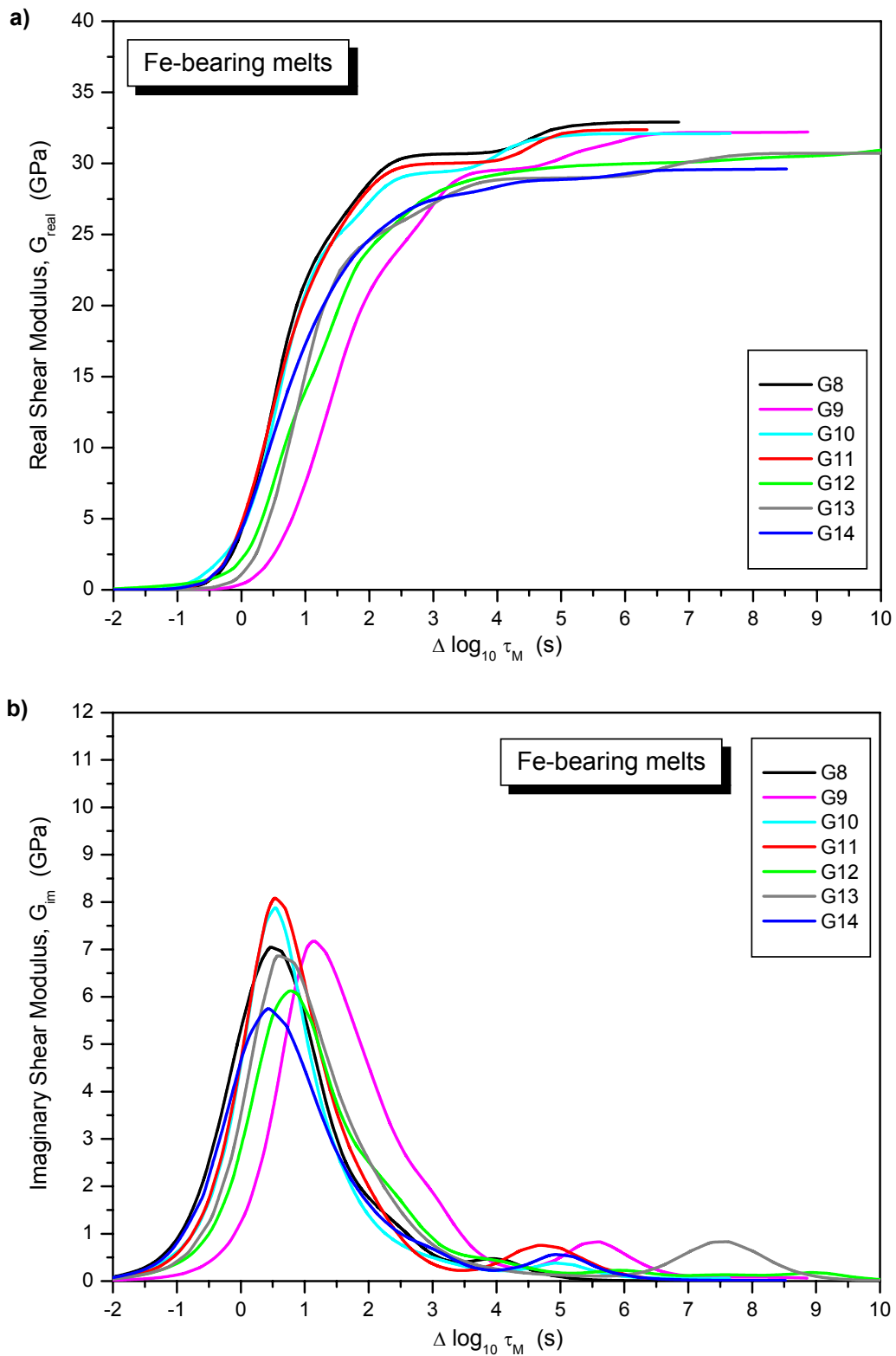


Fig. 69. The fits to the shear modulus data for Fe-bearing melts (G8-G14), using Eq. 57. **a)** fitted lines for real shear modulus data; **b)** fitted lines for imaginary shear modulus data. See also Appendix 4c,d.

Instead of assuming the form of the distribution of relaxation time, the data have been fit by a summation of Eq. 57:

$$G^*(\omega\tau) = \sum_{x=-8.5}^{1.5} G_x^*(\omega\tau \cdot 10^x) \quad (\text{Eq. 58})$$

The real and imaginary parts of the data have been fit separately. The resulting calculated distribution of relaxation time is shown in Figures 70 and 71 and the parameters of the fit are given in Appendix 5a,b.

Table 16 compares the G_∞ values determined at 1 Hz, with the average of the frequency independent G_{av} values determined from the forced oscillation measurements, and the room temperature elastic shear moduli determined on the glasses by ultrasonic methods - G_{ultra} . The G_{av} moduli were determined over the temperature range between lowest measured temperatures up to 500-600°C (depending on the sample) and appear to be frequency independent and shows very little temperature dependence over the 50-200°C (depending on the sample) range of calculation. The values of G_{av} and G_{ultra} are shown in Figure 57a,b as a function of the compositional parameter γ .

Tab. 16. Shear moduli G_{av} and G_∞ from the torsion data together with that determined by ultrasonic techniques at room temperature G_{ultra} .

	Torsion Measurements		Pulse Echo Overlap Technique
	G_{av} (GPa)	G_∞ (GPa)	G_{ultra} (GPa)
G0	27.730 ± 0.278	27.45	29.887 ± 0.232
G1	34.431 ± 0.479	34.26	37.389 ± 0.754
G2	34.663 ± 0.265	34.78	37.842 ± 1.091
G3	34.358 ± 0.402	34.43	38.036 ± 0.147
G4	33.984 ± 0.581	34.23	38.074 ± 0.625
G5	33.863 ± 0.219	34.01	37.122 ± 0.155
G6	33.485 ± 0.349	33.47	36.650 ± 0.191
G7	31.034 ± 0.376	31.68	34.284 ± 0.198
G8	31.998 ± 0.746	32.45	34.228 ± 0.292
G9	32.108 ± 0.636	32.94	34.090 ± 0.129
G10	31.825 ± 0.373	32.20	33.555 ± 0.514
G11	31.775 ± 0.472	32.09	33.540 ± 0.362
G12	31.078 ± 0.292	31.42	32.230 ± 0.274
G13	29.810 ± 0.489	30.89	31.256 ± 0.247
G14	29.261 ± 0.378	29.96	30.938 ± 0.189

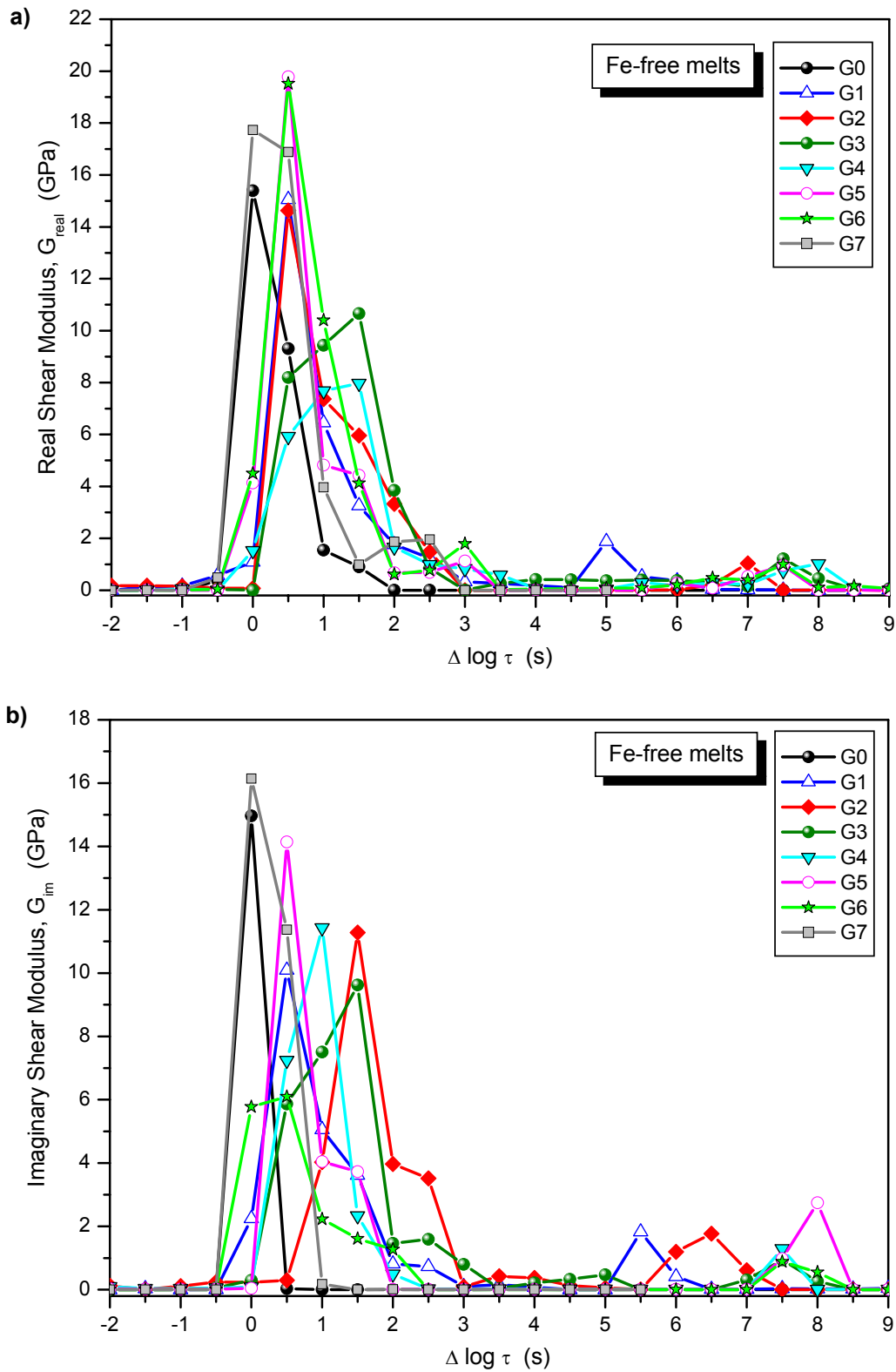


Fig. 70. The distribution of relaxation times for Fe-free samples (G0 and G1-G7) calculated from Eq. 58. The lines on the plot a) are calculated from the real component of the shear modulus, the lines from plot b) show the distributions calculated from the imaginary part of the modulus. The structural relaxation of G7 and G0 is centred on $\Delta \log_{10} \tau \sim 0$, while that of G2 is centred on a timescale 1.5 order of magnitude faster than the Maxwell relaxation time. In all cases, a second relaxation is calculated for relaxation times between ~ 5.5 and ~ 7.5 orders of magnitude faster than the Maxwell relaxation time. See also Appendix 5a.

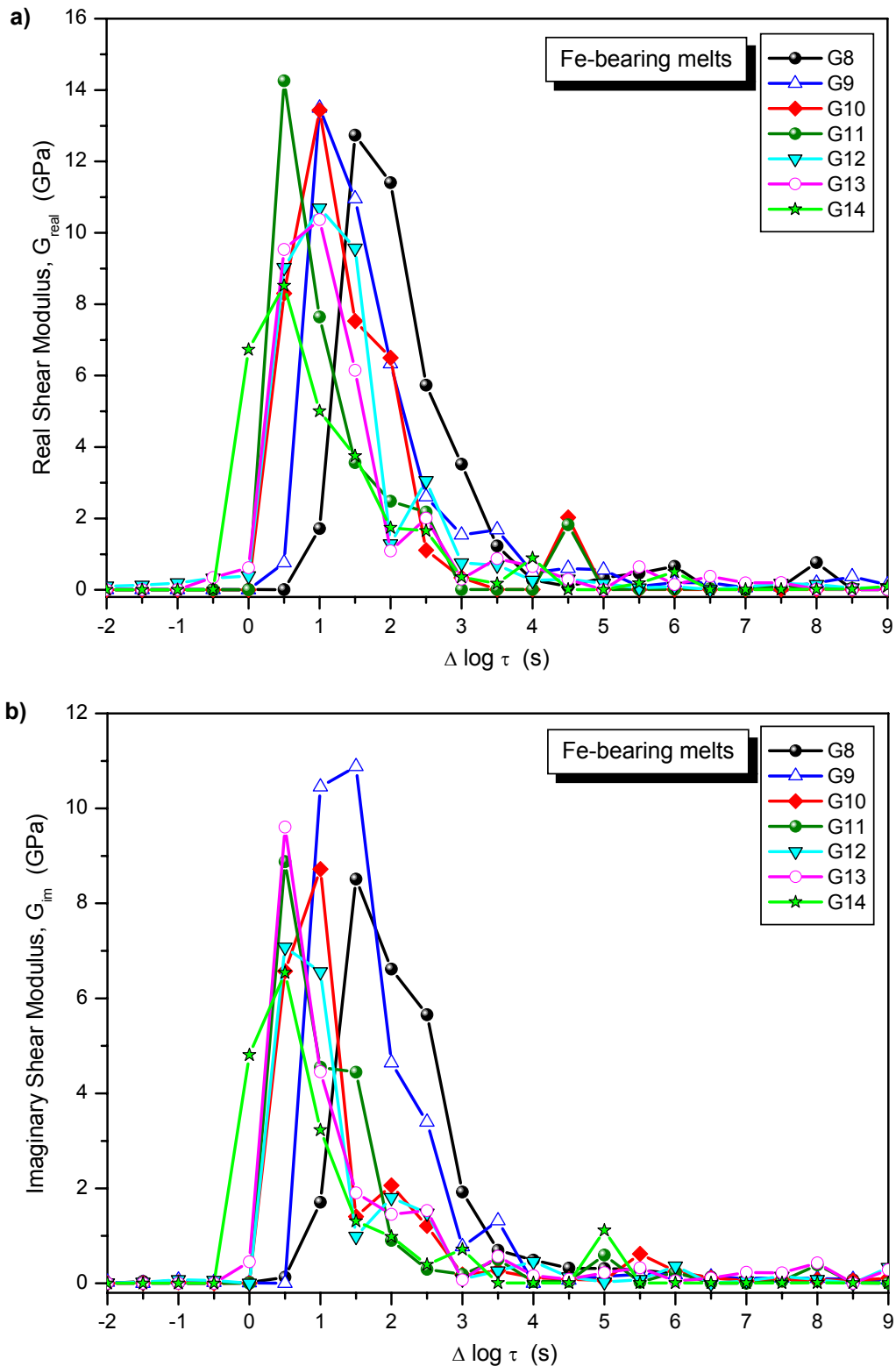


Fig. 71. The distribution of relaxation times for Fe-bearing samples (G8-G14) calculated from Eq. 58. The lines on the plot **a)** are calculated from the real component of the shear modulus, the lines from plot **b)** show the distributions calculated from the imaginary part of the modulus. There is no sample with structural relaxation centred on $\Delta \log_{10} \tau = 0$. The other peaks are centred on a timescale 0.5-1.5 order of magnitude faster than the Maxwell relaxation time. Location of the second relaxation is not clear. See also Appendix 5b.

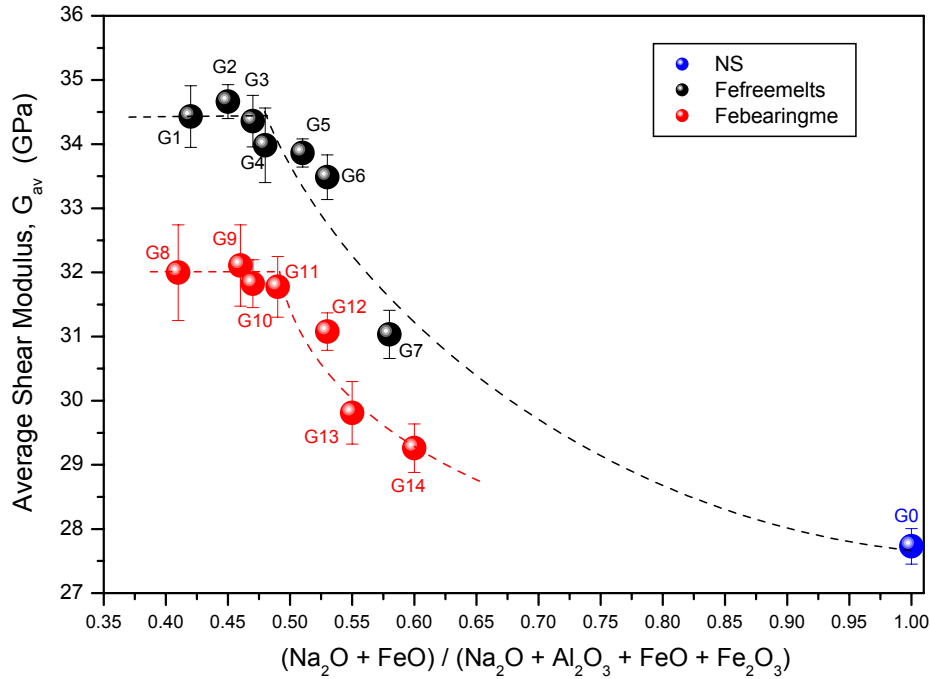


Fig. 72. The average elastic shear moduli as a function of composition – data obtained from torsion apparatus; blue point is for sodium silicate melt NS2 (G0), black points are for data of G_{av} for Fe-free samples (G1-G7), red points – for Fe-bearing melts (G8-G14). The dashed lines are the suggested trends in the data.

Two peaks are observed in the imaginary component of the shear modulus. Both peaks are accompanied by an increase in the real part of the shear modulus. Each peak in the imaginary modulus must be accompanied by an increase in shear modulus. The existence of this second fast relaxation peak is confirmed by the fitting of Eq. 58 independently to the real and imaginary modulus data.

The peak which occurs at the lowest frequencies is the α -relaxation and therefore caused by the loss of energy to the motion of Si and O ions in the melt – the glass transition - which results in the change in shear modulus from 0 to ~35 GPa. The second peak occurs ~5.5-7.5 orders of magnitude faster than the α -peak (depending on the location of α -peak) and is accompanied by a 2-3 GPa increase in the real part of the modulus. There are two energy loss processes (other than that associated with the lifetime of Si-O bonds) expected in these melts – the motion of Al^{3+} ions and the motion of Na^+ ions – see Figure 73.

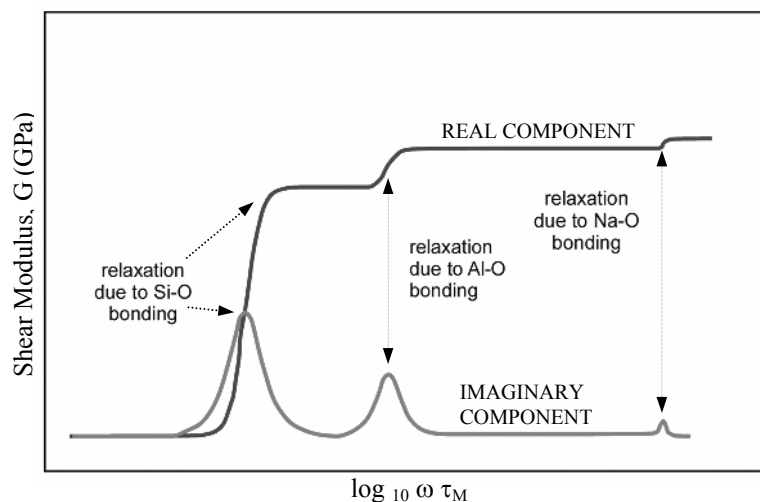


Fig. 73. The known change in modulus with $\omega\tau_M$ for the motion of Si and O atoms in silicate melts together with theoretically expected loss modulus associated with the motion of Al^{3+} and Na^+ atoms in the present melts.

The width of the α -imaginary peak is the same for all the melt compositions with the FWHM (full width at half maximum) for NS2 melt equals 1.13 and the range 1.40-2.68 for G1-G14 (see Table 17) with no clear compositional dependence. However, the position of the peak moves from being centred on τ_M – the Na-rich compositions, to being centred on a timescale 1.5 order of magnitude smaller – the Al-rich compositions.

Such fast relaxation has never been seen before in a silicate melt. The data of Mills (1974), Bagdassarov et al. (1993) and Webb (1992a) all show that the α -peak in silicate melts determined by mechanical spectroscopy is centred on $\log_{10} \omega\tau = 0 \pm 0.5$.

Melt number	FWHM $\log_{10} \omega\tau_M$
G0	1.13
G1	1.90
G2	2.68
G3	1.80
G4	1.40
G5	2.01
G6	1.82
G7	1.52
G8	1.83
G9	1.57
G10	1.67
G11	1.81
G12	1.67
G13	1.69
G14	1.80

Tab. 17. FWHM (full width at half maximum) for α -peak in investigated silicate melts: NS2 (G0), Fe-free (G1-G7) and Fe-bearing (G8-G14)

4.6.2. Comparison of the shear moduli with literature data

Shear modulus data determined in this study can be also compared with data of different silicates.

As seen in Figure 74, the maximum in the imaginary part of the shear modulus of G0 (0.33Na₂O-0.67SiO₂) is centred on log₁₀ ωτ = 0. The data are compared to both the data of Mills (1974) on the same composition at the same deformation frequencies, as well as the theory of Herzfeld & Litovitz (1959) for a melt with a single relaxation time and mechanism. Here, a G_∞ of 27.45 GPa was determined.

Mills (1974) determined G_∞=15 GPa for the same melt composition (see Table 18). The room temperature shear modulus for this melt composition determined by ultrasonic methods is 29.89 GPa, with 24.1 GPa presented in compilation of Ahrens (1995). There is good agreement between the present torsion data and that determination by ultrasonic techniques – for a dG/dT = - 6.9 MPa K⁻¹. (see Table 11, Fig. 57a,b). A dG/dT of -12.0 MPa K⁻¹ is needed to bring Mills' high temperature shear modulus into agreement with the present ultrasonic data. Both of these dG/dT values are reasonable, with values of -7.6MPa K⁻¹ and -10.6 MPa K⁻¹ being found in the literature for 30 and 35 mol% Na₂O glasses (Bansal & Doremus, 1986).

Tab. 18. Shear moduli of melts and glasses measured by different methods and authors.

	Torsion (this study)	Ultrasonic value (this study)	Mills (1974)	Bansal & Doremus (1986)	Ahrens (1995)
(GPa)					
SiO₂			29	31.2 (room temp)	
Borosilicate glass	26.04±1.64 (room temp)	26.37±0.25 (room temp)			
33Na₂O-67SiO₂ (G0)	27.45±2.5 (@400°C)	29.89±0.23 (room temp)	15 (@414°C)		24.1
30Na₂O-70SiO₂				23.80 (room temp)	
35Na₂O-65SiO₂				23.02 (room temp)	
NaAlSi₃O₈					29.2
Na₂Al₂Si₂O₈					30.2

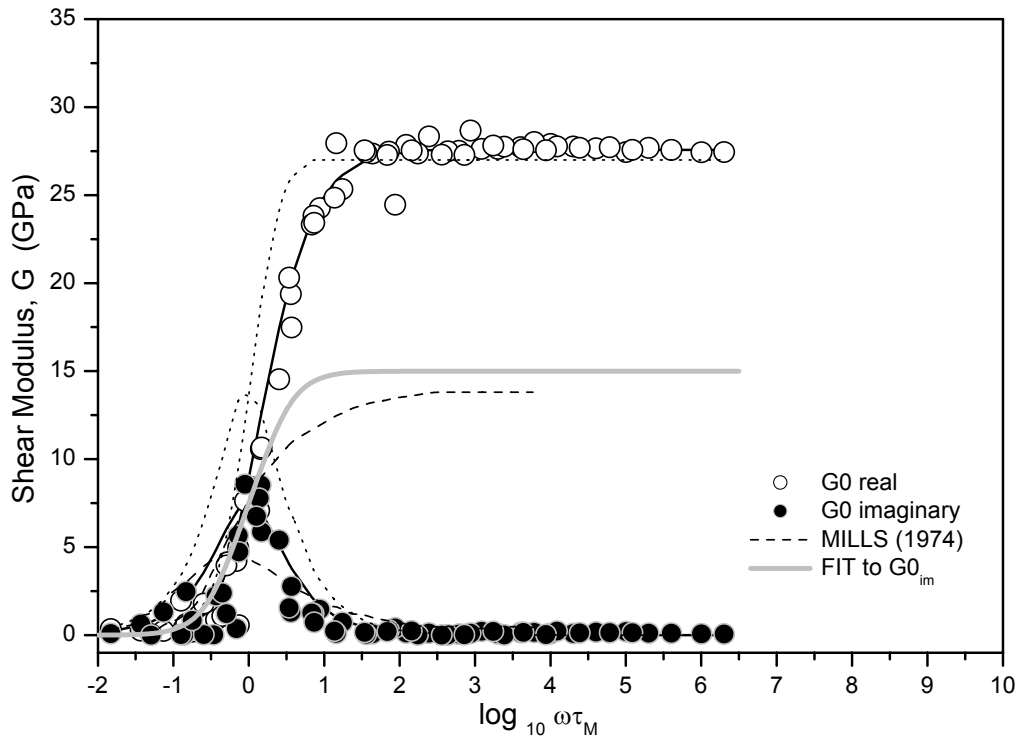


Fig. 74. Frequency dependent real and imaginary components of the shear modulus of $0.33\text{Na}_2\text{O}-0.67\text{SiO}_2$ (NS2, sample G0) The dashed line is the data of Mills (1974) on the same composition; the dotted line of the model of Herzfeld & Litovitz (1959); solid line of the fitting; grey line is fitting to G0 imaginary parameters.

The greatest difficulty in designing a torsion machine is the rigidity of the connection between the torsion rods and the sample. If there is a slippage at this connection, low shear modulus values are measured. In the present work we do not melt the sample directly on the ceramic torsion rods; but use a rhyolite composition melt as glue. The high quality of the bonding between the torsion rods and the melts observed in scanning electron microscope (Fig. 45), together with the similarity between the elastic shear modulus determined by torsion and ultrasonic methods indicate that the low values of elastic shear modulus determined by Mills (1974) are due probably to slippage at the connections between sample and torsion rod. In his experiments, Mills (1974) used clamps between torsion rod and 50 mm long sample. These clamps sat inside his furnace. Mills determined the correct value of shear modulus for SiO_2 melt because this melt was measured as a cylinder 50mm long, which was held by clamps outside the furnace. The only time we get low G values similar to Mills is as the melt is in the process of detaching itself from the rod.

The shear modulus of SiO₂ glass at 27°C is 31.2 GPa (Bansal & Doremus, 1986) (Tab. 18). G at 700°C for a rhyolite composition has been found to be 30.5±2.5 GPa via torsion measurements (Webb, 1992a). Bagdassarov et al. (1993) found G for haplogranitic glasses to vary from 23.90 to 29.61±0.05 GPa at room temperature using ultrasonic techniques to 22.6-26.6±2.2 GPa at temperatures 500-670°C in torsion. Bansal and Doremus (1986) report G for 30Na₂O-70SiO₂ at room temperature of 23.80 GPa and 23.02 GPa for 35Na₂O-65SiO₂. Our value of G_∞ for NS2 (sample G0) equals 27.45 GPa (Tab. 18) is higher than the literature values of 23-24 GPa.

As seen in the Table 16, the G for the present sodium aluminosilicate melts ranges from 31 to 35 GPa. Again these values are slightly higher than the 29-30 GPa in the literature. In addition, the variations in the radius of the ceramic rods may produce as much as ~5% of error in shear modulus.

5. DISCUSSION

5.1. General

Melts present great challenges due to their structural and thermodynamic complexity. With different experimental techniques and measurements it is possible to obtain various properties of glasses and melts which are controlled mostly by composition, but also by pressure, temperature and time. Changes in the physical and thermodynamic properties of melts are caused by rearrangement of the structure as a function of composition, pressure, temperature and time.

In this study melts of only four oxides have been used. The goal of the work was to obtain a good understanding of the relationship between structure and physical properties. There are a large number of studies of the physical properties and structure of silicate glass and melts in the literature. They simply present data without a controlled variation in composition. Here the effect of Al_2O_3 and Fe_2O_3 is investigated in a series of melts with constant SiO_2 content and a controlled variation $\text{Na}_2\text{O}:\text{Al}_2\text{O}_3(\text{Fe}_2\text{O}_3)$ ratio from peralkaline to peraluminous.

An increase of the complexity of the melt structure from only one oxide (SiO_2) towards multioxide compositions allows us to follow the role of each component, what is difficult in very complex systems. The $\text{Na}_2\text{O}-\text{Al}_2\text{O}_3-\text{SiO}_2$ system is very common in both, industry and nature. These three oxides create many natural systems (Neuvill & Mysen, 1996) (i.e. albite, jadeite, nephelinite).

5.2. Density and partial molar volume at room temperature

The densities of the investigated samples (measured at room temperature) decrease in peralkaline melts with increasing Al_2O_3 content. The same trend is observed in Fe-free and Fe-bearing melts (Fig. 54). The breaking point and change of behaviour occurs at $\gamma \sim 0.5$, as the Al_2O_3 content increases in the peraluminous glasses.

In peralkaline melts, an addition of Al_2O_3 to the system $\text{Na}_2\text{O}-\text{SiO}_2$ leads to changes the bond lengths and angles between tetrahedra. In this case not only the bond length between network formers and oxygen changes, but also an intertetrahedral angle network former (T) – oxygen (O) – network former (T) (Taylor & Brown, 1979b; Devine et al., 1987) and its energy (Meagher et al., 1980; Taylor et al., 1980). The Na diffusion channels which exist in sodium silicate melts disappear with increasing Al_2O_3 (Kargl & Meyer, 2004); and Na is used to compensate the negative charge of Al-tetrahedra. Such

rearrangement of the structure results in the decreasing density of the glasses, owing to the building the looser three-dimensional structure.

In peraluminous melt, there is not enough sodium to balance the negative charge of Al-tetrahedra and new structural units are formed, namely triclusters. That causes reduction of the network structure, which becomes denser, and distortions in the structure of tetrahedra. MacDowell & Beall (1969) pointed out, that formation of the triclusters in the melt structure would increase density of the melt. Also Bottinga et al. (1982) indicated high compositional dependence of the density and also viscosity. The authors suggested that changes in the properties of the melt are connected with the changing coordination number of aluminium cation from tetrahedral to octahedral at $\gamma \sim 0.5$, but the percentage of aluminium with new coordination number is not sufficient to change the physical and thermodynamic properties. In this study, this reason was sufficient to assume that triclusters play more important role in the melt structure.

The partial molar volume of the oxides in these glasses has been calculated by a multi-linear regression between mole fraction of the oxide x_i and molar volume of the oxide V_i (see also Tab. 10):

$$V = \sum_i x_i V_i. \quad (\text{Eq. 59})$$

Fits to the molar volume data are presented in the Table 19. Because the very small amount of FeO introduces a large error in this calculation, FeO has been put together with Fe_2O_3 as Fe_2O_3 total. The calculation for each oxide in the glass structure has been separated into four parts:

- (1) for all of the samples with fit $R^2=0.986$. Here one observes that the largest volume units in the melt structure are Al_2O_3 and Fe_2O_3 containing the cations with very high ionisation field strength (Tab. 1) and requiring a charge balancer. The fit parameter for SiO_2 units is always constant and equals $\sim 26 \text{ cm}^3 \text{ mol}^{-1}$;
- (2) for peralkaline composition with fit $R^2=0.989$. The results do not vary significantly from first model;
- (3) for peraluminous composition with fit $R^2=0.957$. Although (3) and (4) are not very different to (1) there is a large variation in Na_2O ;
- (4) for the model assuming the presence of Al_2O_3 in both Al-tetrahedra and triclusters in the peraluminous compositions of the glasses ($R^2=0.987$). Here, there is no large increase in Na_2O partial molar volume and the new structural units (triclusters) take less space in the glass structure than normal Al-tetrahedra. That would explain fast increase in the density with increasing peraluminosity of the glasses, what follows increasing number of triclusters.

Tab. 19. Parameters of the fit to the molar volume data. Calculation has been separated into four models, in which (1) all of the samples have been used, (2) only peralkaline and (3) peraluminous samples and the (4) model including presence of Al_2O_3 in triclusters.

	Partial molar volume ($\text{cm}^3 \text{mol}^{-1}$)			
	all (1)	peralkaline (2)	peraluminous (3)	+ triclusters (4)
SiO₂	27.26 ± 1.67	26.42 ± 5.03	24.81 ± 1.61	26.85 ± 1.71
Al₂O₃	39.01 ± 3.31	41.34 ± 9.75	39.19 ± 2.43	40.41 ± 3.56
Na₂O	20.84 ± 4.03	20.11 ± 10.05	29.57 ± 7.07	19.41 ± 3.47
Fe₂O₃ total	35.34 ± 5.25	39.81 ± 16.85	32.49 ± 3.28	35.29 ± 5.23
Al₂O₃ in triclusters	-	-	-	37.08 ± 3.78
R²	0.986	0.989	0.957	0.987

Comparison of density of the peralkaline melts from this study with other authors (Fig. 55) shows small disagreement, what can be explained by different cooling rates of the glasses. Density depends on a thermal history and especially on quenching rate (Angell, 1981; Angell, 1990). The higher density of the glasses is then caused by lower fictive temperature (Knoche et al., 1994).

5.3. Heat capacity and configurational heat capacity

The heat capacity of glasses is caused by the vibrations between atoms at temperature higher than room temperature (Tangeman & Lange, 1998). With increasing temperature, there are more vibrational modes, what also causes higher heat capacity. The sudden increase in heat capacity just before reaching T_g is explained as a need of additional energy to break the strongest bonds in the melt structure, to change the angles distances between atoms and coordination numbers (Richet & Bottinga, 1995). Above T_g the heat capacity of the liquid becomes constant over the 20°C range of temperature of our measurements.

The configurational state is due to the possibilities of the atoms arrangement over available potential energy minima (Richet & Bottinga, 1995). Increasing temperature produces a heat, which is transformed into the potential energy and atoms are able to reach higher configurational states with higher energy (Fig. 75).

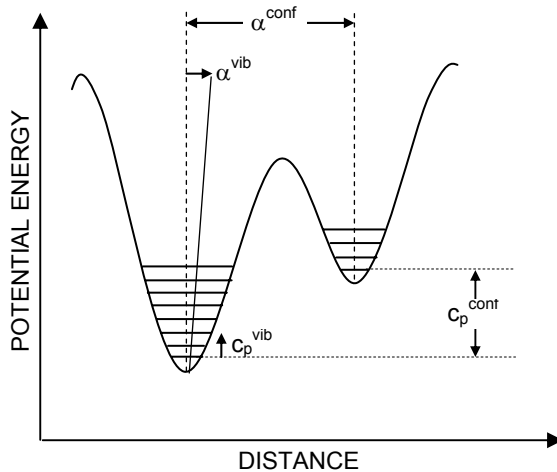


Fig. 75. Schema of the interatomic potentials. Heat capacity consists of vibrational and configurational part. Changes in the interatomic distances between atoms are connected with variations in vibrational and configurational thermal expansion coefficient of the material. Redrawn after Richet & Bottinga, 1995.

Vibrational heat capacity is observed in glasses (below T_g) and glass transition occurs when Dulong – Petit harmonic limit of $3R/g$ atom/K is reached. This kind of heat capacity does not depend strongly from composition (Haggerty et al., 1968; Richet & Bottinga, 1986; Toplis et al., 2001, Roskosz et al., 2004). The compositional dependence is clear above T_g . $3R/g$ atom/K (Fig. 66) introduced by Haggerty et al. (1968) expresses the moment of glass transition in the sample (confirmed by Richet & Bottinga, 1986; Martens et al., 1987).

Configurational heat capacity C_p^{conf} is an energy required for structural changes which are strongly connected with increasing temperature (bond lengths and angles, coordination numbers, distances between atoms). The configurational heat capacity expresses the energy absorbed in reaction to changes of the potential energy, it means of the energy required for structure rearrangement (Simon, 1931; Bernal, 1936).

Configurational heat capacity C_p^{conf} (Tab. 20, Fig. 76) is a difference between heat capacity of the liquid C_{pl} and heat capacity of the glass C_{pg} at T_g (Richet et al., 1986) and has been calculated by Eq. 29, reproduced here: $c_p^{\text{conf}} = c_{pl} - c_{pg}$.

Tab. 20. Table for all of the samples with compositional parameter γ ; heat capacity of the glass c_{pg} and liquid c_{pl} (in $\text{J g}^{-1} \text{K}^{-1}$); configurational heat capacity C_p^{conf} ($\text{J mol}^{-1} \text{K}^{-1}$); parameter of Maier-Kelley equation B_e (kJ mol^{-1}); configurational entropy $S^{\text{conf}}(T)$ ($\text{J mol}^{-1} \text{K}^{-1}$) and parameter $B_e/S^{\text{conf}}(T)$ (10^3K^{-1}).

Melt number	γ	c_{pg} ($\text{J g}^{-1} \text{K}^{-1}$)	c_{pl} ($\text{J g}^{-1} \text{K}^{-1}$)	C_p^{conf} ($\text{J mol}^{-1} \text{K}^{-1}$)	B_e (kJ mol^{-1})	$S^{\text{conf}}(T)$ ($\text{J mol}^{-1} \text{K}^{-1}$)	$B_e/S^{\text{conf}}(T)$ (10^3K)
G0	1.00	1.250	1.450	14.28 \pm 0.42	189.01 \pm 3.93	7.759 \pm 0.172	24.362 \pm 0.523
N33 *	1.00				179.52	7.95	22.572
G1	0.42	1.219	1.370	10.60 \pm 0.42	342.68 \pm 9.84	9.273 \pm 0.292	36.955 \pm 1.112
G2	0.45	1.211	1.356	9.98 \pm 0.45	371.60 \pm 8.38	9.982 \pm 0.239	37.227 \pm 0.866
G3	0.47	1.227	1.366	9.66 \pm 0.47	331.38 \pm 9.02	8.928 \pm 0.258	37.117 \pm 1.041
G4	0.48	1.207	1.366	10.92 \pm 0.48	472.82 \pm 15.77	13.221 \pm 0.462	35.763 \pm 1.221
G5	0.51	1.203	1.340	9.79 \pm 0.51	304.22 \pm 9.69	9.368 \pm 0.316	32.474 \pm 1.065
G6	0.53	1.166	1.310	9.87 \pm 0.53	306.25 \pm 6.43	9.785 \pm 0.220	31.299 \pm 0.680
G7	0.58	1.205	1.355	10.22 \pm 0.58	260.59 \pm 4.88	8.893 \pm 0.176	29.302 \pm 0.565
G8	0.41	1.229	1.403	12.04 \pm 0.41	439.61 \pm 25.71	12.661 \pm 0.795	34.720 \pm 2.105
G9	0.46	1.149	1.290	9.30 \pm 0.46	323.27 \pm 26.03	8.932 \pm 0.744	36.192 \pm 2.964
G10	0.47	1.180	1.290	7.78 \pm 0.47	281.63 \pm 8.62	8.322 \pm 0.269	33.841 \pm 1.065
G11	0.49	1.159	1.296	10.02 \pm 0.49	390.00 \pm 28.11	12.139 \pm 0.941	32.129 \pm 2.403
G12	0.53	1.160	1.290	8.73 \pm 0.53	260.12 \pm 12.45	8.485 \pm 0.430	30.657 \pm 1.511
G13	0.55	1.128	1.280	10.30 \pm 0.55	247.59 \pm 6.41	8.351 \pm 0.228	29.648 \pm 0.789
G14	0.60	1.175	1.340	11.73 \pm 0.60	251.87 \pm 4.93	8.906 \pm 0.188	28.280 \pm 0.576

* sample N33 (compositional equivalent to the sample G0) has been placed in the table to confirm the correctness of the calculation. Data come from Richet (1984).

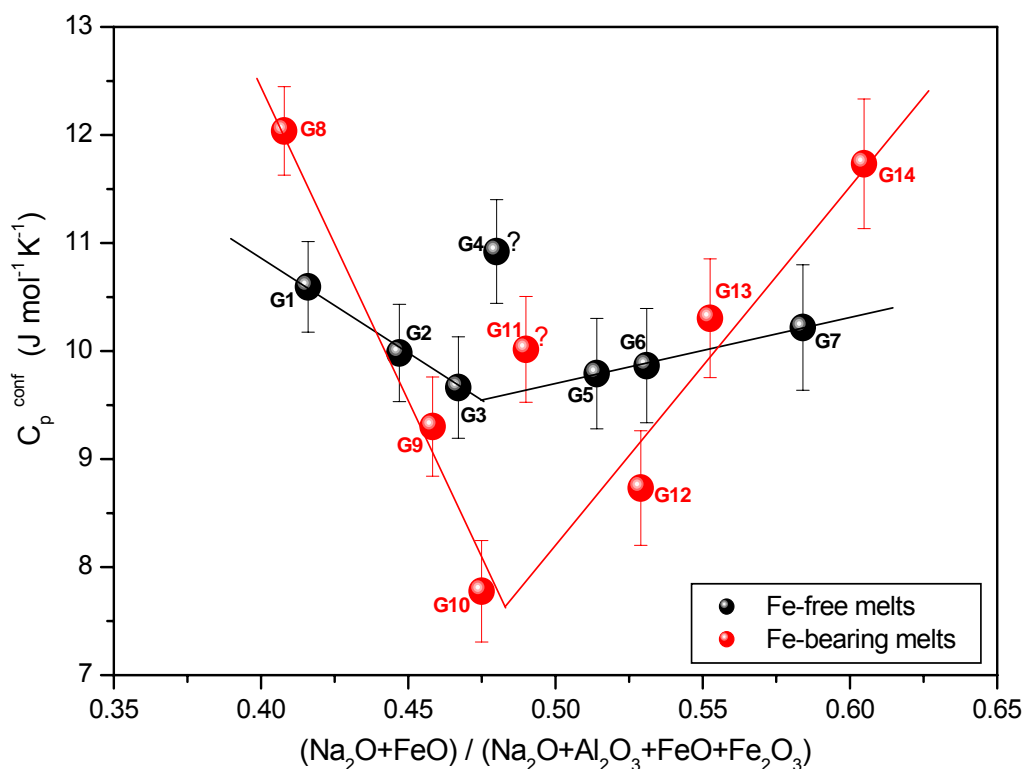


Fig. 76. Configurational heat capacity of the (in $\text{J mol}^{-1} \text{K}^{-1}$) for peralkaline and peraluminous Fe-free (black points) and Fe-bearing (red points) samples as a function of compositional parameter $\gamma = (\text{Na}_2\text{O}+\text{FeO})/(\text{Na}_2\text{O}+\text{Al}_2\text{O}_3+\text{FeO}+\text{Fe}_2\text{O}_3)$. The trends are the guides to the eye.

Figure 76 presents the configurational heat capacity C_p^{conf} (in $\text{J mol}^{-1} \text{K}^{-1}$). The first observation is that trends connecting the data points have deep minimum at $\gamma \sim 0.48$. Addition Al_2O_3 to sodium silicate melts (sample G0) introduces a decrease in the configurational heat capacity because less energy is required for structural rearrangement as Al replaces network modifying Na. At $\gamma \sim 0.48$ C_p^{conf} starts to increase and because of change of structure associated with the formation of triclusters, the more energy is needed for the flow in melt with triclusters. The presence of Fe^{3+} enhanced this effect.

In extreme peraluminous and peralkaline part of the plot the Fe-free melts (G1 and G7) have lower C_p^{conf} than Fe-bearing melts (respectively G8 and G14). For the range $0.43 > \gamma > 0.56$ Fe-free melts have higher configurational heat capacity than Fe-bearing. Samples G4 and G11 are out of the trends. In spite of three repetitions of the measurements for each sample, their location can not be explained. To get satisfactory results one would need to prepare more samples with compositions filling the gap between the melts: G3-G4-G5 and G10-G11-G12.

As a first time the configurational heat capacity data are presented in a controlled series of compositions. In the literature, there exist data only for peralkaline melts (Toplis et al., 2001) and therefore, the breaking point at $\gamma \sim 0.5$ was not presented.

As has been mentioned before (see section 2.3.), in peralkaline range of melts Al is a tetrahedrally coordinated network former. Structure changes in peraluminous melt when Al^{3+} is in excess of Na^+ and there is no more cations to compensate a negative charge of Al-tetrahedra and triclusters are formed. That would explain a change close to the point when $\text{Al} \sim \text{Na}$ ($\gamma \sim 0.5$).

In the case of Fe-bearing peralkaline composition, as a first the complexes with sodium will be formed (NaAl^{4+}) and all Fe^{3+} stays in tetrahedral coordination. Fe^{3+} is then calculated follow the equation: $\text{Fe}^{3+} = (\text{Na}^+) - (\text{Al}^{3+})$. But in peraluminous melts, there is not enough Na to compensate the negative charge of tetrahedra. Al^{3+} and Fe^{3+} stay in tetrahedral coordination and they form triclusters. Weigel et al. (2006) measured that only 5 % of Fe^{3+} changes the coordination number from tetrahedral to octahedral.

5.4. Configurational entropy $S^{conf}(T)$ and B_e parameter

Similar to configurational heat capacity C_p^{conf} , the results of **configurational entropy S^{conf} and B_e parameter have not been shown before in a controlled series of compositions.**

Together with higher energy, the distribution of configurational states occurs, what is measured by configurational entropy S^{conf} (Richet & Bottinga, 1995). The configurational entropy of the melt can be determined e.g. using heat capacity measurements:

$$S^{conf}(T) = S^{conf}(T_g) + \int_{T_g}^T \frac{C_p^{conf}}{T} dT, \quad (\text{Eq. 60})$$

where $S^{conf}(T)$ is constant between 0 K and T_g and $C_p^{conf} = \text{constant}$. $S^{conf}(T_g)$ can be determined from viscosity measurements using the Adam-Gibbs relationship:

$$\eta(T) = \eta_0 \exp\left(\frac{B_e}{T S^{conf}(T)}\right), \quad (\text{Eq. 61})$$

where B_e is a constant (Richet & Neuville, 1992; Toplis, 1998).

Changes in the viscosity and fragility in the investigated melts as a function of composition are connected with changes in configurational parameters. The link between configurational entropy and viscosity lies in Adam – Gibbs theory (Adam & Gibbs, 1965; Richet, 1984; Bottinga & Richet, 1996; Mysen, 1998):

$$\ln \eta = A_c + \frac{B_e}{T S^{conf}(T)} \quad (\text{Eq. 62})$$

(logarithmic form of Eq. 61), where A_c and B_e are constants, independent of temperature, but dependent on composition; and $S^{conf}(T)$ is configurational entropy. This configurational entropy model bonds viscous behaviour of aluminosilicates and their thermodynamic behaviour (Richet & Neuville, 1992; Bottinga, 1994; Mysen, 1995b; Mysen, 1997). Adam – Gibbs theory says that structural relaxation time is function of energy barrier needed to relocate a single silicate unit, and the number of units that must at the same time conquers their energetic barrier to reach a change in configuration (Toplis, 2001).

The height of the peak in the C_p curve (Fig. 66) upon heating can be described as a function of heating and cooling rate in terms of activation energy H , which is found to be identical to that obtained from viscosity measurements (Scherer, 1984; Stevenson et al., 1996); with the structural relaxation time being given by Adam-Gibbs model (Crichton & Moynihan, 1988):

$$\tau_p = \tau_0 \exp\left(\frac{B}{T S^{\text{conf}}(T)}\right). \quad (\text{Eq. 63})$$

The Narayanaswamy model partitions the $B/S^{\text{conf}}(T)$ term into a structure dependent term $(1-x)H$ and a temperature dependent term xH (Wilding et al., 1995; and references therein). Thus the determination of C_p as a function of heating rate can be used to determine changes in melt structure with changing composition as well as the $B/S^{\text{conf}}(T)$ term.

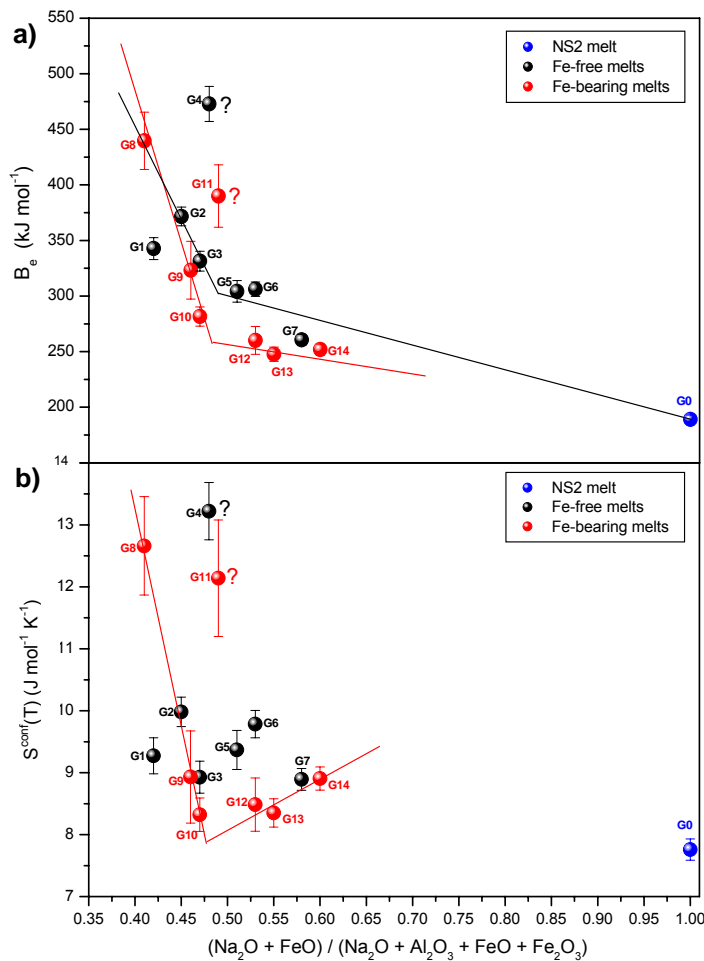


Fig. 77. a) B_e parameter and **b)** configurational entropy $S^{\text{conf}}(T)$ for NS2 (blue point), Fe-free (black points) and Fe-bearing (red points) melts as a function of compositional parameter γ . The trends are the guides to the eye. In the case of Fe-free melts in the plot $S^{\text{conf}}(T)$ vs. composition there is not enough data to support a breaking trend.

How to connect calculated configurational entropy and the structure of the glasses?

The studies of Toplis (1998; 2001) and Russel et al. (2003) (provide an average value of η_0 for silicate melts which allows the calculation of the ratio $B_e/S^{conf}(T)$ and ultimately a calculation of $S^{conf}(T_g)$. $S^{conf}(T_g)$ can be divided into two parts: (1) the topological contribution due to the different bonding within the glass; and (2) the chemical contribution – due to the mixing of different elements on the same structural site (Richet & Neuville, 1992). Both contributions change and new entropies arise.

Similarly, C_p^{conf} is made up of a chemical and topological contribution and can be used to support the interpretation of the variations in $S^{conf}(T)$ with composition. The calculation of $S^{conf}(T)$ as a function of composition will therefore allow discussion of the structure in terms of bonding and site preference of the Al^{3+} and Fe^{3+} atoms. $S^{conf}(T)$ is a measure of the range of structure.

In Figure 77 the B_e parameter (Fig. 77a) and configurational entropy $S^{conf}(T)$ (Fig. 77b) for NS2, Fe-free and Fe-bearing melts as a function of compositional parameter $\gamma = (Na_2O+FeO)/(Na_2O+Al_2O_3+FeO+Fe_2O_3)$ has been presented. B_e is:

$$B_e = \frac{h f}{k_B T}, \quad (\text{Eq. 64})$$

where h is Planck's constant ($6.626068 \cdot 10^{-34} \text{ m}^2 \text{ kg s}^{-1}$), f is frequency, k_B is Boltzmann's constant and T is temperature. B_e was determined analytically from fit to the viscosity curve of the sample which heat capacity is measured (Richet, 1984; Bottinga & Richet, 1996).

B_e is a potential energy barrier to viscous flow and depends on the composition but is assumed to be temperature independent (Toplis, 1998). B_e parameter has been then taken to determine configurational entropy $S^{conf}(T)$ using an Eq. 61 where $\eta(T) = \eta_0 \exp(B_e / S^{conf}(T) T)$. η_0 (marked also as A_0 or A_{VFT} in Eq. 26) is the constant value of viscosity at infinite temperature. In this study this value has been fixed as -2.6 (Toplis, 1998). Choosing another value produces the same trend, just at slightly different absolute values.

The size of the region in the rearranging structure is expressed by the configurational entropy of this region (Adam & Gibbs, 1965). $S^{conf}(T)$ is the sum of the configurational entropy of the smallest rearranging unit occurring in the structure – more precisely: the number of atoms taking part in the viscosity flow (Toplis, 1998; Adam & Gibbs, 1965).

$S^{conf}(T)$ reveals also a temperature dependence. The number of small subsystems increases and as, a consequence, $S^{conf}(T)$ also increases with temperature (Mysen, 1997; Toplis et al., 1997b; Toplis, 1998).

With change of the number of the smallest rearranging unit at glass transition [$Z^*(T_g)$] or height of the average potential energy barrier to viscous flow ($\Delta\mu$), then the ratio $B_e/S^{conf}(T)$ also changes. $B_e/S^{conf}(T)$ relation shows a compositional dependence (Toplis, 1998).

In Figure 77 both B_e and $S^{conf}(T)$ represent the breaking points at $\gamma \sim 0.5$, only in the case of Fe-free melts in the plot $S^{conf}(T)$ vs. composition there is not enough data to support a breaking trend. B_e increases with increasing Al_2O_3 content. In the peralkaline range of composition this increase is small, but in peraluminous melts B_e parameter rises very fast. The breaking point indicates a change in a potential energy barrier to viscous flow, it means that with increasing Al_2O_3 content (close to $\gamma \sim 0.5$) new structure with higher potential energy arises and the flow mechanism is different too.

$S^{conf}(T)$ as a function of composition shows similar behaviour. Together with increasing $S^{conf}(T)$ decreases the size and increases the number of the units causing the rearrangement of the structure. Fe-bearing melts have slightly higher $S^{conf}(T)$ indicating smaller structural units in the network.

Because in the B_e parameter and $S^{conf}(T)$ plots is observed large scatter to describe a structure of the melts is used a ratio $B_e/S^{conf}(T)$. $B_e/S^{conf}(T)$ ratio for the investigated samples as a function of their composition is shown in Figure 78. The trend is exactly the same like on viscosity or shear modulus plot and shows a structural change close to subaluminous point.

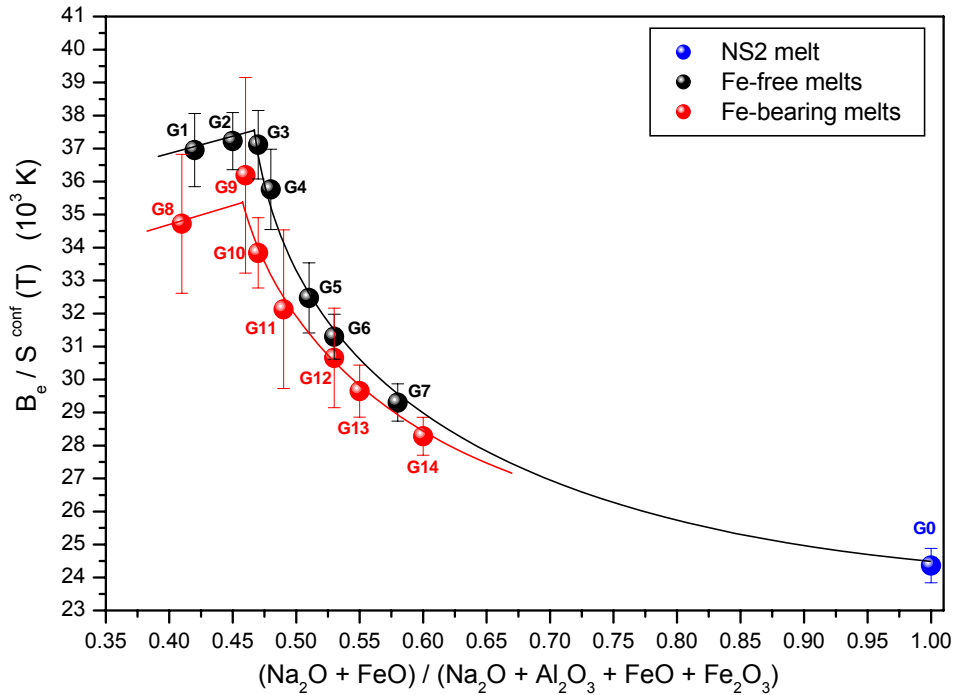


Fig. 78. $B_e/S^{\text{conf}}(T)$ as a function of compositional parameter $\gamma = (\text{Na}_2\text{O}+\text{FeO})/(\text{Na}_2\text{O}+\text{Al}_2\text{O}_3+\text{FeO}+\text{Fe}_2\text{O}_3)$. Blue point is a NS2 melt (G0); black points are for Fe-free melts (G1-G7); red points are for Fe-bearing melts (G8-G14).

5.5. Viscosity and fragility

5.5.1. Viscosity η

Viscosity is temperature and composition dependent (Richet, 1984). The temperature dependence of the viscosity can be discussed using different theories, e.g. (1) Eyring equation (Glasstone et al., 1941), (2) the free volume theory (Cohen & Grest, 1979), (3) Adam – Gibbs theory (Adam & Gibbs, 1965) or (4) the mode coupling theory (Götze, 1991). Description of these theories with regard to the silicate melts viscosity has been done by Bottinga et al. (1995).

In the trend of \log_{10} viscosity as a function of composition (Fig. 60) one observes a clear breaking point at $\gamma \sim 0.47$ for Fe-free melts (in agreement with the viscosity data of Toplis et al., 1997a,b and Webb et al., 2004); and at $\gamma \sim 0.46$ for Fe-bearing melts. For an exact position of the breaking points more compositions are required, especially in the case of Fe-bearing melts.

The viscosity increases from peralkaline composition toward peraluminous with increasing Al_2O_3 and simultaneously decreasing Na_2O . Close to the subaluminous point,

but on the peraluminous side of the composition, the viscosity trend becomes independent on the compositional changes.

In the peralkaline melts amount of Al^{3+} and Fe^{3+} influences the viscosity through the degree of polymerization (Mysen et al., 1985b). The addition of these cations causes an increase of the melt polymerization and following higher viscosity of the peralkaline melts.

Toplis et al. (1997a,b) suggested that maximum in viscosity trends is shifted towards peraluminous composition because triclusters are created before they are necessary and thus some NBOs exist until $\gamma \sim 0.47$. This idea was confirmed with NMR measurements by Stebbins & Xu (1997). It would be explained that not all Na plays a charge balancing role but is still connected with oxygen. Because in the peraluminous composition, there is less Na than Al, then negative charge of Al – tetrahedra needs to be balanced in some different way, does not connected with sodium ions.

Stebbins & Xu (1997) indicated a presence of ~5% NBO on the peraluminous side of the melt composition in anorthite ($\text{CaAl}_2\text{Si}_2\text{O}_8$). That would mean that Al is not connected with charge balancing cations, but built own, fully compensated unit structure, e.g. triclusters.

With increasing amount of Al_2O_3 and Fe_2O_3 degree of polymerization should theoretically increases viscosity, what happens in the peralkaline range of the composition. But despite of higher number of triclusters, nothing like that occurs in the peraluminous melts. Higher peraluminosity does not affect the polymerization of the melt.

Change from tetrahedrally to octahedrally coordinated Al or Fe cations causes an increase the number of NBO and decrease in viscosity (Kozakevitch, 1960; Riebling, 1966; Urbain et al., 1982). Toplis et al. (1997a) did not confirm this theory and says that viscosity of peraluminous melts stays constant. However, the numerous NMR measurements brought an answer, that there is not enough $^{[VI]}\text{Al}$ to influence the viscosity, so any other structural unit which can compensate negative charge of tetrahedra is triclusters. In this study the viscosity trend in peraluminous composition decreases insignificantly with increasing amount of Al_2O_3 .

One observes a decrease in viscosity together with addition to the melt structure the cations with higher electronegativity, what evokes the weakening of network former-oxygen (T-O) bonds and the angle between T-O-T. The viscosity – temperature relationship of these melts increases in order borosilicate < ferrosilicate and galliosilicate < aluminosilicate (Dingwell & Virgo, 1988a). This is consistent with that, what is observed in this study, the Fe-free melts have higher viscosity than Fe-bearing melts.

5.5.2. Frequency dependent shear viscosity $\eta^*(\omega)$ (Pa s) (from torsion)

Viscosity can be also calculated from the torsion data:

$$\eta^*(\omega) = \frac{G^*(\omega)}{i\omega} \quad (\text{Eq. 65})$$

(Webb, 1992a). The real part of the viscosity of each melt is shown in Figure 79 as a function of frequency at each temperature and gathered in the Table 21. The Newtonian viscosity is given by the frequency independent part of the viscosity curve and is calculated at each temperature from the average of the frequency independent data; or where there are not enough data, the Newtonian viscosity is taken to be the lowest frequency datum.

Each of these viscosity data is plotted in Figure 80 as a function of inverse temperature, together with the viscosity data from the micropenetration measurements. The agreement between viscosities determined in the micropenetration and torsion experiments supports the robustness of the torsion $G(\omega)$ data. This illustrates not only that viscosity can be determined from torsion data, but that the temperatures within the two furnaces (micropenetration and torsion) have been calibrated correctly. As the viscosities agree, the temperature calibrations of the two furnaces are correct, and there is no slippage at the torsion rod/melt interface – as also shown from the agreement between the torsion and the ultrasonic shear modulus values.

As the lowest frequency of the torsion measurements is 1 mHz, the highest viscosity expected to be accurately determined is $\sim 10^{13}$ Pa s. Allowing for the distribution in relaxation times; all viscosities $> 10^{15}$ Pa s are not relaxed and therefore slightly lower than the relaxed viscosity (see sample G1 in Figure 79b).

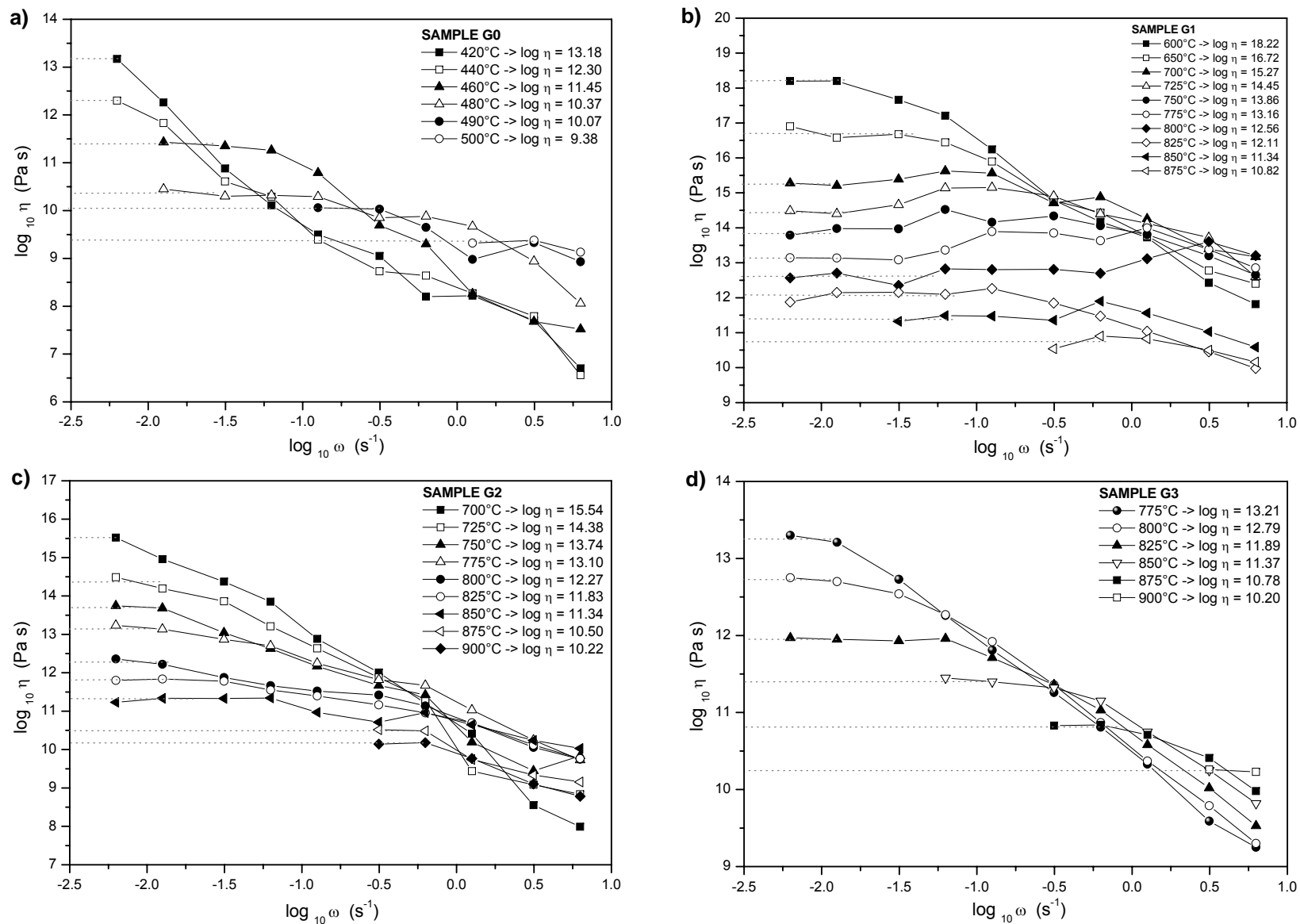


Fig. 79a, b, c, d. Frequency dependent viscosity of the present melts for a range of temperatures. **a)** sample G0; **b)** sample G1; **c)** sample G2; **d)** sample G3.

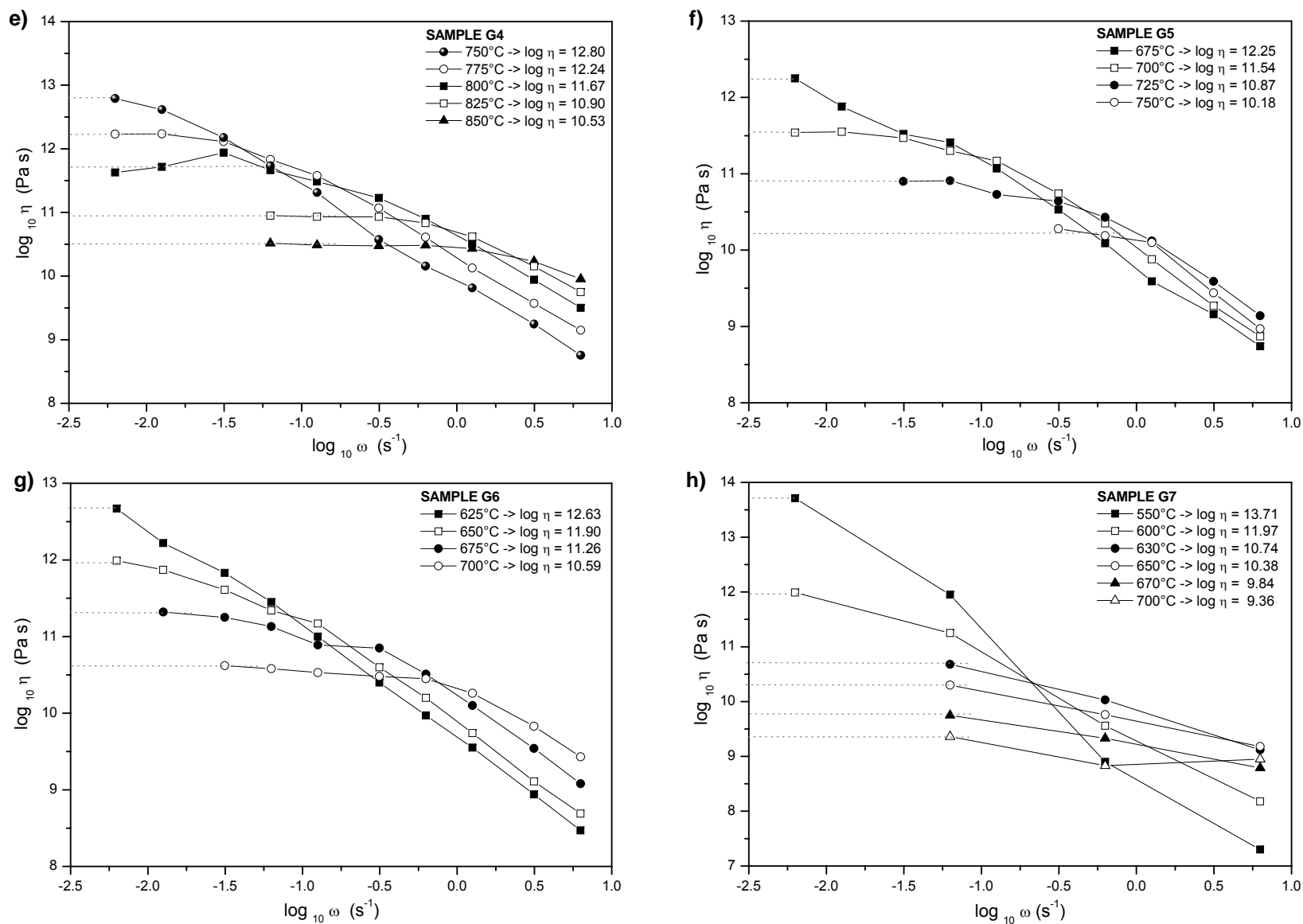


Fig. 79e, f, g, h. Frequency dependent viscosity of the present melts for a range of temperatures. **e)** sample G4; **f)** sample G5; **g)** sample G6; **h)** sample G7.

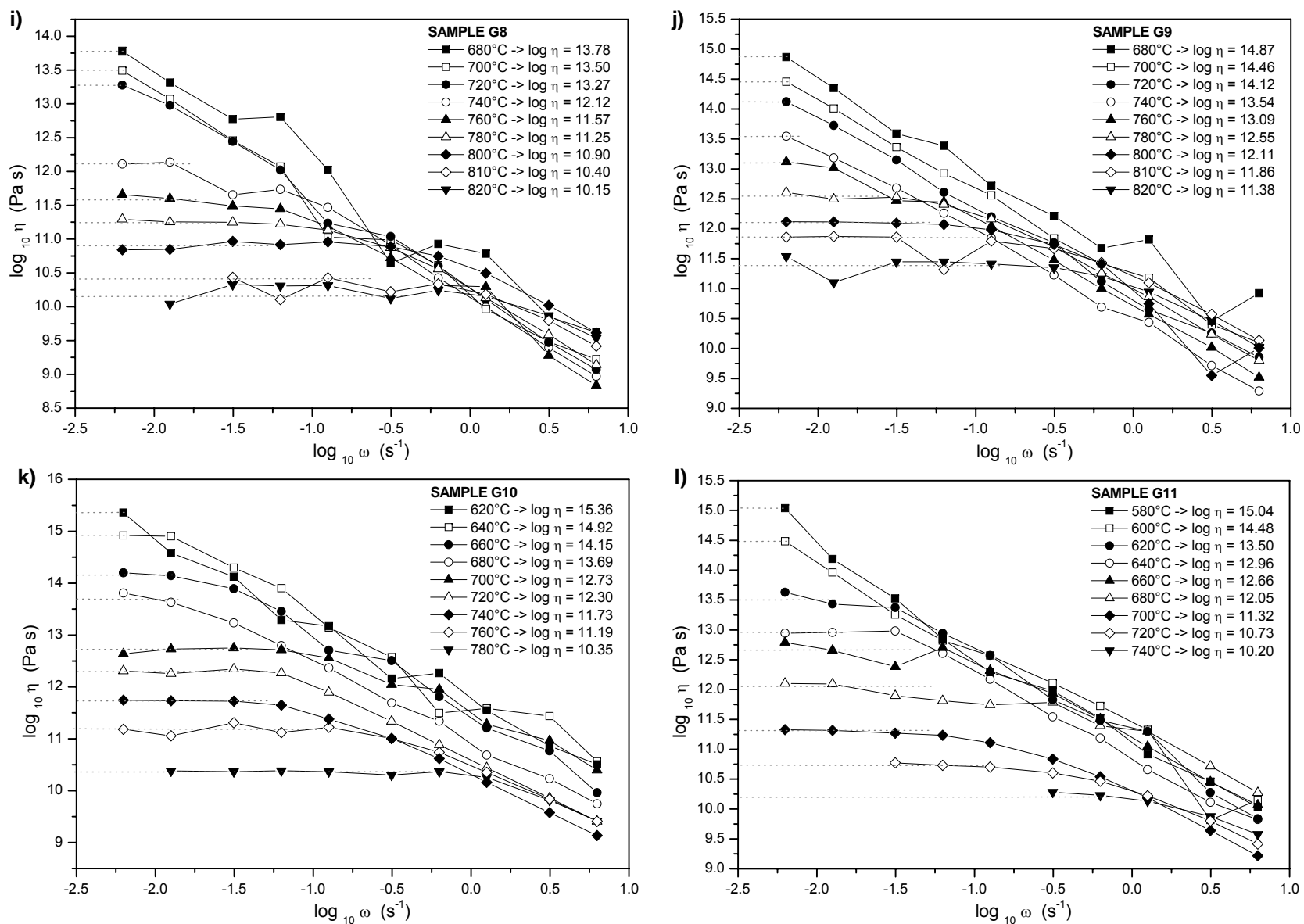


Fig. 79i, j, k, l. Frequency dependent viscosity of the present melts for a range of temperatures. i) sample G8; j) sample G9; k) sample G10; l) sample G11.

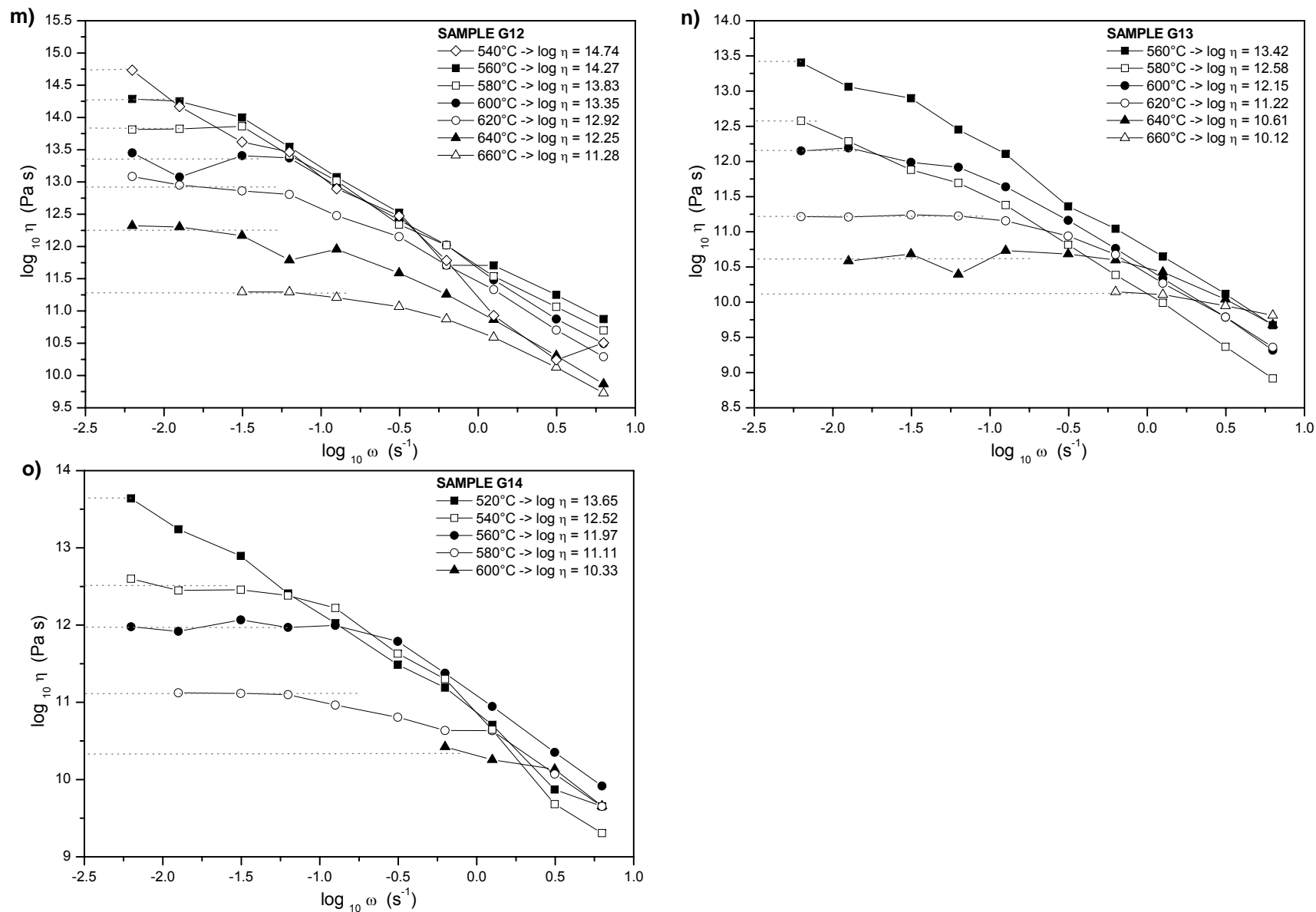


Fig. 79m, n, o. Frequency dependent viscosity of the present melts for a range of temperatures. m) sample G12; n) sample G13; o) sample G14.

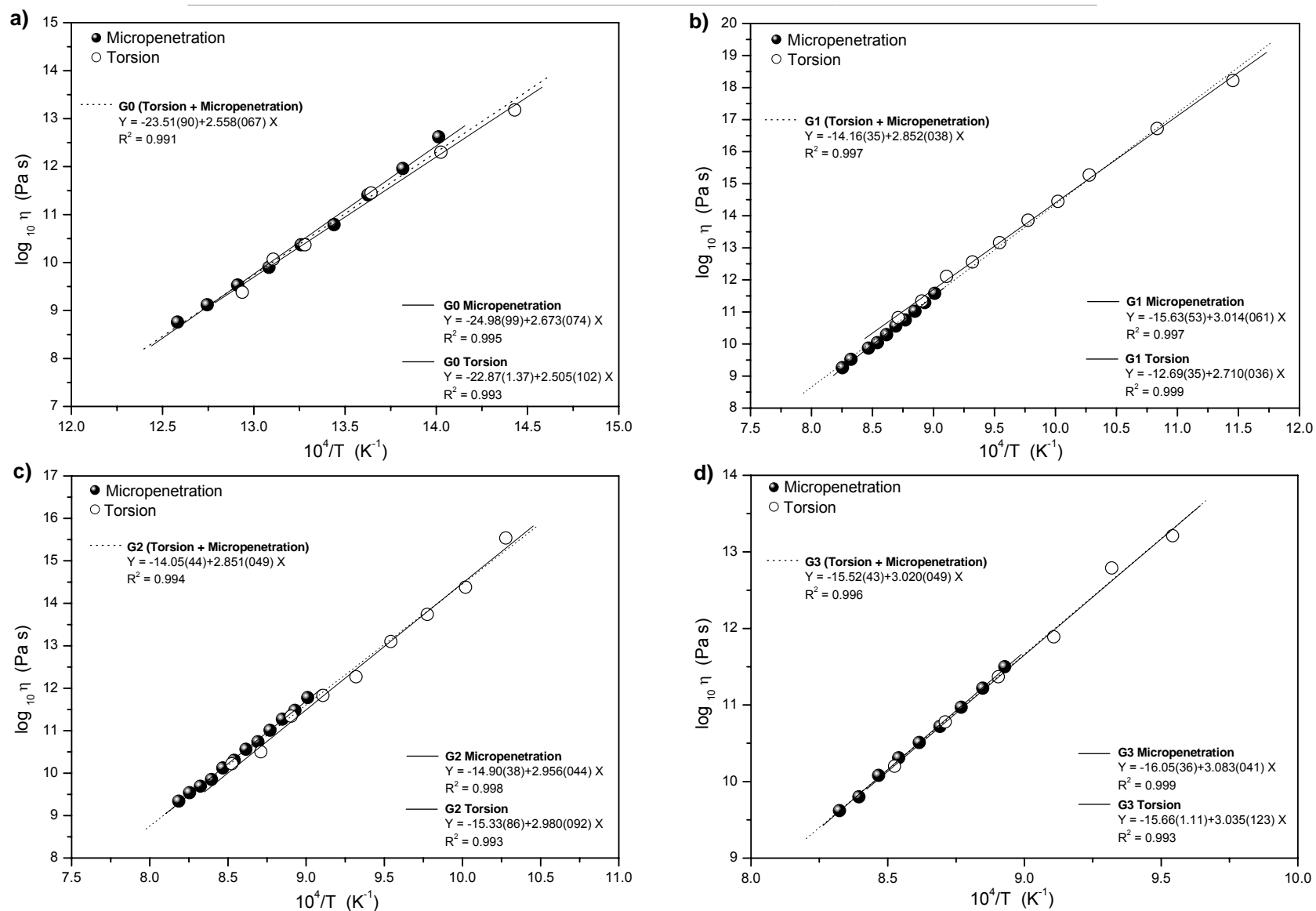


Fig. 80a, b, c, d. Viscosity determined by micropenetration and torsion as a function of inverse temperature. The two sets of viscosity data lie on the same Arrhenian line. **a)** sample G0; **b)** sample G1; **c)** sample G2; **d)** sample G3.

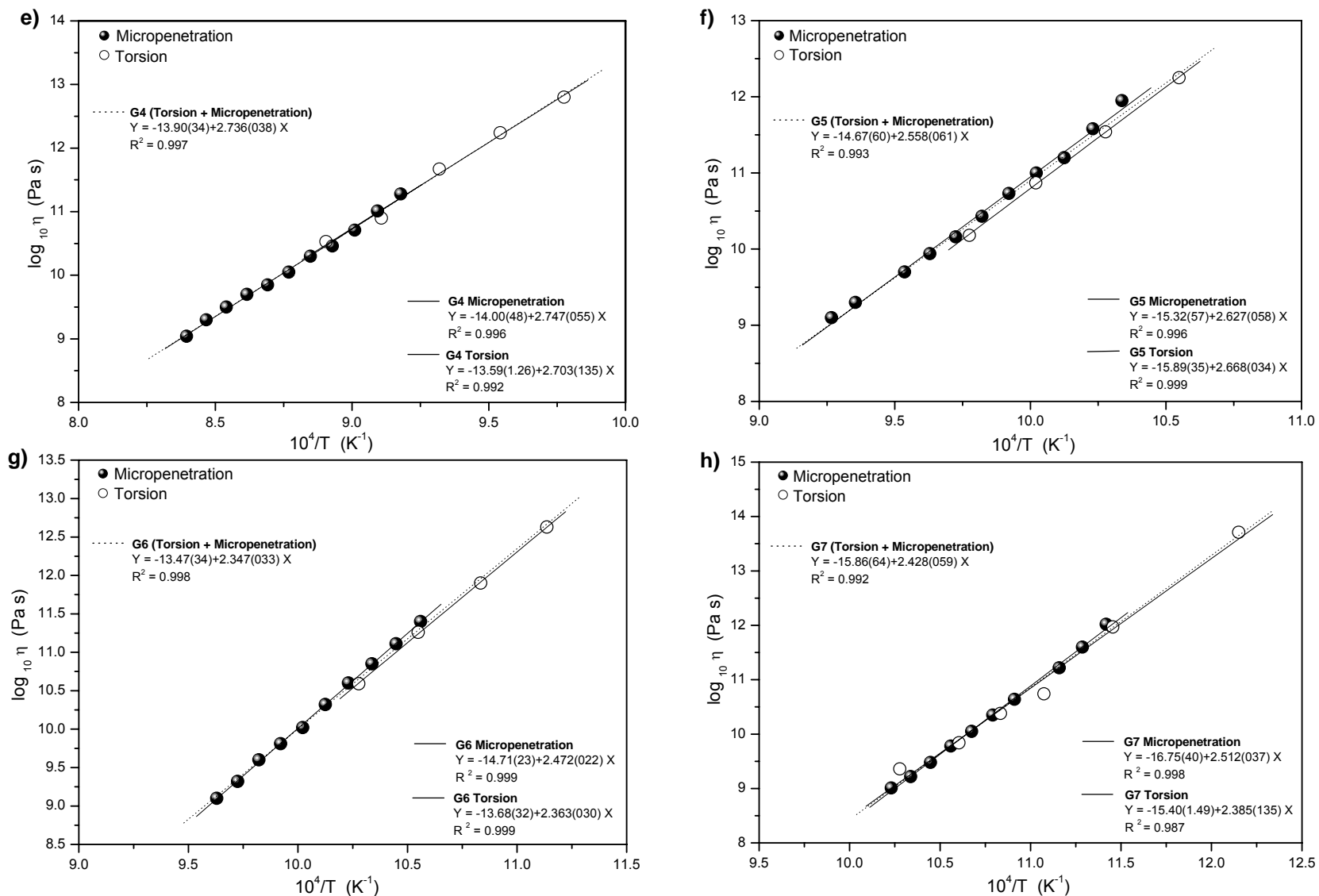


Fig. 80e, f, g, h. Viscosity determined by micropenetration and torsion as a function of inverse temperature. The two sets of viscosity data lie on the same Arrhenian line. **e)** sample G4; **f)** sample G5; **g)** sample G6; **h)** sample G7.

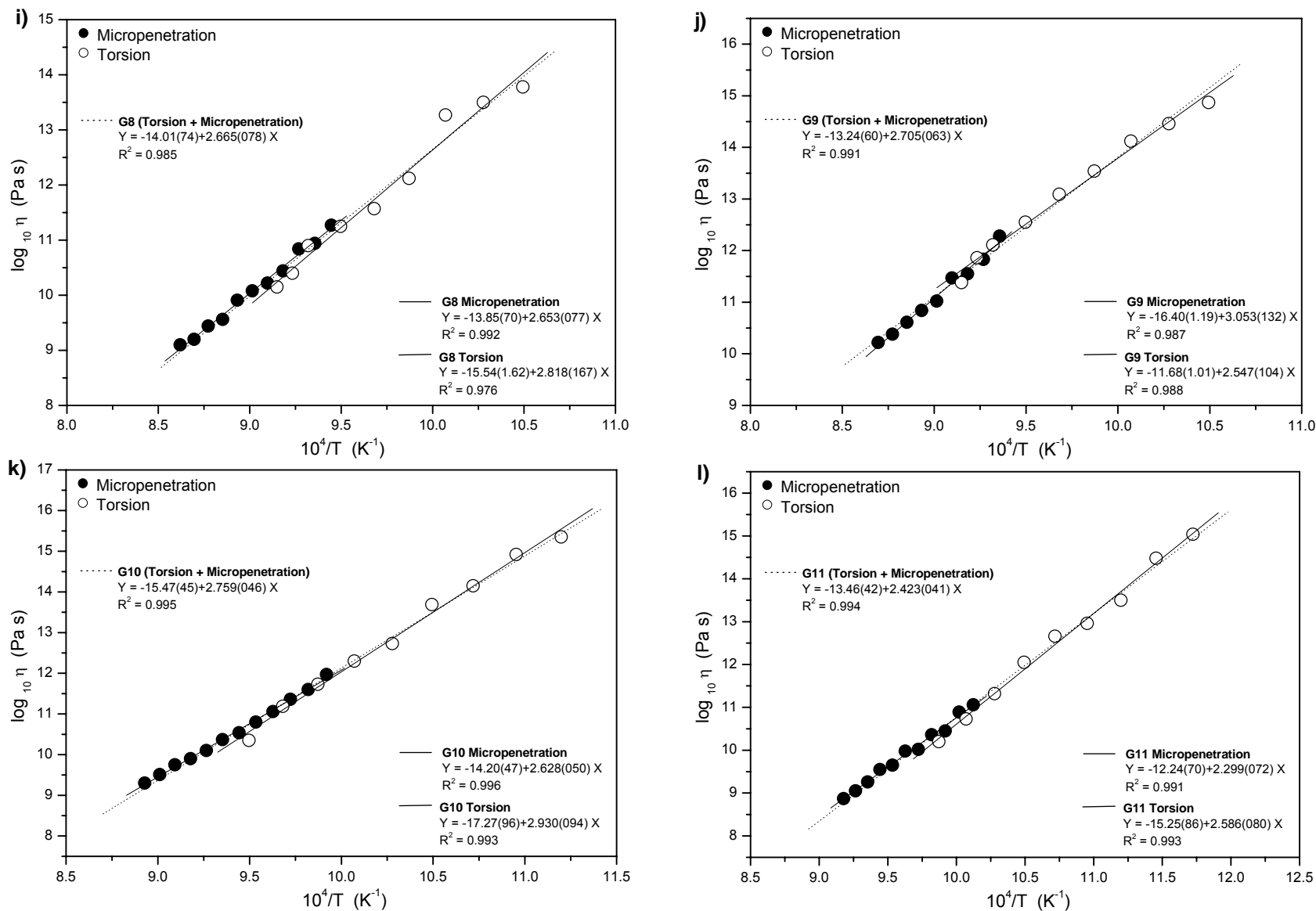


Fig. 80i, j, k, l. Viscosity determined by micropenetration and torsion as a function of inverse temperature. The two sets of viscosity data lie on the same Arrhenius line. **i)** sample G8; **j)** sample G9; **k)** sample G10; **l)** sample G11.

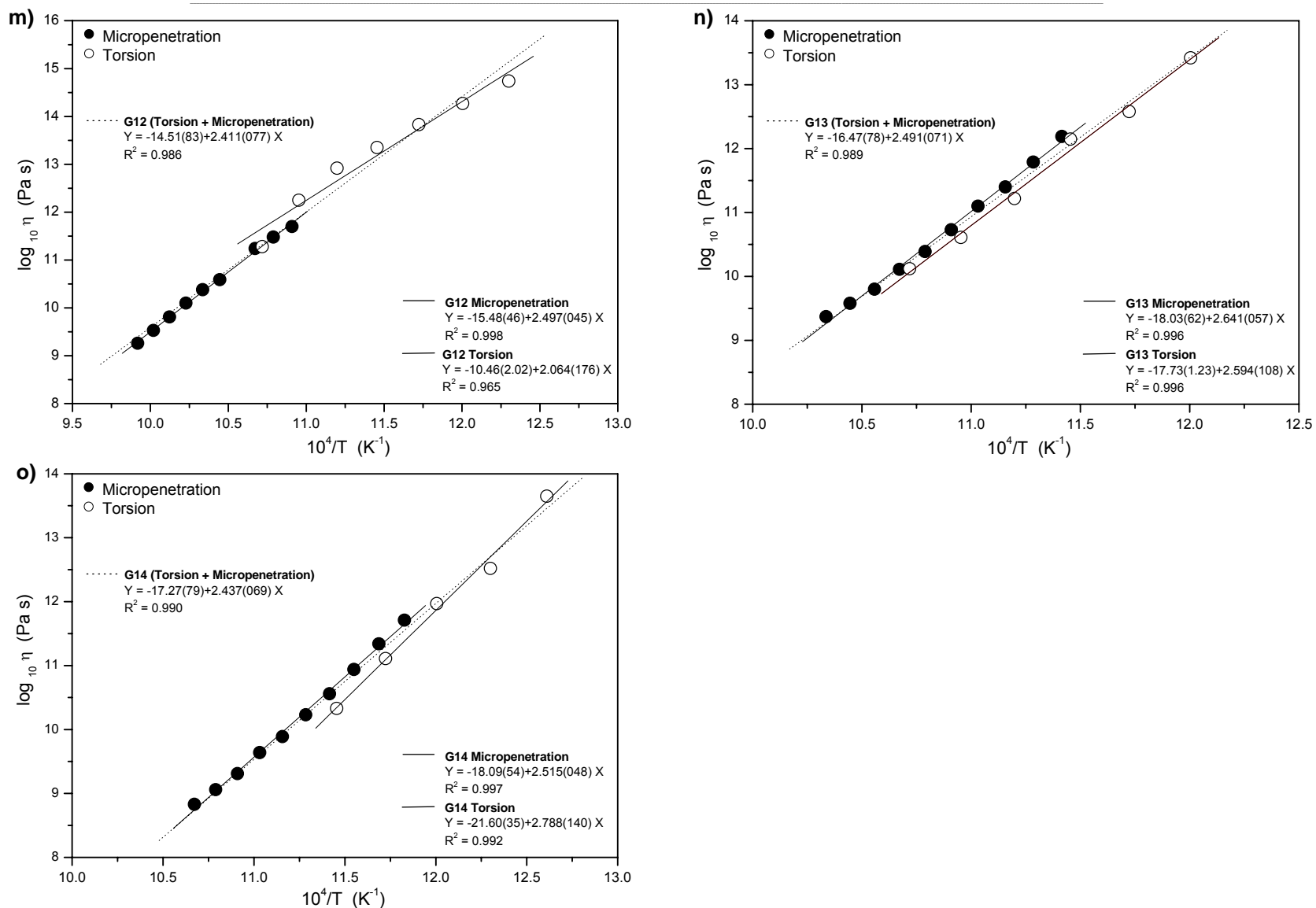


Fig. 80m, n, o. Viscosity determined by micropenetration and torsion as a function of inverse temperature. The two sets of viscosity data lie on the same Arrhenian line. **m)** sample G12; **n)** sample G13; **o)** sample G14.

Tab. 21. Shear viscosity data calculated from torsion data for NS2 melt (G0), Fe-free melts (G1-G7) and Fe-bearing melts (G8-G14) as a function of temperature (presented also in Figure 79).

G0		G1		G2		G3		G4	
T °C	η \log_{10} Pa s	T °C	η \log_{10} Pa s	T °C	η \log_{10} Pa s	T °C	η \log_{10} Pa s	T °C	η \log_{10} Pa s
500	9.38	875	10.82	900	10.22	900	10.20	850	10.53
490	10.07	850	11.34	875	10.50	875	10.78	825	10.90
480	10.37	825	12.11	850	11.34	850	11.37	800	11.67
460	11.45	800	12.56	825	11.83	825	11.89	775	12.24
440	12.30	775	13.16	800	12.27	800	12.79	750	12.80
420	13.18	750	13.86	775	13.10	775	13.21		
		725	14.45	750	13.74				
		700	15.27	725	14.38				
		650	16.72	700	15.54				
		600	18.22						

G5		G6		G7		G8		G9	
T °C	η \log_{10} Pa s	T °C	η \log_{10} Pa s	T °C	η \log_{10} Pa s	T °C	η \log_{10} Pa s	T °C	η \log_{10} Pa s
750	10.18	700	10.59	700	9.36	820	10.15	820	11.38
725	10.87	675	11.26	670	9.84	810	10.40	810	11.86
700	11.54	650	11.90	650	10.38	800	10.90	800	12.11
675	12.25	625	12.63	630	10.74	780	11.25	780	12.55
				600	11.97	760	11.57	760	13.09
				550	13.71	740	12.12	740	13.54
						720	13.27	720	14.12
						700	13.50	700	14.46
						680	13.78	680	14.87

G10		G11		G12		G13		G14	
T °C	η \log_{10} Pa s	T °C	η \log_{10} Pa s	T °C	η \log_{10} Pa s	T °C	η \log_{10} Pa s	T °C	η \log_{10} Pa s
780	10.35	740	10.20	660	11.28	660	10.12	600	10.33
760	11.19	720	10.73	640	12.25	640	10.61	580	11.11
740	11.73	700	11.32	620	12.92	620	11.22	560	11.97
720	12.30	680	12.05	600	13.35	600	12.15	540	12.52
700	12.73	660	12.66	580	13.83	580	12.58	520	13.65
680	13.69	640	12.96	560	14.27	560	13.42		
660	14.15	620	13.50	540	14.74				
640	14.92	600	14.48						
620	15.36	580	15.04						

The agreement between viscosity determined using these two techniques also supports the shift in relaxation times to shorter values being real and not due to errors. The torsion data for stress, strain and strain-rate are correctly measured, as are the temperatures of the furnace. It also proved that there is no slippage on the surface between sample and alumina rod in torsion machine.

5.5.3. Fragility

Fragility (m) is the one parameter used to describe melts (Angell, 1988; Plazek & Ngai, 1991; Böhmer & Angell, 1992). It is not a structural parameter but describes the curvature of viscosity trends. Because the curvature of viscosity data as a function of inverse temperature can be different depending on the composition of the melt, the fragility value describes the shape of the $\log_{10}\eta$ viscosity line as a function of inverse temperature. The widely accepted method to calculate fragility is the gradient of $\log_{10}\eta$ as a function of reduced temperature T_g/T at T_g (Toplis et al., 1997b; Casalini & Roland, 2005; Webb, 2005):

$$\text{fragility} = m = \left. \frac{d(\log_{10} \eta)}{d(T_g/T)} \right|_{T=T_g} \quad (\text{Eq. 66})$$

where T_g is the temperature at which $\eta = 10^{12}$ Pa s; and is the glass transition temperature. Value $m \sim 50$ indicates a fragile melt and shows the highest curvature of the viscosity plot (Fig. 81). Value $m \sim 16$ is almost a straight line and is characteristic for strong melts (SiO_2 -rich). Strong melts agree with Arrhenian equation (Eq. 24), whereas “fragile” have characteristic non-Arrhenian behaviour (Angell, 1988).

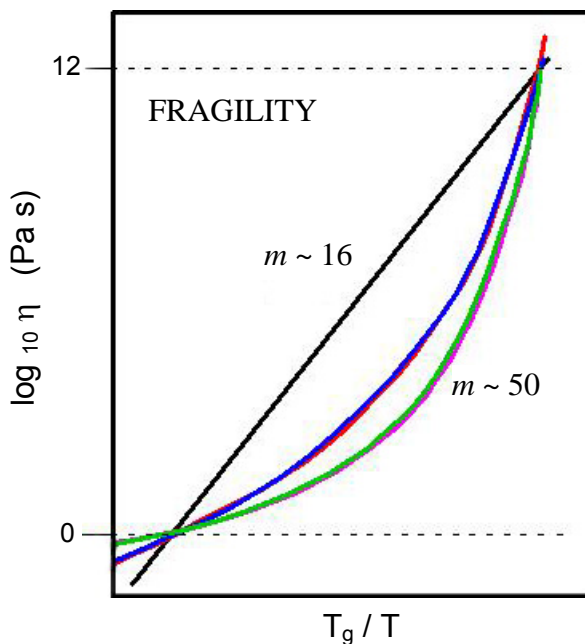


Fig. 81. Fragility of the melts characterised by the curvature of the viscosity plot as a function of reduced temperature.

For the investigated melts fragility has been calculated from the gradient of the viscosity curve at the glass transition temperature using the equation:

$$\text{fragility} = m = \frac{B \cdot 10^4}{T_g^{12}}, \quad (\text{Eq. 67})$$

where B (in K) is the parameter of Arrhenian equation (see Eq. 24) and T_g^{12} (in K) is the temperature, at which the \log_{10} viscosity equals 12 (Toplis et al., 1997b). Data were presented in the Table 22 and showed in Figure 82. Fragility for sodium silicate melt (sample G0) is 36.98 and this is the most fragile sample of all of them. There is clear minimum in the fragility of the Fe-free and Fe-bearing melts at $\gamma \sim 0.49$ indicating some “stronger” than others behaviour of the samples.

Tab. 22. Fragility of the investigated samples calculated using Eq. 67.

Melt number	FRAGILITY m
G0	36.98
G1	27.63
G2	26.90
G3	28.05
G4	26.02
G5	27.32
G6	26.70
G7	28.75
G8	25.85
G9	28.40
G10	26.20
G11	24.24
G12	27.48
G13	30.04
G14	30.10

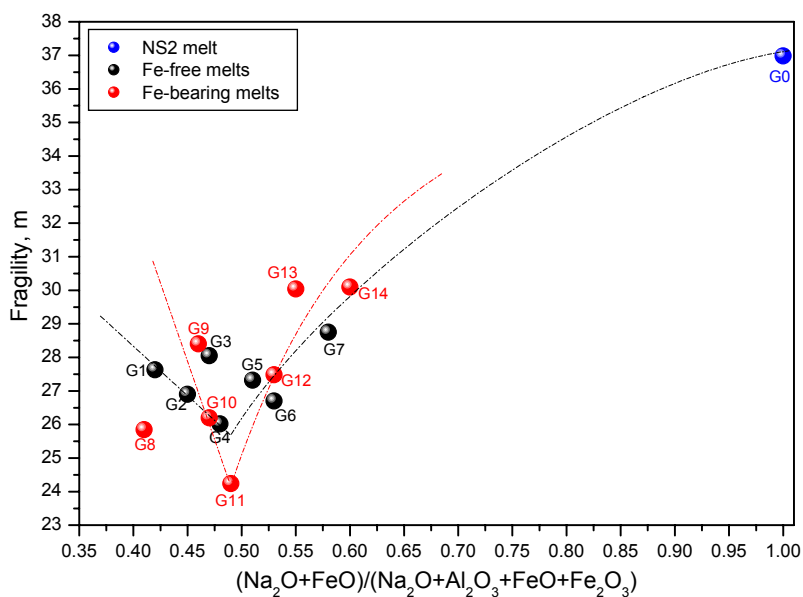


Fig. 82. Fragility of the investigated samples calculated from Eq. 67. The trends are the guides to the eye. Sample G8 lies outside the trend because contain less iron than the others.

5.6. Shear modulus

5.6.1. General

The major observation from the relaxation times of the frequency dependent shear modulus data obtained in this study is that the most of the relaxation times of the samples deviate from Maxwell relaxation time and they are up to 1.3 orders of magnitude faster than Maxwell theory assumes (Fig. 83).

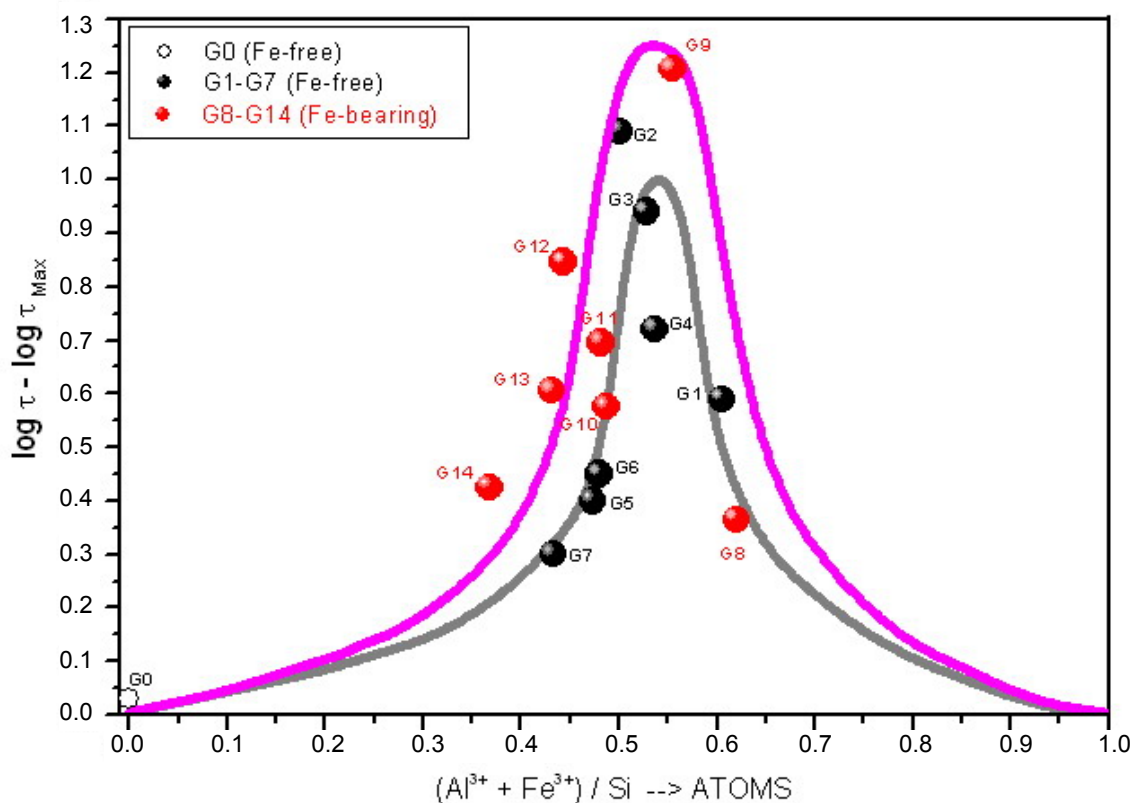


Fig. 83. Deviation of the relaxation times as a function of composition for all of the investigated samples. Sample G8 has only 1mol% Fe_2O_3 , otherwise it will crystallize.

The second major observation is the presence of a second energy loss peak occurring for different samples from ~ 5.5 to ~ 7.5 orders of magnitude faster than the slowest relaxation (Fig. 84).

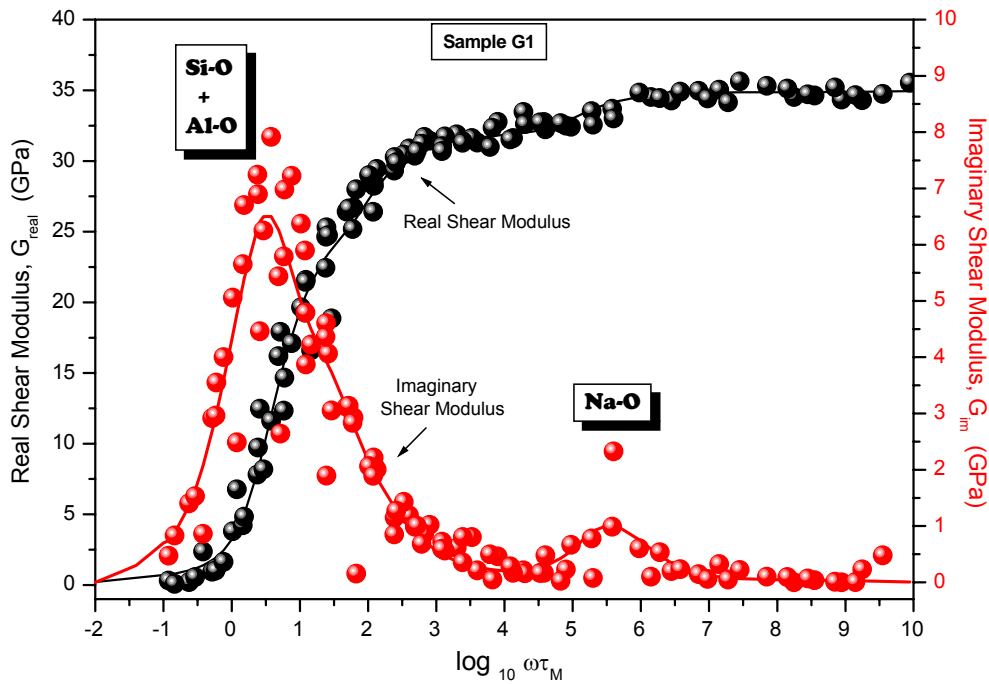


Fig. 84. The real and imaginary components of the shear modulus of G1 – the most peraluminous Fe-free melt composition – as a function of $\log_{10}\omega\tau$. Two peaks in the imaginary shear modulus are observable.

The first question is whether this relaxation faster than Maxwell relaxation time is real. To answer this, the temperature of the furnace was checked and controlled through whole time of the measurements. It needs to be mentioned that $\sim 30^\circ\text{C}$ increase in temperature is equivalent to 1 order of magnitude decrease in viscosity – and therefore also in relaxation time (Webb, 1992b). The torsion furnace has been calibrated and there is a $\pm 3^\circ\text{C}$ temperature variation across the 30 mm of the sample.

If there were a temperature variations during the measurement, the curves as a function of $\log_{10}\omega\tau$ would not be smooth. A further check was the successful comparison of the torsion viscosity with the micropenetration viscosity.

All of the frequency dependent data in Figures 68 and 69 show that a distribution in relaxation timescales is required to describe the observed frequency dependence of the shear modulus. The torsion measurements provide not only the shear modulus, but also the shear viscosity as a function of deformation frequency;

$$\eta = \frac{\sigma}{\dot{\varepsilon}} = \frac{G^*(\omega)}{i\omega} \quad \text{as} \quad G = \frac{\sigma}{\dot{\varepsilon}} \quad (\text{Eq. 68})$$

The shear viscosity determined from torsion data is presented in Figures 79 and 80. In Figure 79, at constant temperature the real component of the shear viscosity increases together with decreasing frequency and becomes independent when it reaches

a relaxed Newtonian viscosity. The value of relaxed Newtonian viscosity from torsion machine should agree with the viscosity obtained at the same temperature with micropenetration technique. As can be observed in Figure 80, the results from both methods are identical. It confirms again that results of faster relaxation time from torsion machine are not due to the error during the measurements.

5.6.2. Diffusion

Of the three peaks expected in the imaginary part of the mechanical spectrum, only 2 are seen (Fig. 84). The second, fast structural relaxation is assumed to be associated with the diffusion of Na^+ in the melt. Given the relatively successful use of the Eyring relationship:

$$D = \frac{k T}{\lambda \eta} \quad (\text{Eq. 69})$$

for diffusivity – D (as a transport property), Boltzmann's constant – k , temperature T , viscosity η , and jump distance λ , there is a relationship between the timescale of diffusion of Si and O and of viscous flow (e.g. Glasstone et al., 1941; Magaritz & Hofmann, 1978; Watson, 1979; Dunn, 1982; Shimizu & Kushiro, 1984; Mysen, 1995b; Reid et al., 2001).

In the calculation the relationship between diffusion, viscosity and relaxation time the other equation are also used. The Stokes equation connects diffusion coefficient D , rigid spheres of radius a and the viscosity of the melt η :

$$D = \frac{k T}{6 \pi a \eta}. \quad (\text{Eq. 70})$$

In the diffusion calculation this equation is combined very often with Einstein – Smoluchowski equation (Farnan & Stebbins, 1990b; Stebbins et al., 1995), which is the relationship between relaxation time τ , diffusion coefficient D and average jump distance d (taken as 0.31nm):

$$D = \frac{d^2}{6 \tau}. \quad (\text{Eq. 71})$$

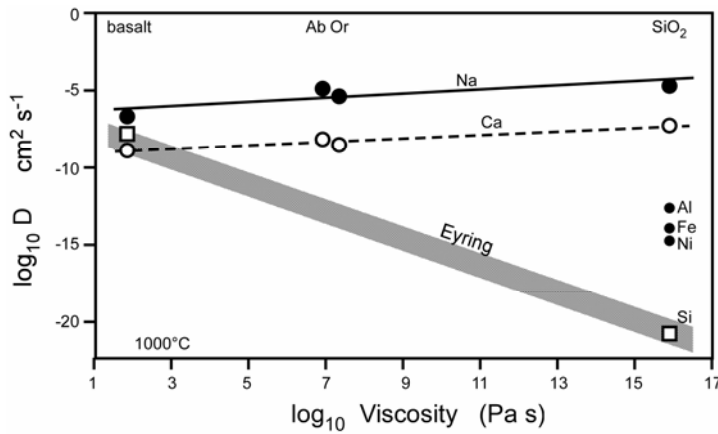


Fig. 85. Na, Ca, Al, Fe, Ni and Si tracer diffusivity data as a function of \log_{10} viscosity (Pa s) for basalt, Ca-Al-Si synthetic oxide melt, albite and orthoclase melts, and SiO₂ melt at 1000°C. Redrawn from Dingwell & Webb, 1990.

The compilation of diffusivity data in Dingwell & Webb (1990) (Fig. 85) illustrate the diffusion rate of Na⁺ approaches that of Si and O in silicate melts at high temperature (low viscosities); but at viscosities of $\sim 10^{12}$ Pa s, the diffusivity of Na⁺ is 12 orders of magnitude faster than that of Si and O for a Na₂O-Al₂O₃-SiO₂ and also for a Na₂O-SiO₂ melt.

The diffusion data of Mungall et al. (1998) (Fig. 86) indicate a ~ 5 -7 orders of magnitude difference between the lifetime of a Na-O bond and a Si-O bond. This indicates that the fast relaxation seen in our measurements is due to Na⁺ diffusion (see also Day & Rindone, 1962).

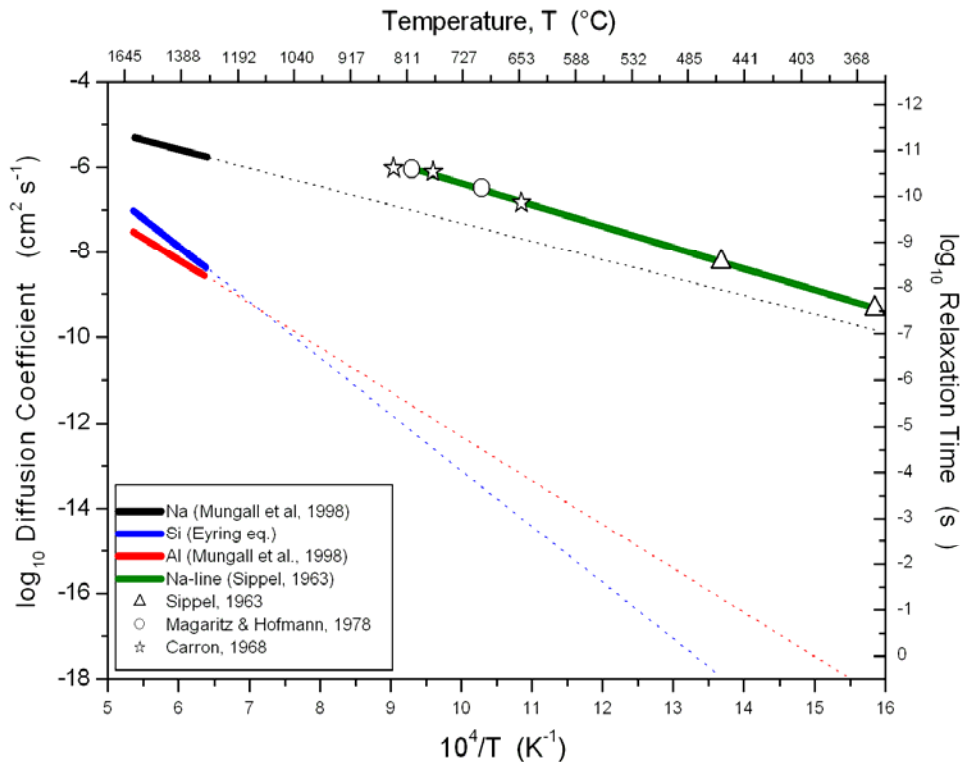


Fig. 86. Diffusivity data for Al, Si and Na in a water-bearing haplogranitic melt (Mungall et al., 1998) – thick black, blue and red lines. These data are extrapolated in temperature to the conditions of the present torsion measurements in order to calculate the timescale of structural motion associated with the diffusion of each of these species. The thick green line shows Na diffusion data in obsidian.

The bonds of the Na with BO are weaker than bonds Na-NBO (George & Stebbins, 1996). From this reason Na can be more mobile and more ionic in the complex melts than in the binary silicates what was suggested by Hsieh et al. (1994) and Lam et al. (1980) with an X-ray photoelectron spectroscopy. Ionicity of sodium can also change the potential barriers to Na motion (Marchi et al., 1988). But the movement of this fast peak to slower times with increasing Al-content (see Fig. 87) agrees with the observations of Kargl & Meyer (2004), who showed that an increase of the amount of Al in the melt composition causes a decrease in sodium mobility and relaxation time of the Na-O bonds becomes slower (peak shifts to the left) (Fig. 87). Such observation is visible in the investigated melts. This further supports our identification of this peak as the Na peak. β -relaxation peak moves at about 2 orders of magnitude with increasing Al_2O_3 content from 15.9 mol% (sample G6) to 19.9 mol% (sample G1) in Fe-free melts. In Fe-bearing melt this correlation is difficult to do.

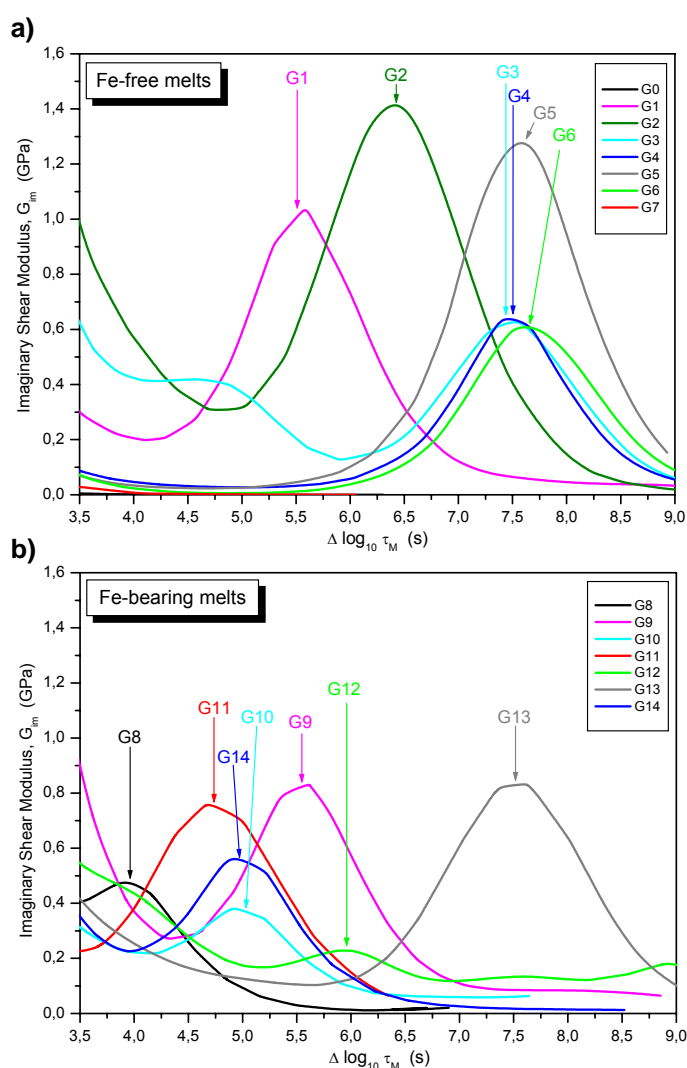


Fig. 87. Shift of the β – relaxation toward slower relaxation time with increasing Al_2O_3 content. **a)** Fe-free melts; there is not enough data for sample G7 to indicate a β -relaxation peak; **b)** Fe-bearing melts.

The expected Al^{3+} -O relaxation peak cannot be resolved in our spectra. The data from Figure 85 as well as the extrapolated diffusion data from Mungall et al (1998) for Al^{3+} diffusion in $\text{Na}_2\text{O-Al}_2\text{O}_3\text{-SiO}_2$ and $\text{Na}_2\text{O-K}_2\text{O-Al}_2\text{O}_3\text{-SiO}_2\text{-H}_2\text{O}$ melts respectively (Fig. 86), suggest that the timescale of Al^{3+} diffusion is close to that of Si and O diffusion at the temperature and viscosity conditions of our measurements. Thus it appears that the Al^{3+} -O peak is part of the Si-O peak (Fig. 86). These two peaks together appear as a broad peak in the imaginary data resulting in the calculation of a distribution of relaxation times. Although there is a large amount of scatter in the FWHM data for these imaginary peaks, the FWHM for $\text{Na}_2\text{O-SiO}_2$ melt (1.13) is much less than that for the Al_2O_3 -bearing melts (1.40-2.68). This supports the conclusion that the Si-O and Al-O peaks form one peak.

It can be seen from the frequency dependence of the shear modulus that the glass transition does not occur at the $\omega\tau_M = 1$ condition as expected from Maxwell theory and the model of Herzfeld & Litovitz (1959). This is in contrast to all of the literature data which shows that the large peak in the imaginary part of the shear modulus is centred on $\omega\tau_M \sim 1$ (see Mills, 1974; Webb, 1991; Bagdassarov et al., 1993). The HPG8 melts of Bagdassarov et al. (1993) with $\text{Al/Si}^{\text{atom}}=0.20$ and $\gamma=0.53$ have structural relaxation times ranging from $3\tau_M$ (for HPG8) to $\sim 0.8\tau_M$ (for HPG8+fluorine). The natural obsidian of Webb (1992a) has a relaxation time $\sim \tau_M$ with $\text{Al/Si}^{\text{atom}}=0.20$ and $\gamma=0.54$. However, the data for the $\text{Na}_2\text{O-SiO}_2$ melt do have the maximum in the imaginary part at $\omega\tau_M=1$. The only difference between the $\text{Na}_2\text{O-SiO}_2$ and the $\text{Na}_2\text{O-Al}_2\text{O}_3\text{-SiO}_2$ melts is the presence of Al_2O_3 . The majority of melts whose structural relaxation time has been compared to the Maxwell relationship have been Al_2O_3 -free or -poor. The present melts have $\text{Al/Si}^{\text{atom}}=0.43$ for the peralkaline melts ($\gamma=0.58$) to $\text{Al/Si}^{\text{atom}}=0.60$ for the peraluminous melts ($\gamma=0.42$).

Thus, instead of the data expected (see Fig. 49) it appears that there is no separate energy loss peak for the lifetime of Al-O bonds. Rather this peak is combined into the Si-O peak. Also FWHM of the slowest peak remains independent of composition.

It is assumed that the Si-O is the longest lived bond in silicate melts, although this was determined on Al-free melts. The Al-O lifetime is therefore shorter than Si-O lifetime, but Mungall's plot (Fig. 86) begins to question this assumption. The relative lifetimes of Si-O and Al-O bonds will be further discussed in section 5.8.

Thus one can begin to interpret the data in Figures 67, 68, 69, 70 and 71. The first energy loss peak is assumed to be associated not only with the lifetime of Si-O bonds, but also of Al-O bonds, with the slightly faster moving Al; and thus creating a faster structural relaxation time than that calculated from the Maxwell equation which assumes a simple mono-structural melt. The second energy loss peak is then associated with the motion of Na in the melt.

The data of Stebbins & Sen (1998) (for borosilicate glass-forming liquid) show that the lifetime of Si-O bonds is not always identified with viscosity. They found the long lived B-O bonds to control flow and determine viscosity; with the shorter lived Si-O bonds forming the β -relaxation (Fig. 88).

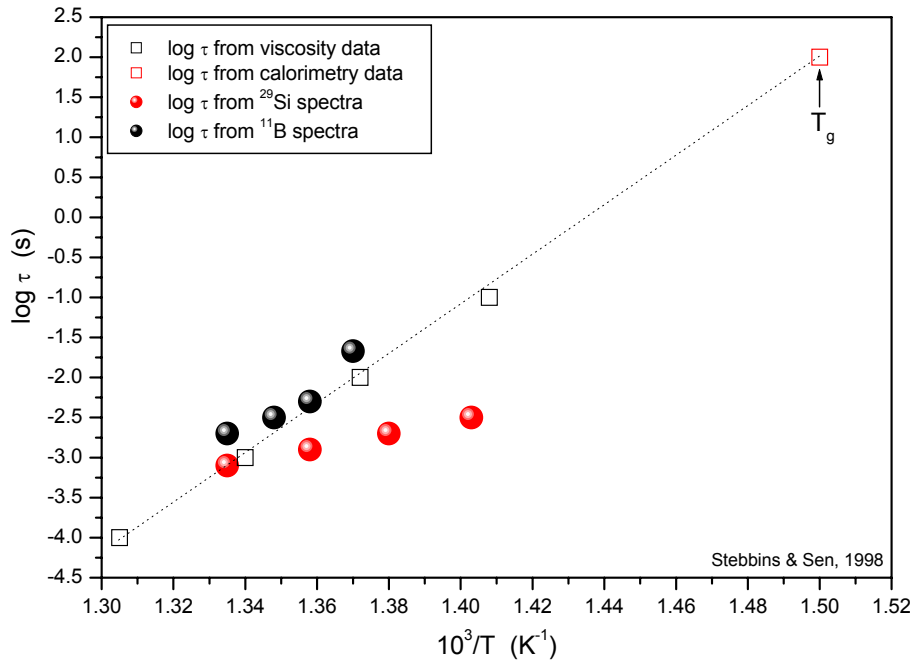


Fig. 88. Log τ derived from high temperature boron-11 (black solid circles) and silicon-29 (red solid circles) magic angle spinning nuclear magnetic resonance spectroscopy (MAS NMR) compared with shear relaxation times calculated from viscosity data (open black squares) and measured by differential scanning calorimetry (open red square). The dashed line is a fit to viscosity data as a guide to the eye. Redrawn after Stebbins & Sen (1998).

5.6.3. Attenuation

The energy loss due to the movement of parts of the melt structure can also be analysed in terms of the attenuation $Q^{-1}(\omega)$ (ratio between imaginary and real part of the shear modulus), where

$$Q^{-1}(\omega) = \frac{J''(\omega)}{J'(\omega)} \quad (\text{Eq. 72})$$

for $J^*(\omega) = G^*(\omega)^{-1}$ (Webb & Jackson, 2003; O'Connell & Budiansky, 1978; Johnston & Toksöz, 1981). Figure 90 shows $\log Q^{-1}$ for all of the melts as a function of inverse temperature. Two straight line trends can be seen in this plot – one associated with the

slowest moving part of the melt structure (taken to be the lifetime of Si-O bonds); and one associated with the faster relaxation. The two regions have been fit separately to the equation:

$$Q^{-1}(\omega) = Q_0^{-1} \omega^\alpha \exp\left(-\frac{\alpha E}{RT}\right) \quad (\text{Eq. 73})$$

(Webb & Jackson, 2003). As the low frequency peak indicates the energy lost in viscous flow its activation energy should be and is identical with the activation energy for viscous flow (see Tab. 23 and 24) in these melts. As there is no separate peak for Si-O and Al-O bonds, it is impossible to calculate the activation energy for both of them separately.

The result of average activation energy obtained in this study for bridging Si-O bonds in Fe-free melts is $543.67 \pm 52.98 \text{ kJ mol}^{-1}$, what is identical with an activation energy of Si-O bond determined by Bockris & Reddy (1970) ($\sim 540 \text{ kJ mol}^{-1}$), who worked with the silicate melts with binary metal oxide – silicate joins. For Fe-bearing melts the average activation energy determined by the attenuation calculation is $497.88 \pm 20.17 \text{ kJ mol}^{-1}$.

The slope in the attenuation calculation in this study allows obtaining activation energy for the faster motion as $126.24 \pm 42.72 \text{ kJ mol}^{-1}$. The activation energy for Na diffusion in silicate melts is $50\text{-}100 \text{ kJ mol}^{-1}$ (Bansal & Doremus, 1986), confirmed also by George & Stebbins (1996) from slope of the relaxation curve as 70 kJ mol^{-1} . This would further suggest that the second energy loss peak is for Na^+ diffusion. There was too much scatter in the plot of attenuation for the second peak in the Fe-bearing melts for it to be fit.

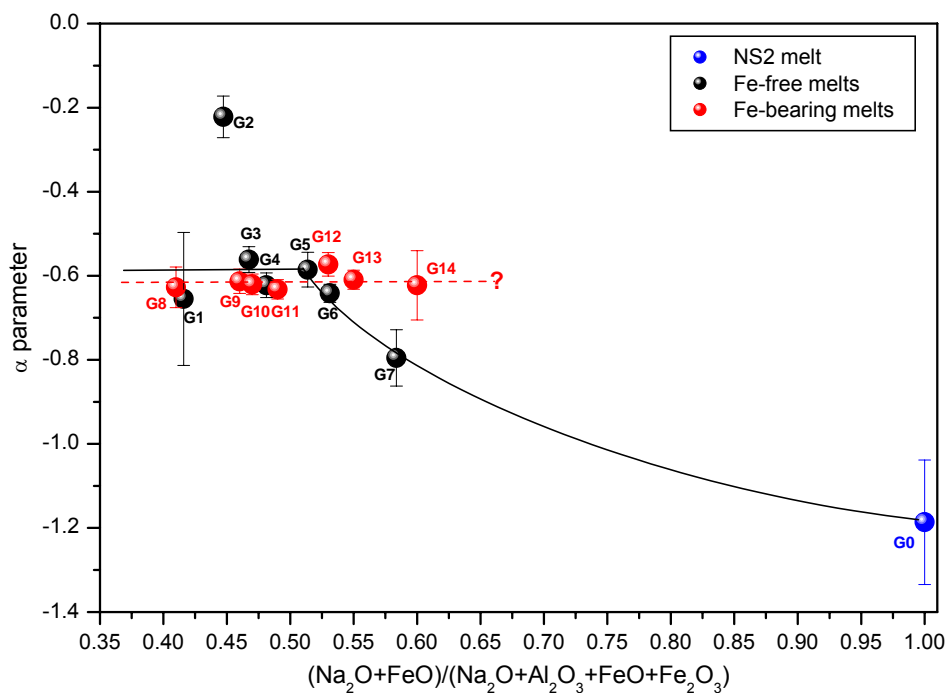
Change of the α parameter (from Eq. 73, see also Tab. 23 and 24) indicates a change in flow mechanism of the melt. Figure 89 presents α parameter as a function of $\gamma = (\text{Na}_2\text{O} + \text{FeO}) / (\text{Na}_2\text{O} + \text{Al}_2\text{O}_3 + \text{FeO} + \text{Fe}_2\text{O}_3)$. Trend of Fe-free melts shows clear breaking point at $\gamma \sim 0.5$, what confirms all previous assumptions. α parameter of Fe-bearing melts seems to be constant, what cannot be explained considering small number of samples.

Tab. 23. Table of fit data Q^{-1} for samples G0-G7 and activation energy for α - and β - relaxation.

	α - relaxation		β - relaxation	
	Alpha α	Activation energy, E_a (kJ mol ⁻¹)	Alpha α	Activation energy, E_a (kJ mol ⁻¹)
G0	-1.19 ± 0.15	531.08 ± 42.37	does not occur	
G1	-0.66 ± 0.16	596.65 ± 45.28	-0.11 ± 0.08	168.03 ± 80.25
G2	-0.22 ± 0.05	569.08 ± 77.44	-0.25 ± 0.09	83.17 ± 44.19
G3	-0.56 ± 0.03	589.96 ± 26.25	-0.27 ± 0.06	100.98 ± 70.60
G4	-0.62 ± 0.03	563.55 ± 16.67	-0.28 ± 0.06	168.63 ± 62.15
G5	-0.59 ± 0.04	495.08 ± 41.11	-0.10 ± 0.05	110.37 ± 167.66
G6	-0.64 ± 0.02	495.42 ± 14.31	-0.22 ± 0.05	164.97 ± 75.33
G7	-0.80 ± 0.07	490.69 ± 30.13	-0.27 ± 0.21	87.50 ± 302.60

Tab. 24. Table of fit data Q^{-1} for samples G0-G14 for α - relaxation.

	γ	Activation energy, E_a (kJ mol ⁻¹)			Alpha α
		Micropenetration	Attenuation	Shear viscosity (from torsion)	
G0	1.00	511.75 ± 14.23	531.08 ± 42.37	479.64 ± 19.53	-1.19 ± 0.15
G1	0.42	577.09 ± 11.68	596.65 ± 45.28	518.89 ± 6.89	-0.66 ± 0.16
G2	0.45	565.99 ± 8.42	569.08 ± 77.44	570.58 ± 17.62	-0.22 ± 0.05
G3	0.47	590.31 ± 7.85	589.96 ± 26.25	590.31 ± 7.85	-0.56 ± 0.03
G4	0.48	525.59 ± 10.53	563.55 ± 16.67	517.55 ± 25.85	-0.62 ± 0.03
G5	0.51	503.00 ± 11.11	495.08 ± 41.11	510.85 ± 6.51	-0.59 ± 0.04
G6	0.53	473.32 ± 4.21	495.42 ± 14.31	452.45 ± 5.74	-0.64 ± 0.02
G7	0.58	480.98 ± 7.08	490.69 ± 30.13	456.66 ± 25.85	-0.80 ± 0.07
G8	0.41	508.17 ± 14.74	505.11 ± 36.21	539.57 ± 31.98	-0.63 ± 0.05
G9	0.46	584.75 ± 25.27	509.27 ± 22.60	487.68 ± 19.91	-0.61 ± 0.03
G10	0.47	503.38 ± 9.57	507.95 ± 21.27	561.01 ± 18.00	-0.62 ± 0.02
G11	0.49	440.38 ± 13.79	493.69 ± 15.82	495.15 ± 15.32	-0.63 ± 0.02
G12	0.53	478.30 ± 8.62	477.71 ± 17.70	395.20 ± 33.70	-0.57 ± 0.03
G13	0.55	505.87 ± 10.91	508.09 ± 11.10	496.68 ± 20.68	-0.61 ± 0.02
G14	0.60	481.55 ± 9.19	518.05 ± 53.47	533.82 ± 26.81	-0.62 ± 0.08

**Fig. 89.** α parameter as a function of $\gamma = (\text{Na}_2\text{O} + \text{FeO}) / (\text{Na}_2\text{O} + \text{Al}_2\text{O}_3 + \text{FeO} + \text{Fe}_2\text{O}_3)$.

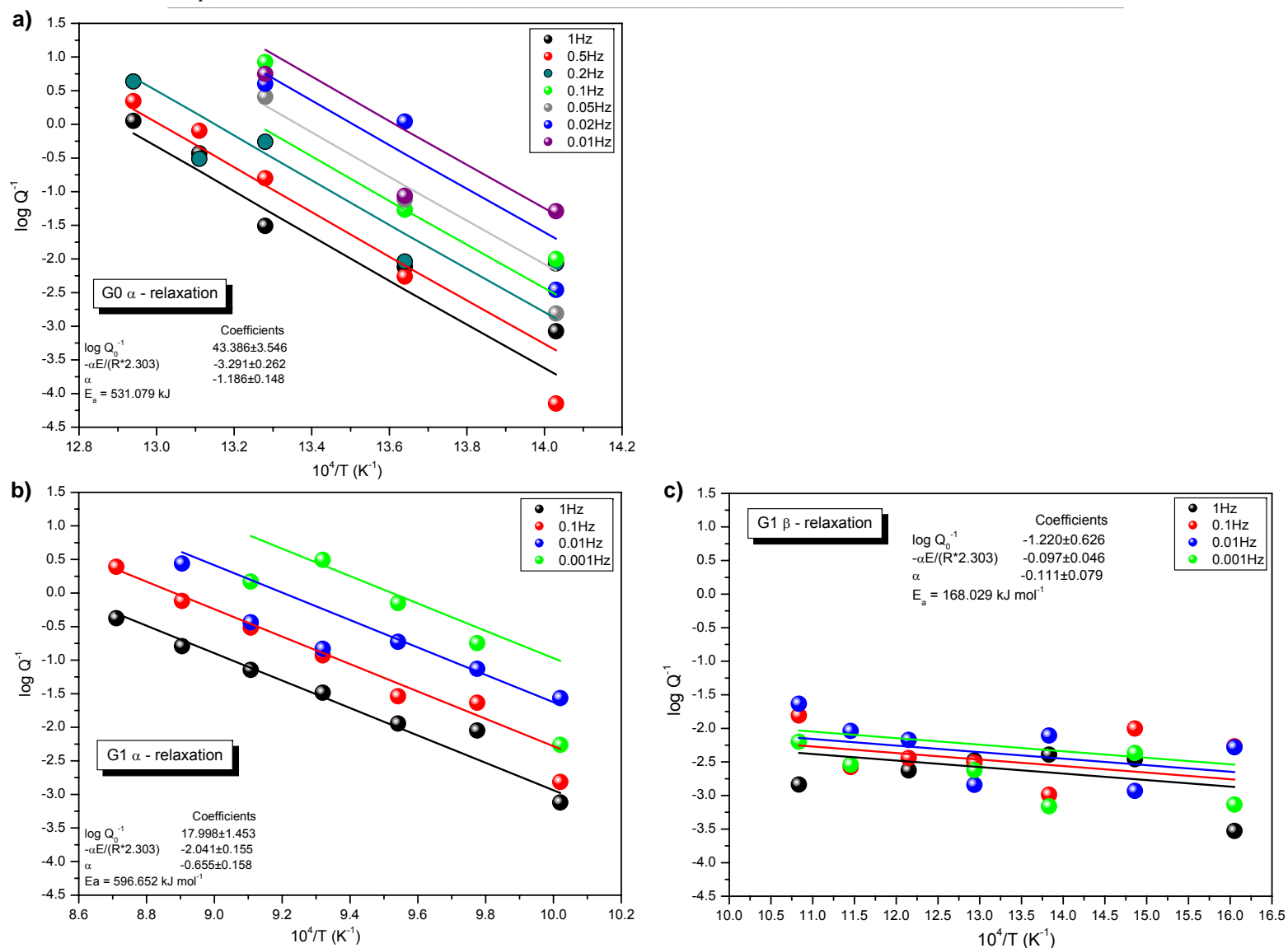


Fig. 90. Attenuation (Q^{-1}) as a function of inverse temperature. The data are fit to Eq. (73). **a)** sample G0 – α -relaxation; **b)** sample G1 – α -relaxation; **c)** sample G1 – β -relaxation.

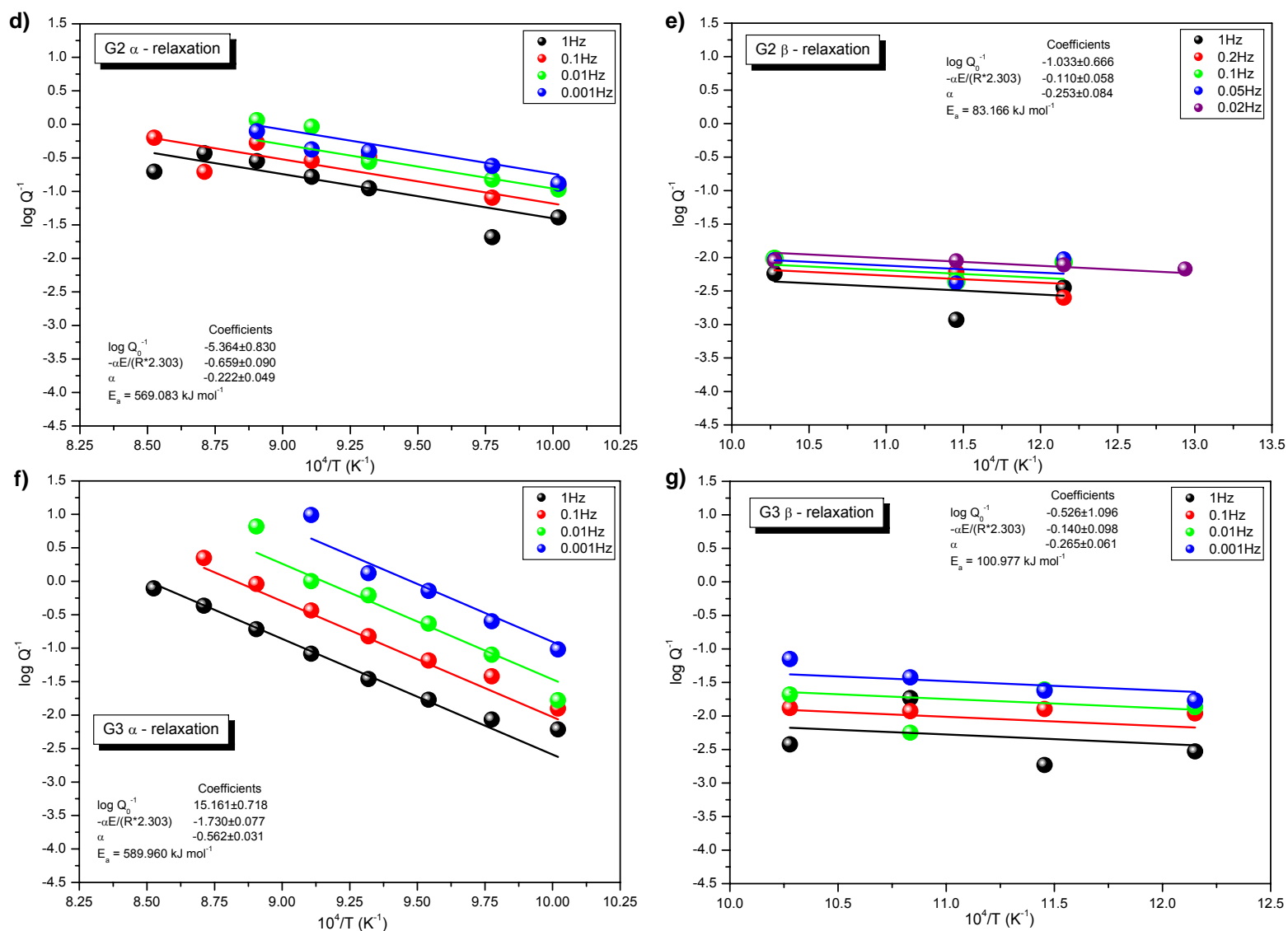


Fig. 90. continuation. Attenuation (Q^{-1}) as a function of inverse temperature. The data are fit to Eq. (73). **d)** sample G2 – α -relaxation; **e)** sample G2 – β -relaxation; **f)** sample G3 – α -relaxation; **g)** sample G3 – β -relaxation.

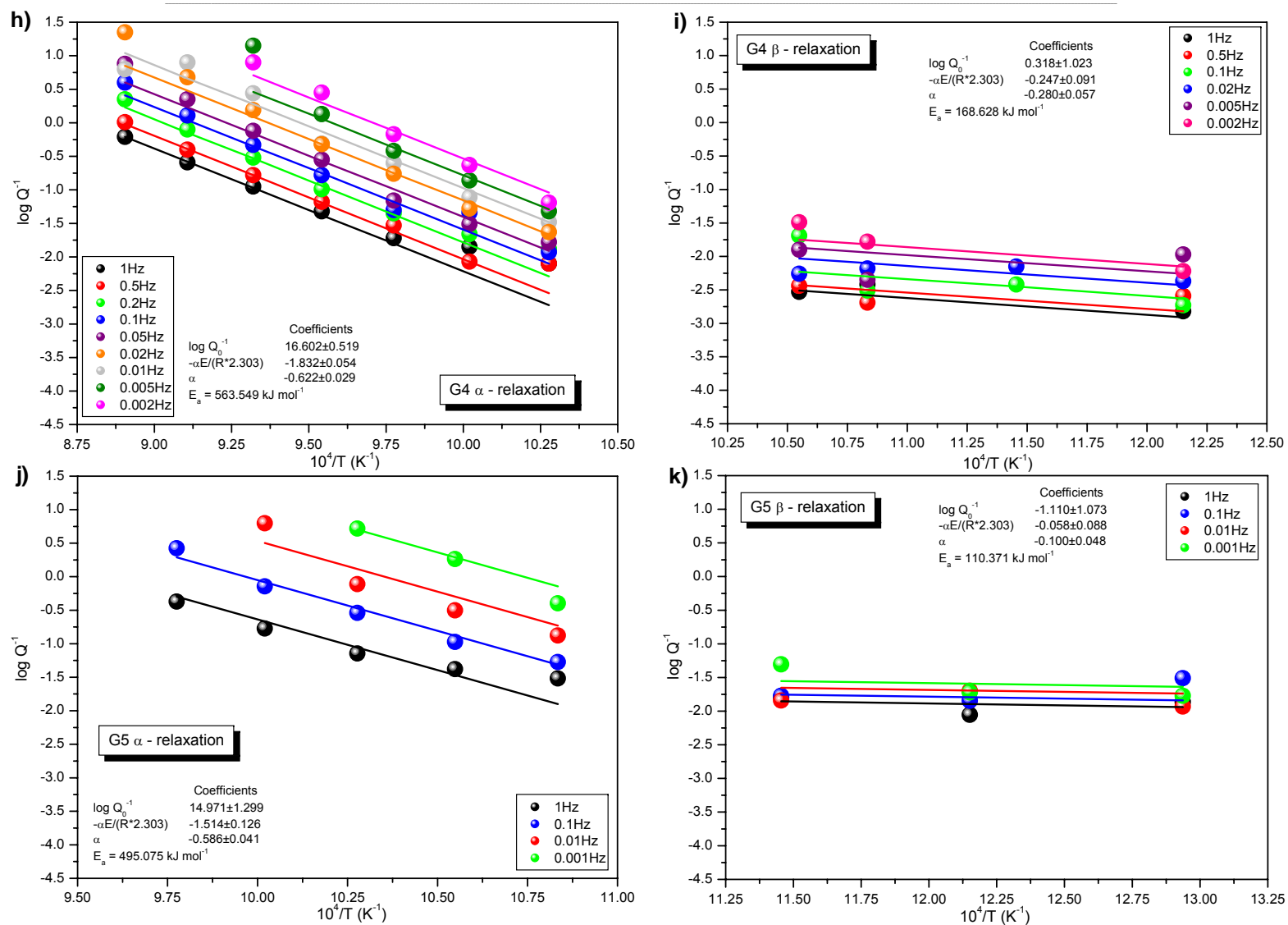


Fig. 90. continuation. Attenuation (Q^{-1}) as a function of inverse temperature. The data are fit to Eq. (73). **h)** sample G4 – α -relaxation; **i)** sample G4 – β -relaxation; **j)** sample G5 – α -relaxation; **k)** sample G5 – β -relaxation.

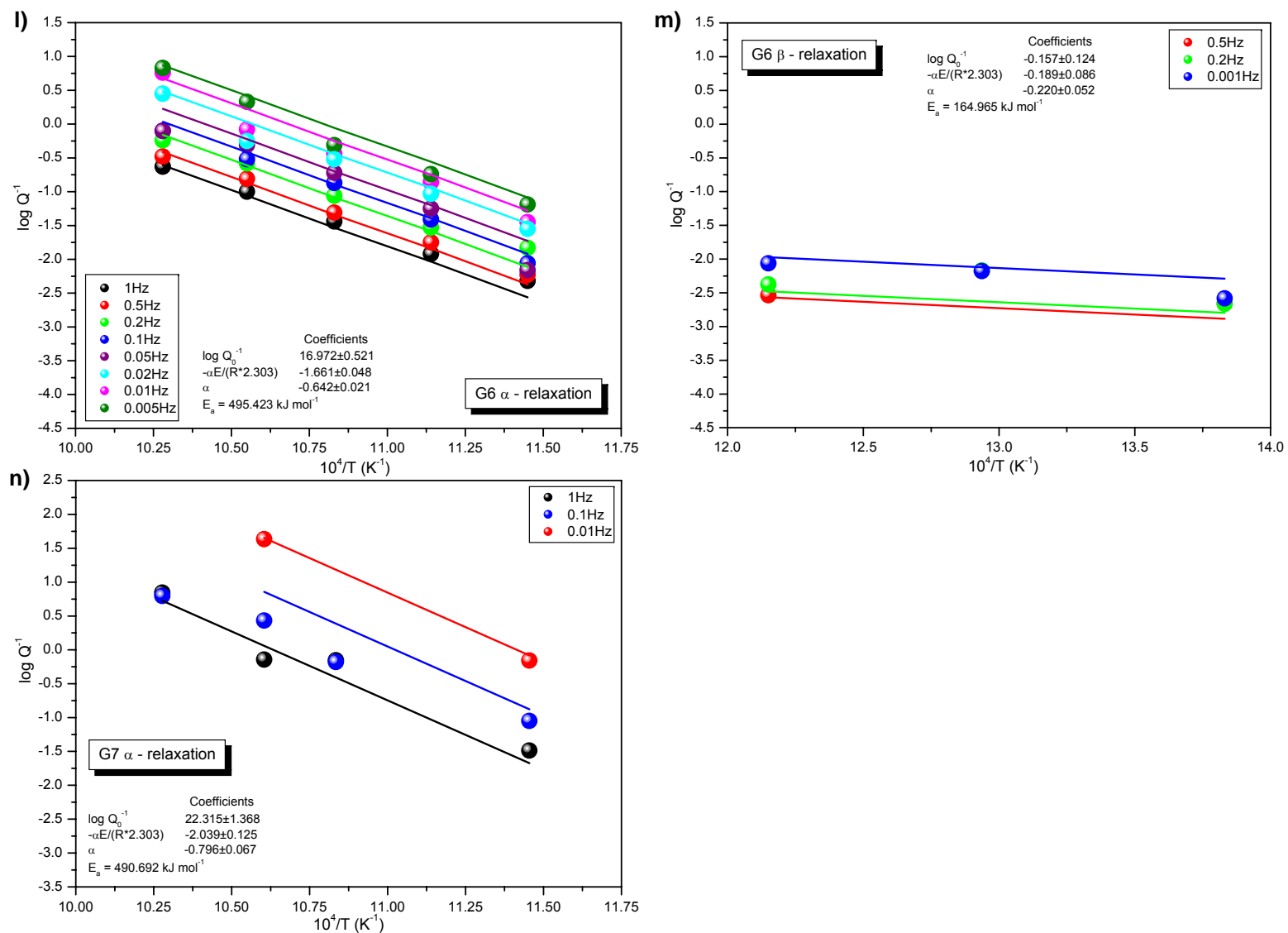


Fig. 90. continuation. Attenuation (Q^{-1}) as a function of inverse temperature. The data are fit to Eq. (73). **l)** sample G6 – α -relaxation; **m)** sample G6 – β -relaxation; **n)** sample G7 – α -relaxation.

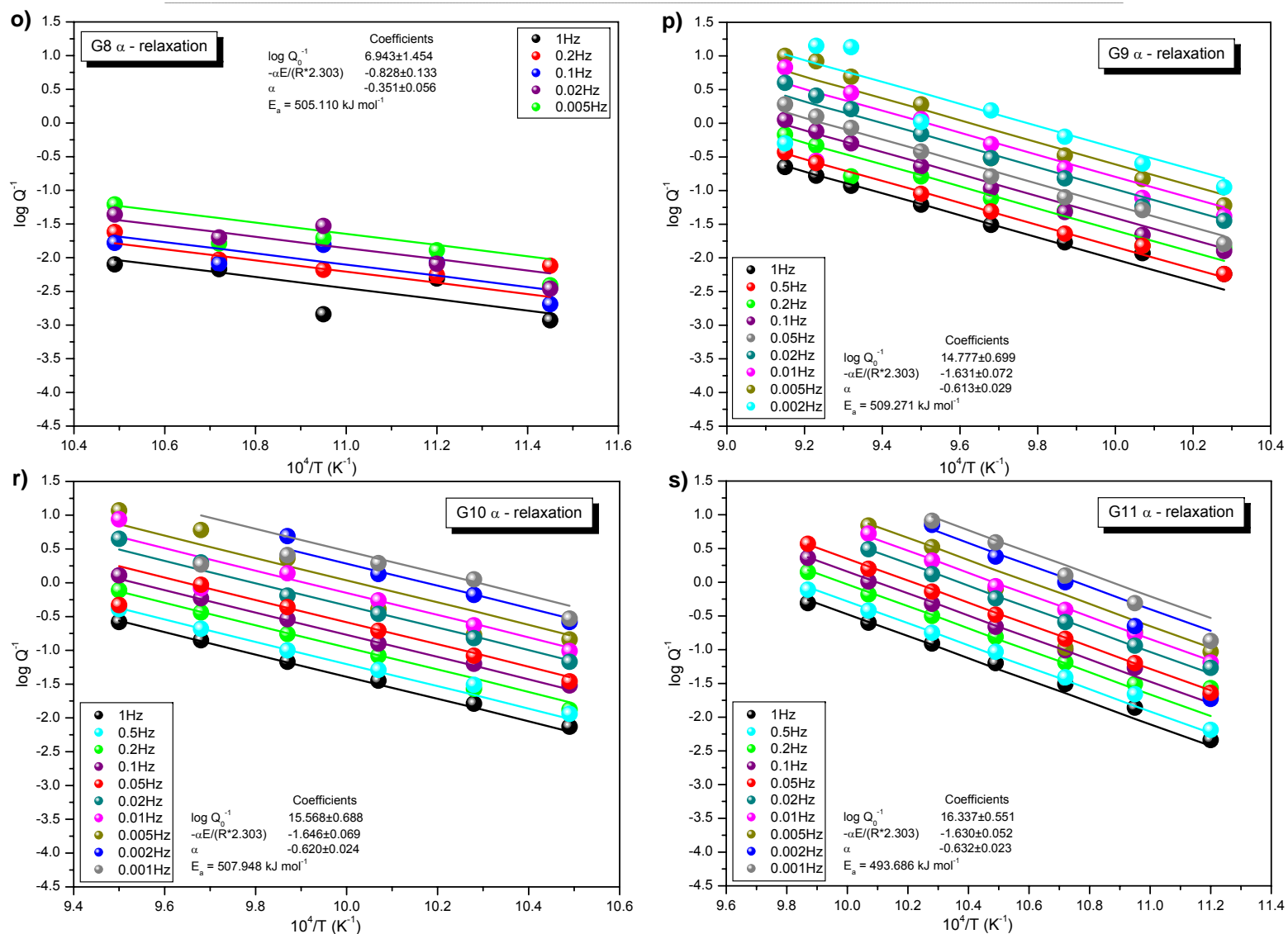


Fig. 90. continuation. Attenuation (Q^{-1}) as a function of inverse temperature. The data are fit to Eq. (73). **o)** sample G8 – α -relaxation; **p)** sample G9 – α -relaxation; **r)** sample G10 – α -relaxation; **s)** sample G11 – α -relaxation.

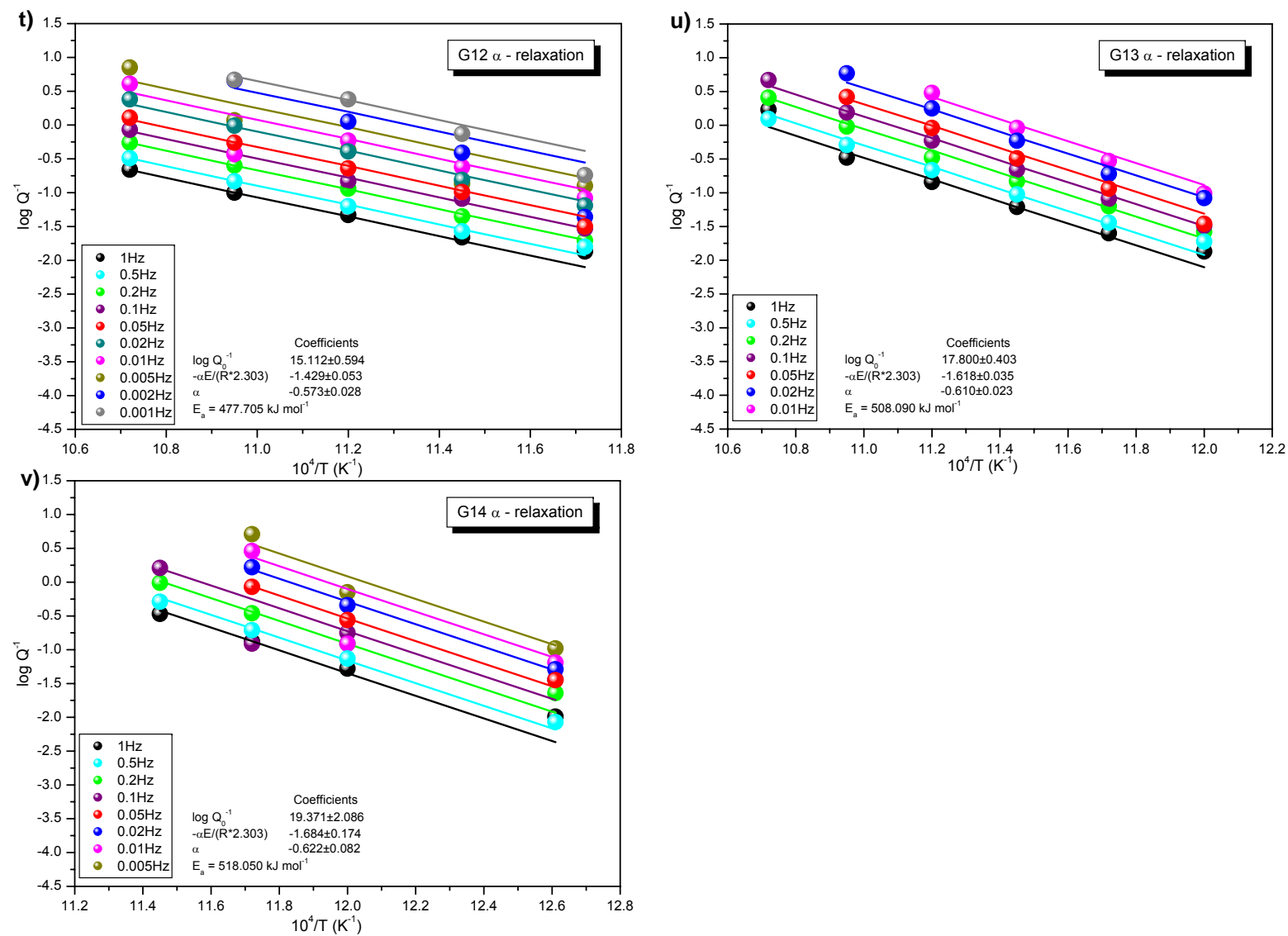


Fig. 90. continuation. Attenuation (Q^{-1}) as a function of inverse temperature. The data are fit to Eq. (73). **t)** sample G12 – α -relaxation; **u)** sample G13 – α -relaxation; **v)** sample G14 – α -relaxation.

5.7. Activation energy from all of the techniques

Activation energy for viscous flow depends on the composition of the sample (Siewert & Rosenhauer, 1997). The change in shape of the activation energy trend may be explained with bonding behaviour (MacKenzie, 1960; Bockris & Reddy, 1970; Stein & Spera, 1993).

Liquid SiO₂ is a non-periodic arrangement of SiO₄ tetrahedra connected by very strong covalent bonds at all corners (Bottinga & Weill, 1972). To start the flow mechanism, these bonds need to be broken and because of their strength the activation energy must be very high (Hofmaier, 1968). The addition of some alkalis and alkali earths introduce new weaker bonds to the melt structure.

With increasing Al₂O₃ content in peralkaline sodium aluminosilicate melts occurs a weakening of the bonds between oxygen and silicate network former and increasing of Al-O bond lengths. As a result of that, activation energy E_a decreases (Mysen et al., 1982; Seifert et al., 1982), what can be seen in Figure 62 in the γ range between 1.00 and 0.53. It is also observed, the activation energy between $1.0 \leq \gamma < 0.53$ does not change significantly. That could be explained by a presence of structural units with similar E_a (Seifert et al., 1982).

In the melts, where Fe²⁺ occurs as a network modifier, bonds between network formers and oxygen are longer and weaker what would explain lower activation energy in Fe-bearing melts. On the other hand, Seifert et al. (1982) suggested, that presence of two different structural units in the melt causes the creation of separate flow units with the weak bond between them.

Changing Na/Al ratio introduces a big spread in the activation energy results. Stein & Spera (1993) shows that in the system NaAlSiO₄ activation energy changes between 515 kJ mol⁻¹ and 340 kJ mol⁻¹ with changing composition .

In this study, the results for samples with $0.42 < \text{Na/Al} < 0.58$ are: for Fe-free melts are between 473.3 ± 4.2 and 590.3 ± 7.8 kJ mol⁻¹, and for Fe-bearing melts: 440.4 ± 13.8 to 584.8 ± 25.3 kJ mol⁻¹.

Activation energies from torsion shear viscosity data and from micropenetration method are comparable, what was earlier shown with light spectroscopy by Lai et al. (1975), Bucaro & Dardy (1977) and Siewert & Rosenhauer (1997). Here, the activation energy using attenuation was also calculated (see Tab. 24). Figure 91 is a plot of activation energy determined from different techniques for all of the samples. So the viscosity should be the same from micropenetration, attenuation and torsion (shear viscosity), this data must plot on a straight line with slope = 1.

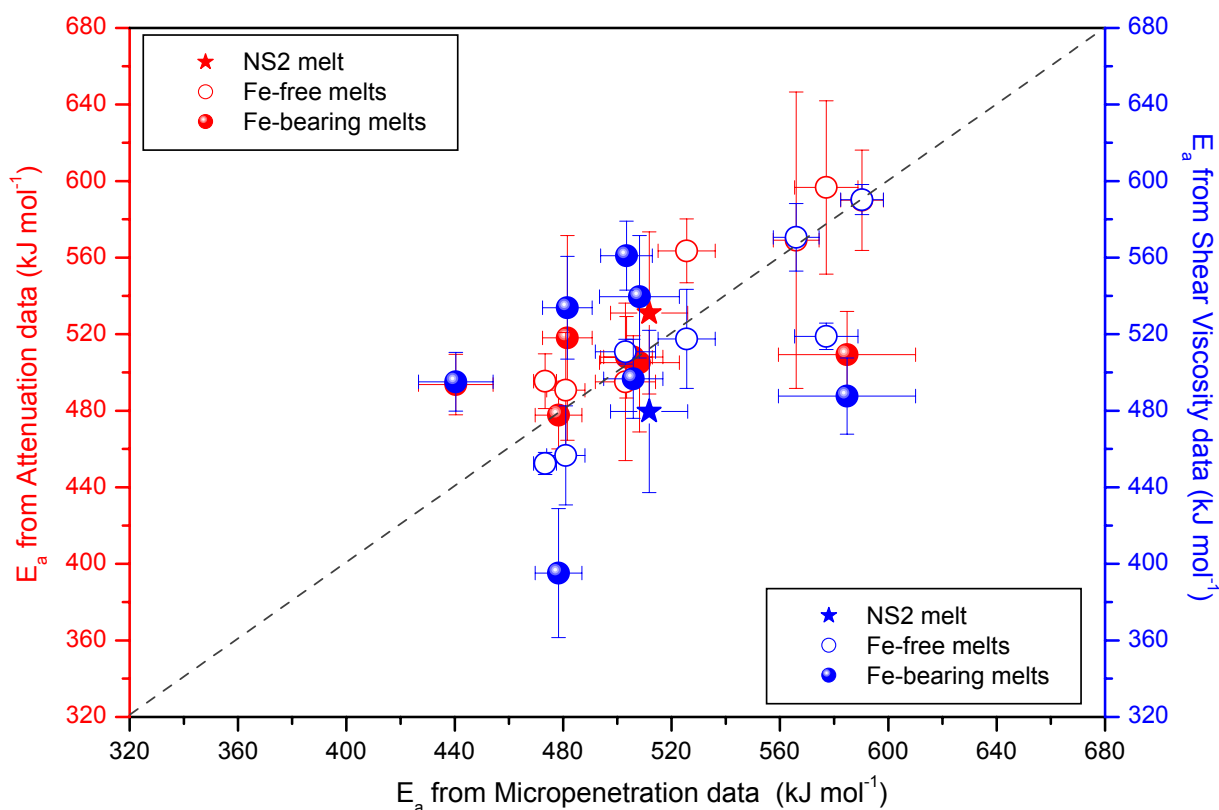


Fig. 91. Plot of the activation energy determined from the attenuation data and the viscosity against the activation energy from micropenetration data. Dashed line indicates slope = 1.

5.8. Fast relaxation time in aluminosilicate melts

The rate of flow in the melts is controlled by the longest lived bonds, whereas there are structural relaxations for each of the bond types in the melt; and the slowest structural relaxation is identified with the rate of flow.

Thermodynamic and rheological properties of magma (viscosity, heat capacity, diffusivity, conductivity, expansivity, compressibility) are required to measure to better interpretation and understanding the flow mechanisms.

Stebbins & Sen (1998) have investigated a microscopic dynamics and viscous flow in a borosilicate glass-forming liquid (44.5 mol% Na_2O , 11.0 mol% B_2O_5 , and 44.5 mol% SiO_2). They have proved with NMR measurements that in multi – component oxide liquids some larger structural groups with different relaxation times are created. In borosilicate, the β – relaxation (connected with breaking of Si-O bonds) occurs at frequencies up to 50 times faster than Maxwell relaxation theory assumed; with the lifetime of B-O bonds being identical to τ_M (Fig. 88). The authors explain this fact with a creation of the polyhedra of

SiO₄, BO₄ and BO₃, which number depends on the temperature. These complex structural units influence the flow mechanism of the melt and lead to separation the measured relaxation time of Si-O bonds and that calculated from Maxwell equation (Eq. 3). Results obtained by Stebbins & Sen (1998) confirm the results for aluminosilicates from this study that Si-O bonds do not always control the flow in silicate melts.

In the case of aluminosilicate melts investigated in this study, it appears that, as suggested by Martens et al. (1987), the Si-rich units are “glued” together by Al-rich units.

The Si-rich units can be called “icebergs” and surrounding them Al-tetrahedra – as sea. The term “iceberg” was discussed by Bockris & Kojonen (1960) for the structure of the alkali silicates and borates (see also references therein).

Stebbins (1995) suggested that Q⁴ species can create the “icebergs” and Q³ units – mica like “sheets”. They move as relatively big parts of the structure and the lifetimes of the bonds creating the “icebergs” can be different than Maxwell theory assumes, because atoms in them are strongly connected. Through the flow the icebergs break the weakest bonds of network modifiers. The idea of such type of structure can explain our results.

Thus, the simple flow mechanism proposed by Farnan & Stebbins (1994) and the relationship between viscosity and Si-O lifetime as determined by Liu et al. (1988) apply only to simple melt.

In the case where large structural units appear in the melt, a more complex relationship between flow mechanism, viscosity and bond lifetime occurs.

Figure 83 shows a difference between Maxwell relaxation time and relaxation times obtained in this study as a function of composition, presented here as (Al³⁺+Fe³⁺)/Si ratio (in atoms). Because in the melts occur also some local changes of structure, the relaxation times of aluminosilicate melts do not agree with Maxwell relaxation theory.

In Si-rich melts the flow mechanism is controlled by the lifetime of the Si-O bonds. Si-O bonds have the longest lifetime in the structure and because silicate melt is a simple melt, Maxwell relaxation works (Fig. 92 a).

With addition more and more Al₂O₃ the structure changes. New network former is introduced into the structure. As long as the ratio between Al and Si does not excess 1:3 (e.g. in albite) the Al-tetrahedra do not influence on the flow mechanism (Fig. 92b). As has been investigate (Dirken et al., 1997) in such melt there is no Al-O-Al bonds.

The increase in the number of Al-tetrahedra causes that these structural units begin to connect with each other, surrounding the separate silica rich clusters (icebergs) (Fig. 92c). The flow mechanism starts to be controlled by the shorter lifetime of Al-O bonds, in spite of presence longer lived Si-O bonds. It means that **the flow mechanism occurs faster than the structure is fully relaxed**, what is observed as a peak in Figure 83.

Figure 92d shows the stage when the melt is almost aluminate with some single Si-tetrahedra. The pure aluminate melt (Fig. 92e) is a simple melt again, where Maxwell relaxation time works.

Here, the original goal of the study – to determine the different behaviour of peralkaline and peraluminous melts – is decoupled from the observations of fast flow mechanism in these Al-rich melts. The existence of triclusters should have an effect on relaxation time and flow mechanism but this is overshadowed by the large effect of a large number of Al-tetrahedra surrounding icebergs of Si-tetrahedra.

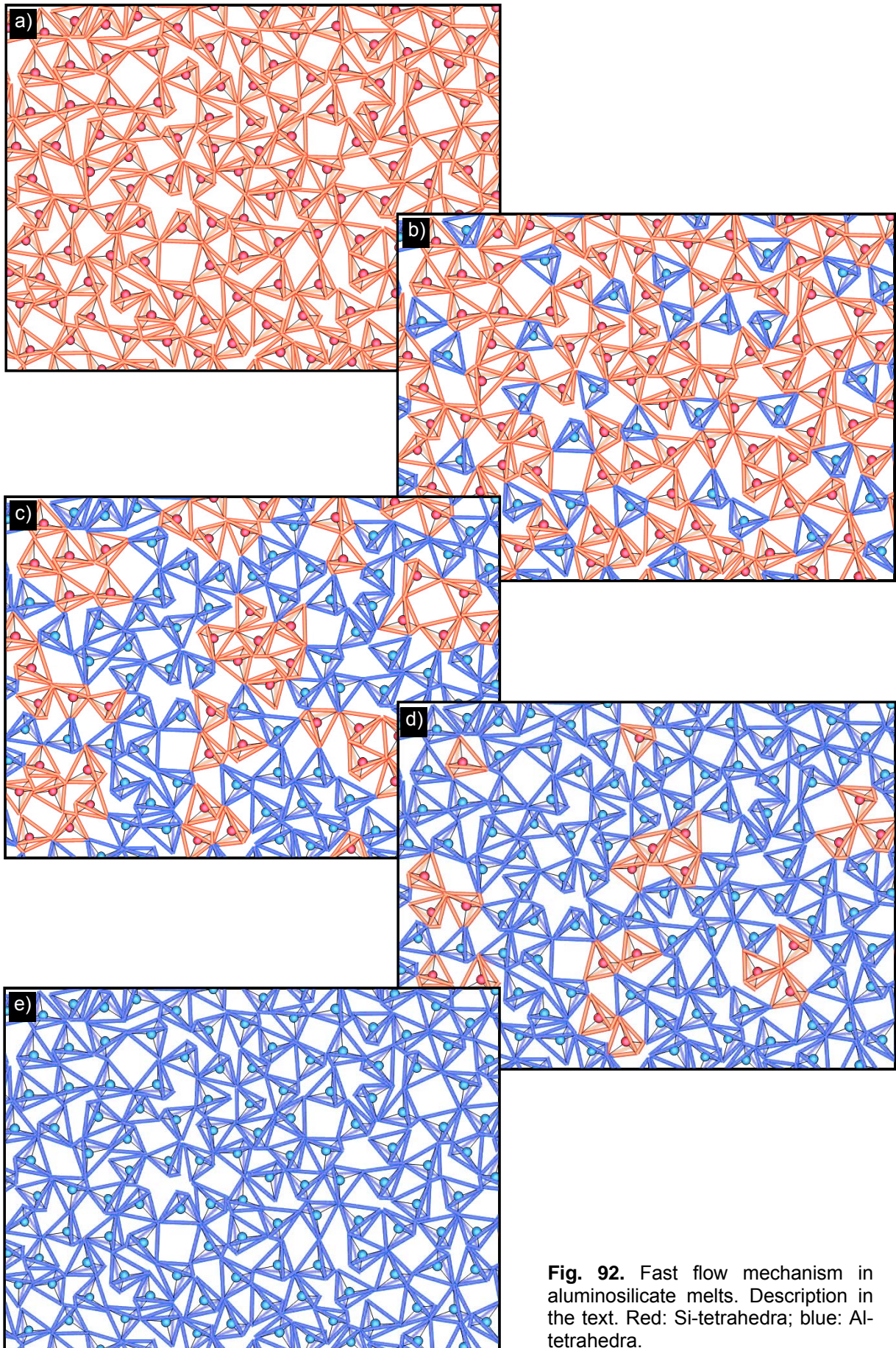


Fig. 92. Fast flow mechanism in aluminosilicate melts. Description in the text. Red: Si-tetrahedra; blue: Al-tetrahedra.

6. CONCLUSIONS

The topology of our planet is dominated by the effect of silicate melts – in the form of mid-oceanic ridges, plumes, subduction zones, volcanoes and the differentiation into mantle and core at the creation of our planet. It therefore behoves us to understand the structure and physical and thermodynamic properties of silicate melts.

The structure of sodium aluminosilicate melts is taken to be built of network formers in tetrahedral coordination; and octahedrally coordinated network modifiers and charge balancers. In peralkaline structure, Si and Al form tetrahedra and Na is a network modifier and charge balancer. In peralkaline Fe-bearing melts Fe^{3+} is placed in tetrahedra and Fe^{2+} is octahedrally coordinated. The structural rearrangement occurs when composition changes into peraluminous ($\gamma \sim 0.5$) - where there is no longer enough Na^+ to charge balance the Al^{3+} in tetrahedral coordination. There is no clear model of the peraluminous structure in aluminosilicate melts and for the purposes of this study here it is assumed that peraluminous structure consists Si, Al (and Fe^{3+} in Fe-bearing melts) in tetrahedra which form triclusters, because of the lack in charge balancers (Na and Fe^{2+}). Negligible part of Fe^{3+} changes coordination from tetrahedral to octahedral, but this amount does not affect the change of structure.

Pure silicate or pure aluminate melt's and glass's networks show high similarity. However, when we start to change composition, one can observe strong variation in physical and thermodynamic properties. Into consideration should be taken not only the kind of the elements playing a network former and network modifiers role, but also the ratio between different ions.

The first observation is that viscosity, heat capacity and shear modulus data show a change in trend at $\gamma \sim 0.5$ indicating different structure in the melts as the composition changes from peralkaline to peraluminous. That is caused by the presence of triclusters. Here, the melt viscosity and glass density data confirm the information from previous studies, that there is a structural and flow mechanism change at $\gamma \sim 0.5$, as expected. The heat capacity data show simple trends as a function of composition.

For the first time the trends in configurational heat capacity as a function of composition indicate the presence of a change in structure. Literature data do not cover a controlled chemical composition range and thus have not observed this. With the addition of $\text{Fe}_2\text{O}_3/\text{Al}_2\text{O}_3$ this effect is additionally enlarged. The configurational entropy indicates that the range of structures available to the melt increases with increasing Al_2O_3 content.

The shear modulus and shear viscosity of $\text{Na}_2\text{O}-\text{Al}_2\text{O}_3-\text{SiO}_2$ melts and the density of the glasses indicate that there is a change in melt structure at $\text{Al} \sim \text{Na}$. Such a change in

structure with composition also requires a change in flow mechanism with composition, and thus a change in the rates at which parts of the melt structure move. The rate of motion of structural units in silicate melts can be determined via forced oscillation methods.

A low-frequency forced oscillation technique has been used to measure the frequency and temperature dependence (to 1000°C) of the shear modulus and viscosity of a range of Na₂O-Al₂O₃-SiO₂ melts. The frequency range is between 1 and 0.001 Hz, and thus the viscosity range is from 10⁸-10¹⁵ Pa s. The frequency-dependence of the shear modulus can be described by simple structural relaxation theory. The measured relaxation times (τ) for the simple peralkaline compositions agree with the Maxwell relaxation time (τ_M). With increasing Al₂O₃ content, the structural relaxation time deviates from the calculated Maxwell relaxation time (gradually become shorter than τ_M) and after (Al³⁺+Fe³⁺)/Si^(atoms) ~ 0.55 goes back and became longer again. The pure aluminate melts seem to be also simple and their relaxation times agree with Maxwell relaxation time (τ_M). This is not effect of triclusters.

Such a decrease in τ/τ_M is observed for the first time. This shortening of relaxation times indicates that the large amount of Al³⁺ in these melts changes not only the structure, but also the flow mechanism of the melt. The shorter Al-O bond lifetimes appear to control the flow mechanism, in spite of the presence of the longer lived Si-O bonds. The structure flows faster than whole structure is relaxed. This has never been seen before. But also melts in this study have a much higher (Al³⁺+Fe³⁺)/Si^(atoms) ratio (0.62) than used in previous studies (0.2).

The structure of these melts is more complex than first thought. Not only is there the structural change with Na/Al composition, but the large amount of Al³⁺ has created melts in which the motion of Al tetrahedra is as important as the motion of the Si tetrahedra. Thus, the theories created to describe the flow and structure of silicate melts need to be expanded to include the large effect due to the presence of almost as many Al tetrahedra as Si tetrahedra in the melt.

The torsion data show the lifetimes of motion of various structures in the melt. It was not possible to separate the lifetime of Al-O bonds from Si-O bonds, nor was the lifetime of AlSi₂O₅ triclusters determined, but the lifetime of Na-O bonds was measured. A second relaxation peak is seen at timescales ~5.5-7.5 orders of magnitude faster than the slowest relaxation time. This very fast relaxation is associated with the movement of Na⁺ in the melt.

What was determined here for the first time was the effect of a large number of fast X-O lifetimes (X=Al in this case). The difference between Si-O rich melts and shorter lived Al-O rich melt means that a new structure controls the flow mechanism. This is not related

to triclusters but simply to the lifetime of the different bonds. This effect is seen in the failure of the Maxwell relationship to calculate the structural relaxation times of melts with $\text{Si}^{\text{atom}} \sim \text{Al}^{\text{atom}}$.

Figure 93 shows predicted relaxation trend for aluminosilicate melts as a function of the Al/Si ratio. Relaxation times vary depending on the melt composition.

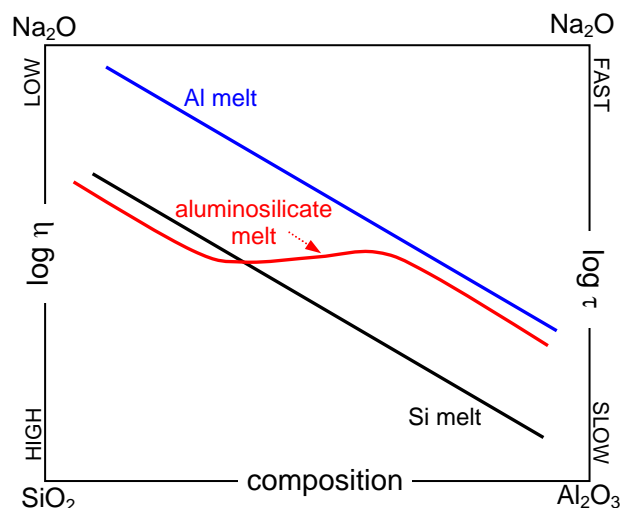


Fig. 93. Predicted relaxation trend for aluminosilicate melts as a function of composition.

Thus studies in which η is related to τ_M and to diffusion of Si or O will be in error in the composition range Si~Al: this applies to phonolite melts, e.g. Laacher See (Eifel, Germany), Tenerife (Canary Islands, Spain), Sardinia (Italy), Dunedin Volcano (East Otago, New Zealand), Mont Dore (Auvergne, France), Bohemian Massif (Czech Republic) or Mount Saint-Hilaire (Québec, Canada).

The error could also occur in the modelling of the dynamic of the phonolitic volcano: wrong cooling rate gives wrong eruption temperature and viscosity, what influence on wrong calculation of the eruption rate and then on magma heat capacity, volume and temperature.

7. OUTLOOK

The work described in this thesis concentrates on the structure of aluminosilicate melts as a function of composition and their physical and thermodynamic properties. In light of presented results the structural rearrangement has been shown to occur close to the subaluminous point. The failure of the Maxwell relaxation theory has been found and faster relaxation time of the complex melts has been measured.

Yet, more detailed studies are required in order to fully understand, what really occurs in these melts, e.g. NMR measurements of the bond lifetimes, diffusion measurements, and other torsion investigations.

To test of the present conclusions, the other series of the melts need to be investigated (Fig. 94), e.g. Ca-aluminosilicates, aluminosilicates with Al- and Si-end or K-Mg or Na-K compositions. Choosing the end members of the series, the influence of triclusters can be omitted and then their effect on viscosity will not be observed, but the effect of changing bond lifetimes as a function of composition and structure will be revealed.

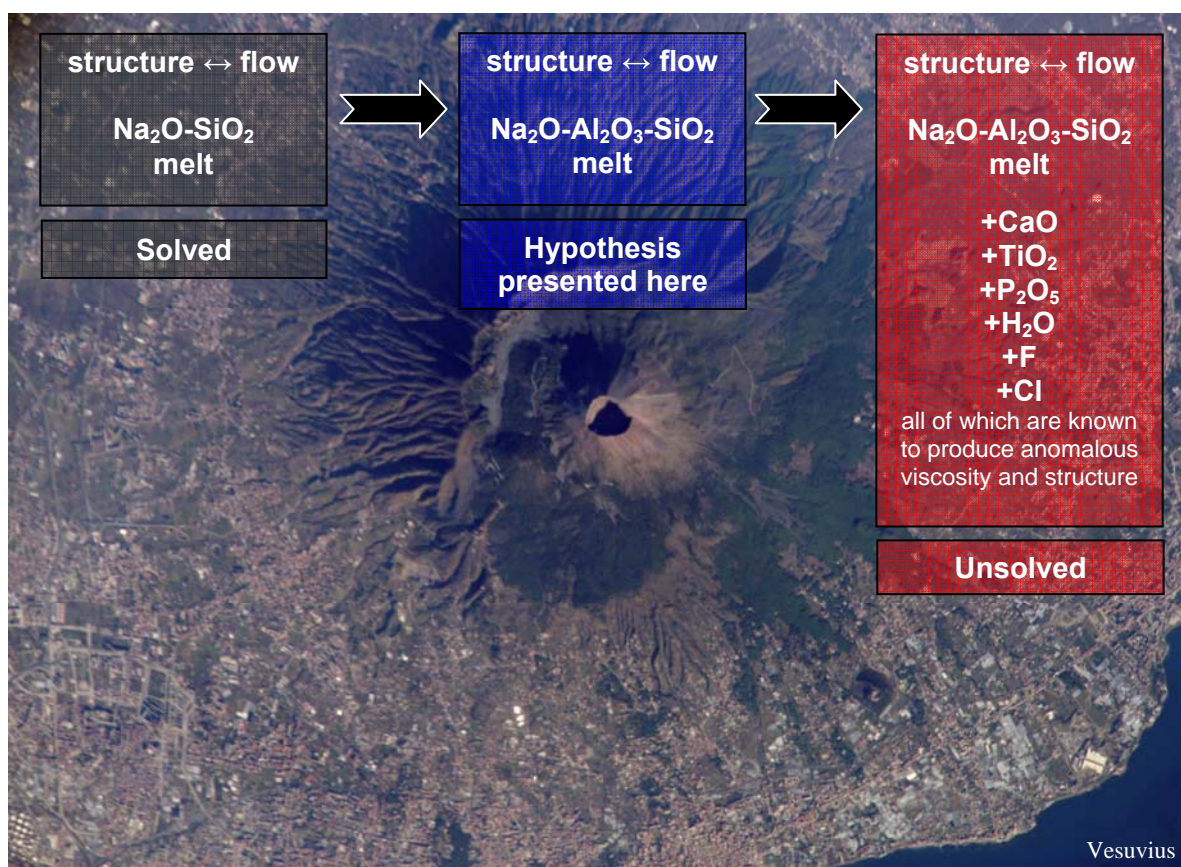


Fig. 94. Past, present and future of the studies of the relationship between structure and flow mechanism in silicate and aluminosilicate melts in the Earth.

8. LITERATURE

- Adam G & JH Gibbs, On the temperature dependence of cooperative relaxation properties in glass – forming liquids. *Journal of Chemical Physics*, 43, 139-146, 1965.
- Ahrens TJ, AGU Mineral Physics & Crystallography. A Handbook of Physical Constants, 1995.
- Allwardt JR, SK Lee & JF Stebbins, Bonding preferences of non-bridging O atoms: Evidence from ¹⁷O MAS and 3QMAS NMR on calcium aluminate and low-silica Ca-aluminosilicate glasses. *American Mineralogist*, 88, 949-954, 2003.
- Angell CA, The glass transition: comparison of computer simulation and laboratory studies. *Annals of the New York Academy of Sciences*, 371, 136-150, 1981.
- Angell CA, Structural instability and relaxation in liquid and glassy phases near the fragile liquid limit. *Journal of Non-Crystalline Solids*, 102, 205-221, 1988.
- Angell CA, Dynamic processes in ionic glasses. *Chemical Review*, 90, 523-542, 1990.
- Angell CA, Relaxation in liquids, polymers and plastic crystals – strong/fragile patterns and problems, *Journal of Non-Crystalline Solids*, 131-133, 13-31, 1991a.
- Angell CA, Thermodynamic aspects of the glass transition in liquids and plastic crystals, *Pure and Applied Chemistry*, 63, 10, 1387-1392, 1991b.
- Angell CA & M Goldstein, eds., Dynamic aspects of structural change in liquids and glasses. *Annals of the New York Academy of Sciences*, 484, 1986.
- Bagdassarov NS, DB Dingwell & SL Webb, Effect of boron, phosphorus and fluorine on shear stress relaxation in haplogranitic melts, *European Journal of Mineralogy*, 5, 409-425, 1993.
- Baker LL & MJ Rutherford, The effect of dissolved water on the oxidation state of silicic melts. *Geochimica et Cosmochimica Acta*, 60, 2179-2187, 1996.
- Bamford CR, A study of magnetic properties of iron in relation to its colouring action in glass. I. Iron in sodium borate glasses melted under oxidizing conditions. *Physics and Chemistry of Glasses*, 1, 159-164, 1960.
- Bansal NP & RH Doremus, Handbook of Glass Properties, 680pp, Academic Press, London, 1986.
- Bell RJ & P Dean. *Discussions of the Faraday Society*, 50, 55-61, 1970.
- Beran A & E Libowitzky, Spectroscopic methods in mineralogy, EMU Notes Mineral., 6, Budapest, Eötvös University Press, p. 661, 2004.
- Bernal JD, An attempt at a molecular theory of liquid structure. *Discussions of the Faraday Society*, 336, 27-40, 1936.
- Berry AJ, HSC O'Neill, KD Jayasuriya, SJ Campbell & GJ Fornan, XANES calibrations for the oxidation state of iron in a silicate glass. *American Mineralogist*, 88, 967-977, 2003.
- Bingham PA, JM Parker, TM Searle & I Smith, Local structure and medium range ordering of tetrahedrally coordinated Fe³⁺ ions in alkali – alkaline earths – silica glasses. *Journal of Non-Crystalline Solids*, 353, 24-25, 2479-2494, 2007.
- Bockris J O'M & E Kojonen, The compressibilities of certain molten alkali silicates and borates. *Journal of the American Ceramic Society*, 82, 4493-4497, 1960.
- Bockris J O'M. & AKN Reddy, Modern electrochemistry, 662, Plenum Press, New York, 1970.
- Bockris J O'M., JD MacKenzie & JA Kitchner, Viscous flow in silicate and binary liquid silicates. *Transactions of the Faraday Society*, 51, 1734-1748, 1955.
- Böhmer R & CA Angell, Correlation of the non-exponentiality and state dependence of mechanical relaxations with bond connectivity in Ge-As-Se supercooled liquids. *Physical Review B*, 45, 17, 10091-10094, 1992.
- Botcharnikov R, J Köpke, F Holtz, C McCammon & M Wilke, The effect of water activity on the oxidation and structural state of Fe in a ferro – basaltic melt. *Geochimica et Cosmochimica Acta*, 69, 5071-5085, 2005.
- Bottinga Y, Configurational entropy and non-Newtonian rheology of homogenous silicate liquids. *Physical Review B*, 49, 1, 1994.

- Bottinga Y & DF Weill, The viscosity of magmatic silicate liquids: a model for calculation. *American Journal of Science*, 272, 438-475, 1972.
- Bottinga Y & P Richet, Silicate melt structural relaxation: rheology, kinetics, and Adam – Gibbs theory. *Chemical Geology*, 128, 129-141, 1996.
- Bottinga Y, P Richet & A Sipp, Viscosity regimes of homogenous silicate melts. *American Mineralogist*, 80, 305-318, 1995.
- Bottinga Y, DF Weill & P Richet, Density calculations for silicate liquids. I. Revised method for aluminosilicate compositions. *Geochimica et Cosmochimica Acta*, 46, 909-919, 1982.
- Brady JB, Chemical components and diffusion. *American Journal of Scienc*, 275, 1073-1088, 1975.
- Brady JB, Diffusion data for silicate minerals, glasses, and liquids. In TJ Ahrens, Ed., *Mineral physics and crystallography: A handbook of physical constants*. American Geophysical Union, Washington, DC., 269-290, 1995.
- Brawer SA, Theory of relaxation in viscous liquids and glasses. *Journal of Chemical Physics*, 81, 2, 954-975, 1984.
- Brawer SA, Relaxation in viscous liquids and glasses. *Journal of the American Ceramic Society*, Columbus, OH, 1985.
- Brown GE Jr., GA Waychunas, CW Ponader, WE Jackson & DA McKeown, EXAFS and NEXAFS studies of cation environments in oxide glasses. *Journal de Physique Colloque*, Paris, 47, 661-668, 1986.
- Brückner R & G Demharter, Systematische Untersuchungen über die Anwendbarkeit von Penetrationsviscosimetern. *Glastechnische Berichte*, 48, 1, 12-18, 1974.
- Brückner R & Y Yue, Non-Newtonian flow behaviour of glass melts as a consequence of viscoelasticity and anisotropic flow. *Journal of Non-Crystalline Solids*, 175, 118-128, 1994.
- Bucaro JA & HD Dardy, High – temperature strain relaxation in silica by optical correlation spectroscopy. *Journal of Non-Crystalline Solids*, 24, 121-129, 1977.
- Bunker BC, RJ Kirkpatrick, RK Brow, GL Turner & C Nelson, Local Structure of Alkaline-Earth Boroaluminate Crystals and Glasses: II, ^{11}B and ^{27}Al MAS NMR Spectroscopy of Alkaline-Earth Boroaluminate Glasses". *Journal of the American Ceramic Society*, 74, 6, 1430-38, 1991.
- Burkhard DJM, Iron – bearing silicate glasses at ambient conditions. *Journal of Non-Crystalline Solids*, 275, 175-188, 2000.
- Burnham CW, Thermodynamics of melting in experimental silicate – volatile systems. *Geochimica et Cosmochimica Acta*, 39, 1077-1084, 1975.
- Bykov VN, VN Anfilogov & SV Kuznetsov, Structure of Al-Si Melts from Raman Sp. Data, *Geokhimija*, 4, 331-337, 1996.
- Bykov VN, AA Osipov & VN Anfilogov, Structure of high-alkali aluminosilicate melts from the high-temperature Raman spectroscopic data, *Glass Physics and Chemistry*, Vol. 29, No. 2, 105-107, 2003.
- Calas G & J Petiau, Coordination of iron in oxide glasses through high – resolution K-edge spectra: information from the pre-edge. *Solid State Communications*, 48, 625-629, 1983.
- Carreño-Morelli E, SE Urreta & R Schaller, Mechanical spectroscopy of thermal stress relaxation at metal-ceramic interfaces in aluminium-based composites. *Acta Materialia*, 48, 18-19, 4725-4733, 2000.
- Carron JP, Autodiffusion du sodium et conductivité électrique dans les obsidiennes granitiques. *Comptes Rendus Acad. Sci. Paris. Serie D*, 266, 854-856, 1968.
- Casalini R & CM Roland, Why liquids are fragile. *Physical Review E*, 72, 031503/1-4, 2005.
- Chakraborty S, Diffusion in silicate melts. *Reviews in Mineralogy*, 32, 411-504, 1995.
- Cohen MH & GS Grest, Liquid – glass transition, a free volume approach. *Physical Review B*, 20, 1077-1098, 1979.
- Crichton SN & CT Moynihan, Structural relaxation of lead silicate glass. *Journal of Non-Crystalline Solids*, 102, 222–227, 1988.

- Cruickshank-Miller C, The Stokes-Einstein Law for Diffusion in Solution *Proceedings of the Royal Society of London. Series A, Containing Papers of a Mathematical and Physical Character*, 106, 740, 724-749, 1924.
- Cukierman M & DR Uhlmann, Effects of iron oxidation state on viscosity, lunar composition 15555. *Journal of Geophysical Research*, 79, 1594-1598, 1974.
- Day DE & EG Rindone, Properties of soda aluminosilicate glasses: I, Refractive index, density, molar refractivity and infrared absorption spectra, *Journal of the American Ceramic Society*, 45, 579-581, 1962.
- DeBolt MA, AJ Easteal, PB Macedo & CT Moynihan, Analysis of structural relaxation in glass using rate heating data. *Journal of the American Ceramic Society*, 59, 16–21, 1976.
- DeGrave E, D Chambaere, P van Iseghem & R de Batist, Mössbauer spectroscopic study of some complex M_2O - Mo - M_2O_3 - SiO_2 glasses. *Journal de Physique Colloque*, Paris, 41, 269-270, 1980.
- Devine RAB, R Dupree, I Farnan & JJ Capponi, Pressure – induced bond – angle variation in amorphous SiO_2 . *Physical Review B*, 35, 2560-2562, 1987.
- Dickenson MP & PC Hess, Redox equilibria and the structural role of iron in aluminosilicate melts. *Contributions to Mineralogy and Petrology*, 78, 352-358, 1981.
- Dickenson JE & PC Hess, The structural role and homogenous redox equilibria of iron in peraluminous, metaluminous and peralkaline silicate melts. *Contributions to Mineralogy and Petrology*, 92, 207-217, 1985.
- Dietzel AZ, Die Kationenfeldstirken und ihre Beziehungen zu Entglasungsvorgängen, zur Verbindungsbildung und zu den Schmelzpunkten von Silikaten. *Z. Elektrochem.*, 48, 9-23, 1942.
- Dingwell DB, Viscosity and Anelasticity of Melts. *Mineral Physics and Crystallography, A Handbook of Physical Constants*, AGU Reference Shelf 2, 209-217, 1995.
- Dingwell DB, Volcanic dilemma – flow or blow? *Science*, 26, 1054-1056, 1996.
- Dingwell DB, R Knoche & SL Webb, The effect of B_2O_3 on the viscosity of haplogranitic liquids, *American Mineralogist*, 77, 457-461, 1992.
- Dingwell DB & D Virgo, Melt viscosities in the Na_2O - FeO - Fe_2O_3 - SiO_2 system and factors controlling the relative viscosities of fully polymerized silicate melts, *Geochimica Cosmochimica Acta*, 52, 395–403, 1988a.
- Dingwell DB & D Virgo, Viscosity – oxidation state relationship for hedenbergitic melt. *Carnegie Inst. Wash. Yearbook*, Vol. 87, 48-53, 1988b.
- Dingwell DB & SL Webb, Structural relaxation in silicate melts and non-Newtonian melt rheology in geologic processes, *Physics and Chemistry of Minerals*, 16, 508-516, 1989.
- Dingwell DB & SL Webb, Relaxation in silicate melts, *European Journal of Mineralogy*, 2, 4, 427-449, 1990.
- Dirken PJ, SC Kohn, ME Smith & ERH vanEck, Complete resolution of Si-O-Si and Si-O-Al arrangements in an aluminosilicate glass by O-17 multiple quantum magic angle spinning NMR spectroscopy. *Chemical Physics Letters*, 266, 568-574, 1997.
- Douglas RW, WL Armstrong, JP Edward & D Hall, A penetration viscometer. *Glass Technology*, 6, 2, 52-55, 1965.
- Dunn T, Oxygen diffusion in three silicate melts along the join diopside anorthite. *Geochimica et Cosmochimica Acta*, 47, 2292–2299, 1982.
- Dyar MD, A review of Mössbauer data on inorganic glasses: the effects of composition on iron valency and coordination. *American Mineralogist*, 70, 304-316, 1985.
- Farnan I & JF Stebbins, High – temperature ^{29}Si NMR investigation of solid and molten silicates. *Journal of the American Ceramic Society*, 112, 32-39, 1990a.
- Farnan I & JF Stebbins, Observation of slow atomic motions close to the glass transition using 2-D ^{29}Si NMR. *Journal of Non-Crystalline Solids*, 124, 207-215, 1990b.
- Farnan I & JF Stebbins, The nature of the glass transition in a silica-rich oxide melt. *Science*, 265, 1206-1209, 1994.

- Fenstermacher JE, Optical absorption due to tetrahedral and octahedral ferric iron in silicate glasses. *Journal of Non-Crystalline Solids*, 38-39, 239-244, 1980.
- Fox KE, T Furakawa & WB White, Transition metal ions in silicate melts. Part 2: Iron in sodium silicate glasses. *Physics and Chemistry of Glasses*, 23, 169-178, 1982.
- Freer R, Diffusion in silicate minerals and glasses: A data digest and guide to the literature. *Contributions to Mineralogy and Petrology*, 76, 440-454, 1981.
- Fulcher GS, Viscosity of simple soda – silicate 500° to 1400°C, *Journal of the American Ceramic Society*, 8, 6, 339, 1925.
- Gaillard F, B Scaillet, M Pichavant & JM Beny, The effect of water and fO_2 on the ferric – ferrous ratio of silicic melts. *Chemical Geology*, 174, 255-273, 2001.
- Gaskell PH, Vibrational spectra of simple silicate glasses. *Discussions of the Faraday Society*, 50, 82, 1970.
- Gaskell PH & AB Mistry, High – resolution transmission electron microscopy of small amorphous silica particles. *Journal of Philosophy*, 39, 245-257, 1979.
- George AM & JF Stebbins, Dynamics of Na in sodium aluminosilicate glasses and liquids. *Physics and Chemistry of Minerals*, 23, 526-534, 1996.
- Giordano D, A Mangiacapra, M Potuzak, JK Russell, C Romano, DB Dingwell & A Di Muro, An expanded non-Arrhenian model for silicate melt viscosity: A treatment for metaluminous, peraluminous and peralkaline liquids. *Chemical Geology*, 229, 42-56, 2006.
- Glasstone S, KJ Laidler & H Eyring, Theory of rate processes. McGraw-Hill, New York, 486, 1941.
- Godovikov AA, *Khimicheskie osnovy sistematiki mineralov (Chemical Properties of Mineral Classification)*, Moskow: Nedra, 1979.
- Goldman DS, Oxidation equilibrium of iron in borosilicate glass. *Journal of the American Ceramic Society*, 66, 205-209, 1983.
- Goldschmidt VM, *Skrifter norske Videnskaps. Akad. Oslo, I: Math.-naturvidensk. Kl.*, 8, 7, 1926.
- Goldstein M & R Simha, eds. The glass transition and the nature of the glassy state. *Annals of the New York Academy of Sciences*, 279, 1976.
- Goto T, S Yamamoto, I Ohno & OL Anderson, Elastic constants of corundum up to 1825 K, *Journal of Geophysical Research*, 94, 7588-7602, 1989.
- Götze W, Aspects of structural glass transitions. In: Hansen JP, D Levsque & J Zin-Justin, Eds., *Liquids, freezing and glass transition. Part I*, 292-503, Elsevier Science, Amsterdam, 1991.
- Greaves GN, N Binsted & CMB Henderson, The environments of modifiers in oxide glasses. In: Hodgson KO, B Hedman & JE Penner-Hahn (eds): *EXAFS and Near Edge Structure III*. Springer – Verlag, Berlin, 297-301, 1984.
- Gwinn R & PC Hess, Iron and titanium solution properties in peraluminous and peralkaline rhyolitic liquids. *Contributions to Mineralogy and Petrology*, 101, 326-338, 1989.
- Haggerty JS, AR Cooper & JH Heasley, Heat capacity of three inorganic glasses and supercooled liquids. *Physics and Chemistry of Glasses*, 5, 130-136, 1968.
- Hannoyer B, M Lenglet, J Dürr & R Cortes, Spectroscopic evidence of octahedral iron (III) in soda – lime silicate glasses. *Journal of Non-Crystalline Solids*, 151, 209-216, 1992.
- Hawthorne FC, Spectroscopic methods in mineralogy and geology, *Reviews in Mineralogy*, 18, Washington (D.C.): Mineralogical Society of America, 1988.
- Heinrichs H & AG Herrmann, *Praktikum der Analytischen Geochemie*. Springer-Verlag, 420-425, 1998.
- Hennet L, S Krishnan, A Bytchkov, T Key, D Thiaudière, P Melin, I Pozdnyakova, ML Saboungi & DL Price, X-ray Diffraction on High-Temperature Liquids: Evolution Towards Time-Resolved Studies. *International Journal of Thermophysics*, 26, 4, 1127-1135, 2005.
- Herrmann AG, *Praktikum der Gesteinsanalyse: Chemisch-instrumentelle Methoden zur Bestimmung der Hauptkomponenten*. Springer-Verlag, Berlin, 114-119, 1975.
- Herzfeld KF & TA Litovitz, *Absorption and Dispersion of Ultrasonic Waves*, 535, Academic Press, New York, 1959.

- Hess, KU and Dingwell DB, Viscosities of hydrous leucogranitic melts: A non-Arrhenian model. *American Mineralogist*, 81, 1297-1300, 1996.
- Hess, PC & MI Wood, Aluminium coordination in metaluminous and peralkaline silicate melts. *Contributions to Mineralogy and Petrology*, 81, 103-112, 1982.
- Hirao K, N Soga & M Kunugi, Mössbauer and ESR analysis of the distribution of Fe³⁺ in leucite-type iron silicate glasses and crystals. *Journal of the American Ceramic Society*, 62, 109-110, 1979.
- Hofmaier G, Viskosität und Struktur flüssiger Silikate: Berg und Hüttenin. *Monatsh. Montan. Hochschule in Löben*, 113, 270-281, 1968.
- Hsieh CH, H Jain, AC Miller & EI Kamitsos, X-ray photoelectron spectroscopy of Al- and B-substituted sodium trisilicate glasses. *Journal of Non-Crystalline Solids*, 168, 247-257, 1994.
- Hummel W & J Arndt, Variation of viscosity with temperature and composition in the plagioclase system. *Contributions to Mineralogy and Petrology*, 90, 83-92, 1985.
- Hunold K & R Brückner, Physikalische Eigenschaften und strukturelle Feinbau von Natrium-Aluminosilicatgläsern und -schmelzen. *Glastechnische Berichte*, 6S, 149-161, 1980.
- Isard JO, *Trans. Soc. Glass Technology*, 43, 113, 1959.
- Iuga D, C Morais, Z Gan, DR Neuville, L Cormier & D Massiot, NMR Heteronuclear Correlation between Quadrupolar Nuclei in Solids. *Journal of the American Ceramic Society*, 127, 11540-11541, 2005.
- Jaeger JC and NGW Cook. *Fundamentals of rock mechanics* (3rd ed.), Chapman and Hall, New York, 593, 1979.
- Jackson I, The laboratory study of seismic wave attenuation. In *Mineral and Rock Deformation-Laboratory Studies, Geophys. Monogr. Ser.* 36:11-23, ed. B. E. Hobbs, H. C. Heard. Washington: American Geophysical Union, 1986.
- Jeoung JS, WH Poisl & MC Weinberg, Effect of oxidation state of iron on phase separation in sodium silicate glasses. *Journal of the American Ceramic Society*, 84, 8, 1859-1864, 2001.
- Johnston WD, Oxidation – reduction equilibria in iron – containing glass. *Journal of the American Ceramic Society*, 47, 198-201, 1964.
- Johnstone DH & MN Toksöz, Definitions and terminology. Seismic wave attenuation. MN Toksöz and DH Johnstone, *Society of Exploration Geophysics*, 1-5, 1981.
- Kargl F & A Meyer, Inelastic neutron scattering on sodium aluminosilicate melts: sodium diffusion and intermediate range order, *Chemical Geology*, 213- 165-172, 2004.
- Kilinc A, ISE Carmichael, ML Rivers & RO Sack, The ferric – ferrous ratio of natural silicate liquids equilibrated in air. *Contributions to Mineralogy and Petrology*, 83, 136-140, 1983.
- King IJ & RWB Stephens, Experimental acoustics: Part I: Measurement of velocity of sound in terms of elastic modulus. *Physics Education*, 10, 6, 420-423, 1975.
- Knoche R, DB Dingwell, FA Seifert & SL Webb, Non-linear properties of supercooled liquids in the system Na₂O-SiO₂. *Chemical Geology*, 116, 1-6, 1994.
- Kress VC & Carmichael ISE, The compressibility of silicate liquids containing Fe₂O₃ and the effect of composition, temperature, oxygen fugacity and pressure on their redox states. *Contributions to Mineralogy and Petrology*, 108, 82-92, 1991.
- Kozakevitch P, Viscosité et elements structuraux des alumino-silicates fondues: laitiers CaO-Al₂O₃-SiO₂ entre 100 et 2000°C. *Review Métallurgie*, 57, 149-160, 1960.
- Krupka KM, RA Robie & BS Hemingway, High-temperature heat capacities of corundum, periclase, anorthite, CaAl₂Si₂O₈ glass, moscovite, pyrophyllite, KAlSi₃O₈ glass, grossular, and NaAlSi₃O₈ glass. *American Mineralogist*, 64, 86-101, 1979.
- Kubicki JD & MJ Toplis, Molecular orbital calculations on aluminosilicate tricluster molecules: implications for the structure of aluminosilicate glasses. *American Mineralogist*, 87, 668-679, 2002.
- Kurkjian CR & EA Sigety, Coordination of the ferric ion in glass. *Physics and Chemistry of Glasses*, 9, 73-83, 1968.

- Kuryaeva RG, Degree of polymerization of aluminosilicate glasses and melts, *Fiz. Khim. Stekla*, 30, 2, 212–224, 2004 [*Glass Phys. Chem. (Engl. transl.)*, 30, 2, 157–166, 2004].
- Kushiro I, Changes in viscosity and structure of melt of $\text{MaAlSi}_2\text{O}_6$ composition at high pressures. *Journal of Geophysical Research*, 81, 6347-6350, 1976.
- Lacy ED, Aluminum in glasses and melts. *Physics and Chemistry of Glasses*, 4, 234–238, 1963.
- Lacy ED, Configuration change in silicates with particular reference to network structures. *Acta Crystallographica*, 18, 141, 1965.
- Lai CC, PB Macedo & CJ Montrose, Light-scattering measurements of structural relaxation in glass by digital correlation spectroscopy. *Journal of the American Ceramic Society*, 58, 3-4, 120-123, 1975.
- Lam DJ, AP Paulikas & BW Veal, X-ray photoemission spectroscopy studies of soda aluminosilicate glasses. *Journal of Non-Crystalline Solids*, 42, 41-47, 1980.
- Lapp JC & JE Shelby, Viscosity and thermal expansion of sodium and potassium galliosilicate glasses. *Journal of the American Ceramic Society*, 69, 2, 126-131, 1986.
- Lee SK, GD Cody, Y Fei & BO Mysen, The effect of Na/Si on the structure of sodium silicate and aluminosilicate glasses quenched from melts at high pressure: A multi-nuclear (Al-27, Na-23, O-17) 1D and 2D solid – state NMR study. *Chemical Geology*, 229, 162-172, 2006.
- Levy RA, CHP Lupis & PA Flinn, Mössbauer analysis of the valence and coordination of iron cations in $\text{SiO}_2\text{-Na}_2\text{O-CaO}$ gasses. *Physics and Chemistry of Glasses*, 17, 94-103, 1976.
- Litovitz TA & P Macedo, Ultrasonic relaxation, viscosity and free volume in molten glasses. In: JA Prins, Ed., *Physics of non-crystalline solids*, Proceedings of the International Conference, North-Holland Publishing Co., Amsterdam, 220-230, 1965.
- Liu SB, JF Stebbins, E Schneider & A Pines, Diffusive motion in alkali-silicate melts: an NMR study at high temperature, *Geochimica et Cosmochimica Acta*, 52, 527- 538, 1988.
- MacDowell JF & GH Beall, Immiscibility and crystallization in $\text{Al}_2\text{O}_3\text{-SiO}_2$ glasses. *Journal of the American Ceramic Society*, 52, 17-25, 1969.
- MacFarlane RE & JA Rayne, Ultrasonic attenuation of the noble metals. *Physical Review*, 162, 532-545, 1967.
- MacKenzie JD, Structure of some inorganic glasses from high – temperature studies. In: MacKenzie JD, *Modern Aspects of the Vitreous State*, 188-218, Butterworths, Woburn, Mass., 1960.
- Magaritz M & AW Hofmann, Diffusion of Sr, Ba and Na in obsidian. *Geochimica et Cosmochimica Acta*, 42, 595-605, 1978.
- Magnien V, DR Neuville, L Cormier, BO Mysen, V Briois, S Belin, O Pinet & P Richet, Kinetics of iron oxidation in silicate melts: a preliminary XANES study. *Chemical Geology*, 213, 253-263, 2004.
- Maier CG & ICK Kelly, An equation for the representation of high temperature heat content data. *Journal of the American Chemical Society*, 54, 3243-3246, 1932.
- Marchi GD, P Mazzoldi & A Miotello, Analysis of ionic conductivity in alkali and mixed – alkali aluminosilicate glasses. *Journal of Non-Crystalline Solids*, 105, 307-312, 1988.
- Martens RM, M Rosenhauer, H Büttner & K von Gehlen, Heat capacity and kinetic parameters in the glass transformation interval of diopside, anorthite and albite glass. *Chemical Geology*, 62, 49-70, 1987.
- Matsumura T, D Okuyama, S Niioka, H Ishida, T Satoh, Y Murakami, H Toyosaki, Y Yamada, T Fukumura & M Kawasaki, X-ray anomalous scattering of diluted magnetic oxide semiconductors: Possible evidence of lattice deformation for high temperature ferromagnetism. *Physical Review B*, 76, 115320-115325, 2007.
- Maxwell JC, On the Dynamical Theory of Gases, *Proceedings of the Royal Society of London* 15, 167–171, (Also appeared in *Philosophical Magazine*, 32, 129–145), 1867.
- May JE, Precise measurement of time delay. *IRE International Convention Record*, 6 (Pt. 2): 134-42, 1958.
- McMillan PF & B Piriou, The structures and vibrational spectra of crystals and glasses in the silica-alumina system. *Journal of Non-Crystalline Solids*, 53, 279-298, 1982.

- McMillan PF, BT Poe, P Gillet & B Reynard, A study of SiO₂ glass and supercooled liquid to 1950K via high temperature Raman spectroscopy, *Geochimica et Cosmochimica Acta*, 58, 3653-3664, 1994.
- McSkimin HJ, Pulse superposition method for measuring ultrasonic wave velocities in solids. *Journal of the Acoustical Society of America*, 33, 12-16, 1961.
- McSkimin HJ & P Aadreatch, Analysis of pulse superposition method for measuring ultrasonic wave velocities as a function of temperature and pressure. *Journal of the Acoustical Society of America*, 34, 609-615, 1962.
- Meade C, RJ Hemley & HL Mao, High-pressure x-ray diffraction of SiO₂ glass. *Physical Review Letters*, 69, 9, 1387-1390, 1992.
- Meagher EP, DK Swanson & GV Gibbs, The calculation of tetrahedral Si-O and Al-O bridging bond lengths and angles (abstract). *EOS*, 61, 408, 1980.
- Mills JJ, Low frequency storage and loss moduli of soda-silica glasses in the transformation range, *Journal of Non-Crystalline Solids*, 14, 255-268, 1974.
- Moynihan CT, Structural relaxation and the glass transition. *Reviews in Mineralogy and Geochemistry*, 32, 1, 1-19, 1995.
- Moynihan CT, Correlation between the width of the glass transition region and the temperature dependence of the viscosity of high-T_g glasses. *Journal of the American Ceramic Society*, 76, 5, 1081-1087, 1993.
- Moynihan CT, PB Macedo, CJ Montrose, CJ Montrose, PK Gupta, MA DeBolt, JF Dill, BE Dom, PW Drake, AJ Easteal, PB Elterman, RP Moeller, H Sasabe, JA Wilder, The glass transition and the nature of the glassy state. In: *Structural relaxation in vitreous materials*. *Annals of the New York Academy of Sciences*, 279, 1, 15-35, 1976.
- Mungall JE, C Romano & DB Dingwell, Multicomponent diffusion in the molten system K₂O-Na₂O-Al₂O₃-SiO₂-H₂O, *American Mineralogist*, 83, 685-699, 1998.
- Mysen BO, Melting curves of rocks and viscosity of rock-forming melts. In: Touloukian YS, WR Judd & RF Roy (eds), *Physical Properties of Rocks and Minerals*, of McGraw-Hill/CINDAS Data Series on Material Properties, Vol. II, McGraw-Hill, New York, 361-407, 1981.
- Mysen BO, Magmatic silicate melts: Relations between bulk composition, structure and properties. In: *Magmatic Processes: Physicochemical Principles* (ed.: BO Mysen), 375-400. *Geochemical Society, Special Publications*, 1, 1987.
- Mysen BO, Structure and properties of silicate melts, 354, Elsevier, Amsterdam, 1988.
- Mysen BO, Role of the Al in depolymerized, peralkaline aluminosilicate melts in the systems LiO₂-Al₂O₃-SiO₂, Na₂O-Al₂O₃-SiO₂, and K₂O-Al₂O₃-SiO₂. *American Mineralogist*, 75, 1-2, 120-134, 1990.
- Mysen BO, Structural behaviour of Al³⁺ in silicate melts: in-situ, high-temperature measurements as a function of bulk chemical composition. *Geochimica et Cosmochimica Acta*, 59, 455-474, 1995a.
- Mysen BO, Experimental, in-situ, high-temperature studies of properties and structure of silicate melts relevant to magmatic temperatures. *European Journal of Mineralogy*, 7, 745-766, 1995b.
- Mysen BO, Aluminosilicate melts: structure, composition and temperature. *Contributions to Mineralogy and Petrology*, 127, 104-118, 1997.
- Mysen BO, Transport and configurational properties of silicate melts: relationship to melt structure at magmatic temperatures. *Physics of the Earth and Planetary Interiors*, 107, 23-32, 1998.
- Mysen BO & JD Frantz, Alkali silicate glass and melt structure in the temperature range 25-1651°C at atmospheric pressure and implications for mixing behaviour of structural units. *Contributions to Mineralogy and Petrology*, 117, 1-14, 1994a.
- Mysen BO & D Virgo, Influence of pressure, temperature, and bulk composition on melt structures in the system NaAlSi₂O₆-NaFe³⁺Si₂O₆. *Journal of the American Ceramic Society*, 278, 1307-1322, 1978.
- Mysen BO & D Virgo, Trace element partitioning and melt structure: an experimental study at 1 atm. pressure. *Geochimica et Cosmochimica Acta*, 44, 1917-1930, 1980.

- Mysen BO & D Virgo, Iron bearing silicate melts – relations between pressure and redox equilibria. *Physics and Chemistry of Minerals*, 12, 4, 191-200, 1985.
- Mysen BO, FA Seifert & D Virgo, Structure and redox equilibria of iron – bearing silicate melts. *American Mineralogist*, 65, 867-884, 1980a.
- Mysen BO, D Virgo & FA Seifert, Relations between the anionic structure and viscosity of silicate melts – a Raman spectroscopic study. *American Mineralogist*, 65, 690-710, 1980b.
- Mysen BO, D Virgo & I Kushiro, The structural role of aluminium in silicate melts – a Raman spectroscopic study at 1 atmosphere. *American Mineralogist*, 66, 678-701, 1981a.
- Mysen BO, D Virgo & FA Seifert, Ferric iron as a network former and as a network modifier in melts relevant to petrological processes. *Carnegie Institution of Washington Year Book*, 80, 311-312, 1981b.
- Mysen BO, D Virgo & FA Seifert, The structure of silicate melts: implications for chemical and physical properties of natural magma, *Reviews of Geophysics and Space Physics*, 20, 3, 353-383, 1982.
- Mysen BO, D Virgo & FA Seifert, Redox equilibria of iron in alkaline earth silicate melts: relationships between melt structure, oxygen fugacity, temperature and properties of iron-bearing silicate liquids. *American Mineralogist*, 69, 834-847, 1984.
- Mysen BO, D Virgo, ER Neumann & FA Seifert, Redox equilibria and the structural states of ferric and ferrous iron in the melts in the system CaO-MgO-Al₂O₃-SiO₂-Fe-O: relationships between redox equilibria, melt structure and liquidus phase equilibria. *American Mineralogist*, 70, 317-331, 1985a.
- Mysen BO, D Virgo, CM Scarfe & DJ Cronin, Viscosity and structure of iron- and aluminium – bearing calcium silicate melts. *American Mineralogist*, 70, 487-498, 1985b.
- Mysen BO, A Lucier & GD Cody, The structural behaviour of Al³⁺ in peralkaline melts and glasses in the system Na₂O-Al₂O₃-SiO₂. *American Mineralogist*, 88, 1668-1678, 2003.
- Nagel R & AG Balogh, Atomic transport in metal/ceramic interfaces under heavy ion irradiation, *Nuclear Instruments and Methods*, B156, 135-142, 1999.
- Narayanaswamy OS, Model of structural relaxation in glass. *Journal of the American Ceramic Society*, 54, 491-498, 1971.
- Narayanaswamy OS, Thermorheological simplicity in the glass transition, *Journal of the American Ceramic Society*, 71, 10, 900-904, 1988.
- Neuvill DR & BO Mysen, Role of the aluminium in the silicate network: in-situ, high-temperature study of glasses and melts on the join SiO₂-NaAlO₂. *Geochimica et Cosmochimica Acta*, 60, 1727-1738, 1996.
- Neuvill DR, L Cormier, V Montouillout & D Massiot, Local Al site distribution in aluminosilicate glasses by ²⁷Al MQMAS NMR. *Journal of Non-Crystalline Solids*, 353, 180-184, 2007.
- Neuvill DR, P Courtial, DB Dingwell & P Richet, Thermodynamic and rheological properties of rhyolite and andesite melts. *Contributions to Mineralogy and Petrology*, 113, 572-581, 1993.
- Nolet DA, RG Burns, SL Flamm & JR Besancon, Spectra of Fe-Ti silicate glasses: implications to remote – sensing of planetary surfaces. *Proceedings of the 10th Lunar and Planetary Science Conference*, 1775-1786, 1979.
- Nowick AS & BS Berry, *Anelastic Relaxation in Solids*. Academic Press, New York, U.S.A., 1972.
- O'Connell RJ & B Budiansky, Measures of dissipation in viscoelastic media, *Geophysical Research Letters*, 5, 5-8, 1978.
- O'Reilly JM & M Goldstein, eds., *Structure and mobility in molecular and atomic glasses*. *Annals of the New York Academy of Sciences*, 371, 1981.
- Ohno I, S Yamamoto & OL Anderson, Determination of elastic constants of trigonal crystals by the rectangular parallelepiped resonance method, *Journal of Non-Crystalline Solids*, 47, 1103-1108, 1986.
- Okuno M, N Zotov, M Schmücker & H Schneider, Structure of SiO₂-Al₂O₃ glasses: Combined X-ray diffraction, IR and Raman studies. *Journal of Non-Crystalline Solids*, 351, 1032-1038, 2005.
- Papadakis EP, Ultrasonic diffraction loss and phase change in anisotropic materials. *Journal of the Acoustical Society of America*, 40, 863-76, 1966.

- Papadakis EP, Ultrasonic velocity and attenuation: measurement methods with scientific and industrial applications. (Mason W P & Thurston R N, eds.) *Physical acoustics: principles and methods*. New York: Academic Press, 12, 277-374, 1976.
- Paul A, Oxidation – reduction equilibria in glass. *Journal of Non-Crystalline Solids*, 123, 354-362, 1990.
- Piguet JL & JE Shelby, Transformation-range behaviour of lithium galliosilicate glasses. *Journal of the American Ceramic Society*, 68, C232-C233, 1985.
- Piguet JL, JC Lapp & JE Shelby, Transformation range behavior of lithium galliosilicate glasses. *Journal of the American Ceramic Society*, 68, 6, 326-329, 1985.
- Plazek DJ & KL Ngai, Correlation of polymer segmental chain dynamics with temperature dependent time – scale shifts. *Macromolecules*, 24, 1222-1224, 1991.
- Pocklington HC, Rough measurement of high viscosities. *Proceedings of the Cambridge Philosophical Society*, 36, 507–508, 1940.
- Poe BT, PF McMillan, CA Angell & RK Sato, Al and Si coordination in SiO₂-Al₂O₃ glasses and liquids: a study by NMR and IR spectroscopy and MD simulations. *Chemical Geology*, 96, 333-349, 1992.
- Poe BT, PF McMillan, B Côté, D Massiot & JP Coutures, Structure and dynamics in calcium aluminate liquids: High temperature ²⁷Al NMR and Raman spectroscopy. *Journal of the American Ceramic Society*, 77, 1832-1838, 1994.
- Poe B, F Seifert, TG Sharp & Z Wu, ELNES spectroscopy of mixed Si coordination minerals. *Physics and Chemistry of Minerals*, 24, 477-487, 1997.
- Reid JE, BT Poe, DC Rubie, N Zotov & M Wiedenbeck, The self-diffusion of silicon and oxygen in diopside (CaMgSi₂O₆) liquid up to 15 GPa. *Chemical Geology*, 174, 77-86, 2001.
- Reid JE, A Suzuki, KI Funakoshi, H Terasaki, BT Poe, DC Rubie & E Ohtani, The viscosity of CaMgSi₂O₆ liquid at pressures up to 13 GPa, *Physics of the Earth and Planetary Interiors*, 139, 45– 54, 2003.
- Richet P, Viscosity and configurational entropy of silicate melts. *Geochimica et Cosmochimica Acta*, 48, 471-483, 1984.
- Richet P, Heat capacity of silicate glasses. *Chemical Geology*, 62, 111-124, 1987.
- Richet P, The physical basis of thermodynamics. With application to chemistry. Plenum Publishing, New York, 2001.
- Richet P, Enthalpy, volume and structural relaxation in glass – forming silicate melts. *Journal of Thermal Analysis and Calorimetry*, 69, 739-750, 2002.
- Richet P & Y Bottinga, Heat capacity of aluminium – free liquid silicates. *Geochimica et Cosmochimica Acta*, 49, 471-486, 1985.
- Richet P & Y Bottinga, Thermochemical properties of silicate glasses and liquids. A review, *Review Geophysics*, 24, 1-25, 1986.
- Richet P & Y Bottinga, Rheology and configurational entropy of silicate melts. In Stebbins JF, McMillan PF and Dingwell DB, Eds., *Structure, Dynamics and Properties of Silicate Melts*, 32, 67-93. *Reviews in Mineralogy*, Mineralogical Society of America, Washington, D.C., 1995.
- Richet P & DR Neuville, Thermodynamics of silicate melts: configurational properties. In: Saxena S., Ed., *Thermodynamic data systematics and estimation*, *Advances in Physical Geochemistry*, 132-160, Springer – Verlag, Berlin, 1992.
- Richet P & MJ Toplis, Thermodynamic aspects of the glass transition of silicates. *Comptes Rendus de l'Académie des Sciences (Paris), série II. Sciences de la Terre et des planètes*, 2, 191-202, 2001
- Richet P, RA Robie & BS Hemingway, Low-temperature heat capacity of diopside glass (CaMgSi₂O₆): A calorimetric test of the configurational-entropy theory applied to the viscosity of liquid silicates. *Geochimica et Cosmochimica Acta*, 50, 7, 1521-1533, 1986.
- Riebling EF, Structure of magnesium aluminosilicate liquids at 1700°C. *Canadian Journal of Chemistry*, 42, 2811-2821, 1964.

- Riebling EF, Structure of aluminosilicate melts containing at least 50 mole % SiO₂ at 1500°C. *Journal of Chemical Physics*, 44, 2857-2865, 1966.
- Riebling EF, Structural similarities between a glass and its melt. *Journal of the American Ceramic Society*, 51, 143-149, 1968.
- Riley WF, LD Sturges & DH Morris, Mechanics of materials: Torsional loading of shafts, 272-344, John Wiley & Sons, Inc., New York, 1999.
- Risbud SH, RJ Kirkpatrick, AP Tagliavere & B Montez, Solid-state NMR evidence of 4-, 5-, and 6-fold aluminum sites in roller-quenched SiO₂-Al₂O₃ glasses. *Journal of the American Ceramic Society*, 70, C10-C70, 1987.
- Rivers ML & LSE Carmichael, Ultrasonic studies of silicate melts. *Journal of Geophysical Research*, 92, 9247-9270, 1987.
- Robie RA, BS Hemingway & JR Fisher, Thermodynamic properties of minerals and related substances at 298.15 K and 1 bar (105 Pascals) pressure and at higher temperatures. *United States Geological Survey Bulletin*, 1452, 456, 1979.
- Roselieb K, W Rammensee, H Büttner & M Rosenhauer, Solubility and diffusion of noble gases in vitreous albite. *Chemical Geology*, 96, 241-266, 1992.
- Roskosz M, MJ Toplis & P Richet, The structural role of Ti in aluminosilicate liquids in the glass transition range: insights from heat capacity and shear viscosity measurements. *Geochimica et Cosmochimica Acta*, 68, 3, 591-606, 2004.
- Russel C & A Wiedenroth, The effect of glass composition on the thermodynamic of the Fe²⁺/Fe³⁺ equilibrium and the iron diffusivity in Na₂O/MgO/CaO/Al₂O₃/SiO₂ melts. *Chemical Geology*, 213, 1-3, 125-135, 2004.
- Russel JK, D Giordano & DB Dingwell, High-temperature limits on viscosity of non-Arrhenian silicate melts, *American Mineralogist*, 88, 1390-1394, 2003.
- Sack RO, ISE Carmichael, ML Rivers & M Ghiorso, Ferric – ferrous equilibria in natural silicate liquids at 1 bar. *Contributions to Mineralogy and Petrology*, 75, 369-376, 1980.
- Sartorius, Sartorius YDK 01, YDK 01-OD, YDK 01 LP. Density Determination Kit, User's manual. 2004
- Sass F, Ch Bouché & A Leitner, *Dubbels Taschenbuch für den Maschinenbau*, Springer – Verlag, 382-384, 1966.
- Sato RK, PF MacMillan, P Dennison & R Dupree, High-resolution ²⁷Al and ²⁹Si MAS NMR investigation of SiO₂-Al₂O₃ glasses. *Journal of Physical Chemistry*, 95, 11, 483-4489, 1991a.
- Sato RK, PF MacMillan, P Dennison & R Dupree, A structural investigation of high alumina glasses in the CaO-Al₂O₃-SiO₂ system via Raman and magic angle spinning nuclear magnetic resonance spectroscopy. *Physics and Chemistry of Glasses*, 32, 149-154, 1991b.
- Scherer GW, Use of the Adam – Gibbs equation in the analysis of structural relaxation. *Journal of the American Ceramic Society*, 67, 7, 504-511, 1984.
- Scherer GW, *Relaxation in glass and composites*. 331, Wiley, New York, 1986.
- Scherer GW, Theories of relaxation. *Journal of Non-Crystalline Solids*, 123, 75-89, 1990.
- Schramm CM, BHWS DeJong & VF Parziale, ²⁹Si magic angle spinning NMR study of local silicon environments in-amorphous and crystalline lithium silicates. *Journal of the American Ceramic Society*, 106, 4396-4402, 1984.
- Secco RA, MH Manghnani & TC Liu, The bulk modulus – attenuation – viscosity systematics for diopside – anorthite melts. *Geophysical Research Letters*, 18, 1, 93-96, 1991.
- Seifert FA & M Olesch, Mössbauer spectroscopy of grandidierite, (Mg, Fe)Al₃BSiO₉. *American Mineralogist*, 62, 547-553, 1977.
- Seifert FA, BO Mysen & D Virgo, Three – dimensional network structure of quenched melts (glass) in the system SiO₂-NaAlO₂, SiO₂-CaAl₂O₄ and SiO₂-MgAl₂O₄. *American Mineralogist*, 67, 696-717, 1982.
- Seifert FA, D Virgo & BO Mysen, Melt structures and redox equilibria in the system Na₂O-FeO-Fe₂O₃-Al₂O₃-SiO₂. *Carnegie Inst. Wash. Yearbook*, 78, 511-519, 1979.
- Shelby JE, Viscosity and thermal expansion of lithium aluminosilicate glasses. *Journal of Applied Physics*, 49, 12, 5885-5891, 1978.

- Shelby JE, Treatise on materials science and technology, 17, Glass II, Chapter 1, 1-40, 1979.
- Shelby JE, Formation and properties of calcium aluminosilicate glasses. *Journal of the American Ceramic Society*, 68, 3, 155-158, 1985.
- Shelby JE, Properties and structure of soda-lime aluminosilicate glasses. *Journal of Applied Physics*, 66, 5, 1947-1950, 1989.
- Shelby JE, Introduction to glass science and technology. 2nd ed. The Royal Society of Chemistry, Cambridge, 2005.
- Shimizu N & I Kushiro, Diffusivity of oxygen in jadeite and diopside melts at high pressures. *Geochimica et Cosmochimica Acta*, 48, 1295-1303, 1984.
- Siewert R & M Rosenhauer, Viscoelastic relaxation measurements in the system SiO₂-NaAlSiO₄ by photon correlation spectroscopy. *American Mineralogist*, 82, 1063-1072, 1997.
- Simon F, Über der Zustand der unterkühlten Flüssigkeiten and Gläser. *Zeitschrift für anorganische und allgemeine Chemie*, 203, 219-227, 1931.
- Sippel RF, Sodium self diffusion in natural minerals. *Geochimica et Cosmochimica Acta*, 27, 107-120, 1963.
- Spiering B & FA Seifert, Iron in silicate glasses of granitic composition: a Mössbauer spectroscopic study. *Contributions to Mineralogy and Petrology*, 90, 63-73, 1985.
- Stebbins JF, NMR evidence for five-coordinated silicon in a silicate glass at atmospheric pressure. *Nature*, 351, 638-639, 1991.
- Stebbins JF, Dynamics and structure of silicate and oxide melts: nuclear magnetic resonance studies, In: Structure, Dynamics and Properties of Silicate Melts, Stebbins JF, PF McMillan & DB Dingwell (eds), *Reviews in Mineralogy*, Mineralogical Society of America, Washington DC, 32, 191-246, 1995.
- Stebbins JF & I Farnan, The effects of temperature on silicate liquid structure: a multi-nuclear, high temperature NMR study. *Science*, 255, 586-589, 1992.
- Stebbins JF & PF McMillan, Compositional and temperature effects on five-coordinated silicon in ambient pressure silicate glasses, *Journal of Non-Crystalline Solids*, 160, 116-125, 1993.
- Stebbins JF & S Sen, Microscopic dynamics and viscous flow in a borosilicate glass – forming liquid. *Journal of Non-Crystalline Solids*, 224, 80-85, 1998.
- Stebbins JF & Z Xu, NMR evidence for excess non-bridging oxygen in an aluminosilicate glass, *Nature*, 390, 60-62, 1997.
- Stebbins JF, ISE Carmichael & LK Moret, Heat capacities and entropies of silicate liquids and glasses. *Contributions to Mineralogy and Petrology*, 86, 131-148, 1984.
- Stebbins JF, JV Ogelsby & SK Lee, Oxygen sites in silicate glasses; a new view from oxygen-17 NMR; *Chemical Geology*, 174, 63-75, 2001.
- Stebbins JF, S Sen & I Farnan, Silicate species exchange, viscosity, and crystallization in a low – silica melt: In situ high – temperature MAS NMR spectroscopy. *American Mineralogist*, 80, 861-864, 1995.
- Steele FN & RW Douglas, The absorption of iron in silicate and borate glasses. *Physics and Chemistry of Glasses*, 6, 246-252, 1965.
- Stein DJ & FJ Spera, Experimental rheometry of melts and supercooled liquids in the system NaAlSiO₄-SiO₂: Implications for structure and dynamics. *American Mineralogist*, 78, 710-723, 1993.
- Stevenson RJ, DB Dingwell, SL Webb & NS Bagdassarov, The equivalence of enthalpy and shear stress relaxation in rhyolitic obsidian and quantification of the liquid-glass transition in volcanic processes, *Journal of Volcanology and Geothermal Research*, 68, 297-306, 1995.
- Tammann G, Kristallisieren und Schmelzen. Johann Ambrosius Barth, Leipzig, 26-46, 1903.
- Tammann G, Der Glaszustand. Leopold Voss, Leipzig, 123, 1933.
- Tammann G, Aggregatzustände. Die Zustandsänderungen der Materie in Abhängigkeit von Druck und Temperatur. Leopold Voss, Leipzig, 2nd Edition, 1923.

- Tammann G & W Hesse, Die Abhängigkeit der Viskosität von der Temperatur bei unterkühlten Flüssigkeiten, *Zeitschrift für anorganische und allgemeine Chemie*, 156, 1, 245-257, 1926.
- Tangeman JA & RA Lange, The effect of Al^{3+} , Fe^{3+} , and Ti^{4+} on the configurational heat capacities of sodium silicate liquids. *Physics and Chemistry of Minerals*, 26, 83-99, 1998.
- Taylor MP & GE Brown Jr., Structure of mineral glasses. I. The feldspar glasses $\text{NaAlSi}_3\text{O}_8$, KAlSi_3O_8 , $\text{CaAl}_2\text{Si}_2\text{O}_8$. *Geochimica et Cosmochimica Acta*, 43, 61-77, 1979a.
- Taylor MP & GE Brown Jr., Structure of mineral glasses. II. The SiO_2 - NaAlSiO_4 join. *Geochimica et Cosmochimica Acta*, 43, 1467-1473, 1979b.
- Taylor TD & GE Rindone, Properties of soda aluminosilicate glasses: V, low temperature viscosities. *Journal of the American Ceramic Society*, 53, 692-695, 1970.
- Taylor MP, GE Brown Jr. & PM Fenn, Structure of mineral glasses. III. $\text{NaAlSi}_3\text{O}_8$ supercooled liquid at 850°C and the effects of thermal history. *Geochimica et Cosmochimica Acta*, 44, 109-117, 1980.
- Terai R, Self-diffusion of sodium ions and electrical conductivity in sodium aluminosilicate glasses. *Physics and Chemistry of Glasses*, 10, 146-152, 1969.
- Toplis MJ, Energy barriers to viscous flow and the prediction of glass transition temperatures of molten silicates, *American Mineralogist*, 83, 480-490, 1998.
- Toplis MJ, Quantitative links between microscopic properties and viscosity of liquids in the system SiO_2 - Na_2O . *Chemical Geology*, 174, 321-331, 2001.
- Toplis M, DB Dingwell & T Lenci, Peraluminous viscosity maxima in Na_2O - Al_2O_3 - SiO_2 liquids: The role of triclusters in tectosilicate melts. *Geochimica et Cosmochimica Acta*, 61, 2605-2612, 1997a.
- Toplis M, DB Dingwell, K-U Hess & T Lenci, Viscosity, fragility, and configurational entropy of melts along the join SiO_2 - NaAlSiO_4 . *American Mineralogist*, 82, 979-990, 1997b.
- Toplis MJ, SC Kohn, ME Smith & IJF Poplett, Fivefold – coordinated aluminium in tectosilicate glasses observed by triple quantum MAS NMR. *American Mineralogist*, 85, 1556-1560, 2000.
- Toplis MJ, J Gottsmann, R Knoche & DB Dingwell, Heat capacities of haplogranitic glasses and liquids. *Geochimica et Cosmochimica Acta*, 65, 1985-1994, 2001.
- Truell R, C Elbaum & B Chick, *Ultrasonic Methods in Solid State Physics*, Academic Press, 1969.
- Urbain G, Y Bottinga & P Richet, Viscosity of liquid silica, silicates and aluminosilicates. *Geochimica et Cosmochimica Acta*, 46, 1061-1072, 1982.
- Virgo D & BO Mysen, The structural state of iron in oxidized vs. reduced glasses at 1 atm.: a ^{57}Fe Mössbauer study. *Physics and Chemistry of Minerals*, 12, 65-76, 1985.
- Virgo D, BO Mysen & PA Danckwerth, Redox equilibria and the anionic structure of $\text{Na}_2\text{O} \cdot x\text{SiO}_2$ -Fe-O melts: effects of oxygen fugacity. *Carnegie Institution of Washington Year Book*, 82, 305-309, 1983.
- Virgo D, BO Mysen & FA Seifert, Relationship between the oxidation state of iron and the structure of silicate melts. *Carnegie Institution of Washington Year Book*, 80, 308-311, 1981.
- Virgo D, BO Mysen, PA Danckwerth & FA Seifert, The anionic structure of 1 atm. melts in the system SiO_2 - NaFeO_2 . *Carnegie Institution of Washington Year Book*, 81, 347-349, 1982.
- Virgo D, BO Mysen, PA Danckwerth & FA Seifert, Speciation of Fe^{3+} in 1-atm Na_2O - SiO_2 -Fe-O melts. *Carnegie Institution of Washington Year Book*, 81, 349-353, 1982a.
- Vogel DRW, Structure and crystallization behaviour of glasses. *Angewandte Chemie International Edition*, 4, 2, 112-121, 1965.
- Waff HS, The structural role of ferric iron in silicate melts. *Canadian Mineralogist*, 15, 198-199, 1977.
- Wang CM & H Chen, Mixed coordination of Fe^{3+} and its dependence on the iron content in sodium disilicate glasses. *Physics and Chemistry of Glasses*, 28, 39-47, 1987.
- Wang Z, TF Cooney & SK Sharma, High temperature structural investigations of Na_2O - $0.5\text{Fe}_2\text{O}_3$ - 3SiO_2 and Na_2O -FeO- 3SiO_2 melts and glasses. *Contributions to Mineralogy and Petrology*, 115, 112-122, 1993.

- Wang Z, TF Cooney & SK Sharma, In situ structural investigations of iron – containing silicate liquids and glasses. *Geochimica et Cosmochimica Acta*, 59, 1571-1577, 1995.
- Warren BE, X-ray diffraction in long chain liquids. *Physical Review*, 44, 969-973, 1933.
- Watson EB, Calcium diffusion in a simple silicate melt to 30 kbar. *Geochimica et Cosmochimica Acta*, 43, 313-323, 1979.
- Webb SL, Shear and volume relaxation in $\text{Na}_2\text{Si}_2\text{O}_5$. *American Mineralogist*, 76, 1449-1454, 1991.
- Webb SL, Low-frequency shear and structural relaxation in rhyolite melt. *Physics and Chemistry of Minerals*, 19, 240-245, 1992a.
- Webb SL, Shear, volume, enthalpy and structural relaxation in silicate melts. *Chemical Geology*, 96, 449-457, 1992b.
- Webb SL, Silicate melts at extreme conditions. In Miletich, R., Ed., *Mineral Behaviour at Extreme Conditions*, EMU Notes in Mineralogy, 7, Chapter 3, 65-94, 2005a.
- Webb SL, Structure and rheology of Fe_2O_3 -bearing $\text{Na}_2\text{O}-\text{Al}_2\text{O}_3-\text{SiO}_2$ melts. *European Journal of Mineralogy*, 17, 223-232, 2005b.
- Webb SL & DB Dingwell, The onset of non-Newtonian rheology of silicate melts: A fiber elongation study. *Physics and Chemistry of Minerals*, 17, 125-132, 1990.
- Webb SL & DB Dingwell, Viscoelasticity. *Reviews in Mineralogy and Geochemistry*, 32, 1, 95-119, 1995.
- Webb SL & I Jackson, Anelasticity and microcreep in polycrystalline MgO at high temperature: an exploratory study. *Physics and Chemistry of Minerals*, 30, 157-166, 2003.
- Webb SL, E Müller & H Büttner, Anomalous rheology of peraluminous melts. *American Mineralogist*, 89, 812-818, 2004.
- Webb SL, M Banaszak, U Köhler, S Rausch & G Raschke, The viscosity of $\text{Na}_2\text{O}-\text{CaO}-\text{Al}_2\text{O}_3-\text{SiO}_2$ melts. *European Journal of Mineralogy*, submitted, 02/2007.
- Weigel C, L Cormier, L Galois, G Calas, D Bowron & B Beuneu, Determination of Fe^{3+} sites in a $\text{NaFeSi}_2\text{O}_6$ glass by neutron diffraction with isotopic substitution coupled with numerical simulation. *Applied Physics Letters*, 89, 14, 141911, 2006.
- Wilding MC, SL Webb & DB Dingwell, Evaluation of a relaxation geospeedometer for volcanic glasses. *Chemical Geology*, 125, 137-148, 1995.
- Wilke M, H Behrens, DJM Burkhard & S Rossano, The oxidation state of iron in silicic melt at 500 MPa water pressure. *Chemical Geology*, 189, 55-67, 2002.
- Wilke M, C Schmidt, F Farges, V Malavergne, L Gautron, A Simionovici, M Hahn & PE Petit, Structural environment of iron in hydrous aluminosilicate glass and melt – evidence from X-ray absorption spectroscopy. *Chemical Geology*, 229, 144-161, 2006.
- Wispelaere SD, D Cabaret, C Levelut, S Rossano, AM Flank, P Parent & F Farges, Na-, Al-, and Si K-edge XANES study of sodium silicate and sodium aluminosilicate glasses : influence of the glass surface. *Chemical Geology*, 213, 63-70, 2004.
- Wood MI & PC Hess, The structural role of Al_2O_3 and TiO_2 in immiscible silicate liquids in the system $\text{SiO}_2-\text{MgO}-\text{CaO}-\text{FeO}-\text{TiO}_2-\text{Al}_2\text{O}_3$. *Contributions to Mineralogy and Petrology*, 72, 319-328, 1980.
- Xue X & M Kanzaki, NMR characteristics of possible oxygen sites in aluminosilicate glasses and melts: an ab initio study. *Journal of Physical Chemistry B*, 103, 10816-10830, 1999.
- Yue YZ & R Brückner, A new description and interpretation of the flow behaviour of glass forming melts. *Journal of Non-Crystalline Solids*, 180, 66-79, 1994.
- Zachariasen WH, *Journal of the American Chemical Society*, 54, 3841-3851 (1932).
- Zdaniewski WA, GE Rindone & DE Day, The internal friction of glasses. *Journal of Materials Science*, 14, 763-775, 1979.
- Zotov N & R Delaplane, Structure and crystallization kinetics of sodium tetrasilicate glass: a high temperature neutron diffraction study. *Materials Science Forum*, 321-324, 535-539, 2000.

APPENDICES

Appendix 1	A-1
Heat capacity data (in $\text{J g}^{-1} \text{K}^{-1}$) for all of the samples with step of temperature of 5°C for matched cooling/heating rate of $20^\circ\text{C min}^{-1}$.	
Appendix 2	A-7
Temperature T , $\log_{10} \eta$, frequency f , $\log_{10} \omega\tau_M$, imaginary (G_{im}) and real (G_{real}) shear modulus and shear modulus of the melt (G_{melt}) for the investigated samples.	
Appendix 3	A-39
Temperature T , frequency f , G_∞ , viscosity η , shear viscosity, relaxed Newtonian viscosity and relaxation times τ of the samples, determined by micropenetration and torsion measurements.	
Appendix 4a	A-57
Parameters of the lines fitted to the real shear modulus data for NS2 melt (G0) and Fe-free melts (G1-G7).	
Appendix 4b	A-61
Parameters of the lines fitted to the imaginary shear modulus data for NS2 melt (G0) and Fe-free melts (G1-G7).	
Appendix 4c	A-65
Parameters of the lines fitted to the real shear modulus data for Fe-bearing melts (G8-14).	
Appendix 4d	A-70
Parameters of the lines fitted to the imaginary shear modulus data for Fe-bearing melts (G8-G14).	
Appendix 5a	A-75
Parameters of the fits to Eq. 58 for the NS (G0) and Fe-free melts (G1-G7).	
Appendix 5b	A-76
Parameters of the fits to Eq. 58 for the Fe-bearing melts (G8-G14).	

Appendix 1. Heat capacity data (in $\text{J g}^{-1} \text{K}^{-1}$) for all of the samples with step of temperature of 5°C for matched cooling/heating rate of $20^\circ\text{C min}^{-1}$.

T ($^\circ\text{C}$)	G0	G1	G2	G3	G4	G5	G6	G7	G8	G9	G10	G11	G12	G13	G14
	Heat capacity c_p ($\text{J g}^{-1} \text{K}^{-1}$)														
100	0.981	0.906	0.898	0.906	0.923	0.917	0.918	0.936	0.911	0.882	0.887	0.874	0.888	0.885	0.893
105	0.986	0.917	0.897	0.918	0.921	0.919	0.923	0.943	0.921	0.888	0.907	0.884	0.900	0.899	0.910
110	0.987	0.919	0.898	0.918	0.918	0.924	0.936	0.948	0.926	0.899	0.911	0.893	0.902	0.904	0.914
115	0.994	0.915	0.902	0.922	0.926	0.928	0.935	0.946	0.933	0.908	0.903	0.898	0.896	0.899	0.910
120	1.001	0.918	0.908	0.928	0.935	0.938	0.939	0.951	0.940	0.915	0.909	0.903	0.902	0.903	0.913
125	1.005	0.930	0.915	0.935	0.944	0.943	0.943	0.955	0.945	0.920	0.913	0.910	0.907	0.905	0.921
130	1.008	0.940	0.927	0.941	0.948	0.947	0.947	0.965	0.947	0.921	0.918	0.923	0.915	0.906	0.926
135	1.015	0.948	0.933	0.945	0.950	0.949	0.950	0.973	0.950	0.924	0.931	0.931	0.929	0.911	0.936
140	1.019	0.953	0.933	0.951	0.946	0.948	0.940	0.963	0.956	0.930	0.936	0.934	0.937	0.916	0.942
145	1.023	0.957	0.936	0.956	0.950	0.951	0.942	0.966	0.959	0.932	0.939	0.941	0.940	0.921	0.945
150	1.024	0.952	0.943	0.961	0.955	0.955	0.946	0.972	0.964	0.937	0.933	0.947	0.934	0.916	0.939
155	1.027	0.957	0.949	0.965	0.960	0.958	0.951	0.977	0.971	0.944	0.936	0.952	0.936	0.921	0.942
160	1.034	0.960	0.953	0.971	0.965	0.963	0.955	0.981	0.977	0.949	0.939	0.958	0.940	0.925	0.947
165	1.036	0.965	0.958	0.976	0.969	0.968	0.958	0.984	0.981	0.952	0.943	0.960	0.945	0.928	0.952
170	1.041	0.970	0.963	0.981	0.974	0.970	0.960	0.987	0.984	0.956	0.948	0.964	0.949	0.932	0.956
175	1.045	0.974	0.967	0.985	0.978	0.977	0.963	0.991	0.986	0.957	0.952	0.966	0.953	0.933	0.960
180	1.047	0.979	0.972	0.991	0.983	0.982	0.968	0.994	0.987	0.961	0.957	0.971	0.957	0.935	0.964
185	1.050	0.982	0.977	0.994	0.987	0.986	0.972	0.997	0.990	0.963	0.959	0.976	0.960	0.938	0.967
190	1.054	0.986	0.980	0.998	0.990	0.989	0.976	1.001	0.994	0.966	0.963	0.980	0.964	0.942	0.971
195	1.057	0.990	0.986	1.003	0.995	0.994	0.979	1.006	0.999	0.971	0.967	0.985	0.968	0.946	0.975
200	1.066	0.995	0.991	1.009	1.000	0.999	0.982	1.008	1.006	0.979	0.972	0.990	0.971	0.949	0.979
205	1.069	0.998	0.996	1.012	1.006	1.003	0.985	1.010	1.010	0.982	0.974	0.992	0.975	0.952	0.982
210	1.072	1.003	1.000	1.017	1.009	1.007	0.989	1.015	1.014	0.985	0.979	0.995	0.979	0.955	0.986
215	1.076	1.007	1.002	1.020	1.012	1.011	0.992	1.017	1.016	0.989	0.982	0.998	0.983	0.959	0.990
220	1.079	1.010	1.006	1.022	1.016	1.013	0.996	1.020	1.019	0.991	0.985	1.001	0.986	0.962	0.995
225	1.081	1.014	1.010	1.027	1.019	1.017	0.999	1.024	1.021	0.992	0.989	1.004	0.990	0.966	0.998
230	1.086	1.017	1.013	1.031	1.021	1.020	1.003	1.028	1.027	0.996	0.993	1.006	0.994	0.969	1.001
235	1.090	1.020	1.018	1.035	1.026	1.025	1.005	1.030	1.031	1.000	0.996	1.007	0.997	0.972	1.005
240	1.094	1.023	1.023	1.040	1.030	1.029	1.008	1.033	1.035	1.003	0.999	1.011	1.000	0.976	1.008
245	1.097	1.027	1.028	1.045	1.034	1.034	1.010	1.036	1.036	1.005	1.003	1.015	1.003	0.980	1.012
250	1.100	1.030	1.031	1.048	1.038	1.038	1.013	1.038	1.039	1.007	1.006	1.018	1.005	0.982	1.015
255	1.104	1.034	1.035	1.053	1.042	1.042	1.016	1.040	1.042	1.010	1.010	1.021	1.009	0.987	1.020
260	1.108	1.039	1.037	1.054	1.044	1.044	1.021	1.044	1.047	1.014	1.013	1.023	1.012	0.989	1.023
265	1.109	1.043	1.042	1.057	1.048	1.047	1.025	1.049	1.049	1.016	1.017	1.028	1.016	0.993	1.027
270	1.113	1.045	1.044	1.059	1.051	1.050	1.030	1.053	1.052	1.018	1.020	1.030	1.020	0.998	1.031
275	1.114	1.048	1.046	1.063	1.055	1.052	1.033	1.056	1.053	1.020	1.023	1.034	1.023	1.001	1.033
280	1.117	1.050	1.049	1.065	1.057	1.054	1.034	1.058	1.055	1.023	1.024	1.037	1.025	1.003	1.034
285	1.120	1.054	1.052	1.068	1.060	1.058	1.038	1.062	1.058	1.026	1.029	1.039	1.028	1.007	1.038
290	1.122	1.056	1.055	1.072	1.064	1.061	1.040	1.064	1.059	1.029	1.031	1.043	1.029	1.007	1.040

Appendix 1. Heat capacity data (in $\text{J g}^{-1} \text{K}^{-1}$) for all of the samples with step of temperature of 5°C for matched cooling/heating rate of $20^\circ\text{C min}^{-1}$. Continuation...

T ($^\circ\text{C}$)	G0	G1	G2	G3	G4	G5	G6	G7	G8	G9	G10	G11	G12	G13	G14
	Heat capacity c_p ($\text{J g}^{-1} \text{K}^{-1}$)														
295	1.125	1.059	1.059	1.076	1.069	1.065	1.044	1.066	1.063	1.031	1.033	1.045	1.030	1.010	1.041
300	1.129	1.062	1.061	1.078	1.071	1.068	1.043	1.066	1.066	1.034	1.035	1.047	1.033	1.012	1.045
305	1.132	1.066	1.063	1.080	1.072	1.070	1.045	1.070	1.068	1.035	1.039	1.050	1.036	1.016	1.047
310	1.137	1.070	1.068	1.083	1.075	1.074	1.048	1.072	1.072	1.039	1.043	1.051	1.040	1.019	1.050
315	1.140	1.073	1.069	1.085	1.077	1.076	1.051	1.074	1.076	1.042	1.044	1.053	1.043	1.021	1.052
320	1.142	1.076	1.073	1.088	1.079	1.078	1.053	1.074	1.077	1.042	1.047	1.057	1.046	1.024	1.054
325	1.144	1.078	1.075	1.090	1.081	1.081	1.055	1.077	1.079	1.044	1.049	1.060	1.048	1.024	1.056
330	1.149	1.081	1.079	1.093	1.084	1.084	1.060	1.081	1.083	1.047	1.051	1.063	1.050	1.027	1.058
335	1.152	1.084	1.081	1.096	1.086	1.087	1.063	1.084	1.086	1.050	1.053	1.064	1.055	1.030	1.060
340	1.157	1.085	1.084	1.098	1.089	1.090	1.064	1.087	1.091	1.055	1.055	1.066	1.055	1.030	1.063
345	1.161	1.087	1.084	1.099	1.089	1.091	1.066	1.089	1.093	1.059	1.058	1.070	1.057	1.032	1.065
350	1.163	1.092	1.087	1.102	1.093	1.095	1.066	1.091	1.095	1.060	1.060	1.071	1.060	1.034	1.067
355	1.167	1.095	1.089	1.106	1.094	1.098	1.068	1.093	1.098	1.062	1.061	1.073	1.062	1.036	1.069
360	1.167	1.096	1.091	1.107	1.097	1.100	1.072	1.097	1.099	1.063	1.064	1.076	1.064	1.038	1.072
365	1.171	1.098	1.092	1.109	1.099	1.101	1.076	1.100	1.101	1.064	1.065	1.077	1.065	1.039	1.073
370	1.172	1.099	1.092	1.110	1.101	1.104	1.079	1.103	1.102	1.065	1.068	1.078	1.067	1.041	1.076
375	1.174	1.102	1.096	1.113	1.104	1.107	1.081	1.106	1.105	1.067	1.071	1.078	1.071	1.044	1.079
380	1.178	1.104	1.098	1.114	1.106	1.109	1.082	1.107	1.108	1.070	1.073	1.081	1.072	1.045	1.081
385	1.179	1.104	1.100	1.115	1.107	1.110	1.081	1.109	1.109	1.071	1.075	1.082	1.073	1.046	1.083
390	1.180	1.107	1.100	1.116	1.109	1.112	1.083	1.110	1.110	1.070	1.077	1.082	1.078	1.049	1.086
395	1.183	1.110	1.102	1.118	1.110	1.112	1.085	1.112	1.112	1.072	1.080	1.085	1.080	1.050	1.087
400	1.186	1.111	1.106	1.122	1.112	1.114	1.089	1.114	1.116	1.076	1.081	1.086	1.081	1.052	1.090
405	1.189	1.114	1.109	1.122	1.113	1.116	1.091	1.117	1.118	1.079	1.083	1.087	1.081	1.055	1.092
410	1.192	1.116	1.111	1.126	1.116	1.118	1.092	1.117	1.120	1.080	1.087	1.089	1.083	1.057	1.094
415	1.196	1.119	1.114	1.127	1.118	1.119	1.094	1.119	1.121	1.081	1.088	1.090	1.085	1.060	1.096
420	1.198	1.120	1.116	1.130	1.120	1.122	1.097	1.123	1.123	1.083	1.091	1.092	1.088	1.062	1.099
425	1.202	1.121	1.118	1.134	1.123	1.124	1.098	1.124	1.124	1.084	1.090	1.094	1.089	1.063	1.099
430	1.207	1.122	1.120	1.135	1.124	1.126	1.099	1.126	1.125	1.087	1.091	1.096	1.089	1.063	1.101
435	1.210	1.124	1.120	1.137	1.125	1.126	1.099	1.126	1.125	1.089	1.093	1.097	1.091	1.065	1.102
440	1.214	1.128	1.122	1.138	1.125	1.127	1.101	1.128	1.126	1.090	1.096	1.100	1.093	1.067	1.106
445	1.222	1.128	1.124	1.140	1.126	1.130	1.102	1.130	1.129	1.091	1.096	1.101	1.094	1.068	1.105
450	1.233	1.129	1.127	1.142	1.128	1.132	1.104	1.132	1.132	1.094	1.098	1.103	1.095	1.070	1.107
455	1.247	1.130	1.130	1.146	1.131	1.135	1.106	1.135	1.134	1.095	1.101	1.103	1.096	1.072	1.109
460	1.267	1.131	1.131	1.146	1.134	1.138	1.108	1.136	1.134	1.097	1.103	1.104	1.098	1.073	1.111
465	1.294	1.131	1.131	1.148	1.136	1.138	1.111	1.139	1.135	1.099	1.102	1.106	1.099	1.074	1.111
470	1.333	1.134	1.130	1.145	1.134	1.137	1.111	1.140	1.138	1.102	1.105	1.107	1.103	1.076	1.115
475	1.381	1.134	1.133	1.148	1.136	1.139	1.112	1.141	1.137	1.103	1.106	1.109	1.103	1.077	1.115
480	1.445	1.137	1.136	1.150	1.139	1.142	1.114	1.144	1.140	1.104	1.107	1.108	1.104	1.078	1.116
485	1.507	1.140	1.137	1.151	1.140	1.144	1.116	1.145	1.142	1.106	1.111	1.110	1.107	1.081	1.120

Appendix 1. Heat capacity data (in $\text{J g}^{-1} \text{K}^{-1}$) for all of the samples with step of temperature of 5°C for matched cooling/heating rate of $20^\circ\text{C min}^{-1}$. Continuation...

T ($^\circ\text{C}$)	G0	G1	G2	G3	G4	G5	G6	G7	G8	G9	G10	G11	G12	G13	G14
	Heat capacity c_p ($\text{J g}^{-1} \text{K}^{-1}$)														
490	1.555	1.143	1.140	1.153	1.142	1.147	1.116	1.146	1.144	1.107	1.114	1.112	1.109	1.084	1.122
495	1.576	1.143	1.140	1.155	1.143	1.147	1.117	1.147	1.149	1.114	1.115	1.114	1.110	1.086	1.123
500	1.559	1.147	1.140	1.155	1.142	1.146	1.120	1.150	1.150	1.115	1.117	1.115	1.111	1.086	1.127
505	1.531	1.146	1.142	1.156	1.144	1.148	1.119	1.150	1.151	1.115	1.118	1.115	1.110	1.086	1.127
510	1.510	1.148	1.146	1.160	1.147	1.152	1.119	1.149	1.151	1.116	1.120	1.116	1.113	1.088	1.131
515	1.499	1.149	1.149	1.162	1.150	1.154	1.121	1.153	1.154	1.118	1.121	1.118	1.112	1.089	1.132
520	1.490	1.150	1.149	1.163	1.152	1.155	1.123	1.155	1.153	1.118	1.119	1.119	1.113	1.090	1.134
525		1.151	1.150	1.165	1.154	1.154	1.124	1.155	1.155	1.117	1.123	1.121	1.115	1.091	1.135
530		1.152	1.150	1.164	1.153	1.154	1.125	1.156	1.155	1.115	1.123	1.123	1.116	1.092	1.138
535		1.153	1.153	1.168	1.156	1.158	1.127	1.157	1.158	1.115	1.125	1.122	1.117	1.093	1.142
540		1.155	1.155	1.171	1.157	1.158	1.130	1.161	1.159	1.113	1.127	1.124	1.119	1.095	1.146
545		1.156	1.156	1.173	1.159	1.160	1.131	1.164	1.161	1.113	1.128	1.124	1.121	1.097	1.151
550		1.157	1.155	1.174	1.160	1.159	1.128	1.164	1.164	1.115	1.130	1.126	1.123	1.099	1.156
555		1.157	1.160	1.176	1.163	1.163	1.130	1.166	1.163	1.114	1.131	1.124	1.123	1.100	1.163
560		1.160	1.163	1.179	1.163	1.165	1.132	1.166	1.165	1.114	1.131	1.124	1.125	1.102	1.174
565		1.163	1.159	1.177	1.159	1.159	1.133	1.168	1.166	1.115	1.133	1.127	1.127	1.107	1.188
570		1.164	1.160	1.176	1.159	1.160	1.134	1.171	1.168	1.116	1.131	1.128	1.127	1.109	1.203
575		1.165	1.159	1.176	1.161	1.163	1.133	1.171	1.168	1.116	1.130	1.128	1.128	1.111	1.223
580		1.166	1.161	1.179	1.163	1.165	1.134	1.177	1.172	1.119	1.130	1.127	1.132	1.113	1.248
585		1.168	1.164	1.182	1.165	1.167	1.134	1.183	1.175	1.120	1.130	1.127	1.133	1.119	1.279
590		1.167	1.169	1.184	1.169	1.169	1.137	1.191	1.177	1.117	1.128	1.130	1.133	1.125	1.314
595		1.168	1.173	1.185	1.169	1.172	1.142	1.199	1.177	1.120	1.127	1.132	1.137	1.132	1.353
600		1.168	1.173	1.185	1.168	1.172	1.141	1.210	1.179	1.123	1.129	1.131	1.138	1.141	1.385
605		1.169	1.172	1.183	1.169	1.171	1.142	1.221	1.180	1.122	1.129	1.133	1.141	1.152	1.407
610		1.171	1.170	1.182	1.167	1.170	1.142	1.234	1.180	1.122	1.129	1.132	1.146	1.169	1.416
615		1.172	1.170	1.182	1.169	1.170	1.144	1.253	1.181	1.123	1.129	1.133	1.153	1.188	1.405
620		1.173	1.172	1.183	1.171	1.173	1.147	1.276	1.181	1.123	1.129	1.131	1.160	1.211	1.388
625		1.172	1.172	1.184	1.172	1.177	1.149	1.307	1.183	1.123	1.129	1.135	1.168	1.234	1.373
630		1.173	1.173	1.184	1.171	1.177	1.152	1.333	1.183	1.124	1.127	1.137	1.177	1.261	1.360
635		1.175	1.172	1.185	1.171	1.176	1.158	1.371	1.184	1.122	1.127	1.140	1.189	1.287	1.352
640		1.178	1.172	1.183	1.171	1.178	1.162	1.402	1.183	1.124	1.130	1.144	1.204	1.309	1.347
645		1.177	1.175	1.189	1.176	1.182	1.166	1.421	1.185	1.125	1.129	1.143	1.220	1.324	1.343
650		1.178	1.174	1.184	1.173	1.181	1.173	1.425	1.189	1.127	1.131	1.149	1.239	1.329	1.341
655		1.181	1.172	1.186	1.172	1.184	1.181	1.414	1.189	1.128	1.132	1.151	1.260	1.327	1.341
660		1.179	1.173	1.188	1.175	1.190	1.195	1.397	1.187	1.125	1.131	1.155	1.280	1.317	
665		1.179	1.176	1.191	1.176	1.194	1.210	1.382	1.192	1.129	1.130	1.157	1.297	1.306	
670		1.179	1.176	1.192	1.176	1.197	1.225	1.370	1.191	1.127	1.131	1.167	1.311	1.296	
675		1.182	1.177	1.194	1.177	1.200	1.248	1.366	1.192	1.128	1.135	1.175	1.325	1.291	
680		1.182	1.177	1.193	1.178	1.211	1.274	1.363	1.193	1.129	1.134	1.184	1.328	1.284	

Appendix 1. Heat capacity data (in $\text{J g}^{-1} \text{K}^{-1}$) for all of the samples with step of temperature of 5°C for matched cooling/heating rate of $20^\circ\text{C min}^{-1}$. Continuation...

T ($^\circ\text{C}$)	G0	G1	G2	G3	G4	G5	G6	G7	G8	G9	G10	G11	G12	G13	G14
	Heat capacity c_p ($\text{J g}^{-1} \text{K}^{-1}$)														
685		1.185	1.179	1.194	1.181	1.223	1.299	1.359	1.193	1.130	1.138	1.198	1.334	1.283	
690		1.187	1.184	1.198	1.184	1.236	1.326	1.352	1.195	1.131	1.140	1.208	1.334		
695		1.188	1.185	1.200	1.184	1.255	1.349	1.353	1.199	1.133	1.141	1.223	1.331		
700		1.187	1.182	1.198	1.182	1.269	1.365		1.203	1.134	1.142	1.238	1.326		
705		1.188	1.185	1.192	1.182	1.291	1.368		1.206	1.136	1.146	1.253	1.323		
710		1.190	1.185	1.197	1.184	1.317	1.362		1.204	1.134	1.149	1.268	1.318		
715		1.192	1.185	1.200	1.182	1.341	1.350		1.205	1.134	1.153	1.281	1.314		
720		1.193	1.187	1.200	1.186	1.366	1.336		1.210	1.136	1.156	1.294	1.309		
725		1.189	1.187	1.201	1.184	1.383	1.326		1.209	1.136	1.164	1.306	1.308		
730		1.189	1.187	1.203	1.185	1.395	1.319		1.215	1.139	1.166	1.312	1.300		
735		1.192	1.185	1.199	1.185	1.393	1.315		1.215	1.138	1.177	1.318	1.303		
740		1.191	1.189	1.203	1.190	1.391	1.315		1.223	1.139	1.187	1.320	1.298		
745		1.193	1.192	1.202	1.191	1.377	1.310		1.230	1.142	1.199	1.318	1.297		
750		1.195	1.193	1.203	1.192	1.366	1.312		1.237	1.147	1.216	1.315			
755		1.191	1.189	1.202	1.192	1.355			1.245	1.148	1.229	1.308			
760		1.191	1.191	1.204	1.199	1.351			1.257	1.154	1.248	1.304			
765		1.195	1.191	1.206	1.205	1.344			1.269	1.158	1.267	1.300			
770		1.200	1.193	1.207	1.211	1.344			1.289	1.167	1.285	1.299			
775		1.200	1.197	1.210	1.222	1.346			1.305	1.168	1.298	1.296			
780		1.204	1.197	1.211	1.233	1.344			1.327	1.181	1.312	1.297			
785		1.207	1.199	1.214	1.242	1.334			1.353	1.194	1.318	1.296			
790		1.205	1.200	1.218	1.257	1.341			1.379	1.207	1.317				
795		1.209	1.202	1.225	1.272				1.401	1.218	1.317				
800		1.211	1.205	1.218	1.288				1.421	1.238	1.311				
805		1.219	1.209	1.219	1.306				1.433	1.253	1.303				
810		1.227	1.217	1.228	1.331				1.436	1.268	1.300				
815		1.227	1.224	1.236	1.355				1.432	1.286	1.291				
820		1.239	1.225	1.236	1.372				1.422	1.301	1.286				
825		1.250	1.236	1.245	1.386				1.412	1.316	1.287				
830		1.262	1.248	1.257	1.403				1.403	1.319	1.283				
835		1.279	1.261	1.267	1.408					1.319					
840		1.298	1.274	1.284	1.406					1.314					
845		1.322	1.292	1.303	1.400					1.309					
850		1.347	1.311	1.317	1.387					1.301					
855		1.375	1.341	1.339	1.382					1.295					
860		1.402	1.362	1.363	1.376					1.290					
865		1.425	1.388	1.386	1.374										
870		1.450	1.408	1.404	1.366										
875		1.459	1.425	1.424	1.367										

Appendix 1. Heat capacity data (in $\text{J g}^{-1} \text{K}^{-1}$) for all of the samples with step of temperature of 5°C for matched cooling/heating rate of $20^\circ\text{C min}^{-1}$.
Continuation...

T ($^\circ\text{C}$)	G0	G1	G2	G3	G4	G5	G6	G7	G8	G9	G10	G11	G12	G13	G14
	Heat capacity c_p ($\text{J g}^{-1} \text{K}^{-1}$)														
880		1.451	1.432	1.431	1.366										
885		1.434	1.424	1.427											
890		1.417	1.404	1.410											
895		1.404	1.395	1.400											
900		1.396	1.379	1.383											
905		1.392	1.373	1.377											
910		1.387	1.363	1.369											
915		1.382	1.359	1.366											
920		1.382	1.356	1.366											
925		1.378	1.350												

Appendix 2. Temperature T , $\log_{10} \eta$, frequency f , $\log_{10} \omega\tau_M$, imaginary (G_{im}) and real (G_{real}) shear modulus and shear modulus of the melt (G_{melt}) for the investigated samples.

SAMPLE G0						
T (°C)	$\log_{10} \eta$ (Pa s)	f (Hz)	$\log_{10} \omega\tau_M$	G_{im} (GPa)	G_{real} (GPa)	G_{melt} (GPa)
380	15.94	1	6.305	0.065	27.446	27.446
380		0.5	6.004	0.067	27.436	27.436
380		0.2	5.606	0.107	27.565	27.565
380		0.1	5.305	0.107	27.687	27.687
380		0.05	5.004	0.201	27.449	27.450
380		0.02	4.606	0.170	27.657	27.658
380		0.01	4.305	0.092	27.763	27.763
380		0.005	4.004	0.079	27.906	27.907
380		0.002	3.606	0.146	27.725	27.726
380		0.001	3.305	0.076	27.632	27.632
400	14.73	1	5.088	0.137	27.570	27.571
400		0.5	4.787	0.141	27.721	27.722
400		0.2	4.389	0.121	27.691	27.691
400		0.1	4.088	0.226	27.764	27.765
400		0.05	3.787	0.155	28.019	28.019
400		0.02	3.389	0.010	27.756	27.756
400		0.01	3.088	0.215	27.628	27.629
400		0.005	2.787	0.056	27.514	27.514
400		0.002	2.389	0.113	28.334	28.335
400		0.001	2.088	0.119	27.852	27.853
420	13.58	1	3.942	0.031	27.552	27.552
420		0.5	3.641	0.157	27.609	27.610
420		0.2	3.243	0.208	27.815	27.815
420		0.1	2.942	0.100	28.666	28.666
420		0.05	2.641	0.011	27.493	27.493
420		0.02	2.243	0.013	27.365	27.365
420		0.01	1.942	0.409	24.453	24.457
420		0.005	1.641	0.076	27.360	27.360
420		0.002	1.243	0.724	25.341	25.351
420		0.001	0.942	1.464	24.261	24.305

SAMPLE G0						
T (°C)	$\log_{10} \eta$ (Pa s)	f (Hz)	$\log_{10} \omega\tau_M$	G_{im} (GPa)	G_{real} (GPa)	G_{melt} (GPa)
440	12.50	1	2.860	0.023	27.287	27.287
440		0.5	2.559	0.002	27.303	27.303
440		0.2	2.161	0.235	27.540	27.541
440		0.1	1.860	0.274	27.474	27.476
440		0.05	1.559	0.042	27.430	27.430
440		0.02	1.161	0.097	27.948	27.948
440		0.01	0.860	1.223	23.827	23.858
440		0.005	0.559	1.289	19.371	19.413
440		0.002	0.161	8.520	10.572	13.578
440		0.001	-0.140	5.656	4.959	7.521
460	11.48	1	1.838	0.207	27.279	27.280
460		0.5	1.537	0.151	27.547	27.548
460		0.2	1.139	0.227	24.857	24.858
460		0.1	0.838	1.253	23.324	23.358
460		0.05	0.537	1.554	20.310	20.370
460		0.02	0.139	7.773	7.074	10.510
460		0.01	-0.162	0.365	4.210	4.225
460		0.005	-0.463	0.014	1.532	1.532
460		0.002	-0.861	0.003	0.382	0.382
480		10.51	1	0.869	0.726	23.425
480	0.5		0.568	2.767	17.474	17.692
480	0.2		0.170	5.869	10.652	12.162
480	0.1		-0.131	4.727	0.559	4.760
480	0.05		-0.432	2.231	0.871	2.395
480	0.02		-0.830	2.467	0.619	2.543
480	0.01		-1.131	1.312	0.235	1.332
480	0.005		-1.432	0.626	0.255	0.676
480	0.002		-1.830	0.088	0.343	0.354

Appendix 2. Temperature T , $\log_{10} \eta$, frequency f , $\log_{10} \omega\tau_M$, imaginary (G_{im}) and real (G_{real}) shear modulus and shear modulus of the melt (G_{melt}) for the investigated samples – continuation...

SAMPLE G0						
T (°C)	$\log_{10} \eta$ (Pa s)	f (Hz)	$\log_{10} \omega\tau_M$	G_{im} (GPa)	G_{real} (GPa)	G_{melt} (GPa)
490	10.04	1	0.404	5.399	14.534	15.504
490		0.5	0.103	6.747	8.415	10.786
490		0.2	-0.295	1.212	3.954	4.135
490		0.1	-0.596	0.028	1.794	1.794
490		0.05	-0.897	0.034	1.956	1.956
490		0.02	-1.295	0.001	0.050	0.050
500		9.59	1	-0.049	8.567	7.623
500	0.5		-0.350	2.392	1.081	2.625
500	0.2		-0.748	0.836	0.193	0.858

SAMPLE G1						
T (°C)	$\log_{10} \eta$ (Pa s)	f (Hz)	$\log_{10} \omega\tau_M$	G_{im} (GPa)	G_{real} (GPa)	G_{melt} (GPa)
350	32.74	1	23.002	0.010	34.259	34.259
350		0.5	22.701	0.099	33.948	33.948
350		0.2	22.303	0.145	34.363	34.364
350		0.1	22.002	0.182	33.721	33.722
350		0.05	21.701	0.110	33.693	33.693
350		0.02	21.303	0.066	33.456	33.456
350		0.01	21.002	0.179	34.354	34.355
350		0.005	20.701	0.226	33.834	33.835
350		0.002	20.303	0.015	34.135	34.135
350		0.001	20.002	0.025	34.235	34.235
400	29.14	1	19.408	0.119	34.217	34.218
400		0.5	19.107	0.043	34.270	34.270
400		0.2	18.709	0.027	33.731	33.731
400		0.1	18.408	0.340	34.173	34.175
400		0.05	18.107	0.008	34.121	34.121
400		0.02	17.709	0.210	33.822	33.823
400		0.01	17.408	0.041	35.062	35.062
400		0.005	17.107	0.034	34.413	34.413
400		0.002	16.709	0.111	34.651	34.651
400	0.001	16.408	0.150	34.741	34.741	
450	26.05	1	16.311	0.141	34.787	34.787
450		0.5	16.010	0.031	34.621	34.621
450		0.2	15.612	0.037	34.913	34.913
450		0.1	15.311	0.036	34.792	34.792
450		0.05	15.010	0.181	35.527	35.528
450		0.02	14.612	0.088	35.295	35.295
450		0.01	14.311	0.268	34.269	34.270
450		0.005	14.010	0.183	35.692	35.692
450		0.002	13.612	0.123	34.414	34.414
450		0.001	13.311	0.024	34.510	34.510

Appendix 2. Temperature T , $\log_{10} \eta$, frequency f , $\log_{10} \omega\tau_M$, imaginary (G_{im}) and real (G_{real}) shear modulus and shear modulus of the melt (G_{melt}) for the investigated samples – continuation...

SAMPLE G1						
T (°C)	$\log_{10} \eta$ (Pa s)	f (Hz)	$\log_{10} \omega\tau_M$	G_{im} (GPa)	G_{real} (GPa)	G_{melt} (GPa)
500	23.35	1	13.615	0.113	34.257	34.258
500		0.5	13.314	0.069	34.596	34.596
500		0.2	12.916	0.117	34.408	34.408
500		0.1	12.615	0.107	34.703	34.704
500		0.05	12.314	0.024	34.692	34.692
500		0.02	11.916	0.132	34.584	34.584
500		0.01	11.615	0.049	34.218	34.218
500		0.005	11.314	0.177	34.921	34.922
500		0.002	10.916	0.341	33.956	33.958
500		0.001	10.615	0.082	34.319	34.319
550	20.98	1	11.247	0.081	34.376	34.376
550		0.5	10.946	0.096	34.231	34.231
550		0.2	10.548	0.074	34.461	34.461
550		0.1	10.247	0.123	34.022	34.022
550		0.05	9.946	0.141	35.531	35.531
550		0.02	9.548	0.478	34.744	34.748
550		0.01	9.247	0.231	34.306	34.307
550		0.005	8.946	0.000	34.341	34.341
550		0.002	8.548	0.036	34.630	34.630
550		0.001	8.247	0.001	34.516	34.516
600	18.89	1	9.149	0.004	34.661	34.661
600		0.5	8.848	0.008	35.200	35.200
600		0.2	8.451	0.067	34.721	34.721
600		0.1	8.149	0.093	35.122	35.122
600		0.05	7.848	0.098	35.320	35.320
600		0.02	7.451	0.219	35.628	35.629
600		0.01	7.149	0.321	35.043	35.044
600		0.005	6.848	0.145	34.962	34.962
600		0.002	6.451	0.200	34.281	34.281
600		0.001	6.149	0.099	34.517	34.517

SAMPLE G1						
T (°C)	$\log_{10} \eta$ (Pa s)	f (Hz)	$\log_{10} \omega\tau_M$	G_{im} (GPa)	G_{real} (GPa)	G_{melt} (GPa)
650	17.02	1	7.279	0.050	34.157	34.157
650		0.5	6.978	0.060	34.418	34.418
650		0.2	6.581	0.232	34.898	34.899
650		0.1	6.279	0.535	34.446	34.450
650		0.05	5.978	0.605	34.838	34.843
650		0.02	5.581	0.989	33.686	33.700
650		0.01	5.279	0.780	33.520	33.529
650		0.005	4.978	0.667	32.420	34.427
650		0.002	4.581	0.169	32.755	33.756
650		0.001	4.279	0.212	33.477	33.478
700	15.34	1	5.602	2.329	33.004	33.086
700		0.5	5.301	0.077	32.563	32.563
700		0.2	4.903	0.226	32.500	32.500
700		0.1	4.602	0.479	32.234	32.238
700		0.05	4.301	0.161	32.606	32.606
700		0.02	3.903	0.459	32.767	32.770
700		0.01	3.602	0.211	31.305	31.306
700		0.005	3.301	0.611	31.889	31.894
700		0.002	2.903	1.021	31.431	31.448
700		0.001	2.602	1.188	30.883	30.906
725	14.56	1	4.826	0.025	32.677	32.677
725		0.5	4.525	0.165	32.730	32.730
725		0.2	4.127	0.168	31.623	31.623
725		0.1	3.826	0.050	32.344	32.345
725		0.05	3.525	0.803	31.622	31.632
725		0.02	3.127	0.565	31.736	31.741
725		0.01	2.826	0.862	31.708	31.720
725		0.005	2.525	1.430	30.452	30.486
725		0.002	2.127	2.006	29.429	29.497
725		0.001	1.826	0.153	27.987	27.987

Appendix 2. Temperature T , $\log_{10} \eta$, frequency f , $\log_{10} \omega\tau_M$, imaginary (G_{im}) and real (G_{real}) shear modulus and shear modulus of the melt (G_{melt}) for the investigated samples – continuation...

SAMPLE G1						
T (°C)	$\log_{10} \eta$ (Pa s)	f (Hz)	$\log_{10} \omega\tau_M$	G_{im} (GPa)	G_{real} (GPa)	G_{melt} (GPa)
750	13.82	1	4.088	0.282	31.523	31.524
750		0.5	3.787	0.497	30.993	30.997
750		0.2	3.389	0.803	31.401	31.411
750		0.1	3.088	0.720	31.044	31.052
750		0.05	2.787	0.685	31.232	31.240
750		0.02	2.389	1.150	30.269	30.291
750		0.01	2.088	2.094	28.235	28.313
750		0.005	1.787	2.930	26.700	26.860
750		0.002	1.389	1.896	25.313	25.384
750		0.001	1.088	1.088	3.872	21.589
775	13.12	1	3.385	0.356	31.285	31.287
775		0.5	3.084	0.594	30.698	30.704
775		0.2	2.686	0.989	30.377	30.393
775		0.1	2.385	0.851	29.313	29.326
775		0.05	2.084	2.217	28.516	28.602
775		0.02	1.686	3.119	26.414	26.597
775		0.01	1.385	4.606	24.633	25.060
775		0.005	1.084	4.792	21.454	21.982
775		0.002	0.686	5.438	16.193	17.082
775		0.001	0.385	6.898	9.730	11.927
800	12.45	1	2.715	1.006	30.672	30.688
800		0.5	2.414	1.268	29.907	29.934
800		0.2	2.016	2.063	28.996	29.069
800		0.1	1.715	3.135	26.642	26.826
800		0.05	1.414	4.066	24.749	25.081
800		0.02	1.016	6.374	19.652	20.660
800		0.01	0.715	2.643	17.912	18.106
800		0.005	0.414	4.460	12.468	13.242
800		0.002	0.016	5.057	3.808	6.331
800		0.001	-0.285	2.918	0.935	3.064

SAMPLE G1							
T (°C)	$\log_{10} \eta$ (Pa s)	f (Hz)	$\log_{10} \omega\tau_M$	G_{im} (GPa)	G_{real} (GPa)	G_{melt} (GPa)	
825	11.81	1	2.076	1.891	26.412	26.480	
825		0.5	1.775	2.833	25.190	25.349	
825		0.2	1.377	4.359	22.440	22.859	
825		0.1	1.076	5.895	19.273	20.155	
825		0.05	0.775	6.981	14.673	16.249	
825		0.02	0.377	7.244	7.812	10.654	
825		0.01	0.076	2.487	6.773	7.215	
825		0.005	-0.225	3.550	1.193	3.745	
825		0.002	-0.623	1.401	0.206	1.416	
825		0.001	-0.924	0.472	0.320	0.571	
850	11.20	1	1.465	3.054	18.866	19.112	
850		0.5	1.164	4.224	16.595	17.124	
850		0.2	0.766	5.791	12.343	13.634	
850		0.1	0.465	6.250	8.192	10.304	
850		0.05	0.164	5.654	4.217	7.053	
850		0.02	-0.234	2.963	1.021	3.134	
850		0.01	-0.535	1.531	0.556	1.629	
850		0.005	-0.836	0.830	0.082	0.835	
875		10.62	1	0.880	7.222	17.109	18.571
875			0.5	0.579	7.916	11.614	14.055
875	0.2		0.181	6.704	4.831	8.263	
875	0.1		-0.120	4.000	1.630	4.320	
875	0.05		-0.421	0.862	2.373	2.524	

Appendix 2. Temperature T , $\log_{10} \eta$, frequency f , $\log_{10} \omega\tau_M$, imaginary (G_{im}) and real (G_{real}) shear modulus and shear modulus of the melt (G_{melt}) for the investigated samples – continuation...

SAMPLE G2						
T (°C)	$\log_{10} \eta$ (Pa s)	f (Hz)	$\log_{10} \omega\tau_M$	G_{im} (GPa)	G_{real} (GPa)	G_{melt} (GPa)
500	23.33	1	13.590	0.503	34.780	34.784
500		0.5	13.289	0.526	34.868	34.872
500		0.2	12.891	0.440	34.738	34.741
500		0.1	12.590	0.439	34.663	34.666
500		0.05	12.289	0.620	34.897	34.903
500		0.02	11.891	0.234	34.744	34.744
500		0.01	11.590	0.107	34.596	34.596
500		0.005	11.289	0.574	34.868	34.873
500		0.002	10.891	0.168	34.824	34.824
500		0.001	10.590	0.390	35.283	35.285
550	21.01	1	11.267	0.122	34.411	34.411
550		0.5	10.966	0.010	34.366	34.366
550		0.2	10.568	0.086	34.497	34.497
550		0.1	10.267	0.293	34.580	34.581
550		0.05	9.966	0.332	34.662	34.663
550		0.02	9.568	0.266	34.217	34.218
550		0.01	9.267	0.043	34.445	34.445
550		0.005	8.966	0.108	34.459	34.459
550		0.002	8.568	0.077	34.237	34.237
550		0.001	8.267	0.104	34.745	34.745
600	18.95	1	9.210	0.041	34.792	34.792
600		0.5	8.909	0.022	34.816	34.816
600		0.2	8.511	0.209	34.730	34.731
600		0.1	8.210	0.148	34.316	34.317
600		0.05	7.909	0.146	35.289	35.289
600		0.02	7.511	0.311	34.764	34.765
600		0.01	7.210	0.818	34.508	34.509
600		0.005	6.909	1.379	34.431	34.432
600		0.002	6.511	1.128	33.085	33.085
600		0.001	6.210	1.591	33.225	33.225

SAMPLE G2						
T (°C)	$\log_{10} \eta$ (Pa s)	f (Hz)	$\log_{10} \omega\tau_M$	G_{im} (GPa)	G_{real} (GPa)	G_{melt} (GPa)
650	17.12	1	7.376	0.547	33.812	33.812
650		0.5	7.075	1.161	33.920	33.921
650		0.2	6.677	1.327	33.818	33.819
650		0.1	6.376	1.544	34.002	34.002
650		0.05	6.075	1.119	33.577	33.577
650		0.02	5.677	1.051	33.750	33.750
650		0.01	5.376	0.207	34.133	34.134
650		0.005	5.075	0.066	33.784	33.784
650		0.002	4.677	0.121	33.772	33.772
650		0.001	4.376	0.199	34.542	34.543
700	15.47	1	5.730	0.195	33.587	33.587
700		0.5	5.429	0.222	33.433	33.434
700		0.2	5.031	0.326	33.505	33.506
700		0.1	4.730	0.321	33.763	33.765
700		0.05	4.429	0.317	33.719	33.721
700						
725	14.71	1	4.970	1.360	33.314	33.341
725		0.5	4.668	1.205	33.330	33.352
725		0.2	4.271	0.346	33.565	33.567
725		0.1	3.970	3.951	32.479	32.719
725		0.05	3.668	2.361	32.572	32.657
725		0.02	3.271	2.162	32.923	32.993
725		0.01	2.970	3.227	30.306	30.478
725		0.005	2.668	4.557	30.103	30.446
725		0.002	2.271	3.923	30.205	30.458
725		0.001	1.970	3.866	29.690	29.940

Appendix 2. Temperature T , $\log_{10} \eta$, frequency f , $\log_{10} \omega\tau_M$, imaginary (G_{im}) and real (G_{real}) shear modulus and shear modulus of the melt (G_{melt}) for the investigated samples – continuation...

SAMPLE G2						
T (°C)	$\log_{10} \eta$ (Pa s)	f (Hz)	$\log_{10} \omega\tau_M$	G_{im} (GPa)	G_{real} (GPa)	G_{melt} (GPa)
750	13.99	1	4.246	0.679	32.835	32.842
750		0.5	3.945	0.139	32.993	32.994
750		0.2	3.547	0.196	33.189	33.189
750		0.1	3.246	2.640	32.855	32.960
750		0.05	2.945	2.327	28.868	28.962
750		0.02	2.547	2.932	29.642	29.787
750		0.01	2.246	4.232	28.188	28.503
750		0.005	1.945	5.503	24.635	25.242
750		0.002	1.547	8.552	23.147	24.676
750		0.001	1.246	12.46	5.555	23.239
800	12.64	1	2.900	3.508	31.538	31.733
800		0.5	2.598	8.998	30.799	32.086
800		0.2	2.201	6.051	30.106	30.708
800		0.1	1.900	8.572	26.067	27.440
800		0.05	1.598	8.240	23.249	24.666
800		0.02	1.201	5.271	23.179	23.771
800		0.01	0.900	4.612	16.775	17.398
800		0.005	0.598	2.967	16.206	16.475
800		0.002	0.201	3.323	8.745	9.355
800		0.001	-0.100	-0.100	3.223	8.169
825	12.02	1	2.272	5.162	31.273	31.696
825		0.5	1.971	5.814	29.223	29.796
825		0.02	0.573	4.446	7.664	8.860
825		0.01	0.272	5.595	6.067	8.253
825		0.005	-0.029	4.765	5.268	7.104
825		0.002	-0.427	2.175	3.264	3.922
825		0.001	-0.728	0.562	1.336	1.449

SAMPLE G2						
T (°C)	$\log_{10} \eta$ (Pa s)	f (Hz)	$\log_{10} \omega\tau_M$	G_{im} (GPa)	G_{real} (GPa)	G_{melt} (GPa)
850	11.42	1	1.673	8.469	30.002	30.496
850		0.5	1.372	9.691	28.864	30.447
850		0.2	0.974	9.896	30.499	32.065
850		0.1	0.673	10.243	19.339	21.884
850		0.05	0.372	2.887	18.954	19.172
850		0.02	-0.026	2.081	18.085	18.204
850		0.01	-0.327	3.480	3.016	4.605
850		0.005	-0.628	0.424	2.278	2.318
850		0.002	-1.026	0.483	0.779	0.916
850		0.001	-1.327	0.190	0.241	0.307
875	10.84	1	1.100	8.998	24.342	25.952
875		0.5	0.799	10.842	21.656	24.219
875		0.2	0.401	6.928	12.106	13.948
875		0.1	0.100	1.532	7.825	7.973
875		0.05	-0.201	0.164	2.015	2.022
875						
900	10.29	1	0.551	3.793	19.308	19.678
900		0.5	0.250	3.984	5.503	6.794
900		0.2	-0.148	0.734	3.618	3.692
900		0.1	-0.449	0.950	1.506	1.781
900		0.05	-0.750	0.347	0.687	0.770
900						
900						

Appendix 2. Temperature T , $\log_{10} \eta$, frequency f , $\log_{10} \omega\tau_M$, imaginary (G_{im}) and real (G_{real}) shear modulus and shear modulus of the melt (G_{melt}) for the investigated samples – continuation...

SAMPLE G3						
T (°C)	$\log_{10} \eta$ (Pa s)	f (Hz)	$\log_{10} \omega\tau_M$	G_{im} (GPa)	G_{real} (GPa)	G_{melt} (GPa)
550	21.41	1	11.671	0.102	34.434	34.434
550		0.5	11.370	0.037	34.650	34.650
550		0.2	10.972	0.081	34.381	34.381
550		0.1	10.671	0.379	34.737	34.739
550		0.05	10.370	0.319	33.786	33.788
550		0.02	9.972	0.290	34.250	34.251
550		0.01	9.671	0.455	33.474	33.477
550		0.005	9.370	0.217	34.424	34.425
550		0.002	8.972	0.329	34.511	34.512
550		0.001	8.671	0.579	34.068	34.073
600	19.26	1	9.526	0.064	34.375	34.375
600		0.5	9.225	0.276	34.705	34.706
600		0.2	8.827	0.033	34.097	34.097
600		0.1	8.526	0.446	35.138	35.141
600		0.05	8.225	0.076	34.313	34.313
600		0.02	7.827	0.236	33.850	33.851
600		0.01	7.526	0.853	34.361	34.361
600		0.005	7.225	0.008	32.915	32.915
600		0.002	6.827	0.117	32.467	32.468
600		0.001	6.526	0.807	33.896	33.906
650	17.35	1	7.613	0.626	33.900	33.900
650		0.5	7.312	0.707	34.110	34.110
650		0.2	6.914	0.214	33.292	33.292
650		0.1	6.613	0.397	33.635	33.637
650		0.05	6.312	0.105	32.811	32.811
650		0.02	5.914	0.598	33.017	33.023
650		0.01	5.613	0.181	32.059	32.059
650		0.005	5.312	0.070	32.044	32.044
650		0.002	4.914	0.614	31.656	31.662
650		0.001	4.613	1.236	32.858	32.881

SAMPLE G3						
T (°C)	$\log_{10} \eta$ (Pa s)	f (Hz)	$\log_{10} \omega\tau_M$	G_{im} (GPa)	G_{real} (GPa)	G_{melt} (GPa)
700	15.64	1	5.897	0.122	32.258	32.258
700		0.5	5.596	0.091	32.154	32.154
700		0.2	5.198	0.275	31.222	31.223
700		0.1	4.897	0.424	32.188	32.190
700		0.05	4.596	0.461	32.267	32.270
700		0.02	4.198	0.039	31.405	31.405
700		0.01	3.897	0.664	31.811	31.818
700		0.005	3.596	0.553	29.366	29.371
700		0.002	3.198	1.048	29.891	29.909
700		0.001	2.897	2.037	28.894	28.966
725	14.84	1	5.103	0.191	31.182	31.182
725		0.5	4.802	0.191	31.453	31.454
725		0.2	4.404	0.120	30.616	30.616
725		0.1	4.103	0.397	31.709	31.711
725		0.05	3.802	0.077	30.695	30.695
725		0.02	3.404	0.343	30.484	30.486
725		0.01	3.103	0.491	29.424	29.428
725		0.005	2.802	1.517	27.796	27.838
725		0.002	2.404	2.484	27.307	27.420
725		0.001	2.103	2.478	25.918	25.922
750	14.09	1	4.348	0.267	31.077	31.078
750		0.5	4.047	0.175	31.256	31.257
750		0.2	3.649	0.487	30.459	30.463
750		0.1	3.348	1.168	30.819	30.841
750		0.05	3.047	1.279	29.718	29.745
750		0.02	2.649	1.868	28.176	28.238
750		0.01	2.348	2.255	28.240	28.330
750		0.005	2.047	3.167	25.186	25.384
750		0.002	1.649	4.299	23.560	23.596
750		0.001	1.348	4.810	19.065	19.662

Appendix 2. Temperature T , $\log_{10} \eta$, frequency f , $\log_{10} \omega\tau_M$, imaginary (G_{im}) and real (G_{real}) shear modulus and shear modulus of the melt (G_{melt}) for the investigated samples – continuation...

SAMPLE G3							
T (°C)	$\log_{10} \eta$ (Pa s)	f (Hz)	$\log_{10} \omega\tau_M$	G_{im} (GPa)	G_{real} (GPa)	G_{melt} (GPa)	
775	13.37	1	3.629	0.503	29.680	29.684	
775		0.5	3.328	0.548	29.408	29.413	
775		0.2	2.930	1.194	27.877	27.902	
775		0.1	2.629	1.832	28.013	28.073	
775		0.05	2.328	2.571	26.855	26.978	
775		0.02	1.930	3.609	24.408	24.674	
775		0.01	1.629	5.078	21.782	22.367	
775		0.005	1.328	7.497	19.060	20.482	
775		0.002	0.930	7.162	14.676	15.013	
775		0.001	0.629	0.629	7.836	9.650	
800	12.68	1	2.944	0.991	28.670	28.687	
800		0.5	2.643	1.528	28.079	28.121	
800		0.2	2.245	2.339	26.191	26.296	
800		0.1	1.944	3.680	24.426	24.702	
800		0.05	1.643	4.555	21.746	22.218	
800		0.02	1.245	6.564	17.111	18.327	
800		0.01	0.944	7.409	11.975	14.082	
800		0.005	0.643	6.875	10.039	10.761	
800		0.002	0.245	3.931	3.066	4.986	
800		0.001	-0.056	-0.056	2.225	1.685	2.791
825	12.03	1	2.290	2.114	25.566	25.653	
825		0.5	1.989	3.303	24.462	24.684	
825		0.2	1.591	4.734	20.622	21.159	
825		0.1	1.290	6.747	18.410	18.613	
825		0.05	0.989	7.130	13.213	15.014	
825		0.02	0.591	6.393	6.215	8.916	
825		0.01	0.290	5.665	5.645	7.997	
825		0.005	-0.011	-0.011	2.659	0.818	2.782
825		0.002	-0.409	-0.409	1.117	0.143	1.127
825		0.001	-0.710	-0.710	0.582	0.060	0.585

SAMPLE G3						
T (°C)	$\log_{10} \eta$ (Pa s)	f (Hz)	$\log_{10} \omega\tau_M$	G_{im} (GPa)	G_{real} (GPa)	G_{melt} (GPa)
850	11.40	1	1.665	4.118	21.420	21.813
850		0.5	1.364	5.600	18.408	19.241
850		0.2	0.966	7.015	12.796	14.593
850		0.1	0.665	6.994	7.681	10.388
850		0.05	0.364	5.223	3.477	6.275
850		0.02	-0.034	2.484	1.304	2.805
850		0.01	-0.335	1.402	0.213	1.418
850		0.005	-0.636	0.659	0.054	0.661
850		0.002	-1.034	0.034	0.259	0.261
850		0.001	-1.034	0.034	0.259	0.261
875	10.81	1	1.067	6.035	14.009	15.253
875		0.5	0.766	6.343	6.934	8.182
875		0.2	0.368	4.053	3.251	5.196
875		0.1	0.067	2.774	1.245	3.040
875		0.05	-0.234	1.356	0.719	1.535
875		0.02	-0.234	1.356	0.719	1.535
900	10.23	1	1.067	6.664	8.517	12.881
900		0.5	0.766	5.680	3.913	10.441

Appendix 2. Temperature T , $\log_{10} \eta$, frequency f , $\log_{10} \omega\tau_M$, imaginary (G_{im}) and real (G_{real}) shear modulus and shear modulus of the melt (G_{melt}) for the investigated samples – continuation...

SAMPLE G4						
T (°C)	$\log_{10} \eta$ (Pa s)	f (Hz)	$\log_{10} \omega\tau_M$	G_{im} (GPa)	G_{real} (GPa)	G_{melt} (GPa)
550	19.38	1	9.643	0.052	34.233	34.233
550		0.5	9.342	0.088	34.215	34.215
550		0.2	8.944	0.256	34.421	34.422
550		0.1	8.643	0.063	34.122	34.122
550		0.05	8.342	0.117	34.290	34.290
550		0.02	7.944	0.146	34.081	34.081
550		0.01	7.643	0.908	33.542	33.548
550		0.005	7.342	0.368	34.386	34.388
550		0.002	6.944	0.203	33.757	33.757
550		0.001	6.643	0.083	32.231	32.231
600	17.47	1	7.731	0.585	34.193	34.193
600		0.5	7.430	1.047	34.291	34.291
600		0.2	7.032	0.017	34.023	34.023
600		0.1	6.731	0.128	33.918	33.918
600		0.05	6.430	0.233	34.461	34.461
600		0.02	6.032	0.239	33.932	33.932
600		0.01	5.731	0.045	34.220	34.220
600		0.005	5.430	0.135	33.869	33.869
600		0.002	5.032	0.045	33.792	33.792
600		0.001	4.731	0.175	33.446	33.447
650	15.76	1	6.026	0.129	33.678	33.678
650		0.5	5.725	0.069	33.438	33.438
650		0.2	5.327	0.063	33.008	33.008
650		0.1	5.026	0.101	32.839	32.839
650		0.05	4.725	0.019	33.370	33.370
650		0.02	4.327	0.219	32.803	32.804
650		0.01	4.026	0.578	32.667	32.672
650		0.005	3.725	0.149	33.461	33.462
650		0.002	3.327	0.545	32.556	32.560
650		0.001	3.026	0.313	32.318	32.319

SAMPLE G4						
T (°C)	$\log_{10} \eta$ (Pa s)	f (Hz)	$\log_{10} \omega\tau_M$	G_{im} (GPa)	G_{real} (GPa)	G_{melt} (GPa)
675	14.98	1	5.242	0.097	32.778	32.778
675		0.5	4.941	0.120	32.812	32.812
675		0.2	4.543	0.230	32.970	32.971
675		0.1	4.242	0.663	32.281	32.288
675		0.05	3.941	0.036	32.664	32.664
675		0.02	3.543	0.176	31.898	31.898
675		0.01	3.242	0.579	31.494	31.500
675		0.005	2.941	0.397	31.634	31.636
675		0.002	2.543	0.959	29.504	29.520
675		0.001	2.242	1.563	30.592	30.632
700	14.23	1	4.497	0.248	31.335	31.336
700		0.5	4.196	0.252	31.374	31.375
700		0.2	3.798	0.403	30.700	30.703
700		0.1	3.497	0.364	30.786	30.788
700		0.05	3.196	0.495	29.906	29.910
700		0.02	2.798	0.724	31.013	31.021
700		0.01	2.497	0.975	29.757	29.773
700		0.005	2.196	1.386	28.993	29.026
700		0.002	1.798	1.767	27.346	27.403
700		0.001	1.497	0.701	26.231	26.241
725	13.53	1	3.790	0.449	31.526	31.529
725		0.5	3.489	0.269	31.307	31.308
725		0.2	3.091	0.673	31.064	31.071
725		0.1	2.790	1.387	30.432	30.463
725		0.05	2.489	0.950	30.529	30.544
725		0.02	2.091	1.543	29.317	29.358
725		0.01	1.790	2.136	27.375	27.458
725		0.005	1.489	3.646	26.113	26.366
725		0.002	1.091	5.299	22.650	23.261
725		0.001	0.790	6.916	19.926	20.524

Appendix 2. Temperature T , $\log_{10} \eta$, frequency f , $\log_{10} \omega\tau_M$, imaginary (G_{im}) and real (G_{real}) shear modulus and shear modulus of the melt (G_{melt}) for the investigated samples – continuation...

SAMPLE G4						
T (°C)	$\log_{10} \eta$ (Pa s)	f (Hz)	$\log_{10} \omega\tau_M$	G_{im} (GPa)	G_{real} (GPa)	G_{melt} (GPa)
750	12.85	1	3.117	0.565	29.964	29.969
750		0.5	2.816	0.878	29.474	29.487
750		0.2	2.418	1.298	28.959	28.988
750		0.1	2.117	1.430	28.265	28.301
750		0.05	1.816	1.860	26.752	26.816
750		0.02	1.418	4.101	23.780	24.131
750		0.01	1.117	5.374	21.531	22.192
750		0.005	0.816	7.497	19.753	21.127
750		0.002	0.418	8.260	12.200	13.712
750		0.001	0.117	6.165	5.819	8.478
775	12.21	1	2.477	1.404	29.255	29.289
775		0.5	2.176	1.853	28.316	28.377
775		0.2	1.778	2.668	25.914	26.051
775		0.1	1.477	4.069	24.727	25.060
775		0.05	1.176	5.848	20.886	21.690
775		0.02	0.778	7.553	15.852	17.560
775		0.01	0.477	6.804	13.978	14.001
775		0.005	0.176	6.471	4.759	8.033
775		0.002	-0.222	3.430	1.214	3.639
775		0.001	-0.523	1.701	0.652	1.822
800	11.60	1	1.866	3.143	28.058	28.233
800		0.5	1.565	4.341	26.065	26.424
800		0.2	1.167	6.459	21.566	22.512
800		0.1	0.866	7.890	16.895	18.646
800		0.05	0.565	8.447	11.020	13.885
800		0.02	0.167	6.095	3.927	7.251
800		0.01	-0.134	3.668	1.336	3.903
800		0.005	-0.435	5.452	0.382	5.466
800		0.002	-0.833	0.825	0.105	0.831
800		0.001	-1.134	0.424	0.177	0.459

SAMPLE G4						
T (°C)	$\log_{10} \eta$ (Pa s)	f (Hz)	$\log_{10} \omega\tau_M$	G_{im} (GPa)	G_{real} (GPa)	G_{melt} (GPa)
825	11.02	1	1.283	5.577	21.685	22.391
825		0.5	0.982	7.084	17.716	19.080
825		0.2	0.584	8.265	10.519	13.377
825		0.1	0.283	6.798	5.225	8.574
825		0.05	-0.018	4.245	1.893	4.648
825		0.02	-0.416	1.703	0.357	1.740
825		0.01	-0.717	0.891	0.112	0.898
825						
850	10.46	1	0.726	7.264	11.851	13.900
850		0.5	0.425	6.848	6.682	9.568
850		0.2	0.027	4.367	1.970	4.791
850		0.1	-0.274	2.459	0.619	2.535
850		0.05	-0.575	1.207	0.160	1.217
850		0.02	-0.973	0.497	0.022	0.498
850		0.01	-1.274	0.265	0.042	0.269
850						

Appendix 2. Temperature T , $\log_{10} \eta$, frequency f , $\log_{10} \omega\tau_M$, imaginary (G_{im}) and real (G_{real}) shear modulus and shear modulus of the melt (G_{melt}) for the investigated samples – continuation...

SAMPLE G5						
T (°C)	$\log_{10} \eta$ (Pa s)	f (Hz)	$\log_{10} \omega\tau_M$	G_{im} (GPa)	G_{real} (GPa)	G_{melt} (GPa)
500	18.66	1	8.929	0.465	34.004	34.007
500		0.5	8.628	0.439	33.968	33.970
500		0.2	8.230	0.396	33.608	33.611
500		0.1	7.929	1.023	33.098	33.133
500		0.05	7.628	1.560	33.038	33.043
500		0.02	7.230	0.985	33.331	33.343
500		0.01	6.929	0.385	32.903	32.905
500		0.005	6.628	0.508	32.716	32.720
500		0.002	6.230	0.311	33.436	33.437
500		0.001	5.929	0.549	32.448	32.453
550	16.60	1	6.864	0.289	32.735	32.736
550		0.5	6.563	0.634	32.548	32.554
550		0.2	6.165	0.667	32.238	32.245
550		0.1	5.864	0.459	32.105	32.108
550		0.05	5.563	0.130	31.503	31.504
550		0.02	5.165	0.272	31.283	31.284
550		0.01	4.864	0.639	31.909	31.915
550		0.005	4.563	0.306	31.566	31.568
550		0.002	4.165	0.449	31.352	31.355
550		0.001	3.864	0.587	30.799	30.804
600	14.77	1	5.036	0.502	31.524	31.528
600		0.5	4.735	0.522	31.396	31.400
600		0.2	4.337	0.401	31.339	31.342
600		0.1	4.036	0.529	31.350	31.354
600		0.05	3.735	1.021	31.146	31.162
600		0.02	3.337	0.540	31.131	31.135
600		0.01	3.036	0.429	29.807	29.810
600		0.005	2.735	0.722	29.647	29.656
600		0.002	2.337	1.348	29.209	29.240
600		0.001	2.036	1.419	28.554	28.589

SAMPLE G5						
T (°C)	$\log_{10} \eta$ (Pa s)	f (Hz)	$\log_{10} \omega\tau_M$	G_{im} (GPa)	G_{real} (GPa)	G_{melt} (GPa)
625	13.93	1	4.198	0.510	30.835	30.839
625		0.5	3.897	0.396	30.709	30.712
625		0.2	3.499	0.520	30.292	30.297
625		0.1	3.198	0.980	30.106	30.122
625		0.05	2.897	1.028	29.215	29.233
625		0.02	2.499	1.544	29.753	29.793
625		0.01	2.198	1.719	28.392	28.444
625		0.005	1.897	2.114	27.700	27.781
625		0.002	1.499	2.846	26.574	26.726
625		0.001	1.198	1.107	25.487	25.511
650	13.14	1	3.406	0.920	30.333	30.346
650		0.5	3.105	1.022	30.305	30.322
650		0.2	2.707	1.216	29.979	30.004
650		0.1	2.406	1.561	29.278	29.320
650		0.05	2.105	1.654	28.754	28.801
650		0.02	1.707	2.352	27.211	27.312
650		0.01	1.406	3.433	25.843	26.070
650		0.005	1.105	4.342	23.686	24.081
650		0.002	0.707	3.225	20.969	21.216
650		0.001	0.406	6.447	16.107	17.350
675	12.39	1	2.655	1.226	29.327	29.352
675		0.5	2.354	1.605	28.183	28.228
675		0.2	1.956	1.746	26.652	26.709
675		0.1	1.655	2.762	25.955	26.101
675		0.05	1.354	3.735	24.125	24.412
675		0.02	0.956	5.252	20.607	21.266
675		0.01	0.655	5.740	18.224	19.107
675		0.005	0.354	6.685	15.089	15.532
675		0.002	-0.044	7.378	8.480	9.128
675		0.001	-0.345	3.988	2.175	4.543

Appendix 2. Temperature T , $\log_{10} \eta$, frequency f , $\log_{10} \omega\tau_M$, imaginary (G_{im}) and real (G_{real}) shear modulus and shear modulus of the melt (G_{melt}) for the investigated samples – continuation...

SAMPLE G5						
T (°C)	$\log_{10} \eta$ (Pa s)	f (Hz)	$\log_{10} \omega\tau_M$	G_{im} (GPa)	G_{real} (GPa)	G_{melt} (GPa)
700	11.68	1	1.943	1.845	25.748	25.814
700		0.5	1.642	2.330	24.235	24.347
700		0.2	1.244	3.783	22.278	22.597
700		0.1	0.943	5.643	19.567	20.364
700		0.05	0.642	6.940	15.758	17.219
700		0.02	0.244	6.465	8.638	11.417
700		0.01	-0.057	6.494	8.397	8.412
700		0.005	-0.358	3.707	1.615	4.043
700		0.002	-0.756	1.771	0.386	1.812
700		0.001	-1.057	-0.865	0.166	0.881
725	11.00	1	1.267	3.904	23.141	23.468
725		0.5	0.966	5.464	20.439	21.157
725		0.2	0.568	6.374	14.856	16.585
725		0.1	0.267	6.553	9.131	11.850
725		0.05	-0.034	6.104	4.324	7.481
725		0.02	-0.432	3.040	1.014	3.205
725		0.01	-0.733	2.261	0.361	2.290
725		0.005	-1.034	1.107	0.131	1.115
750	10.36	1	0.624	6.554	15.428	16.762
750		0.5	0.323	3.444	15.342	15.724
750		0.2	-0.075	6.345	4.200	7.609
750		0.1	-0.376	3.892	1.465	4.158
750		0.05	-0.677	2.361	0.482	2.410

SAMPLE G6						
T (°C)	$\log_{10} \eta$ (Pa s)	f (Hz)	$\log_{10} \omega\tau_M$	G_{im} (GPa)	G_{real} (GPa)	G_{melt} (GPa)
450	19.48	1	9.757	0.122	33.471	33.471
450		0.5	9.456	0.074	33.626	33.626
450		0.2	9.058	0.074	34.231	34.231
450		0.1	8.757	0.222	33.451	33.162
450		0.05	8.456	0.047	33.393	33.293
450		0.02	8.058	0.304	33.727	33.428
450		0.01	7.757	1.051	33.840	33.540
450		0.005	7.456	0.536	33.330	33.130
450		0.002	7.058	0.409	32.915	32.915
450		0.001	6.757	0.086	33.001	33.001
500	17.27	1	7.545	0.708	32.946	32.946
500		0.5	7.244	0.031	32.593	32.593
500		0.2	6.846	0.222	32.771	32.771
500		0.1	6.545	0.324	32.451	32.451
500		0.05	6.244	0.197	32.079	32.079
500		0.02	5.846	0.100	31.556	31.556
500		0.01	5.545	0.164	32.509	32.509
500		0.005	5.244	0.059	32.360	32.360
500		0.002	4.846	0.133	33.327	33.327
500		0.001	4.545	0.212	32.051	32.052
550	15.33	1	5.602	0.155	31.754	31.754
550		0.5	5.300	0.094	32.058	32.058
550		0.2	4.903	0.133	31.710	31.710
550		0.1	4.602	0.101	31.574	31.574
550		0.05	4.300	0.425	32.198	32.201
550		0.02	3.903	0.322	31.934	31.935
550		0.01	3.602	0.004	31.402	31.402
550		0.005	3.300	0.149	31.609	31.609
550		0.002	2.903	0.206	28.179	28.179
550		0.001	2.602	0.251	29.024	29.025

Appendix 2. Temperature T , $\log_{10} \eta$, frequency f , $\log_{10} \omega\tau_M$, imaginary (G_{im}) and real (G_{real}) shear modulus and shear modulus of the melt (G_{melt}) for the investigated samples – continuation...

SAMPLE G6						
T (°C)	$\log_{10} \eta$ (Pa s)	f (Hz)	$\log_{10} \omega\tau_M$	G_{im} (GPa)	G_{real} (GPa)	G_{melt} (GPa)
575	14.44	1	4.716	0.089	31.713	31.713
575		0.5	4.415	0.145	31.252	31.252
575		0.2	4.017	0.129	31.477	31.478
575		0.1	3.716	0.230	30.783	30.784
575		0.05	3.415	0.404	31.434	31.437
575		0.02	3.017	0.100	31.140	31.140
575		0.01	2.716	0.672	30.341	30.348
575		0.005	2.415	0.447	30.200	30.203
575		0.002	2.017	0.357	30.200	30.202
575		0.001	1.716	0.738	28.570	28.580
600	13.61	1	3.881	0.153	31.620	31.621
600		0.5	3.580	0.185	31.435	31.436
600		0.2	3.182	0.453	30.880	30.883
600		0.1	2.881	0.267	30.551	30.552
600		0.05	2.580	0.210	30.645	30.646
600		0.02	2.182	0.845	29.936	29.947
600		0.01	1.881	1.067	29.826	29.845
600		0.005	1.580	1.871	28.865	28.926
600		0.002	1.182	1.713	26.844	26.899
600		0.001	0.881	1.123	25.201	25.226
625	12.82	1	3.092	0.373	31.168	31.171
625		0.5	2.791	0.548	30.810	30.815
625		0.2	2.393	0.885	30.346	30.359
625		0.1	2.092	1.170	29.847	29.870
625		0.05	1.791	1.584	28.380	28.424
625		0.02	1.393	2.494	26.927	27.042
625		0.01	1.092	3.517	25.350	25.593
625		0.005	0.791	4.218	23.059	23.441
625		0.002	0.393	5.202	18.798	19.262
625		0.001	0.092	5.892	14.194	15.369

SAMPLE G6						
T (°C)	$\log_{10} \eta$ (Pa s)	f (Hz)	$\log_{10} \omega\tau_M$	G_{im} (GPa)	G_{real} (GPa)	G_{melt} (GPa)
650	12.07	1	2.347	1.099	30.177	30.197
650		0.5	2.046	1.450	29.310	29.346
650		0.2	1.648	2.439	27.769	27.876
650		0.1	1.347	3.519	26.137	26.373
650		0.05	1.046	4.425	23.413	23.828
650		0.02	0.648	5.613	18.769	19.900
650		0.01	0.347	5.823	15.940	16.653
650		0.005	0.046	5.566	11.260	12.150
650		0.002	-0.352	2.637	2.979	3.979
650		0.001	-0.653	2.169	1.346	2.553
675	11.37	1	1.640	2.710	26.795	26.932
675		0.5	1.339	3.837	24.926	25.220
675		0.2	0.941	5.599	21.155	21.883
675		0.1	0.640	5.181	17.101	18.548
675		0.05	0.339	5.710	11.673	14.101
675		0.02	-0.059	4.862	8.698	9.157
675		0.01	-0.360	3.001	3.626	4.707
675		0.005	-0.661	1.960	0.917	2.164
675		0.002	-1.059	0.930	0.230	0.958
700		10.70	1	0.970	5.074	21.440
700	0.5		0.669	5.732	17.167	18.746
700	0.2		0.271	5.498	9.540	12.513
700	0.1		-0.030	3.482	4.367	7.651
700	0.05		-0.331	3.396	4.228	4.555
700	0.02		-0.729	1.512	0.542	1.606
700	0.01		-1.030	0.849	0.146	0.861
700	0.005		-1.331	0.460	0.068	0.465

Appendix 2. Temperature T , $\log_{10} \eta$, frequency f , $\log_{10} \omega\tau_M$, imaginary (G_{im}) and real (G_{real}) shear modulus and shear modulus of the melt (G_{melt}) for the investigated samples – continuation...

SAMPLE G7						
T (°C)	$\log_{10} \eta$ (Pa s)	f (Hz)	$\log_{10} \omega\tau_M$	G_{im} (GPa)	G_{real} (GPa)	G_{melt} (GPa)
500		1	6.047	0.111	31.678	31.678
500		0.1	5.047	0.062	31.228	31.228
500		0.01	4.047	0.286	30.903	30.904
500		0.001	3.047	0.071	30.588	30.588
550		1	4.073	0.126	30.864	30.864
550		0.1	3.073	0.050	30.941	30.941
550		0.01	2.073	0.547	28.555	28.561
550		0.001	1.073	3.132	24.156	24.358
600		1	2.325	0.958	29.439	29.454
600		0.1	1.325	2.269	25.392	25.493
600		0.01	0.325	11.212	16.151	19.661
600		0.001	-0.675	6.136	8.244	10.277
630		1	0.686	8.227	20.892	22.453
630		0.1	-0.314	6.671	10.092	12.098
630		0.01	-1.314	0.760	1.927	2.071
650		1	-0.135	9.480	13.520	16.546
650		0.1	-1.135	3.589	1.325	3.826
650		0.01	-2.135	0.503	0.249	0.561
670		1	-0.632	3.868	5.388	6.633
670		0.1	-1.632	1.353	0.216	1.370
670		0.01	-2.632	0.140	0.003	0.140

SAMPLE G7						
T (°C)	$\log_{10} \eta$ (Pa s)	f (Hz)	$\log_{10} \omega\tau_M$	G_{im} (GPa)	G_{real} (GPa)	G_{melt} (GPa)
700		1	-0.632	5.569	0.795	5.625
700		0.1	-1.632	0.424	0.683	0.804
700		0.01	-2.632	0.158	0.404	0.434

Appendix 2. Temperature T , $\log_{10} \eta$, frequency f , $\log_{10} \omega\tau_M$, imaginary (G_{im}) and real (G_{real}) shear modulus and shear modulus of the melt (G_{melt}) for the investigated samples – continuation...

SAMPLE G8						
T (°C)	$\log_{10} \eta$ (Pa s)	f (Hz)	$\log_{10} \omega\tau_M$	G_{im} (GPa)	G_{real} (GPa)	G_{melt} (GPa)
600	16.55	1	6.838	0.039	32.451	32.451
600		0.5	6.537	0.233	32.827	32.828
600		0.2	6.139	0.250	33.358	33.359
600		0.1	5.838	0.064	31.715	31.715
600		0.05	5.537	0.340	31.789	31.791
600		0.02	5.139	0.115	32.863	32.863
600		0.01	4.838	0.232	32.225	32.225
600		0.005	4.537	0.123	31.683	31.683
600		0.002	4.139	0.214	31.715	31.716
600		0.001	3.838	0.540	31.493	31.498
620	15.87	1	6.157	0.163	32.947	32.947
620		0.5	5.856	0.056	32.487	32.487
620		0.2	5.458	0.176	32.355	32.355
620		0.1	5.157	0.277	32.514	32.515
620		0.05	4.856	0.248	32.629	32.630
620		0.02	4.458	0.260	31.918	31.919
620		0.01	4.157	0.016	31.073	31.073
620		0.005	3.856	0.416	32.313	32.315
620		0.002	3.458	0.244	32.230	32.230
620		0.001	3.157	0.475	31.131	31.134
640	15.22	1	5.506	0.047	32.180	32.180
640		0.5	5.205	0.056	32.132	32.132
640		0.2	4.807	0.217	32.526	32.527
640		0.1	4.506	0.505	32.523	32.526
640		0.05	4.205	0.538	30.993	30.997
640		0.02	3.807	0.943	32.140	32.154
640		0.01	3.506	0.746	32.078	32.086
640		0.005	3.205	0.598	30.846	30.852
640		0.002	2.807	0.153	30.659	30.659
640		0.001	2.506	0.190	30.101	30.102

SAMPLE G8						
T (°C)	$\log_{10} \eta$ (Pa s)	f (Hz)	$\log_{10} \omega\tau_M$	G_{im} (GPa)	G_{real} (GPa)	G_{melt} (GPa)
660	14.60	1	4.883	0.211	31.373	31.373
660		0.5	4.582	0.294	31.529	31.530
660		0.2	4.184	0.292	31.364	31.365
660		0.1	3.883	0.255	31.233	31.234
660		0.05	3.582	0.568	30.949	30.954
660		0.02	3.184	0.597	30.130	30.136
660		0.01	2.883	0.789	30.813	30.823
660		0.005	2.582	0.485	29.628	29.632
660		0.002	2.184	1.177	28.799	28.823
660		0.001	1.883	1.667	28.205	28.254
680	14.00	1	4.286	0.250	31.176	31.177
680		0.5	3.985	0.214	30.848	30.849
680		0.2	3.587	0.730	30.604	30.613
680		0.1	3.286	0.510	30.508	30.512
680		0.05	2.985	0.132	30.189	30.189
680		0.02	2.587	1.267	28.783	28.811
680		0.01	2.286	3.854	28.844	29.101
680		0.005	1.985	1.786	28.815	28.870
680		0.002	1.587	2.477	26.840	26.954
680		0.001	1.286	3.645	25.166	25.428
700	13.43	1	3.713	0.332	30.346	30.348
700		0.5	3.412	0.300	30.411	30.413
700		0.2	3.014	0.365	30.056	30.058
700		0.1	2.713	0.816	30.769	30.779
700		0.05	2.412	0.967	29.375	29.391
700		0.02	2.014	0.423	28.814	28.817
700		0.01	1.713	2.349	27.404	27.505
700		0.005	1.412	2.843	24.986	25.147
700		0.002	1.014	4.692	22.443	22.928
700		0.001	0.713	6.148	19.292	20.248

Appendix 2. Temperature T , $\log_{10} \eta$, frequency f , $\log_{10} \omega\tau_M$, imaginary (G_{im}) and real (G_{real}) shear modulus and shear modulus of the melt (G_{melt}) for the investigated samples – continuation...

SAMPLE G8						
T (°C)	$\log_{10} \eta$ (Pa s)	f (Hz)	$\log_{10} \omega\tau_M$	G_{im} (GPa)	G_{real} (GPa)	G_{melt} (GPa)
720	12.88	1	3.164	0.469	30.447	30.451
720		0.5	2.863	0.590	30.304	30.310
720		0.2	2.465	1.021	29.700	29.717
720		0.1	2.164	1.588	28.907	28.950
720		0.05	1.863	2.163	27.446	27.532
720		0.02	1.465	1.364	26.849	26.883
720		0.01	1.164	4.171	23.818	24.180
720		0.005	0.863	0.863	5.520	20.227
720		0.002	0.465	0.465	7.540	14.450
720		0.001	0.164	0.164	7.525	8.931
740	12.35	1	2.636	0.931	29.987	30.001
740		0.5	2.335	1.232	29.401	29.427
740		0.2	1.937	1.966	28.236	28.304
740		0.1	1.636	2.654	26.377	26.510
740		0.05	1.335	4.097	24.377	24.719
740		0.02	0.937	5.848	21.074	21.870
740		0.01	0.636	5.413	17.407	18.229
740		0.005	0.335	0.335	14.833	14.837
740		0.002	-0.063	-0.063	2.732	7.807
740		0.001	-0.364	-0.364	2.565	3.788
760	11.84	1	2.129	1.711	29.235	29.286
760		0.5	1.828	2.385	28.008	28.109
760		0.2	1.430	0.312	25.470	25.471
760		0.1	1.129	5.181	23.207	23.778
760		0.05	0.828	6.643	19.138	20.258
760		0.02	0.430	7.765	11.883	14.195
760		0.01	0.129	7.015	6.649	9.665
760		0.005	-0.172	1.542	6.066	6.259
760		0.002	-0.570	-0.570	2.000	0.618
760		0.001	-0.871	-0.871	1.137	0.165

SAMPLE G8						
T (°C)	$\log_{10} \eta$ (Pa s)	f (Hz)	$\log_{10} \omega\tau_M$	G_{im} (GPa)	G_{real} (GPa)	G_{melt} (GPa)
780	11.35	1	1.641	2.755	24.357	24.512
780		0.5	1.340	3.840	22.471	22.797
780		0.2	0.942	5.369	18.526	19.288
780		0.1	0.641	7.180	14.744	16.399
780		0.05	0.340	7.426	9.485	12.046
780		0.02	-0.058	5.392	3.551	6.456
780		0.01	-0.359	3.292	1.263	3.526
780		0.005	-0.660	1.760	0.351	1.794
780		0.002	-1.058	0.713	0.081	0.717
780		0.001	-1.359	0.391	0.033	0.393
800	10.88	1	1.171	5.167	22.627	23.209
800		0.5	0.870	6.580	18.682	19.807
800		0.2	0.472	7.872	11.968	14.325
800		0.1	0.171	6.987	6.488	9.535
800		0.05	-0.130	4.852	2.713	5.559
800		0.02	-0.528	2.279	0.601	2.357
800		0.01	-0.829	1.036	0.659	1.228
800		0.005	-1.130	0.580	0.058	0.582
800		0.002	-1.528	0.176	0.178	0.251
800		0.001	-1.829	0.055	0.097	0.112
810	10.66	1	0.943	6.543	19.918	20.965
810		0.5	0.642	7.836	15.148	17.055
810		0.2	0.244	7.643	7.622	10.794
810		0.1	-0.057	5.455	3.316	6.384
810		0.05	-0.358	2.077	3.115	3.744
810		0.02	-0.756	1.339	0.229	1.358
810		0.01	-1.057	0.320	0.651	0.725
810		0.005	-1.358	0.339	0.054	0.343

Appendix 2. Temperature T , $\log_{10} \eta$, frequency f , $\log_{10} \omega\tau_M$, imaginary (G_{im}) and real (G_{real}) shear modulus and shear modulus of the melt (G_{melt}) for the investigated samples – continuation...

SAMPLE G8						
T (°C)	$\log_{10} \eta$ (Pa s)	f (Hz)	$\log_{10} \omega\tau_M$	G_{im} (GPa)	G_{real} (GPa)	G_{melt} (GPa)
820	10.43	1	0.719	6.853	14.943	16.439
820		0.5	0.418	7.306	9.913	12.315
820		0.2	0.020	5.646	3.856	6.837
820		0.1	-0.281	3.481	1.424	3.761
820		0.05	-0.582	1.316	1.579	2.055
820		0.02	-0.980	0.820	0.094	0.825
820		0.01	-1.281	0.405	0.025	0.405
820		0.005	-1.582	0.212	0.003	0.212
820		0.002	-1.980	0.039	0.072	0.082

SAMPLE G9						
T (°C)	$\log_{10} \eta$ (Pa s)	f (Hz)	$\log_{10} \omega\tau_M$	G_{im} (GPa)	G_{real} (GPa)	G_{melt} (GPa)
600	18.58	1	8.856	0.110	32.941	32.942
600		0.5	8.555	0.086	32.510	32.510
600		0.2	8.157	0.219	33.441	33.442
600		0.1	7.856	0.241	32.030	32.030
600		0.05	7.555	0.659	31.174	31.181
600		0.02	7.157	0.169	32.491	32.491
600		0.01	6.856	0.228	32.212	32.213
600		0.005	6.555	0.233	32.800	32.800
600		0.002	6.157	0.184	31.920	31.921
600		0.001	5.856	0.207	32.100	32.101
620	17.79	1	8.073	0.114	31.710	31.710
620		0.5	7.772	0.058	31.840	31.840
620		0.2	7.374	0.157	32.101	32.102
620		0.1	7.073	0.124	31.876	31.876
620		0.05	6.772	0.339	32.837	32.838
620		0.02	6.374	0.064	32.583	32.583
620		0.01	6.073	0.588	31.924	31.929
620		0.005	5.772	0.261	31.413	31.414
620		0.002	5.374	0.130	31.175	31.175
620		0.001	5.073	0.272	31.066	31.068
640	17.04	1	7.324	0.046	31.849	31.849
640		0.5	7.023	0.055	31.660	31.660
640		0.2	6.625	0.207	31.015	31.015
640		0.1	6.324	0.489	31.488	31.492
640		0.05	6.023	0.545	31.421	31.426
640		0.02	5.625	0.908	30.950	30.963
640		0.01	5.324	0.708	30.420	30.428
640		0.005	5.023	0.601	31.039	31.045
640		0.002	4.625	0.153	30.640	30.640
640		0.001	4.324	0.192	30.415	30.415

Appendix 2. Temperature T , $\log_{10} \eta$, frequency f , $\log_{10} \omega\tau_M$, imaginary (G_{im}) and real (G_{real}) shear modulus and shear modulus of the melt (G_{melt}) for the investigated samples – continuation...

SAMPLE G9						
T (°C)	$\log_{10} \eta$ (Pa s)	f (Hz)	$\log_{10} \omega\tau_M$	G_{im} (GPa)	G_{real} (GPa)	G_{melt} (GPa)
660	16.33	1	6.607	0.023	31.616	31.616
660		0.5	6.306	0.182	31.371	31.371
660		0.2	5.908	0.130	30.909	30.909
660		0.1	5.607	0.234	31.615	31.615
660		0.05	5.306	0.175	31.477	31.478
660		0.02	4.908	0.394	30.723	30.725
660		0.01	4.607	0.527	30.257	30.262
660		0.005	4.306	0.625	30.185	30.192
660		0.002	3.908	0.698	29.582	29.590
660		0.001	3.607	1.296	29.569	29.598
680	15.64	1	5.920	0.263	30.827	30.828
680		0.5	5.619	0.045	30.956	30.956
680		0.2	5.221	0.417	30.587	30.589
680		0.1	4.920	0.150	30.809	30.809
680		0.05	4.619	0.257	30.127	30.128
680		0.02	4.221	0.328	30.628	30.630
680		0.01	3.920	0.764	30.232	30.242
680		0.005	3.619	0.611	29.277	29.283
680		0.002	3.221	1.413	28.123	28.158
680		0.001	2.920	2.320	26.826	26.926
700	14.98	1	5.261	0.176	30.600	30.601
700		0.5	4.960	0.177	30.486	30.486
700		0.2	4.562	0.426	29.893	29.896
700		0.1	4.261	0.368	29.240	29.242
700		0.05	3.960	0.486	30.029	30.033
700		0.02	3.562	1.018	28.910	28.928
700		0.01	3.261	1.182	28.438	28.463
700		0.005	2.960	1.629	27.175	27.224
700		0.002	2.562	2.875	25.430	25.592
700		0.001	2.261	4.031	24.026	24.362

SAMPLE G9						
T (°C)	$\log_{10} \eta$ (Pa s)	f (Hz)	$\log_{10} \omega\tau_M$	G_{im} (GPa)	G_{real} (GPa)	G_{melt} (GPa)
720	14.35	1	4.629	0.355	30.065	30.067
720		0.5	4.328	0.452	29.524	29.527
720		0.2	3.930	0.445	29.257	29.260
720		0.1	3.629	0.655	29.594	29.601
720		0.05	3.328	1.455	28.189	28.226
720		0.02	2.930	1.576	27.171	27.217
720		0.01	2.629	2.029	26.163	26.242
720		0.005	2.328	3.535	23.885	24.145
720		0.002	1.930	5.296	20.870	21.531
720		0.001	1.629	6.632	17.153	18.390
740	13.74	1	4.022	0.488	28.423	28.428
740		0.5	3.721	0.647	28.331	28.339
740		0.2	3.323	1.365	27.184	27.218
740		0.1	3.022	1.232	26.015	26.044
740		0.05	2.721	2.115	26.878	26.961
740		0.02	2.323	3.517	23.410	23.673
740		0.01	2.022	4.559	21.450	21.929
740		0.005	1.721	5.996	18.060	19.029
740		0.002	1.323	7.642	12.155	14.358
740		0.001	1.022	6.960	6.959	9.842
760	13.16	1	3.438	0.826	26.730	26.743
760		0.5	3.137	1.304	26.523	26.555
760		0.2	2.739	1.870	24.757	24.827
760		0.1	2.438	2.494	23.399	23.532
760		0.05	2.137	3.723	22.875	23.176
760		0.02	1.739	5.552	18.196	19.024
760		0.01	1.438	7.004	14.249	15.877
760		0.005	1.137	3.673	12.029	12.578
760		0.002	0.739	5.196	3.380	6.199
760		0.001	0.438	3.284	1.910	3.799

Appendix 2. Temperature T , $\log_{10} \eta$, frequency f , $\log_{10} \omega\tau_M$, imaginary (G_{im}) and real (G_{real}) shear modulus and shear modulus of the melt (G_{melt}) for the investigated samples – continuation...

SAMPLE G9							
T (°C)	$\log_{10} \eta$ (Pa s)	f (Hz)	$\log_{10} \omega\tau_M$	G_{im} (GPa)	G_{real} (GPa)	G_{melt} (GPa)	
780	12.60	1	2.876	1.575	25.275	25.324	
780		0.5	2.575	2.161	24.261	24.357	
780		0.2	2.177	3.647	22.268	22.564	
780		0.1	1.876	4.520	19.528	20.044	
780		0.05	1.575	6.198	16.195	17.341	
780		0.02	1.177	7.260	10.473	12.743	
780		0.01	0.876	6.365	5.539	8.438	
780		0.005	0.575	4.236	2.234	4.789	
780		0.002	0.177	1.563	1.503	2.168	
780		0.001	0.001	-0.124	1.016	0.456	1.114
800	12.06	1	2.336	2.553	21.642	21.792	
800		0.5	2.035	0.443	20.748	20.753	
800		0.2	1.637	2.811	17.498	17.723	
800		0.1	1.336	6.445	12.774	14.308	
800		0.05	1.035	6.865	8.150	10.656	
800		0.02	0.637	4.817	2.946	5.646	
800		0.01	0.336	2.938	1.048	3.119	
800		0.005	0.035	1.556	0.321	1.589	
800		0.002	0.002	-0.363	0.653	0.049	0.655
800		0.001	0.001	-0.664	0.327	0.024	0.328
810	11.79	1	2.073	3.409	20.424	20.706	
810		0.5	1.772	4.656	18.269	18.853	
810		0.2	1.374	6.258	13.405	14.793	
810		0.1	1.073	6.822	9.034	11.320	
810		0.05	0.772	5.865	4.660	7.491	
810		0.02	0.374	3.120	1.211	3.347	
810		0.01	0.073	0.521	1.905	1.975	
810		0.005	0.005	-0.228	0.907	0.110	0.913
810		0.002	0.002	-0.626	0.372	0.026	0.373
810		0.001	0.001	-0.927	0.181	0.012	0.181

SAMPLE G9						
T (°C)	$\log_{10} \eta$ (Pa s)	f (Hz)	$\log_{10} \omega\tau_M$	G_{im} (GPa)	G_{real} (GPa)	G_{melt} (GPa)
820	11.53	1	1.815	3.700	16.569	16.977
820		0.5	1.514	5.149	14.011	14.928
820		0.2	1.116	6.213	9.261	11.151
820		0.1	0.815	5.698	5.068	7.626
820		0.05	0.514	3.967	2.066	4.473
820		0.02	0.116	1.831	0.461	1.888
820		0.01	-0.185	0.992	0.146	1.003
820		0.005	-0.486	0.497	0.049	0.499
820		0.002	-0.884	0.089	0.178	0.199
820		0.001	-1.185	0.122	0.047	0.130

Appendix 2. Temperature T , $\log_{10} \eta$, frequency f , $\log_{10} \omega\tau_M$, imaginary (G_{im}) and real (G_{real}) shear modulus and shear modulus of the melt (G_{melt}) for the investigated samples – continuation...

SAMPLE G10						
T (°C)	$\log_{10} \eta$ (Pa s)	f (Hz)	$\log_{10} \omega\tau_M$	G_{im} (GPa)	G_{real} (GPa)	G_{melt} (GPa)
560	17.35	1	7.642	0.062	32.199	32.199
560		0.5	7.341	0.135	31.958	31.958
560		0.2	6.943	0.051	31.723	31.723
560		0.1	6.642	0.076	32.019	32.020
560		0.05	6.341	0.207	32.229	32.230
560		0.02	5.943	0.132	32.489	32.489
560		0.01	5.642	0.212	32.040	32.040
560		0.005	5.341	0.241	31.658	31.658
560		0.002	4.943	0.116	31.503	31.503
560		0.001	4.642	0.383	31.462	31.464
580	16.61	1	6.902	0.110	31.927	31.927
580		0.5	6.601	0.102	31.881	31.881
580		0.2	6.203	0.196	31.973	31.974
580		0.1	5.902	0.262	31.925	31.926
580		0.05	5.601	0.058	31.824	31.824
580		0.02	5.203	0.298	31.577	31.579
580		0.01	4.902	0.280	31.833	31.834
580		0.005	4.601	0.364	31.578	31.580
580		0.002	4.203	0.134	31.523	31.523
580		0.001	3.902	0.191	30.974	30.975
600	15.91	1	6.196	0.046	31.825	31.825
600		0.5	5.895	0.056	32.028	32.028
600		0.2	5.497	0.212	31.906	31.907
600		0.1	5.196	0.486	31.281	31.285
600		0.05	4.895	0.546	31.454	31.459
600		0.02	4.497	0.928	31.619	31.633
600		0.01	4.196	0.763	32.821	32.830
600		0.005	3.895	0.577	29.762	29.768
600		0.002	3.497	0.155	31.057	31.057
600		0.001	3.196	0.185	29.281	29.282

SAMPLE G10						
T (°C)	$\log_{10} \eta$ (Pa s)	f (Hz)	$\log_{10} \omega\tau_M$	G_{im} (GPa)	G_{real} (GPa)	G_{melt} (GPa)
620	15.23	1	5.522	0.032	31.980	31.980
620		0.5	5.221	0.036	32.103	32.103
620		0.2	4.823	0.070	31.455	31.455
620		0.1	4.522	0.183	31.362	31.362
620		0.05	4.221	0.045	31.906	31.906
620		0.02	3.823	0.295	30.188	30.189
620		0.01	3.522	0.077	28.928	28.928
620		0.005	3.221	0.660	29.598	29.606
620		0.002	2.823	0.302	29.709	29.710
620		0.001	2.522	2.287	30.618	30.703
640	14.59	1	4.877	0.046	31.334	31.334
640		0.5	4.576	0.171	30.488	30.488
640		0.2	4.178	0.096	30.242	30.242
640		0.1	3.877	0.039	30.857	30.857
640		0.05	3.576	0.234	30.548	30.549
640		0.02	3.178	0.350	29.566	29.568
640		0.01	2.877	0.632	28.953	28.960
640		0.005	2.576	0.785	28.665	28.676
640		0.002	2.178	1.421	27.977	28.013
640		0.001	1.877	0.329	26.758	26.760
660	13.97	1	4.260	0.058	30.604	30.604
660		0.5	3.959	0.184	30.377	30.378
660		0.2	3.561	0.202	30.316	30.317
660		0.1	3.260	0.406	29.775	29.778
660		0.05	2.959	0.800	28.802	28.813
660		0.02	2.561	0.508	28.543	28.548
660		0.01	2.260	1.425	28.377	28.413
660		0.005	1.959	1.947	27.117	27.187
660		0.002	1.561	3.114	25.487	25.676
660		0.001	1.260	1.769	21.563	21.635

Appendix 2. Temperature T , $\log_{10} \eta$, frequency f , $\log_{10} \omega\tau_M$, imaginary (G_{im}) and real (G_{real}) shear modulus and shear modulus of the melt (G_{melt}) for the investigated samples – continuation...

SAMPLE G10							
T (°C)	$\log_{10} \eta$ (Pa s)	f (Hz)	$\log_{10} \omega\tau_M$	G_{im} (GPa)	G_{real} (GPa)	G_{melt} (GPa)	
680	13.38	1	3.669	0.221	29.710	29.711	
680		0.5	3.368	0.338	29.522	29.524	
680		0.2	2.970	0.384	29.138	29.141	
680		0.1	2.669	0.863	28.250	28.263	
680		0.05	2.368	0.977	28.262	28.279	
680		0.02	1.970	1.847	27.060	27.123	
680		0.01	1.669	2.470	25.502	25.621	
680		0.005	1.368	3.390	23.515	23.758	
680		0.002	0.970	5.377	20.318	21.017	
680		0.001	0.669	0.669	5.093	17.371	18.103
700	12.81	1	3.102	0.494	30.312	30.316	
700		0.5	2.801	0.918	29.977	29.991	
700		0.2	2.403	0.756	28.191	28.201	
700		0.1	2.102	1.780	27.941	27.997	
700		0.05	1.801	2.199	26.345	26.437	
700		0.02	1.403	3.599	23.868	24.137	
700		0.01	1.102	5.158	21.840	22.441	
700		0.005	0.801	0.801	3.147	18.397	18.664
700		0.002	0.403	0.403	7.573	11.522	13.788
700		0.001	0.102	0.102	6.830	6.134	9.180
720	12.27	1	2.558	1.020	28.492	28.510	
720		0.5	2.257	1.438	27.750	27.788	
720		0.2	1.859	2.185	26.087	26.178	
720		0.1	1.558	3.040	24.297	24.486	
720		0.05	1.257	4.304	22.137	22.552	
720		0.02	0.859	6.218	17.770	18.827	
720		0.01	0.558	7.354	13.420	15.303	
720		0.005	0.257	4.391	10.896	11.748	
720		0.002	-0.141	-0.141	4.537	3.344	5.636
720		0.001	-0.442	-0.442	2.554	1.319	2.874

SAMPLE G10						
T (°C)	$\log_{10} \eta$ (Pa s)	f (Hz)	$\log_{10} \omega\tau_M$	G_{im} (GPa)	G_{real} (GPa)	G_{melt} (GPa)
740	11.74	1	2.035	1.921	28.149	28.214
740		0.5	1.734	2.648	26.645	26.777
740		0.2	1.336	4.078	23.249	23.604
740		0.1	1.035	5.851	20.483	21.302
740		0.05	0.734	7.144	16.489	17.970
740		0.02	0.336	6.776	10.391	12.405
740		0.01	0.035	6.256	4.484	7.697
740		0.005	-0.266	3.743	1.625	4.080
740		0.002	-0.664	1.516	0.308	1.547
740		0.001	-0.965	0.780	0.301	0.836
760	11.24	1	1.533	3.601	25.780	26.030
760		0.5	1.232	4.829	23.290	23.786
760		0.2	0.834	6.340	17.470	18.585
760		0.1	0.533	7.735	13.038	15.159
760		0.05	0.232	7.074	7.603	10.384
760		0.02	-0.166	4.678	2.327	5.225
760		0.01	-0.467	1.851	2.238	2.904
760		0.005	-0.768	1.435	0.236	1.454
760		0.002	-1.166	0.320	0.443	0.546
760		0.001	-1.467	0.214	0.116	0.244
780	10.76	1	1.049	5.172	19.464	20.140
780		0.5	0.748	6.473	15.765	17.043
780		0.2	0.350	7.178	9.247	11.706
780		0.1	0.049	5.811	4.486	7.341
780		0.05	-0.252	1.987	4.206	4.652
780		0.02	-0.650	1.643	0.368	1.684
780		0.01	-0.951	0.855	0.097	0.861
780		0.005	-1.252	0.410	0.035	0.411
780		0.002	-1.650	0.061	0.122	0.136

Appendix 2. Temperature T , $\log_{10} \eta$, frequency f , $\log_{10} \omega\tau_M$, imaginary (G_{im}) and real (G_{real}) shear modulus and shear modulus of the melt (G_{melt}) for the investigated samples – continuation...

SAMPLE G11						
T (°C)	$\log_{10} \eta$ (Pa s)	f (Hz)	$\log_{10} \omega\tau_M$	G_{im} (GPa)	G_{real} (GPa)	G_{melt} (GPa)
540	16.05	1	6.343	0.047	32.094	32.094
540		0.5	6.042	0.056	32.240	32.240
540		0.2	5.644	0.218	32.761	32.762
540		0.1	5.343	0.496	31.973	31.977
540		0.05	5.042	0.557	32.085	32.090
540		0.02	4.644	0.944	32.166	32.179
540		0.01	4.343	0.730	31.402	31.411
540		0.005	4.042	0.605	31.223	31.229
540		0.002	3.644	0.157	31.408	31.408
540		0.001	3.343	0.202	32.001	32.002
560	15.37	1	5.664	0.151	32.055	32.055
560		0.5	5.362	0.006	31.614	31.614
560		0.2	4.965	0.070	31.939	31.939
560		0.1	4.664	0.077	31.354	31.354
560		0.05	4.362	0.487	31.385	31.389
560		0.02	3.965	0.046	30.852	30.852
560		0.01	3.664	0.160	31.584	31.585
560		0.005	3.362	0.314	30.941	30.942
560		0.002	2.965	0.612	31.704	31.710
560		0.001	2.664	0.421	29.909	29.912
580	14.72	1	5.016	0.084	31.325	31.325
580		0.5	4.715	0.113	30.928	30.928
580		0.2	4.317	0.131	30.725	30.725
580		0.1	4.016	0.262	30.761	30.762
580		0.05	3.715	0.376	30.195	30.198
580		0.02	3.317	0.311	30.239	30.240
580		0.01	3.016	0.553	29.968	29.974
580		0.005	2.715	0.528	30.440	30.444
580		0.002	2.317	0.485	27.398	27.403
580		0.001	2.016	1.722	29.673	29.723

SAMPLE G11						
T (°C)	$\log_{10} \eta$ (Pa s)	f (Hz)	$\log_{10} \omega\tau_M$	G_{im} (GPa)	G_{real} (GPa)	G_{melt} (GPa)
600	14.11	1	4.398	0.141	30.629	30.629
600		0.5	4.097	0.033	30.642	30.642
600		0.2	3.699	0.421	30.087	30.090
600		0.1	3.398	0.529	30.330	30.335
600		0.05	3.097	0.637	29.577	29.584
600		0.02	2.699	0.740	29.144	29.154
600		0.01	2.398	0.662	29.088	29.096
600		0.005	2.097	0.894	28.278	28.292
600		0.002	1.699	1.818	26.671	26.732
600		0.001	1.398	2.408	25.431	25.545
620	13.52	1	3.808	0.137	29.776	29.776
620		0.5	3.507	0.188	29.041	29.041
620		0.2	3.109	0.790	29.600	29.611
620		0.1	2.808	0.604	28.133	28.140
620		0.05	2.507	0.669	28.907	28.914
620		0.02	2.109	1.483	27.636	27.676
620		0.01	1.808	1.741	26.708	26.765
620		0.005	1.507	2.345	25.297	25.406
620		0.002	1.109	0.428	23.176	23.180
620		0.001	0.808	2.680	19.965	20.144
640	12.95	1	3.244	0.419	30.480	30.482
640		0.5	2.943	0.646	29.684	29.691
640		0.2	2.545	0.912	29.235	29.249
640		0.1	2.244	1.531	28.373	28.414
640		0.05	1.943	1.745	27.515	27.570
640		0.02	1.545	2.960	25.819	25.988
640		0.01	1.244	4.014	23.389	23.731
640		0.005	0.943	3.791	20.361	20.711
640		0.002	0.545	3.615	16.288	16.684
640		0.001	0.244	5.529	11.363	12.637

Appendix 2. Temperature T , $\log_{10} \eta$, frequency f , $\log_{10} \omega\tau_M$, imaginary (G_{im}) and real (G_{real}) shear modulus and shear modulus of the melt (G_{melt}) for the investigated samples – continuation...

SAMPLE G11						
T (°C)	$\log_{10} \eta$ (Pa s)	f (Hz)	$\log_{10} \omega\tau_M$	G_{im} (GPa)	G_{real} (GPa)	G_{melt} (GPa)
660	12.41	1	2.704	0.919	29.430	29.445
660		0.5	2.403	1.121	28.581	28.603
660		0.2	2.005	1.759	27.217	27.273
660		0.1	1.704	2.549	25.909	26.034
660		0.05	1.403	3.398	23.421	23.666
660		0.02	1.005	5.227	20.121	20.789
660		0.01	0.704	6.324	16.304	17.487
660		0.005	0.403	1.509	14.208	14.288
660		0.002	0.005	5.719	5.716	8.086
660		0.001	0.001	-0.296	3.886	3.109
680	11.89	1	2.187	1.872	29.551	29.610
680		0.5	1.886	2.596	27.816	27.937
680		0.2	1.488	3.969	25.480	25.788
680		0.1	1.187	4.924	22.429	22.963
680		0.05	0.886	6.073	18.334	19.313
680		0.02	0.488	6.971	12.199	14.051
680		0.01	0.187	6.481	7.370	9.814
680		0.005	-0.114	3.922	4.931	6.301
680		0.002	-0.512	2.472	1.034	2.680
680		0.001	-0.813	1.266	0.328	1.308
700	11.40	1	1.691	3.267	26.436	26.637
700		0.5	1.390	4.334	24.124	24.510
700		0.2	0.992	6.142	19.337	20.289
700		0.1	0.691	6.911	14.572	16.128
700		0.05	0.390	6.798	9.463	11.651
700		0.02	-0.008	5.124	3.893	6.435
700		0.01	-0.309	3.398	1.635	3.771
700		0.005	-0.610	1.854	0.564	1.938
700		0.002	-1.008	0.822	0.115	0.830
700		0.001	-1.309	0.424	0.052	0.427

SAMPLE G11							
T (°C)	$\log_{10} \eta$ (Pa s)	f (Hz)	$\log_{10} \omega\tau_M$	G_{im} (GPa)	G_{real} (GPa)	G_{melt} (GPa)	
720	10.92	1	1.214	5.767	22.990	23.703	
720		0.5	0.913	7.066	18.776	20.061	
720		0.2	0.516	7.456	11.183	13.441	
720		0.1	0.214	6.517	6.408	9.140	
720		0.05	-0.087	4.472	2.791	5.272	
720		0.02	-0.484	2.246	0.730	2.362	
720		0.01	-0.786	1.202	0.231	1.224	
720		0.005	-1.087	0.662	0.095	0.669	
740		10.46	1	0.757	7.477	15.163	16.906
740			0.5	0.456	7.467	9.702	12.243
740	0.2		0.058	5.407	3.822	6.621	
740	0.1		-0.243	3.372	1.478	3.682	
740	0.05		-0.544	1.902	0.508	1.969	
740							

Appendix 2. Temperature T , $\log_{10} \eta$, frequency f , $\log_{10} \omega\tau_M$, imaginary (G_{im}) and real (G_{real}) shear modulus and shear modulus of the melt (G_{melt}) for the investigated samples – continuation...

SAMPLE G12						
T (°C)	$\log_{10} \eta$ (Pa s)	f (Hz)	$\log_{10} \omega\tau_M$	G_{im} (GPa)	G_{real} (GPa)	G_{melt} (GPa)
340	25.27	1	15.576	0.022	31.420	31.420
340		0.5	15.275	0.037	31.316	31.316
340		0.2	14.877	0.028	31.543	31.543
340		0.1	14.576	0.044	30.880	30.880
340		0.05	14.275	0.222	31.072	31.073
340		0.02	13.877	0.018	31.320	31.320
340		0.01	13.576	0.057	31.180	31.180
340		0.005	13.275	0.251	30.946	30.947
340		0.002	12.877	0.107	31.006	31.006
340		0.001	12.576	0.034	31.092	31.092
360	23.99	1	14.289	0.014	31.494	31.494
360		0.5	13.988	0.018	31.404	31.404
360		0.2	13.590	0.017	31.006	31.006
360		0.1	13.289	0.206	30.914	30.915
360		0.05	12.988	0.278	30.938	30.939
360		0.02	12.590	0.267	31.384	31.385
360		0.01	12.289	0.095	31.217	31.217
360		0.005	11.988	0.117	30.869	30.869
360		0.002	11.590	0.050	30.643	30.643
360		0.001	11.289	0.185	30.700	30.701
380	22.78	1	13.080	0.045	31.212	31.212
380		0.5	12.779	0.053	30.630	30.630
380		0.2	12.381	0.210	31.531	31.532
380		0.1	12.080	0.484	31.190	31.194
380		0.05	11.779	0.545	31.397	31.401
380		0.02	11.381	0.909	30.959	30.972
380		0.01	11.080	0.722	31.029	31.037
380		0.005	10.779	0.592	30.580	30.586
380		0.002	10.381	0.155	30.910	30.911
380		0.001	10.080	0.193	30.524	30.525

SAMPLE G12						
T (°C)	$\log_{10} \eta$ (Pa s)	f (Hz)	$\log_{10} \omega\tau_M$	G_{im} (GPa)	G_{real} (GPa)	G_{melt} (GPa)
400	21.64	1	11.943	0.035	30.681	30.681
400		0.5	11.642	0.023	30.972	30.972
400		0.2	11.244	0.061	30.895	30.895
400		0.1	10.943	0.230	31.664	31.665
400		0.05	10.642	0.201	30.857	30.858
400		0.02	10.244	0.035	30.407	30.407
400		0.01	9.943	0.001	31.149	31.149
400		0.005	9.642	0.145	30.712	30.712
400		0.002	9.244	0.107	30.540	30.540
400		0.001	8.943	0.182	30.820	30.820
420	20.57	1	10.871	0.105	31.261	31.261
420		0.5	10.570	0.012	30.934	30.934
420		0.2	10.173	0.009	30.693	30.693
420		0.1	9.871	0.220	31.353	31.354
420		0.05	9.570	0.091	30.449	30.449
420		0.02	9.173	0.132	30.640	30.640
420		0.01	8.871	0.343	30.527	30.529
420		0.005	8.570	0.025	30.567	30.567
420		0.002	8.173	0.032	31.141	31.141
420		0.001	7.871	0.177	30.318	30.318
440	19.56	1	9.860	0.046	30.605	30.605
440		0.5	9.559	0.011	30.328	30.328
440		0.2	9.161	0.067	29.815	29.815
440		0.1	8.860	0.088	30.353	30.353
440		0.05	8.559	0.123	29.808	29.809
440		0.02	8.161	0.010	30.372	30.372
440		0.01	7.860	0.330	30.045	30.046
440		0.005	7.559	0.039	29.963	29.963
440		0.002	7.161	0.038	30.033	30.033
440		0.001	6.860	0.125	29.364	29.364

Appendix 2. Temperature T , $\log_{10} \eta$, frequency f , $\log_{10} \omega\tau_M$, imaginary (G_{im}) and real (G_{real}) shear modulus and shear modulus of the melt (G_{melt}) for the investigated samples – continuation...

SAMPLE G12						
T (°C)	$\log_{10} \eta$ (Pa s)	f (Hz)	$\log_{10} \omega\tau_M$	G_{im} (GPa)	G_{real} (GPa)	G_{melt} (GPa)
460	18.60	1	8.904	0.083	30.516	30.516
460		0.5	8.603	0.066	30.663	30.663
460		0.2	8.205	0.101	29.968	29.969
460		0.1	7.904	0.112	30.367	30.367
460		0.05	7.603	0.157	30.376	30.376
460		0.02	7.205	0.097	30.374	30.375
460		0.01	6.904	0.036	29.757	29.757
460		0.005	6.603	0.011	30.204	30.204
460		0.002	6.205	0.053	29.795	29.795
460		0.001	5.904	0.193	29.842	29.843
480	17.70	1	7.999	0.015	30.536	30.536
480		0.5	7.698	0.151	30.051	30.052
480		0.2	7.300	0.065	30.008	30.008
480		0.1	6.999	0.209	29.827	29.828
480		0.05	6.698	0.319	30.110	30.111
480		0.02	6.300	0.006	29.549	29.549
480		0.01	5.999	0.303	29.038	29.040
480		0.005	5.698	0.095	29.490	29.490
480		0.002	5.300	0.141	29.161	29.161
480		0.001	4.999	0.335	29.677	29.679
500	16.84	1	7.141	0.151	30.061	30.061
500		0.5	6.840	0.072	29.813	29.813
500		0.2	6.442	0.040	29.775	29.775
500		0.1	6.141	0.162	30.520	30.520
500		0.05	5.840	0.633	29.927	29.934
500		0.02	5.442	0.012	30.383	30.383
500		0.01	5.141	0.072	29.809	29.809
500		0.005	4.840	0.383	29.433	29.435
500		0.002	4.442	0.271	29.223	29.224
500		0.001	4.141	0.349	28.923	28.925

SAMPLE G12						
T (°C)	$\log_{10} \eta$ (Pa s)	f (Hz)	$\log_{10} \omega\tau_M$	G_{im} (GPa)	G_{real} (GPa)	G_{melt} (GPa)
520	16.02	1	6.325	0.119	30.446	30.447
520		0.5	6.024	0.347	30.245	30.247
520		0.2	5.626	0.090	30.252	30.252
520		0.1	5.325	0.397	29.979	29.981
520		0.05	5.024	0.052	29.383	29.383
520		0.02	4.626	0.093	30.176	30.176
520		0.01	4.325	0.634	29.735	29.742
520		0.005	4.024	0.397	28.881	28.884
520		0.002	3.626	0.462	29.236	29.239
520		0.001	3.325	0.743	28.762	28.771
540	15.25	1	5.550	0.090	30.084	30.084
540		0.5	5.249	0.024	29.987	29.987
540		0.2	4.851	0.048	30.561	30.561
540		0.1	4.550	0.170	29.603	29.603
540		0.05	4.249	0.417	29.259	29.262
540		0.02	3.851	0.442	29.260	29.263
540		0.01	3.550	0.820	28.929	28.941
540		0.005	3.249	0.586	28.836	28.842
540		0.002	2.851	0.827	27.731	27.744
540		0.001	2.550	1.519	27.628	27.670
560	14.51	1	4.813	0.236	29.632	29.633
560		0.5	4.512	0.280	29.437	29.438
560		0.2	4.114	0.320	29.130	29.132
560		0.1	3.813	0.162	28.939	28.940
560		0.05	3.512	0.526	28.508	28.513
560		0.02	3.114	0.747	27.897	27.907
560		0.01	2.813	1.098	27.343	27.365
560		0.005	2.512	1.566	26.644	26.690
560		0.002	2.114	2.240	25.083	25.183
560		0.001	1.813	0.384	23.918	23.921

Appendix 2. Temperature T , $\log_{10} \eta$, frequency f , $\log_{10} \omega\tau_M$, imaginary (G_{im}) and real (G_{real}) shear modulus and shear modulus of the melt (G_{melt}) for the investigated samples – continuation...

SAMPLE G12							
T (°C)	$\log_{10} \eta$ (Pa s)	f (Hz)	$\log_{10} \omega\tau_M$	G_{im} (GPa)	G_{real} (GPa)	G_{melt} (GPa)	
580	13.81	1	4.109	0.395	29.235	29.237	
580		0.5	3.808	0.460	29.003	29.006	
580		0.2	3.411	0.543	27.869	27.874	
580		0.1	3.109	0.826	28.288	28.300	
580		0.05	2.808	0.865	27.135	27.148	
580		0.02	2.411	1.654	25.852	25.905	
580		0.01	2.109	2.046	24.676	24.761	
580		0.005	1.808	2.883	23.044	23.223	
580		0.002	1.411	1.411	23.928	23.951	
580		0.001	1.109	1.109	3.244	17.804	18.097
600	13.14	1	3.439	0.622	28.329	28.336	
600		0.5	3.137	0.745	27.629	27.639	
600		0.2	2.740	1.207	27.149	27.176	
600		0.1	2.439	2.097	25.825	25.910	
600		0.05	2.137	2.543	24.662	24.793	
600		0.02	1.740	3.450	22.222	22.488	
600		0.01	1.439	4.673	19.411	19.965	
600		0.005	1.137	2.537	18.681	18.852	
600		0.002	0.740	0.740	4.746	12.308	13.191
600		0.001	0.439	0.439	5.608	7.623	9.464
620	12.50	1	2.798	1.229	26.073	26.102	
620		0.5	2.497	1.588	25.307	25.357	
620		0.2	2.099	2.699	23.542	23.697	
620		0.1	1.798	3.224	21.723	21.961	
620		0.05	1.497	4.454	19.309	19.816	
620		0.02	1.099	6.001	14.741	15.915	
620		0.01	0.798	6.381	10.846	12.584	
620		0.005	0.497	3.626	8.565	9.301	
620		0.002	0.099	0.099	3.565	3.189	4.783
620		0.001	-0.202	-0.202	2.420	0.999	2.618

SAMPLE G12						
T (°C)	$\log_{10} \eta$ (Pa s)	f (Hz)	$\log_{10} \omega\tau_M$	G_{im} (GPa)	G_{real} (GPa)	G_{melt} (GPa)
640	11.88	1	2.185	2.318	23.108	23.224
640		0.5	1.884	3.193	21.537	21.772
640		0.2	1.486	4.616	18.524	19.091
640		0.1	1.185	5.688	15.053	16.091
640		0.05	0.884	6.119	11.103	12.677
640		0.02	0.486	5.705	5.879	8.192
640		0.01	0.185	1.938	5.157	5.509
640		0.005	-0.116	2.319	1.978	3.048
640		0.002	-0.514	1.265	0.276	1.294
640		0.001	-0.815	0.660	0.140	0.675
660	11.30	1	1.598	4.221	19.098	19.559
660		0.5	1.297	5.288	16.190	17.032
660		0.2	0.899	6.177	11.161	12.756
660		0.1	0.598	5.927	7.016	9.185
660		0.05	0.297	4.607	3.565	5.825
660		0.02	-0.101	2.543	1.051	2.752
660		0.01	-0.402	1.556	0.384	1.603
660		0.005	-0.703	0.779	0.110	0.787

Appendix 2. Temperature T , $\log_{10} \eta$, frequency f , $\log_{10} \omega\tau_M$, imaginary (G_{im}) and real (G_{real}) shear modulus and shear modulus of the melt (G_{melt}) for the investigated samples – continuation...

SAMPLE G13						
T (°C)	$\log_{10} \eta$ (Pa s)	f (Hz)	$\log_{10} \omega\tau_M$	G_{im} (GPa)	G_{real} (GPa)	G_{melt} (GPa)
320	26.51	1	16.820	0.088	30.887	30.887
320		0.5	16.519	0.067	30.945	30.945
320		0.2	16.121	0.185	31.151	31.151
320		0.1	15.820	0.121	30.608	30.609
320		0.05	15.519	0.415	30.654	30.657
320		0.02	15.121	0.259	30.719	30.720
320		0.01	14.820	0.093	30.988	30.988
320		0.005	14.519	0.251	30.609	30.610
320		0.002	14.121	0.027	29.761	29.761
320		0.001	13.820	0.317	32.020	32.021
340	25.06	1	15.367	0.059	30.701	30.701
340		0.5	15.066	0.076	30.779	30.780
340		0.2	14.668	0.193	30.813	30.813
340		0.1	14.367	0.023	30.890	30.890
340		0.05	14.066	0.627	30.840	30.846
340		0.02	13.668	0.127	30.043	30.043
340		0.01	13.367	0.000	30.766	30.766
340		0.005	13.066			
340		0.002	12.668	0.048	29.934	29.934
340		0.001	12.367	0.919	30.672	30.686
360	23.70	1	14.005	0.058	30.838	30.838
360		0.5	13.704	0.052	30.627	30.627
360		0.2	13.306	0.221	30.701	30.702
360		0.1	13.005	0.152	30.487	30.488
360		0.05	12.704	0.213	30.307	30.308
360		0.02	12.306	0.082	30.785	30.785
360		0.01	12.005	0.003	30.323	30.323
360		0.005	11.704	0.252	30.560	30.561
360		0.002	11.306	0.249	30.166	30.167
360		0.001	11.005	0.384	28.952	28.954

SAMPLE G13						
T (°C)	$\log_{10} \eta$ (Pa s)	f (Hz)	$\log_{10} \omega\tau_M$	G_{im} (GPa)	G_{real} (GPa)	G_{melt} (GPa)
380	22.42	1	12.727	0.101	30.675	30.675
380		0.5	12.426	0.049	30.440	30.440
380		0.2	12.028	0.100	30.398	30.398
380		0.1	11.727	0.160	30.728	30.729
380		0.05	11.426	0.146	31.022	31.023
380		0.02	11.028	0.056	30.441	30.441
380		0.01	10.727	0.239	30.521	30.522
380		0.005	10.426	0.048	30.876	30.876
380		0.002	10.028	0.181	29.714	29.714
380		0.001	9.727	0.320	30.013	30.015
400	21.22	1	11.525	0.107	30.912	30.913
400		0.5	11.223	0.093	30.610	30.610
400		0.2	10.826	0.203	30.752	30.752
400		0.1	10.525	0.080	30.580	30.580
400		0.05	10.223	0.061	30.527	30.527
400		0.02	9.826	0.362	30.992	30.994
400		0.01	9.525	0.034	30.760	30.760
400		0.005	9.223	0.170	30.779	30.779
400		0.002	8.826	0.212	30.635	30.636
400		0.001	8.525	0.307	30.538	30.539
420	20.08	1	10.392	0.035	30.840	30.840
420		0.5	10.091	0.008	30.823	30.823
420		0.2	9.693	0.041	31.013	31.013
420		0.1	9.392	0.125	30.809	30.809
420		0.05	9.091	0.046	31.167	31.167
420		0.02	8.693	0.295	30.867	30.868
420		0.01	8.392	0.094	30.480	30.480
420		0.005	8.091	0.359	30.486	30.488
420		0.002	7.693	0.010	32.251	32.251
420		0.001	7.392	0.162	30.627	30.627

Appendix 2. Temperature T , $\log_{10} \eta$, frequency f , $\log_{10} \omega\tau_M$, imaginary (G_{im}) and real (G_{real}) shear modulus and shear modulus of the melt (G_{melt}) for the investigated samples – continuation...

SAMPLE G13						
T (°C)	$\log_{10} \eta$ (Pa s)	f (Hz)	$\log_{10} \omega\tau_M$	G_{im} (GPa)	G_{real} (GPa)	G_{melt} (GPa)
440	19.01	1	9.322	0.045	30.803	30.803
440		0.5	9.021	0.054	31.278	31.278
440		0.2	8.623	0.208	31.166	31.167
440		0.1	8.322	0.482	31.069	31.073
440		0.05	8.021	0.529	30.463	30.467
440		0.02	7.623	0.897	30.576	30.589
440		0.01	7.322	0.718	30.868	30.877
440		0.005	7.021	0.583	30.088	30.094
440		0.002	6.623	0.153	30.573	30.573
440		0.001	6.322	0.197	31.108	31.109
460	18.00	1	8.311	0.024	29.688	29.688
460		0.5	8.010	0.036	29.434	29.435
460		0.2	7.612	0.259	29.783	29.784
460		0.1	7.311	0.050	29.722	29.722
460		0.05	7.010	0.181	29.160	29.161
460		0.02	6.612	0.217	28.842	28.843
460		0.01	6.311	0.261	29.038	29.039
460		0.005	6.010	0.117	30.344	30.344
460		0.002	5.612	0.351	29.098	29.101
460		0.001	5.311	0.497	29.140	29.144
480	17.04	1	7.354	0.074	30.621	30.621
480		0.5	7.053	0.043	30.282	30.282
480		0.2	6.655	0.166	30.628	30.629
480		0.1	6.354	0.159	30.732	30.733
480		0.05	6.053	0.112	29.934	29.934
480		0.02	5.655	0.334	31.310	31.312
480		0.01	5.354	0.448	30.644	30.647
480		0.005	5.053	0.053	30.051	30.051
480		0.002	4.655	0.441	29.850	29.853
480		0.001	4.354	0.136	30.212	30.213

SAMPLE G13						
T (°C)	$\log_{10} \eta$ (Pa s)	f (Hz)	$\log_{10} \omega\tau_M$	G_{im} (GPa)	G_{real} (GPa)	G_{melt} (GPa)
500	16.14	1	6.446	0.193	29.402	29.403
500		0.5	6.145	0.161	29.320	29.320
500		0.2	5.747	0.065	29.617	29.617
500		0.1	5.446	0.241	29.582	29.583
500		0.05	5.145	0.131	29.328	29.328
500		0.02	4.747	0.315	29.069	29.070
500		0.01	4.446	0.086	28.877	28.877
500		0.005	4.145	0.403	29.061	29.064
500		0.002	3.747	0.459	28.603	28.606
500		0.001	3.446	0.549	27.319	27.324
520	15.28	1	5.584	0.010	29.091	29.091
520		0.5	5.283	0.069	28.480	28.480
520		0.2	4.885	0.346	28.351	28.353
520		0.1	4.584	0.024	28.160	28.160
520		0.05	4.283	0.233	28.858	28.859
520		0.02	3.885	0.611	28.489	28.496
520		0.01	3.584	0.633	28.239	28.246
520		0.005	3.283	0.587	28.155	28.161
520		0.002	2.885	0.773	26.869	26.880
520		0.001	2.584	1.465	26.190	26.231
540	14.46	1	4.765	0.147	29.408	29.409
540		0.5	4.464	0.209	29.108	29.108
540		0.2	4.066	0.027	29.191	29.191
540		0.1	3.765	0.027	28.524	28.524
540		0.05	3.464	0.655	27.794	27.802
540		0.02	3.066	0.573	27.941	27.947
540		0.01	2.765	1.334	27.684	27.716
540		0.005	2.464	1.630	26.101	26.151
540		0.002	2.066	2.303	24.901	25.007
540		0.001	1.765	0.915	24.611	24.628

Appendix 2. Temperature T , $\log_{10} \eta$, frequency f , $\log_{10} \omega\tau_M$, imaginary (G_{im}) and real (G_{real}) shear modulus and shear modulus of the melt (G_{melt}) for the investigated samples – continuation...

SAMPLE G13						
T (°C)	$\log_{10} \eta$ (Pa s)	f (Hz)	$\log_{10} \omega\tau_M$	G_{im} (GPa)	G_{real} (GPa)	G_{melt} (GPa)
560	13.68	1	3.984	0.372	27.790	27.792
560		0.5	3.683	0.518	27.457	27.461
560		0.2	3.285	0.706	26.990	26.999
560		0.1	2.984	0.874	27.027	27.041
560		0.05	2.683	0.906	26.197	26.213
560		0.02	2.285	2.022	24.440	24.524
560		0.01	1.984	2.242	23.076	23.185
560		0.005	1.683	3.119	21.777	21.999
560		0.002	1.285	4.457	21.206	21.211
560		0.001	0.984	4.009	16.129	16.620
580	12.93	1	3.241	0.651	25.993	26.001
580		0.5	2.940	0.921	25.556	25.572
580		0.2	2.542	1.550	24.628	24.677
580		0.1	2.241	1.930	23.953	24.031
580		0.05	1.940	2.585	22.270	22.419
580		0.02	1.542	3.793	19.688	20.050
580		0.01	1.241	4.921	16.857	17.560
580		0.005	0.940	4.753	14.302	15.071
580		0.002	0.542	4.855	9.208	10.410
580		0.001	0.241	4.738	4.500	6.534
600	12.22	1	2.531	1.641	26.659	26.710
600		0.5	2.230	2.422	25.574	25.688
600		0.2	1.832	3.443	23.189	23.444
600		0.1	1.531	4.590	21.141	21.634
600		0.05	1.230	5.743	17.591	18.505
600		0.02	0.832	6.900	11.849	13.712
600		0.01	0.531	6.533	7.100	9.649
600		0.005	0.230	3.853	4.981	6.298
600		0.002	-0.168	2.466	0.793	2.590
600		0.001	-0.469	1.115	1.139	1.595

SAMPLE G13						
T (°C)	$\log_{10} \eta$ (Pa s)	f (Hz)	$\log_{10} \omega\tau_M$	G_{im} (GPa)	G_{real} (GPa)	G_{melt} (GPa)
620	11.54	1	1.853	3.614	25.171	25.430
620		0.5	1.552	4.856	22.442	22.962
620		0.2	1.154	5.873	17.714	18.662
620		0.1	0.853	7.517	12.755	14.805
620		0.05	0.552	6.856	7.562	10.207
620		0.02	0.154	4.512	2.514	5.165
620		0.01	-0.147	2.643	0.875	2.784
620		0.005	-0.448	1.375	0.234	1.395
620		0.002	-0.846	0.512	0.045	0.514
620		0.001	-1.147	0.259	0.018	0.259
640	10.90	1	1.205	5.983	17.900	18.873
640		0.5	0.904	6.889	13.467	15.127
640		0.2	0.506	6.693	7.004	9.687
640		0.1	0.205	4.976	3.204	5.919
640		0.05	-0.096	3.026	1.159	3.241
640		0.02	-0.494	1.358	0.229	1.378
640		0.01	-0.795	0.196	0.639	0.668
640		0.005	-1.096	0.303	0.023	0.304
640		0.002	-1.494	0.061	0.106	0.123
660		10.28	1	0.585	8.150	4.784
660	0.5		0.284	5.579	4.481	7.156
660	0.2		-0.114	3.217	1.246	3.450
660	0.1		-0.415	1.763	0.379	1.803
680	9.68	1	-0.009	4.141	2.150	4.666

Appendix 2. Temperature T , $\log_{10} \eta$, frequency f , $\log_{10} \omega\tau_M$, imaginary (G_{im}) and real (G_{real}) shear modulus and shear modulus of the melt (G_{melt}) for the investigated samples – continuation...

SAMPLE G14						
T (°C)	$\log_{10} \eta$ (Pa s)	f (Hz)	$\log_{10} \omega\tau_M$	G_{im} (GPa)	G_{real} (GPa)	G_{melt} (GPa)
420	18.20	1	8.521	0.094	29.965	29.965
420		0.5	8.220	0.098	29.764	29.764
420		0.2	7.822	0.097	30.055	30.055
420		0.1	7.521	0.209	29.573	29.574
420		0.05	7.220	0.112	29.665	29.665
420		0.02	6.822	0.059	28.705	28.705
420		0.01	6.521	0.187	29.158	29.159
420		0.005	6.220	0.266	29.470	29.471
420		0.002	5.822	0.036	29.067	29.067
420		0.001	5.521	0.339	28.728	28.730
440	17.18	1	7.503	0.034	29.471	29.471
440		0.5	7.202	0.034	29.503	29.503
440		0.2	6.804	0.219	29.034	29.035
440		0.1	6.503	0.249	29.072	29.073
440		0.05	6.202	0.035	29.362	29.362
440		0.02	5.804	0.035	29.505	29.505
440		0.01	5.503	0.181	28.797	28.798
440		0.005	5.202	0.042	28.956	28.956
440		0.002	4.804	0.824	28.819	28.831
440		0.001	4.503	0.749	29.109	29.119
460	16.22	1	6.541	0.027	29.456	29.456
460		0.5	6.240	0.182	29.391	29.391
460		0.2	5.842	0.138	28.959	28.960
460		0.1	5.541	0.015	28.942	28.942
460		0.05	5.240	0.234	28.979	28.980
460		0.02	4.842	0.665	27.961	27.969
460		0.01	4.541	0.748	28.671	28.681
460		0.005				
460		0.002	3.842	0.315	28.303	28.304
460		0.001	3.541	0.288	28.312	28.314

SAMPLE G14						
T (°C)	$\log_{10} \eta$ (Pa s)	f (Hz)	$\log_{10} \omega\tau_M$	G_{im} (GPa)	G_{real} (GPa)	G_{melt} (GPa)
480	15.31	1	5.629	0.030	29.281	29.281
480		0.5	5.328	0.070	29.173	29.173
480		0.2	4.930	1.290	28.647	28.676
480		0.1	4.629	0.200	28.830	28.831
480		0.05	4.328	0.367	29.391	29.393
480		0.02	3.930	0.130	28.943	28.943
480		0.01	3.629	0.384	28.028	28.030
480		0.005	3.328	0.687	27.860	27.868
480		0.002	2.930	0.640	27.131	27.139
480		0.001	2.629	0.947	27.207	27.223
500	14.44	1	4.765	0.361	28.803	28.806
500		0.5	4.464	0.171	28.566	28.567
500		0.2	4.066	0.069	28.070	28.070
500		0.1	3.765	0.123	27.541	27.541
500		0.05	3.464	0.300	27.963	27.964
500		0.02	3.066	0.491	27.308	27.312
500		0.01	2.765	0.648	27.224	27.232
500		0.005	2.464	0.937	26.610	26.627
500		0.002	2.066	1.525	25.254	25.300
500		0.001	1.765	0.317	24.875	24.878
520	13.62	1	3.944	0.282	27.902	27.904
520		0.5	3.643	0.233	27.579	27.580
520		0.2	3.245	0.641	27.997	28.004
520		0.1	2.944	0.976	26.902	26.919
520		0.05	2.643	0.965	26.953	26.970
520		0.02	2.245	1.328	25.848	25.882
520		0.01	1.944	1.607	24.717	24.770
520		0.005	1.643	2.469	23.733	23.861
520		0.002	1.245	0.069	21.908	21.908
520		0.001	0.944	2.743	19.629	19.819

Appendix 2. Temperature T , $\log_{10} \eta$, frequency f , $\log_{10} \omega\tau_M$, imaginary (G_{im}) and real (G_{real}) shear modulus and shear modulus of the melt (G_{melt}) for the investigated samples – continuation...

SAMPLE G14						
T (°C)	$\log_{10} \eta$ (Pa s)	f (Hz)	$\log_{10} \omega\tau_M$	G_{im} (GPa)	G_{real} (GPa)	G_{melt} (GPa)
540	12.84	1	3.164	0.040	27.629	27.629
540		0.5	2.863	0.048	27.570	27.570
540		0.2	2.465	0.176	26.358	26.359
540		0.1	2.164	0.398	25.660	25.663
540		0.05	1.863	0.424	24.410	24.414
540		0.02	1.465	0.663	22.597	22.607
540		0.01	1.164	0.480	20.647	20.653
540		0.005	0.863	0.359	18.550	18.553
540		0.002	0.465	0.070	14.095	14.096
540		0.001	0.164	0.164	0.063	9.949
560	12.10	1	2.421	1.304	25.025	25.059
560		0.5	2.120	1.773	24.154	24.219
560		0.2	1.722	2.792	22.456	22.629
560		0.1	1.421	3.761	20.924	21.259
560		0.05	1.120	4.861	17.754	18.407
560		0.02	0.722	6.225	13.507	14.872
560		0.01	0.421	1.472	11.962	12.052
560		0.005	0.120	4.617	6.494	7.968
560		0.002	-0.278	3.291	1.412	3.581
560		0.001	-0.579	0.150	0.150	2.135
580	11.39	1	1.713	2.829	21.262	21.450
580		0.5	1.412	3.705	19.125	19.480
580		0.2	1.014	5.400	15.555	16.465
580		0.1	0.713	1.717	13.993	14.098
580		0.05	0.412	6.365	7.534	9.862
580		0.02	0.014	4.619	2.797	5.399
580		0.01	-0.287	3.143	1.089	3.327
580		0.005	-0.588	1.632	0.317	1.663
580		0.002	-0.986	0.665	0.052	0.667

SAMPLE G14						
T (°C)	$\log_{10} \eta$ (Pa s)	f (Hz)	$\log_{10} \omega\tau_M$	G_{im} (GPa)	G_{real} (GPa)	G_{melt} (GPa)
600	10.72	1	1.037	4.532	13.462	14.204
600		0.5	0.736	5.369	10.364	11.672
600		0.2	0.338	5.691	5.795	8.122
600		0.1	0.037	4.174	2.547	4.890

Appendix 3. Temperature T , frequency f , G_{∞} , viscosity, shear viscosity, relaxed Newtonian viscosity and relaxation times of the samples, determined by micropenetration and torsion measurements.

			MICROPENETRATION				TORSION		
T	f	G_{∞}	A	B	$\log_{10} \eta$	τ	Shear visc. $\log_{10} \eta$	Relaxed Newt. visc. $\log_{10} \eta$	τ
°C	Hz	GPa	$\log_{10} \text{ Pa s}$	K	Pa s	s	Pa s	Pa s	s
SAMPLE G0									
500	1	27.45	-24.98±0.99	2.673 ±0.074	9.59	0.142	9.13	9.38	0.087
	0.5						9.38		
	0.2						9.32		
490	1	27.45	-24.98±0.99	2.673 ±0.074	10.04	0.403	8.93	10.07	0.428
	0.5						9.33		
	0.2						8.98		
	0.1						9.65		
	0.05						10.03		
	0.02						10.06		
480	1	27.45	-24.98±0.99	2.673 ±0.074	10.51	1.177	8.06	10.37	0.854
	0.5						8.94		
	0.2						9.67		
	0.1						9.88		
	0.05						9.85		
	0.02						10.29		
	0.01						10.32		
	0.005						10.30		
	0.002						10.45		
460	1	27.45	-24.98±0.99	2.673 ±0.074	11.48	10.948	7.52	11.45	10.269
	0.5						7.68		
	0.2						8.26		
	0.1						9.30		
	0.05						9.69		
	0.02						10.79		
	0.01						11.26		
	0.005						11.35		
	0.002						11.43		
440	1	27.45	-24.98±0.99	2.673 ±0.074	12.50	115.386	6.56	12.30	72.698
	0.5						7.79		
	0.2						8.27		
	0.1						8.64		
	0.05						8.73		
	0.02						9.39		
	0.01						10.29		
	0.005						10.61		
	0.002						11.83		
	0.001						12.30		
420	1	27.45	-24.98±0.99	2.673 ±0.074	13.58	1393.121	6.70	13.18	551.468
	0.5						7.70		
	0.2						8.22		
	0.1						8.20		
	0.05						9.05		
	0.02						9.50		
	0.01						10.11		
	0.005						10.88		
	0.002						12.26		
	0.001						13.17		
400		27.45	-24.98±0.99	2.673 ±0.074	14.73	19503.938	-	-	-
380		27.45	-24.98±0.99	2.673 ±0.074	15.94	320968.90	-	-	-
SAMPLE G1									
875	1	34.26	-15.63±0.53	3.014 ±0.061	10.62	1.208	10.16	10.82	1.928
	0.5						10.50		
	0.2						10.83		
	0.1						10.90		
	0.05						10.54		
850	1	34.26	-15.63±0.53	3.014 ±0.061	11.20	4.640	10.59	11.34	6.386
	0.5						11.03		
	0.2						11.56		
	0.1						11.90		
	0.05						11.36		
	0.02						11.47		

Appendix 3. Temperature T , frequency f , G_{∞} , viscosity, shear viscosity, relaxed Newtonian viscosity and relaxation times of the samples, determined by micropenetration and torsion measurements. Continuation...

			MICROPENETRATION				TORSION		
T	f	G_{∞}	A	B	$\log_{10} \eta$	τ	Shear visc. $\log_{10} \eta$	Relaxed Newt. visc. $\log_{10} \eta$	τ
°C	Hz	GPa	$\log_{10} \text{ Pa s}$	K	Pa s	s	Pa s	Pa s	s
SAMPLE G1									
850	0.01		-15.63±0.53		11.20	4.640	11.49	11.34	6.386
	0.005						11.32		
825	1	34.26	-15.63±0.53	3.014 ±0.061	11.81	18.945	9.98	12.11	37.603
	0.5						10.46		
	0.2						11.04		
	0.1						11.47		
	0.05						11.85		
	0.02						12.26		
	0.01						12.10		
	0.005						12.15		
	0.002						12.15		
	0.001						11.88		
800	1	34.26	-15.63±0.53	3.014 ±0.061	12.45	82.598	13.20	12.56	105.981
	0.5						13.61		
	0.2						13.12		
	0.1						12.70		
	0.05						12.81		
	0.02						12.80		
	0.01						12.82		
	0.005						12.35		
	0.002						12.70		
	0.001						12.57		
775	1	34.26	-15.63±0.53	3.014 ±0.061	13.12	386.329	12.85	13.16	421.917
	0.5						13.38		
	0.2						14.00		
	0.1						13.63		
	0.05						13.85		
	0.02						13.90		
	0.01						13.36		
	0.005						13.08		
	0.002						13.14		
	0.001						13.14		
750	1	34.26	-15.63±0.53	3.014 ±0.061	13.82	1948.454	12.65	13.86	2114.594
	0.5						13.20		
	0.2						13.81		
	0.1						14.06		
	0.05						14.34		
	0.02						14.16		
	0.01						14.52		
	0.005						13.97		
	0.002						13.98		
	0.001						13.79		
725	1	34.26	-15.63±0.53	3.014 ±0.061	14.56	10656.877	12.60	14.45	8226.725
	0.5						13.72		
	0.2						14.12		
	0.1						14.40		
	0.05						14.91		
	0.02						15.15		
	0.01						15.14		
	0.005						14.66		
	0.002						14.40		
	0.001						14.49		
700	1	34.26	-15.63±0.53	3.014 ±0.061	15.34	63604.893	13.17	15.27	54353.433
	0.5						13.39		
	0.2						14.26		
	0.1						14.88		
	0.05						14.71		
	0.02						15.56		
	0.01						15.63		
	0.005						15.39		
	0.002						15.21		
	0.001						15.28		
650	1	34.26	-15.63±0.53	3.014 ±0.061	17.02	3029002	12.40	16.72	1531887.9
	0.5						12.78		
	0.2						13.77		

Appendix 3. Temperature T , frequency f , G_{∞} , viscosity, shear viscosity, relaxed Newtonian viscosity and relaxation times of the samples, determined by micropenetration and torsion measurements. Continuation...

			MICROPENETRATION				TORSION		
T	f	G_{∞}	A	B	$\log_{10} \eta$	τ	Shear visc. $\log_{10} \eta$	Relaxed Newt. visc. $\log_{10} \eta$	τ
°C	Hz	GPa	$\log_{10} \text{ Pa s}$	K	Pa s	s	Pa s	Pa s	s
SAMPLE G1									
650	0.1	34.26	-15.63±0.53	3.014 ±0.061	17.02	3029002	14.43	16.72	1531887.9
	0.05						14.78		
	0.02						15.90		
	0.01						16.44		
	0.005						16.68		
	0.002						16.58		
	0.001						16.90		
600	1	34.26	-15.63±0.53	3.014 ±0.061	18.89	224541877	11.82	18.22	48442548.4
	0.5						12.43		
	0.2						13.72		
	0.1						14.17		
	0.05						14.79		
	0.02						16.24		
	0.01						17.21		
	0.005						17.66		
	0.002						18.20		
	0.001						18.20		
550		34.26	-15.63±0.53	3.014 ±0.061	20.98	2.809E+10	-	-	-
500		34.26	-15.63±0.53	3.014 ±0.061	23.35	6.562E+12	-	-	-
450		34.26	-15.63±0.53	3.014 ±0.061	26.05	3.260E+15	-	-	-
400		34.26	-15.63±0.53	3.014 ±0.061	29.14	4.073E+18	-	-	-
350		34.26	-15.63±0.53	3.014 ±0.061	32.74	1.598E+22	-	-	-
SAMPLE G2									
900	1	34.78	-14.90±0.38	2.956 ±0.044	10.29	0.566	8.78	10.22	0.477
	0.5						9.10		
	0.2						9.77		
	0.1						10.18		
	0.05						10.14		
875	1	34.78	-14.90±0.38	2.956 ±0.044	10.84	2.004	9.16	10.50	0.909
	0.5						9.34		
	0.2						9.74		
	0.1						10.49		
	0.05						10.52		
850	1	34.78	-14.90±0.38	2.956 ±0.044	11.42	7.498	10.03	11.34	6.290
	0.5						10.24		
	0.2						10.65		
	0.1						10.96		
	0.05						10.71		
	0.02						10.97		
	0.01						11.34		
	0.005						11.33		
	0.002						11.34		
	0.001						11.23		
825	1	34.78	-14.90±0.38	2.956 ±0.044	12.02	29.797	9.77	11.83	19.437
	0.5						10.12		
	0.2						10.70		
	0.1						10.96		
	0.05						11.16		
	0.02						11.40		
	0.01						11.55		
	0.005						11.78		
	0.002						11.84		
	0.001						11.80		
800	1	34.78	-14.90±0.38	2.956 ±0.044	12.64	126.277	9.75	12.27	53.533
	0.5						10.06		
	0.2						10.68		
	0.1						11.14		

Appendix 3. Temperature T, frequency f, G_∞, viscosity, shear viscosity, relaxed Newtonian viscosity and relaxation times of the samples, determined by micropenetration and torsion measurements. Continuation...

			MICROPENETRATION				TORSION		
T	f	G _∞	A	B	log ₁₀ η	τ	Shear visc. log ₁₀ η	Relaxed Newt. visc. log ₁₀ η	τ
°C	Hz	GPa	log ₁₀ Pa s	K	Pa s	s	Pa s	Pa s	s
SAMPLE G2									
800	0.05	34.78	-14.90±0.38	2.956 ±0.044	12.64	126.277	11.42	12.27	53.533
	0.02						11.52		
	0.01						11.67		
	0.005						11.88		
	0.002						12.22		
	0.001						12.36		
775	1	34.78	-14.90±0.38	2.956 ±0.044	13.30	573.329	9.73	13.10	361.927
	0.5						10.25		
	0.2						11.03		
	0.1						11.67		
	0.05						11.82		
	0.02						12.25		
	0.01						12.70		
	0.005						12.87		
	0.002						13.14		
	0.001						13.24		
750	1	34.78	-14.90±0.38	2.956 ±0.044	13.99	2802.839	9.83	13.74	1579.870
	0.5						9.45		
	0.2						10.19		
	0.1						11.42		
	0.05						11.67		
	0.02						12.17		
	0.01						12.63		
	0.005						13.04		
	0.002						13.68		
	0.001						13.75		
725	1	34.78	-14.90±0.38	2.956 ±0.044	14.71	14836.133	8.84	14.38	6896.381
	0.5						9.08		
	0.2						9.44		
	0.1						11.30		
	0.05						11.88		
	0.02						12.64		
	0.01						13.21		
	0.005						13.86		
	0.002						14.19		
	0.001						14.49		
700	1	34.78	-14.90±0.38	2.956 ±0.044	15.47	85552.678	7.99	15.54	99683.038
	0.5						8.55		
	0.2						10.41		
	0.1						11.21		
	0.05						12.00		
	0.02						12.88		
	0.01						13.85		
	0.005						14.37		
	0.002						14.96		
	0.001						15.52		
650		34.78	-14.90±0.38	2.956 ±0.044	17.12	3781969.52	-	-	-
600		34.78	-14.90±0.38	2.956 ±0.044	18.95	258040948	-	-	-
550		34.78	-14.90±0.38	2.956 ±0.044	21.01	2.941E+10	-	-	-
500		34.78	-14.90±0.38	2.956 ±0.044	23.33	6.186E+12	-	-	-

Appendix 3. Temperature T , frequency f , G_{∞} , viscosity, shear viscosity, relaxed Newtonian viscosity and relaxation times of the samples, determined by micropenetration and torsion measurements. Continuation...

			MICROPENETRATION				TORSION		
T	f	G_{∞}	A	B	$\log_{10} \eta$	τ	Shear visc. $\log_{10} \eta$	Relaxed Newt. visc. $\log_{10} \eta$	τ
°C	Hz	GPa	$\log_{10} \text{ Pa s}$	K	Pa s	s	Pa s	Pa s	s
SAMPLE G3									
900	1	34.43	-16.05±0.36	3.083 ±0.041	10.23	0.497	10.23	10.20	0.460
	0.5						10.26		
875	1	34.43	-16.05±0.36	3.083 ±0.041	10.80	1.857	9.98	10.78	1.750
	0.5						10.41		
	0.2						10.71		
	0.1						10.84		
	0.05						10.83		
850	1	34.43	-16.05±0.36	3.083 ±0.041	11.40	7.356	9.82	11.37	6.808
	0.5						10.25		
	0.2						10.75		
	0.1						11.15		
	0.05						11.32		
	0.02						11.40		
	0.01						11.45		
	0.005						-		
	0.002						-		
825	1	34.43	-16.05±0.36	3.083 ±0.041	12.03	31.022	9.53	11.89	22.543
	0.5						10.02		
	0.2						10.58		
	0.1						11.03		
	0.05						11.36		
	0.02						11.71		
	0.01						11.96		
	0.005						11.93		
	0.002						11.95		
	0.001						11.97		
800	1	34.43	-16.05±0.36	3.083 ±0.041	12.68	139.892	9.30	12.79	179.064
	0.5						9.79		
	0.2						10.37		
	0.1						10.87		
	0.05						11.36		
	0.02						11.92		
	0.01						12.27		
	0.005						12.54		
	0.002						12.70		
	0.001						12.75		
775	1	34.43	-16.05±0.36	3.083 ±0.041	13.37	677.838	9.25	13.21	470.985
	0.5						9.59		
	0.2						10.33		
	0.1						10.81		
	0.05						11.26		
	0.02						11.81		
	0.01						12.26		
	0.005						12.73		
	0.002						13.21		
	0.001						13.30		
750		34.43	-16.05±0.36	3.083 ±0.041	14.09	3547.749	-	-	-
725		34.43	-16.05±0.36	3.083 ±0.041	14.84	20174.069	-	-	-
700		34.43	-16.05±0.36	3.083 ±0.041	15.64	125436.353	-	-	-
650		34.43	-16.05±0.36	3.083 ±0.041	17.35	6526177	-	-	-
600		34.43	-16.05±0.36	3.083 ±0.041	19.26	533930613	-	-	-
550		34.43	-16.05±0.36	3.083 ±0.041	21.41	7.460E+10	-	-	-

Appendix 3. Temperature T , frequency f , G_{∞} , viscosity, shear viscosity, relaxed Newtonian viscosity and relaxation times of the samples, determined by micropenetration and torsion measurements. Continuation...

			MICROPENETRATION				TORSION		
T	f	G_{∞}	A	B	$\log_{10} \eta$	τ	Shear visc. $\log_{10} \eta$	Relaxed Newt. visc. $\log_{10} \eta$	τ
°C	Hz	GPa	$\log_{10} \text{ Pa s}$	K	Pa s	s	Pa s	Pa s	s
SAMPLE G4									
850	1	34.23	-14.00±0.48	2.747 ±0.055	10.46	0.847	9.95	10.53	0.990
	0.5						10.23		
	0.2						10.43		
	0.1						10.48		
	0.05						10.47		
	0.02						10.49		
0.01	10.52								
825	1	34.23	-14.00±0.48	2.747 ±0.055	11.02	3.055	9.75	10.90	2.320
	0.5						10.15		
	0.2						10.62		
	0.1						10.83		
	0.05						10.93		
	0.02						10.93		
0.01	10.95								
800	1	34.23	-14.00±0.48	2.747 ±0.055	11.60	11.692	9.50	11.67	13.663
	0.5						9.94		
	0.2						10.51		
	0.1						10.90		
	0.05						11.23		
	0.02						11.49		
	0.01						11.67		
	0.005						11.94		
	0.002						11.72		
	0.001						11.63		
775	1	34.23	-14.00±0.48	2.747 ±0.055	12.21	47.706	9.15	12.24	50.764
	0.5						9.57		
	0.2						10.13		
	0.1						10.61		
	0.05						11.07		
	0.02						11.58		
	0.01						11.83		
	0.005						12.11		
	0.002						12.24		
	0.001						12.23		
750	1	34.23	-14.00±0.48	2.747 ±0.055	12.85	208.505	8.75	12.80	184.312
	0.5						9.25		
	0.2						9.81		
	0.1						10.16		
	0.05						10.57		
	0.02						11.31		
	0.01						11.73		
	0.005						12.18		
	0.002						12.62		
	0.001						12.79		
725		34.23	-14.00±0.48	2.747 ±0.055	13.53	981.190	-	-	-
700		34.23	-14.00±0.48	2.747 ±0.055	14.23	4999.810	-	-	-
675		34.23	-14.00±0.48	2.747 ±0.055	14.98	27762.193	-	-	-
650		34.23	-14.00±0.48	2.747 ±0.055	15.76	169154.854	-	-	-
600		34.23	-14.00±0.48	2.747 ±0.055	17.47	8566363.46	-	-	-
550		34.23	-14.00±0.48	2.747 ±0.055	19.38	698904974	-	-	-

Appendix 3. Temperature T, frequency *f*, G_{∞} , viscosity, shear viscosity, relaxed Newtonian viscosity and relaxation times of the samples, determined by micropenetration and torsion measurements. Continuation...

			MICROPENETRATION				TORSION		
T	f	G_{∞}	A	B	$\log_{10} \eta$	τ	Shear visc. $\log_{10} \eta$	Relaxed Newt. visc. $\log_{10} \eta$	τ
°C	Hz	GPa	\log_{10} Pa s	K	Pa s	s	Pa s	Pa s	s
SAMPLE G5									
750	1	34.01	-15.32±0.57	2.627 ±0.058	10.36	0.669	8.97	10.18	0.445
	0.5						9.44		
	0.2						10.10		
	0.1						10.19		
	0.05						10.28		
725	1	34.01	-15.32±0.57	2.627 ±0.058	11.00	2.944	9.14	10.87	2.180
	0.5						9.59		
	0.2						10.12		
	0.1						10.43		
	0.05						10.64		
	0.02						10.73		
	0.01						10.91		
	0.005						10.90		
700	1	34.01	-15.32±0.57	2.627 ±0.058	11.68	13.970	8.87	11.54	10.195
	0.5						9.27		
	0.2						9.88		
	0.1						10.35		
	0.05						10.74		
	0.02						11.17		
	0.01						11.30		
	0.005						11.47		
	0.002						11.55		
	0.001						11.54		
	675						1		
0.5		9.16							
0.2		9.59							
0.1		10.09							
0.05		10.53							
0.02		11.07							
0.01		11.41							
0.005		11.52							
0.002		11.88							
0.001		12.25							
650		34.01	-15.32±0.57	2.627 ±0.058	13.14	405.235	-	-	-
625		34.01	-15.32±0.57	2.627 ±0.058	13.93	2512.110	-	-	-
600		34.01	-15.32±0.57	2.627 ±0.058	14.77	17288.228	-	-	-
550		34.01	-15.32±0.57	2.627 ±0.058	16.60	1163738.49	-	-	-
500		34.01	-15.32±0.57	2.627 ±0.058	18.66	135037734	-	-	-
SAMPLE G6									
700	1	33.47	-14.71±0.23	2.472 ±0.022	10.70	1.485	9.43	10.59	1.162
	0.5						9.83		
	0.2						10.26		
	0.1						10.45		
	0.05						10.48		
	0.02						10.53		
	0.01						10.58		
	0.005						10.62		
675	1	33.47	-14.71±0.23	2.472 ±0.022	11.37	6.950	9.08	11.26	5.437
	0.5						9.54		
	0.2						10.10		
	0.1						10.51		
	0.05						10.85		
	0.02						10.89		
	0.01						11.13		
	0.005						11.25		
	0.002						11.32		

Appendix 3. Temperature T , frequency f , G_{∞} , viscosity, shear viscosity, relaxed Newtonian viscosity and relaxation times of the samples. determined by micropenetration and torsion measurements. Continuation...

			MICROPENETRATION				TORSION		
T	f	G_{∞}	A	B	$\log_{10} \eta$	τ	Shear visc. $\log_{10} \eta$	Relaxed Newt. visc. $\log_{10} \eta$	τ
°C	Hz	GPa	$\log_{10} \text{ Pa s}$	K	Pa s	s	Pa s	Pa s	s
SAMPLE G6									
650	1	33.47	-14.71±0.23	2.472 ±0.022	12.07	35.353	8.69	11.90	23.732
	0.5						9.11		
	0.2						9.74		
	0.1						10.20		
	0.05						10.60		
	0.02						11.17		
	0.01						11.34		
	0.005						11.61		
	0.002						11.87		
	0.001						11.99		
625	1	33.47	-14.71±0.23	2.472 ±0.022	12.82	196.877	8.47	12.63	127.451
	0.5						8.94		
	0.2						9.55		
	0.1						9.97		
	0.05						10.40		
	0.02						11.00		
	0.01						11.45		
	0.005						11.83		
	0.002						12.22		
	0.001						12.67		
600		33.47	-14.71±0.23	2.472 ±0.022	13.61	1209.697	-	-	-
575		33.47	-14.71±0.23	2.472 ±0.022	14.44	8272.708	-	-	-
550		33.47	-14.71±0.23	2.472 ±0.022	15.33	63583.751	-	-	-
500		33.47	-14.71±0.23	2.472 ±0.022	17.27	5579716.25	-	-	-
450		33.47	-14.71±0.23	2.472 ±0.022	19.48	909193294	-	-	-

SAMPLE G7									
700	1	31.68	-16.75±0.40	2.512 ±0.037	9.07	0.037	8.95	9.36	0.072
	0.1						8.83		
	0.01						9.36		
670	1	31.68	-16.75±0.40	2.512 ±0.037	9.89	0.246	8.79	9.84	0.218
	0.1						9.33		
	0.01						9.75		
650	1	31.68	-16.75±0.40	2.512 ±0.037	10.47	0.929	9.18	10.38	0.757
	0.1						9.76		
	0.01						10.30		
630	1	31.68	-16.75±0.40	2.512 ±0.037	11.07	3.723	9.12	10.74	1.735
	0.1						10.03		
	0.01						10.68		
600	1	31.68	-16.75±0.40	2.512 ±0.037	12.03	33.640	8.18	11.97	29.461
	0.1						9.56		
	0.01						11.25		
	0.001						11.99		
550	1	31.68	-16.75±0.40	2.512 ±0.037	13.78	1883.505	7.30	13.71	1618.984
	0.1						8.90		
	0.01						11.95		
	0.001						13.71		
500		31.68	-16.75±0.40	2.512 ±0.037	15.75	177513.061	-	-	-

Appendix 3. Temperature T , frequency f , G_{∞} , viscosity, shear viscosity, relaxed Newtonian viscosity and relaxation times of the samples. determined by micropenetration and torsion measurements. Continuation...

			MICROPENETRATION				TORSION		
T	f	G_{∞}	A	B	$\log_{10} \eta$	τ	Shear visc. $\log_{10} \eta$	Relaxed Newt. visc. $\log_{10} \eta$	τ
°C	Hz	GPa	$\log_{10} \text{ Pa s}$	K	Pa s	s	Pa s	Pa s	s
SAMPLE G8									
820	1	32.45	-13.85±0.70	2.654 ±0.077	10.43	0.833	9.54	10.15	0.435
	0.5						9.87		
	0.2						10.15		
	0.1						10.24		
	0.05						10.12		
	0.02						10.31		
	0.01						10.31		
	0.005						10.33		
	0.002						10.04		
810	1	32.45	-13.85±0.70	2.654 ±0.077	10.66	1.396	9.42	10.40	0.774
	0.5						9.80		
	0.2						10.18		
	0.1						10.34		
	0.05						10.22		
	0.02						10.43		
	0.01						10.11		
	0.005						10.43		
	0.002								
800	1	32.45	-13.85±0.70	2.654 ±0.077	10.88	2.361	9.62	10.90	2.448
	0.5						10.02		
	0.2						10.50		
	0.1						10.75		
	0.05						10.89		
	0.02						10.96		
	0.01						10.92		
	0.005						10.97		
	0.002						10.85		
0.001	10.84								
780	1	32.45	-13.85±0.70	2.654 ±0.077	11.35	6.965	9.14	11.25	5.480
	0.5						9.59		
	0.2						10.13		
	0.1						10.56		
	0.05						10.87		
	0.02						11.13		
	0.01						11.22		
	0.005						11.25		
	0.002						11.25		
0.001	11.29								
760	1	32.45	-13.85±0.70	2.654 ±0.077	11.84	21.425	8.84	11.57	11.449
	0.5						9.28		
	0.2						10.29		
	0.1						10.32		
	0.05						10.73		
	0.02						11.19		
	0.01						11.45		
	0.005						11.49		
	0.002						11.60		
0.001	11.66								
740	1	32.45	-13.85±0.70	2.654 ±0.077	12.35	68.893	8.97	12.12.	40.623
	0.5						9.39		
	0.2						9.99		
	0.1						10.43		
	0.05						10.92		
	0.02						11.47		
	0.01						11.74		
	0.005						11.66		
	0.002						12.14		
0.001	12.11								
720	1	32.45	-13.85±0.70	2.654 ±0.077	12.88	232.198	9.07	13.27	573.810
	0.5						9.47		
	0.2						10.11		
	0.1						10.60		
	0.05						11.04		
	0.02						11.24		
	0.01						12.02		
	0.005						12.44		

Appendix 3. Temperature T , frequency f , G_{∞} , viscosity, shear viscosity, relaxed Newtonian viscosity and relaxation times of the samples. determined by micropenetration and torsion measurements. Continuation...

			MICROPENETRATION				TORSION		
T	f	G_{∞}	A	B	$\log_{10} \eta$	τ	Shear visc. $\log_{10} \eta$	Relaxed Newt. visc. $\log_{10} \eta$	τ
°C	Hz	GPa	$\log_{10} \text{ Pa s}$	K	Pa s	s	Pa s	Pa s	s
SAMPLE G8									
720	0.002	32.45	-13.85±0.70	2.654 ±0.077	12.88	232.198	12.98	13.27	573.810
	0.001						13.28		
700	1	32.45	-13.85±0.70	2.654 ±0.077	13.43	822.684	9.22	13.50	974.470
	0.5						9.48		
	0.2						9.96		
	0.1						10.61		
	0.05						10.99		
	0.02						11.03		
	0.01						12.07		
	0.005						12.46		
	0.002						13.07		
	0.001						13.49		
680	1	32.45	-13.85±0.70	2.654 ±0.077	14.00	3073.737	9.62	13.78	1856.814
	0.5						9.85		
	0.2						10.78		
	0.1						10.93		
	0.05						10.64		
	0.02						12.02		
	0.01						12.81		
	0.005						12.77		
	0.002						13.31		
	0.001						13.78		
660		32.45	-13.85±0.70	2.654 ±0.077	14.60	12151.838	-	-	-
640		32.45	-13.85±0.70	2.654 ±0.077	15.22	51023.674	-	-	-
620		32.45	-13.85±0.70	2.654 ±0.077	15.87	228461.612	-	-	-
600		32.45	-13.85±0.70	2.654 ±0.077	16.55	1095682.75	-	-	-
SAMPLE G9									
820	1	32.94	-16.40±1.19	3.054 ±0.132	11.53	10.396	10.02	11.38	7.282
	0.5						10.46		
	0.2						10.94		
	0.1						11.21		
	0.05						11.35		
	0.02						11.41		
	0.01						11.45		
	0.005						11.45		
	0.002						11.10		
	0.001						11.54		
810	1	32.94	-16.40±1.19	3.054 ±0.132	11.79	18.831	10.13	11.86	21.992
	0.5						10.57		
	0.2						11.10		
	0.1						11.44		
	0.05						11.67		
	0.02						11.80		
	0.01						11.32		
	0.005						11.86		
	0.002						11.87		
	0.001						11.86		
800	1	32.94	-16.40±1.19	3.054 ±0.132	12.06	34.489	10.01	12.11	39.107
	0.5						9.55		
	0.2						10.75		
	0.1						11.41		
	0.05						11.74		
	0.02						11.98		
	0.01						12.07		
	0.005						12.09		
	0.002						12.12		
	0.001						12.12		

Appendix 3. Temperature T , frequency f , G_{∞} , viscosity, shear viscosity, relaxed Newtonian viscosity and relaxation times of the samples. determined by micropenetration and torsion measurements. Continuation...

			MICROPENETRATION				TORSION		
T	f	G_{∞}	A	B	$\log_{10} \eta$	τ	Shear visc. $\log_{10} \eta$	Relaxed Newt. visc. $\log_{10} \eta$	τ
°C	Hz	GPa	$\log_{10} \text{ Pa s}$	K	Pa s	s	Pa s	Pa s	s
SAMPLE G9									
780	1	32.94	-16.40±1.19	3.054 ±0.132	12.60	119.746	9.80	12.55	107.710
	0.5						10.24		
	0.2						10.86		
	0.1						11.26		
	0.05						11.70		
	0.02						12.16		
	0.01						12.41		
	0.005						12.53		
	0.002						12.49		
	0.001						12.61		
760	1	32.94	-16.40±1.19	3.054 ±0.132	13.16	436.285	9.52	13.09	373.470
	0.5						10.02		
	0.2						10.57		
	0.1						11.00		
	0.05						11.47		
	0.02						12.05		
	0.01						12.45		
	0.005						12.47		
	0.002						13.02		
	0.001						13.12		
740	1	32.94	-16.40±1.19	3.054 ±0.132	13.74	1672.833	9.29	13.54	1052.582
	0.5						9.71		
	0.2						10.44		
	0.1						10.69		
	0.05						11.23		
	0.02						11.85		
	0.01						12.26		
	0.005						12.68		
	0.002						13.18		
	0.001						13.54		
720	1	32.94	-16.40±1.19	3.054 ±0.132	14.35	6770.904	9.85	14.12	4001.806
	0.5						10.26		
	0.2						10.65		
	0.1						11.12		
	0.05						11.77		
	0.02						12.20		
	0.01						12.61		
	0.005						13.15		
	0.002						13.72		
	0.001						14.12		
700	1	32.94	-16.40±1.19	3.054 ±0.132	14.98	29027.024	10.10	14.46	8754.997
	0.5						10.40		
	0.2						11.18		
	0.1						11.42		
	0.05						11.84		
	0.02						12.56		
	0.01						12.92		
	0.005						13.36		
	0.002						14.01		
	0.001						14.46		
680	1	32.94	-16.40±1.19	3.054 ±0.132	15.64	132279.22	10.92	14.87	22503.808
	0.5						10.46		
	0.2						11.82		
	0.1						11.68		
	0.05						12.21		
	0.02						12.72		
	0.01						13.39		
	0.005						13.59		
	0.002						14.35		
	0.001						14.87		
660		32.94	-16.40±1.19	3.054 ±0.132	16.33	643310.088	-	-	-
640		32.94	-16.40±1.19	3.054 ±0.132	17.04	3353084.93	-	-	-

Appendix 3. Temperature T , frequency f , G_{∞} , viscosity, shear viscosity, relaxed Newtonian viscosity and relaxation times of the samples. determined by micropenetration and torsion measurements. Continuation...

			MICROPENETRATION				TORSION		
T	f	G_{∞}	A	B	$\log_{10} \eta$	τ	Shear visc. $\log_{10} \eta$	Relaxed Newt. visc. $\log_{10} \eta$	τ
°C	Hz	GPa	$\log_{10} \text{ Pa s}$	K	Pa s	s	Pa s	Pa s	s
SAMPLE G9									
620		32.94	-16.40±1.19	3.054 ±0.132	17.79	18818555.7	-	-	-
600		32.94	-16.40±1.19	3.054 ±0.132	18.58	114301772	-	-	-

SAMPLE G10									
780	1	32.20	-14.20±0.47	2.629 ±0.050	10.76	1.782	9.42	10.35	0.695
	0.5						9.81		
	0.2						10.26		
	0.1						10.37		
	0.05						10.30		
	0.02						10.37		
	0.01						10.38		
	0.005						10.37		
	0.002						10.38		
760	1	32.20	-14.20±0.47	2.629 ±0.050	11.24	5.424	9.41	11.19	4.810
	0.5						9.84		
	0.2						10.35		
	0.1						10.74		
	0.05						11.00		
	0.02						11.22		
	0.01						11.12		
	0.005						11.31		
	0.002						11.06		
0.001	11.18								
740	1	32.20	-14.20±0.47	2.629 ±0.050	11.74	17.249	9.14	11.73	16.678
	0.5						9.58		
	0.2						10.16		
	0.1						10.62		
	0.05						11.01		
	0.02						11.38		
	0.01						11.65		
	0.005						11.73		
	0.002						11.73		
0.001	11.74								
720	1	32.20	-14.20±0.47	2.629 ±0.050	12.27	57.465	9.41	12.30	61.966
	0.5						9.86		
	0.2						10.44		
	0.1						10.88		
	0.05						11.34		
	0.02						11.89		
	0.01						12.27		
	0.005						12.35		
	0.002						12.26		
0.001	12.31								
700	1	32.20	-14.20±0.47	2.629 ±0.050	12.81	201.158	10.40	12.73	166.784
	0.5						10.97		
	0.2						11.28		
	0.1						11.95		
	0.05						12.05		
	0.02						12.56		
	0.01						12.71		
	0.005						12.75		
	0.002						12.73		
0.001	12.64								
680	1	32.20	-14.20±0.47	2.629 ±0.050	13.38	742.172	9.75	13.69	1521.086
	0.5						10.23		
	0.2						10.69		
	0.1						11.34		
	0.05						11.69		
	0.02						12.37		
	0.01						12.79		
	0.005						13.23		
	0.002						13.63		
0.001	13.81								

Appendix 3. Temperature T , frequency f , G_{∞} , viscosity, shear viscosity, relaxed Newtonian viscosity and relaxation times of the samples. determined by micropenetration and torsion measurements. Continuation...

			MICROPENETRATION				TORSION		
T	f	G_{∞}	A	B	$\log_{10} \eta$	τ	Shear visc. $\log_{10} \eta$	Relaxed Newt. visc. $\log_{10} \eta$	τ
°C	Hz	GPa	$\log_{10} \text{ Pa s}$	K	Pa s	s	Pa s	Pa s	s
SAMPLE G10									
660	1	32.20	-14.20±0.47	2.629 ±0.050	13.97	2895.878	9.96	14.15	4386.860
	0.5						10.77		
	0.2						11.21		
	0.1						11.81		
	0.05						12.51		
	0.02						12.71		
	0.01						13.46		
	0.005						13.89		
	0.002						14.14		
	0.001						14.20		
640	1	32.20	-14.20±0.47	2.629 ±0.050	14.59	11993.902	10.57	14.92	25831.746
	0.5						11.44		
	0.2						11.58		
	0.1						11.50		
	0.05						12.57		
	0.02						13.14		
	0.01						13.90		
	0.005						14.30		
	0.002						14.90		
	0.001						14.92		
620	1	32.20	-14.20±0.47	2.629 ±0.050	15.23	52940.246	10.51	15.36	71146.536
	0.5						10.86		
	0.2						11.54		
	0.1						12.27		
	0.05						12.16		
	0.02						13.17		
	0.01						13.29		
	0.005						14.12		
	0.002						14.58		
	0.001						15.36		
600		32.20	-14.20±0.47	2.629 ±0.050	15.91	250124.756	-	-	-
580		32.20	-14.20±0.47	2.629 ±0.050	16.61	1271015.61	-	-	-
560		32.20	-14.20±0.47	2.629 ±0.050	17.35	6983069.65	-	-	-
SAMPLE G11									
740	1	32.09	-12.24±0.70	2.300 ±0.072	10.46	0.910	9.58	10.20	0.494
	0.5						9.88		
	0.2						10.13		
	0.1						10.23		
	0.05						10.28		
720	1	32.09	-12.24±0.70	2.300 ±0.072	10.92	2.608	9.41	10.73	1.673
	0.5						9.80		
	0.2						10.22		
	0.1						10.47		
	0.05						10.60		
	0.02						10.70		
	0.01						10.73		
0.005	10.77								
700	1	32.09	-12.24±0.70	2.300 ±0.072	11.40	7.806	9.22	11.32	6.510
	0.5						9.64		
	0.2						10.19		
	0.1						10.54		
	0.05						10.84		
	0.02						11.11		
	0.01						11.23		
	0.005						11.27		
	0.002						11.32		
0.001	11.33								
680	1	32.09	-12.24±0.70	2.300 ±0.072	11.89	24.462	10.27	12.05	34.960
	0.5						10.72		
	0.2						11.30		
	0.1						11.39		

Appendix 3. Temperature T , frequency f , G_{∞} , viscosity, shear viscosity, relaxed Newtonian viscosity and relaxation times of the samples. determined by micropenetration and torsion measurements. Continuation...

			MICROPENETRATION				TORSION		
T	f	G_{∞}	A	B	$\log_{10} \eta$	τ	Shear visc. $\log_{10} \eta$	Relaxed Newt. visc. $\log_{10} \eta$	τ
°C	Hz	GPa	$\log_{10} \text{ Pa s}$	K	Pa s	s	Pa s	Pa s	s
SAMPLE G11									
680	0.05	32.09	-12.24±0.70	2.300 ±0.072	11.89	24.462	11.79	12.05	34.960
	0.02						11.74		
	0.01						11.81		
	0.005						11.90		
	0.002						12.09		
	0.001						12.10		
660	1	32.09	-12.24±0.70	2.300 ±0.072	12.41	80.513	10.07	12.66	142.421
	0.5						10.45		
	0.2						11.05		
	0.1						11.51		
	0.05						11.93		
	0.02						12.32		
	0.01						12.70		
	0.005						12.38		
	0.002						12.66		
	0.001						12.79		
640	1	32.09	-12.24±0.70	2.300 ±0.072	12.95	279.187	9.82	12.96	284.167
	0.5						10.11		
	0.2						10.66		
	0.1						11.19		
	0.05						11.54		
	0.02						12.17		
	0.01						12.61		
	0.005						12.98		
	0.002						12.96		
	0.001						12.94		
620	1	32.09	-12.24±0.70	2.300 ±0.072	13.52	1023.567	9.84	13.50	985.311
	0.5						10.28		
	0.2						11.30		
	0.1						11.48		
	0.05						11.83		
	0.02						12.57		
	0.01						12.94		
	0.005						13.37		
	0.002						13.43		
	0.001						13.63		
600	1	32.09	-12.24±0.70	2.300 ±0.072	14.11	3982.802	10.15	14.48	9409.647
	0.5						9.82		
	0.2						11.33		
	0.1						11.73		
	0.05						12.11		
	0.02						12.57		
	0.01						12.82		
	0.005						13.25		
	0.002						13.96		
	0.001						14.48		
580	1	32.09	-12.24±0.70	2.300 ±0.072	14.72	16517.018	10.03	15.04	34164.364
	0.5						10.46		
	0.2						10.92		
	0.1						11.52		
	0.05						11.98		
	0.02						12.29		
	0.01						12.84		
	0.005						13.53		
	0.002						14.19		
	0.001						15.04		
560		32.09	-12.24±0.70	2.300 ±0.072	15.37	73339.525	-	-	-
540		32.09	-12.24±0.70	2.300 ±0.072	16.05	350426.752	-	-	-

Appendix 3. Temperature T , frequency f , G_{∞} , viscosity, shear viscosity, relaxed Newtonian viscosity and relaxation times of the samples. determined by micropenetration and torsion measurements. Continuation...

			MICROPENETRATION				TORSION		
T	f	G_{∞}	A	B	$\log_{10} \eta$	τ	Shear visc. $\log_{10} \eta$	Relaxed Newt. visc. $\log_{10} \eta$	τ
°C	Hz	GPa	$\log_{10} \text{ Pa s}$	K	Pa s	s	Pa s	Pa s	s
SAMPLE G12									
660	1	31.42	-15.48±0.46	2.498 ±0.045	11.30	6.310	9.73	11.28	6.064
	0.5						10.13		
	0.2						10.59		
	0.1						10.87		
	0.05						11.07		
	0.02						11.21		
	0.01						11.29		
	0.005						11.29		
640	1	31.42	-15.48±0.46	2.498 ±0.045	11.88	24.354	9.87	12.25	56.598
	0.5						10.31		
	0.2						10.87		
	0.1						11.26		
	0.05						11.59		
	0.02						11.96		
	0.01						11.79		
	0.005						12.17		
	0.002						12.30		
	0.001						12.32		
620	1	31.42	-15.48±0.46	2.498 ±0.045	12.50	99.865	10.29	12.92	264.728
	0.5						10.70		
	0.2						11.33		
	0.1						11.71		
	0.05						12.15		
	0.02						12.48		
	0.01						12.81		
	0.005						12.86		
	0.002						12.95		
	0.001						13.09		
600	1	31.42	-15.48±0.46	2.498 ±0.045	13.14	436.850	10.50	13.35	712.524
	0.5						10.88		
	0.2						11.48		
	0.1						12.02		
	0.05						12.41		
	0.02						12.94		
	0.01						13.37		
	0.005						13.41		
	0.002						13.08		
	0.001						13.45		
580	1	31.42	-15.48±0.46	2.498 ±0.045	13.81	2047.879	10.70	13.83	2151.788
	0.5						11.07		
	0.2						11.54		
	0.1						12.02		
	0.05						12.34		
	0.02						13.02		
	0.01						13.41		
	0.005						13.86		
	0.002						13.82		
	0.001						13.81		
560	1	31.42	-15.48±0.46	2.498 ±0.045	14.51	10339.412	10.87	14.27	5926.515
	0.5						11.25		
	0.2						11.71		
	0.1						11.71		
	0.05						12.52		
	0.02						13.07		
	0.01						13.54		
	0.005						14.00		
	0.002						14.25		
	0.001						14.29		
540	1	31.42	-15.48±0.46	2.498 ±0.045	15.25	56530.742	10.51	14.74	17490.386
	0.5						10.24		
	0.2						10.93		
	0.1						11.78		
	0.05						12.47		
	0.02						12.90		
	0.01						13.47		
	0.005						13.47		

Appendix 3. Temperature T , frequency f , G_{∞} , viscosity, shear viscosity, relaxed Newtonian viscosity and relaxation times of the samples. determined by micropenetration and torsion measurements. Continuation...

			MICROPENETRATION				TORSION		
T	f	G_{∞}	A	B	$\log_{10} \eta$	τ	Shear visc. $\log_{10} \eta$	Relaxed Newt. visc. $\log_{10} \eta$	τ
°C	Hz	GPa	$\log_{10} \text{ Pa s}$	K	Pa s	s	Pa s	Pa s	s
SAMPLE G12									
540	0.005	31.42	-15.48±0.46	2.498 ±0.045	15.25	56530.742	13.62	14.74	17490.386
	0.002						14.17		
	0.001						14.73		
520		31.42	-15.48±0.46	2.498 ±0.045	16.02	336735.264	-	-	-
500		31.42	-15.48±0.46	2.498 ±0.045	16.84	2199865.92	-	-	-
480		31.42	-15.48±0.46	2.498 ±0.045	17.70	15878264.5	-	-	-
460		31.42	-15.48±0.46	2.498 ±0.045	18.60	127659557	-	-	-
440		31.42	-15.48±0.46	2.498 ±0.045	19.56	1153689848	-	-	-
420		31.42	-15.48±0.46	2.498 ±0.045	20.57	1183878995	-	-	-
400		31.42	-15.48±0.46	2.498 ±0.045	21.64	1.395E+11	-	-	-
380		31.42	-15.48±0.46	2.498 ±0.045	22.78	1.912E+12	-	-	-
360		31.42	-15.48±0.46	2.498 ±0.045	23.99	3.093E+13	-	-	-
340		31.42	-15.48±0.46	2.498 ±0.045	25.28	6.000E+14	-	-	-

SAMPLE G13									
660	1	30.89	-18.04±0.62	2.642 ±0.057	10.28	0.612	9.81	10.12	0.427
	0.5						9.95		
	0.2						10.11		
	0.1						10.15		
640	1	30.89	-18.04±0.62	2.642 ±0.057	10.90	2.554	9.68	10.61	1.319
	0.5						10.04		
	0.2						10.43		
	0.1						10.60		
	0.05						10.68		
	0.02						10.73		
	0.01						10.39		
	0.005						10.68		
	0.002						10.59		
620	1	30.89	-18.04±0.62	2.642 ±0.057	11.54	11.357	9.36	11.22	5.373
	0.5						9.79		
	0.2						10.27		
	0.1						10.68		
	0.05						10.94		
	0.02						11.16		
	0.01						11.22		
	0.005						11.24		
	0.002						11.21		
	0.001						11.21		
600	1	30.89	-18.04±0.62	2.642 ±0.057	12.22	54.080	9.32	12.15	45.733
	0.5						9.79		
	0.2						10.34		
	0.1						10.76		
	0.05						11.16		
	0.02						11.64		
	0.01						11.92		
	0.005						11.99		
	0.002						12.19		
	0.001						12.15		
580	1	30.89	-18.04±0.62	2.642 ±0.057	12.93	277.070	8.92	12.58	123.092
	0.5						9.37		
	0.2						9.99		
	0.1						10.39		
	0.05						10.82		
	0.02						11.38		

Appendix 3. Temperature T , frequency f , G_{∞} , viscosity, shear viscosity, relaxed Newtonian viscosity and relaxation times of the samples. determined by micropenetration and torsion measurements. Continuation...

			MICROPENETRATION				TORSION		
T	f	G_{∞}	A	B	$\log_{10} \eta$	τ	Shear visc. $\log_{10} \eta$	Relaxed Newt. visc. $\log_{10} \eta$	τ
°C	Hz	GPa	$\log_{10} \text{ Pa s}$	K	Pa s	s	Pa s	Pa s	s
SAMPLE G13									
580	0.01	30.89	-18.04±0.62	2.642 ±0.057	12.93	277.070	11.69	12.58	123.092
	0.005						11.88		
	0.002						12.29		
	0.001						12.58		
560	1	30.89	-18.04±0.62	2.642 ±0.057	13.68	1535.378	9.67	13.42	851.587
	0.5						10.12		
	0.2						10.65		
	0.1						11.04		
	0.05						11.36		
	0.02						12.11		
	0.01						12.45		
	0.005						12.90		
	0.002						13.06		
	0.001						13.40		
540		30.89	-18.04±0.62	2.642 ±0.057	14.46	9256.079	-	-	-
520		30.89	-18.04±0.62	2.642 ±0.057	15.28	61093.320	-	-	-
500		30.89	-18.04±0.62	2.642 ±0.057	16.14	444600.602	-	-	-
480		30.89	-18.04±0.62	2.642 ±0.057	17.04	3595301.17	-	-	-
460		30.89	-18.04±0.62	2.642 ±0.057	18.00	32586482.1	-	-	-
440		30.89	-18.04±0.62	2.642 ±0.057	19.01	334229901	-	-	-
420		30.89	-18.04±0.62	2.642 ±0.057	20.08	3921105590	-	-	-
400		30.89	-18.04±0.62	2.642 ±0.057	21.22	5.325E+10	-	-	-
380		30.89	-18.04±0.62	2.642 ±0.057	22.42	8.485E+11	-	-	-
360		30.89	-18.04±0.62	2.642 ±0.057	23.70	1.610E+13	-	-	-
340		30.89	-18.04±0.62	2.642 ±0.057	25.06	3.704E+14	-	-	-
320		30.89	-18.04±0.62	2.642 ±0.057	26.51	1.052E+16	-	-	-
SAMPLE G14									
600	1	29.96	-18.10±0.54	2.515 ±0.048	10.72	1.734	9.66	10.33	0.713
	0.5						10.13		
	0.2						10.26		
	0.1						10.42		
580	1	29.96	-18.10±0.54	2.515 ±0.048	11.39	8.217	9.65	11.11	4.299
	0.5						10.07		
	0.2						10.63		
	0.1						10.64		
	0.05						10.81		
	0.02						10.97		
	0.01						11.10		
	0.005						11.12		
	0.002						11.12		
560	1	29.96	-18.10±0.54	2.515 ±0.048	12.10	41.950	9.92	11.97	31.145
	0.5						10.35		
	0.2						10.95		
	0.1						11.38		
	0.05						11.79		
	0.02						12.00		
	0.01						11.97		
	0.005						12.07		
	0.002						11.92		
	0.001						11.98		

Appendix 3. Temperature T , frequency f , G_{∞} , viscosity, shear viscosity, relaxed Newtonian viscosity and relaxation times of the samples. determined by micropenetration and torsion measurements. Continuation...

			MICROPENETRATION				TORSION		
T	f	G_{∞}	A	B	$\log_{10} \eta$	τ	Shear visc. $\log_{10} \eta$	Relaxed Newt. visc. $\log_{10} \eta$	τ
°C	Hz	GPa	\log_{10} Pa s	K	Pa s	s	Pa s	Pa s	s
SAMPLE G14									
540	1	29.96	-18.10±0.54	2.515 ±0.048	12.84	232.052	9.31	12.52	110.506
	0.5						9.68		
	0.2						10.65		
	0.1						11.30		
	0.05						11.63		
	0.02						12.22		
	0.01						12.38		
	0.005						12.46		
	0.002						12.45		
	0.001						12.60		
520	1	29.96	-18.10±0.54	2.515 ±0.048	13.62	1399.289	9.65	13.65	1490.688
	0.5						9.87		
	0.2						10.71		
	0.1						11.19		
	0.05						11.49		
	0.02						12.02		
	0.01						12.41		
	0.005						12.90		
	0.002						13.24		
	0.001						13.64		
500		29.96	-18.10±0.54	2.515 ±0.048	14.44	9259.919	-	-	-
480		29.96	-18.10±0.54	2.515 ±0.048	15.31	67749.071	-	-	-
460		29.96	-18.10±0.54	2.515 ±0.048	16.22	552540.818	-	-	-
440		29.96	-18.10±0.54	2.515 ±0.048	17.18	5069431.36	-	-	-
420		29.96	-18.10±0.54	2.515 ±0.048	18.20	52858539.6	-	-	-

Appendix 4a. Parameters of the lines fitted to the real shear modulus data for NS2 melt (G0) and Fe-free melts (G1-G7). See also Fig. 68a.

FITS TO THE REAL SHEAR MODULUS DATA															
G0		G1		G2		G3		G4		G5		G6		G7	
$\Delta \log_{10}$ τ_M (s)	G_{real} (GPa)	$\Delta \log_{10}$ τ_M (s)	G_{real} (GPa)	$\Delta \log_{10}$ τ_M (s)	G_{real} (GPa)	$\Delta \log_{10}$ τ_M (s)	G_{real} (GPa)	$\Delta \log_{10}$ τ_M (s)	G_{real} (GPa)	$\Delta \log_{10}$ τ_M (s)	G_{real} (GPa)	$\Delta \log_{10}$ τ_M (s)	G_{real} (GPa)	$\Delta \log_{10}$ τ_M (s)	G_{real} (GPa)
-1.830	0.008	-2.000	0.000	-2.000	0.000	-2.000	0.001	-2.000	0.002	-2.000	0.207	-1.057	0.052	-2.632	0.020
-1.432	0.040	-1.500	0.000	-1.600	0.000	-1.600	0.003	-1.800	0.005	-1.800	0.299	-1.034	0.058	-2.632	0.020
-1.295	0.067	-1.000	0.001	-1.300	0.000	-1.300	0.011	-1.600	0.011	-1.600	0.372	-0.756	0.203	-2.135	0.148
-1.131	0.127	-0.500	0.009	-1.000	0.000	-1.034	0.029	-1.400	0.024	-1.400	0.436	-0.733	0.225	-1.632	0.561
-0.897	0.330	0.000	0.081	-0.605	0.002	-0.710	0.076	-1.274	0.038	-1.200	0.528	-0.677	0.288	-1.632	0.561
-0.861	0.383	0.385	0.357	-0.304	0.007	-0.636	0.094	-1.134	0.063	-1.057	0.650	-0.432	0.826	-1.314	1.147
-0.830	0.437	0.414	0.393	-0.088	0.019	-0.409	0.196	-0.973	0.111	-1.034	0.676	-0.376	1.039	-1.135	1.736
-0.748	0.616	0.686	0.849	0.029	0.032	-0.335	0.254	-0.833	0.183	-0.756	1.268	-0.358	1.120	-0.675	4.980
-0.596	1.155	0.715	0.913	0.095	0.044	-0.234	0.369	-0.717	0.281	-0.733	1.346	-0.345	1.180	-0.632	5.448
-0.464	1.960	0.775	1.057	0.213	0.075	-0.056	0.735	-0.575	0.482	-0.677	1.562	-0.075	3.188	-0.632	5.448
-0.432	2.214	1.016	1.888	0.330	0.128	-0.034	0.801	-0.523	0.589	-0.432	2.983	-0.057	3.389	-0.314	9.493
-0.350	3.009	1.076	2.178	0.396	0.174	-0.011	0.877	-0.435	0.829	-0.376	3.426	-0.044	3.536	-0.135	11.826
-0.295	3.670	1.084	2.223	0.490	0.267	0.067	1.190	-0.416	0.892	-0.358	3.584	-0.034	3.648	0.325	17.284
-0.163	5.698	1.088	2.243	0.514	0.298	0.245	2.310	-0.274	1.522	-0.345	3.698	0.244	8.044	0.686	20.849
-0.140	6.107	1.377	4.456	0.692	0.667	0.290	2.698	-0.222	1.830	-0.075	6.727	0.267	8.507	1.073	23.961
-0.131	6.268	1.385	4.542	0.697	0.682	0.364	3.438	-0.134	2.471	-0.057	6.979	0.323	9.709	1.325	25.537
-0.049	7.875	1.389	4.581	0.727	0.783	0.368	3.484	-0.018	3.538	-0.044	7.158	0.354	10.425	2.073	28.615
0.103	11.168	1.414	4.847	0.791	1.039	0.591	6.349	0.027	4.022	-0.034	7.292	0.406	11.640	2.325	29.357
0.139	11.956	1.686	8.308	0.912	1.764	0.629	6.909	0.117	5.097	0.244	11.439	0.568	15.568	3.047	30.616
0.161	12.456	1.715	8.729	0.993	2.493	0.643	7.111	0.167	5.756	0.267	11.788	0.624	16.844	3.073	30.637
0.170	12.647	1.775	9.621	1.029	2.893	0.665	7.439	0.176	5.875	0.323	12.645	0.642	17.249	4.047	31.021
0.404	17.445	1.787	9.808	1.092	3.744	0.766	8.994	0.283	7.470	0.354	13.130	0.655	17.526	4.073	31.030
0.537	19.802	1.826	10.416	1.095	3.783	0.766	8.994	0.418	9.761	0.406	13.923	0.707	18.571	5.047	31.273
0.559	20.172	2.016	13.525	1.213	5.945	0.930	11.629	0.425	9.884	0.568	16.363	0.943	22.077	6.047	31.702
0.568	20.311	2.076	14.503	1.330	8.861	0.944	11.850	0.477	10.824	0.624	17.161	0.956	22.214		
0.838	23.695	2.084	14.641	1.388	10.570	0.966	12.206	0.565	12.467	0.642	17.419	0.966	22.314		
0.860	23.903	2.088	14.702	1.391	10.664	0.989	12.577	0.584	12.825	0.655	17.599	1.105	23.511		
0.869	23.980	2.127	15.329	1.396	10.810	1.067	13.829	0.726	15.421	0.707	18.294	1.198	24.160		
0.942	24.566	2.385	19.110	1.490	13.829	1.067	13.829	0.778	16.323	0.943	21.119	1.244	24.459		
1.139	25.718	2.389	19.160	1.689	20.010	1.245	16.488	0.790	16.533	0.956	21.258	1.267	24.602		
1.161	25.820	2.414	19.491	1.692	20.094	1.290	17.106	0.816	16.981	0.966	21.361	1.354	25.145		
1.243	26.147	2.525	20.869	1.697	20.224	1.328	17.617	0.866	17.811	1.105	22.724	1.406	25.462		
1.537	26.942	2.602	21.753	1.727	21.041	1.348	17.876	0.982	19.644	1.198	23.524	1.499	26.028		
1.559	26.986	2.686	22.654	1.791	22.554	1.364	18.077	1.091	21.212	1.244	23.886	1.642	26.834		
1.641	27.125	2.715	22.948	1.993	25.952	1.591	20.736	1.117	21.565	1.267	24.056	1.655	26.901		
1.838	27.357	2.787	23.640	2.029	26.357	1.629	21.141	1.167	22.205	1.354	24.666	1.707	27.156		
1.860	27.375	2.826	23.998	2.087	26.921	1.643	21.282	1.176	22.312	1.406	24.997	1.897	27.920		

Appendix 4a. Parameters of the lines fitted to the real shear modulus data for NS2 melt (G0) and Fe-free melts (G1-G7) – continuation...

FITS TO THE REAL SHEAR MODULUS DATA															
G0		G1		G2		G3		G4		G5		G6		G7	
$\Delta \log_{10}$ τ_M (s)	G_{real} (GPa)	$\Delta \log_{10}$ τ_M (s)	G_{real} (GPa)	$\Delta \log_{10}$ τ_M (s)	G_{real} (GPa)	$\Delta \log_{10}$ τ_M (s)	G_{real} (GPa)	$\Delta \log_{10}$ τ_M (s)	G_{real} (GPa)	$\Delta \log_{10}$ τ_M (s)	G_{real} (GPa)	$\Delta \log_{10}$ τ_M (s)	G_{real} (GPa)	$\Delta \log_{10}$ τ_M (s)	G_{real} (GPa)
1.942	27.431	2.903	24.672	2.095	26.989	1.649	21.345	1.283	23.547	1.499	25.548	1.943	28.067		
2.088	27.495	3.084	26.103	2.119	27.187	1.665	21.505	1.418	24.867	1.642	26.290	1.956	28.106		
2.161	27.516	3.088	26.130	2.330	28.376	1.930	23.952	1.477	25.368	1.655	26.352	2.036	28.326		
2.243	27.532	3.127	26.408	2.388	28.595	1.944	24.068	1.489	25.467	1.707	26.591	2.105	28.494		
2.389	27.550	3.301	27.519	2.391	28.606	1.989	24.444	1.497	25.533	1.897	27.384	2.198	28.698		
2.559	27.561	3.385	27.993	2.396	28.623	2.047	24.920	1.565	26.052	1.943	27.559	2.337	28.974		
2.641	27.563	3.389	28.013	2.420	28.705	2.103	25.363	1.778	27.385	1.956	27.608	2.354	29.008		
2.787	27.566	3.419	28.169	2.689	29.582	2.245	26.429	1.790	27.450	2.036	27.894	2.406	29.108		
2.860	27.567	3.525	28.694	2.692	29.594	2.290	26.748	1.798	27.493	2.105	28.127	2.499	29.291		
2.942	27.568	3.602	29.037	2.727	29.727	2.328	27.014	1.816	27.585	2.198	28.417	2.655	29.615		
3.088	27.569	3.720	29.501	2.818	30.097	2.348	27.150	1.866	27.829	2.337	28.799	2.707	29.729		
3.243	27.569	3.787	29.734	2.887	30.414	2.404	27.522	2.091	28.753	2.354	28.843	2.735	29.792		
3.305	27.569	3.826	29.858	2.993	30.924	2.629	28.836	2.117	28.845	2.406	28.968	2.897	30.178		
3.389	27.569	3.903	30.084	3.029	31.098	2.643	28.903	2.176	29.039	2.499	29.179	3.036	30.516		
3.606	27.569	4.088	30.534	3.087	31.376	2.649	28.933	2.196	29.103	2.655	29.484	3.105	30.673		
3.641	27.569	4.117	30.594	3.119	31.523	2.802	29.544	2.242	29.241	2.707	29.572	3.198	30.862		
3.787	27.569	4.127	30.612	3.188	31.820	2.897	29.812	2.418	29.715	2.735	29.617	3.337	31.082		
3.942	27.569	4.280	30.872	3.388	32.454	2.930	29.889	2.477	29.854	2.897	29.849	3.406	31.163		
4.004	27.569	4.301	30.902	3.391	32.462	2.944	29.918	2.489	29.883	3.036	30.015	3.499	31.248		
4.088	27.569	4.419	31.052	3.420	32.526	3.047	30.100	2.497	29.902	3.105	30.089	3.735	31.373		
4.305	27.569	4.525	31.165	3.586	32.790	3.103	30.176	2.543	30.004	3.198	30.182	3.864	31.410		
4.389	27.569	4.581	31.217	3.689	32.884	3.198	30.279	2.790	30.499	3.337	30.308	3.897	31.418		
4.606	27.569	4.602	31.236	3.692	32.886	3.328	30.389	2.798	30.514	3.406	30.366	4.036	31.444		
4.787	27.569	4.720	31.335	3.818	32.957	3.348	30.404	2.816	30.547	3.499	30.442	4.165	31.464		
5.004	27.569	4.826	31.418	3.887	32.982	3.404	30.444	2.941	30.765	3.735	30.608	4.198	31.469		
5.088	27.569	4.903	31.477	4.087	33.023	3.596	30.573	3.026	30.906	3.864	30.684	4.337	31.488		
5.305	27.569	4.979	31.536	4.119	33.027	3.629	30.595	3.091	31.008	3.897	30.702	4.563	31.519		
5.606	27.569	5.117	31.647	4.188	33.033	3.649	30.608	3.117	31.048	4.036	30.775	4.735	31.544		
6.004	27.569	5.280	31.785	4.388	33.044	3.802	30.713	3.196	31.164	4.165	30.839	4.864	31.563		
6.305	27.569	5.301	31.804	4.420	33.045	3.897	30.781	3.242	31.227	4.198	30.855	5.036	31.591		
		5.419	31.915	4.586	33.048	4.047	30.896	3.327	31.341	4.337	30.927	5.165	31.613		
		5.581	32.072	4.727	33.049	4.103	30.940	3.489	31.533	4.563	31.069	5.563	31.696		
		5.602	32.093	4.818	33.050	4.198	31.014	3.497	31.542	4.735	31.212	5.864	31.792		
		5.720	32.203	4.887	33.050	4.348	31.134	3.543	31.590	4.864	31.344	5.929	31.819		
		5.979	32.422	5.028	33.050	4.404	31.178	3.725	31.759	5.036	31.538	6.165	31.939		
		6.117	32.520	5.119	33.051	4.596	31.331	3.790	31.809	5.165	31.675	6.230	31.979		
		6.150	32.540	5.188	33.051	4.613	31.345	3.798	31.815	5.563	31.952	6.563	32.233		

Appendix 4a. Parameters of the lines fitted to the real shear modulus data for NS2 melt (G0) and Fe-free melts (G1-G7) – continuation...

FITS TO THE REAL SHEAR MODULUS DATA															
G0		G1		G2		G3		G4		G5		G6		G7	
$\Delta \log_{10}$ τ_M (s)	G_{real} (GPa)	$\Delta \log_{10}$ τ_M (s)	G_{real} (GPa)	$\Delta \log_{10}$ τ_M (s)	G_{real} (GPa)	$\Delta \log_{10}$ τ_M (s)	G_{real} (GPa)	$\Delta \log_{10}$ τ_M (s)	G_{real} (GPa)	$\Delta \log_{10}$ τ_M (s)	G_{real} (GPa)	$\Delta \log_{10}$ τ_M (s)	G_{real} (GPa)	$\Delta \log_{10}$ τ_M (s)	G_{real} (GPa)
		6.280	32.612	5.426	33.051	4.802	31.492	3.941	31.912	5.864	32.114	6.628	32.289		
		6.419	32.676	5.452	33.051	4.897	31.565	4.026	31.969	5.929	32.159	6.864	32.504		
		6.451	32.689	5.586	33.051	4.914	31.578	4.196	32.093	6.165	32.380	6.929	32.567		
		6.581	32.743	5.727	33.051	5.103	31.722	4.242	32.131	6.230	32.459	7.230	32.899		
		6.849	32.889	5.753	33.051	5.198	31.794	4.327	32.211	6.563	32.960	7.628	33.430		
		6.979	32.997	5.887	33.052	5.312	31.881	4.497	32.389	6.628	33.056	7.929	33.720		
		7.150	33.197	6.028	33.052	5.596	32.099	4.543	32.439	6.864	33.324	8.230	33.878		
		7.280	33.402	6.151	33.053	5.613	32.112	4.725	32.619	6.929	33.372	8.628	34.029		
		7.451	33.735	6.426	33.059	5.897	32.325	4.731	32.624	7.230	33.495	8.929	34.162		
		7.849	34.462	6.452	33.061	5.914	32.337	4.941	32.769	7.628	33.546				
		8.150	34.741	6.727	33.085	6.312	32.617	5.026	32.813	7.929	33.580				
		8.247	34.794	6.753	33.089	6.526	32.755	5.032	32.816	8.230	33.643				
		8.451	34.872	7.028	33.177	6.613	32.809	5.242	32.907	8.628	33.822				
		8.548	34.899	7.151	33.257	6.827	32.940	5.327	32.943	8.929	34.063				
		8.849	34.973	7.415	33.555	6.914	32.998	5.430	32.989						
		8.946	34.997	7.426	33.570	7.225	33.282	5.725	33.128						
		9.150	35.043	7.452	33.608	7.312	33.395	5.731	33.130						
		9.247	35.060	7.716	33.994	7.526	33.820	6.026	33.267						
		9.548	35.091	7.727	34.008	7.613	34.000	6.032	33.270						
		9.946	35.102	7.753	34.042	7.827	34.100	6.430	33.482						
		10.247	35.104	8.114	34.396	7.952	34.200	6.643	33.626						
		10.548	35.104	8.151	34.422	8.102	34.300	6.731	33.693						
		10.615	35.104	8.415	34.576	8.253	34.400	6.944	33.869						
		10.916	35.104	8.452	34.594	8.403	34.400	7.032	33.943						
		10.946	35.104	8.716	34.696	8.554	34.400	7.342	34.140						
		11.247	35.104	9.114	34.761	8.704	34.400	7.430	34.174						
		11.314	35.104	9.415	34.773	8.855	34.400	7.643	34.223						
		11.615	35.104	9.625	34.775	9.006	34.400	7.731	34.235						
		11.916	35.104	9.716	34.776	9.156	34.400	7.944	34.256						
		12.314	35.104	9.926	34.776	9.307	34.400	8.342	34.302						
		12.615	35.104	10.114	34.777	9.457	34.400	8.643	34.360						
		12.916	35.104	10.324	34.777	9.608	34.400	8.944	34.451						
		13.311	35.104	10.415	34.777	9.800	34.400	9.342	34.764						
		13.314	35.104	10.625	34.777	10.000	34.400	9.643	35.162						
		13.612	35.104	10.926	34.777	10.200	34.400								
		13.615	35.104	11.324	34.777	10.400	34.400								
		14.010	35.104	11.625	34.777	10.600	34.400								

Appendix 4a. Parameters of the lines fitted to the real shear modulus data for NS2 melt (G0) and Fe-free melts (G1-G7) – continuation...

FITS TO THE REAL SHEAR MODULUS DATA															
G0		G1		G2		G3		G4		G5		G6		G7	
$\Delta \log_{10}$ τ_M (s)	G_{real} (GPa)	$\Delta \log_{10}$ τ_M (s)	G_{real} (GPa)	$\Delta \log_{10}$ τ_M (s)	G_{real} (GPa)	$\Delta \log_{10}$ τ_M (s)	G_{real} (GPa)	$\Delta \log_{10}$ τ_M (s)	G_{real} (GPa)	$\Delta \log_{10}$ τ_M (s)	G_{real} (GPa)	$\Delta \log_{10}$ τ_M (s)	G_{real} (GPa)	$\Delta \log_{10}$ τ_M (s)	G_{real} (GPa)
		14.311	35.104	11.926	34.777	10.800	34.400								
		14.612	35.104	12.133	34.777	11.000	34.400								
		15.010	35.104	12.324	34.777	11.200	34.400								
		15.311	35.104	12.434	34.777	11.400	34.400								
		15.612	35.104	12.625	34.777	11.600	34.400								
				12.832	34.777	11.800	34.400								
				13.133	34.777	12.000	34.400								
				13.434	34.777	12.200	34.400								
				13.832	34.777	12.400	34.400								
				14.133	34.777	12.600	34.400								
				14.434	34.777	12.800	34.400								
				14.832	34.777										
				15.133	34.777										

Appendix 4b. Parameters of the lines fitted to the imaginary shear modulus data for NS2 melt (G0) and Fe-free melts (G1-G7). See also Fig. 68b.

FITS TO THE IMAGINARY SHEAR MODULUS DATA															
G0		G1		G2		G3		G4		G5		G6		G7	
$\Delta \log_{10}$ τ_M (s)	G_{im} (GPa)	$\Delta \log_{10}$ τ_M (s)	G_{im} (GPa)	$\Delta \log_{10}$ τ_M (s)	G_{im} (GPa)	$\Delta \log_{10}$ τ_M (s)	G_{im} (GPa)	$\Delta \log_{10}$ τ_M (s)	G_{im} (GPa)	$\Delta \log_{10}$ τ_M (s)	G_{im} (GPa)	$\Delta \log_{10}$ τ_M (s)	G_{im} (GPa)	$\Delta \log_{10}$ τ_M (s)	G_{im} (GPa)
-1.830	0.222	-1.000	0.032	-0.605	0.042	-1.034	0.297	-1.274	0.247	-1.057	0.426	-1.331	0.372	-2.632	0.046
-1.432	0.553	-0.500	0.102	-0.304	0.085	-0.710	0.617	-1.134	0.316	-1.034	0.448	-1.059	0.694	-2.632	0.046
-1.295	0.757	0.385	0.777	-0.088	0.139	-0.636	0.727	-0.973	0.430	-0.756	0.828	-1.030	0.741	-2.135	0.145
-1.131	1.102	0.414	0.829	0.029	0.182	-0.409	1.192	-0.833	0.569	-0.733	0.871	-0.729	1.454	-1.632	0.461
-0.897	1.868	0.686	1.505	0.095	0.212	-0.335	1.396	-0.717	0.724	-0.677	0.986	-0.661	1.686	-1.632	0.461
-0.861	2.022	0.715	1.601	0.213	0.278	-0.234	1.726	-0.575	0.979	-0.432	1.703	-0.653	1.713	-1.314	0.957
-0.830	2.168	0.775	1.812	0.330	0.364	-0.056	2.469	-0.523	1.092	-0.376	1.925	-0.360	3.070	-1.135	1.440
-0.748	2.591	1.016	2.898	0.396	0.423	-0.034	2.575	-0.435	1.320	-0.358	2.005	-0.352	3.111	-0.675	4.026
-0.596	3.566	1.076	3.219	0.490	0.526	-0.011	2.691	-0.416	1.376	-0.345	2.063	-0.331	3.228	-0.632	4.409
-0.464	4.606	1.084	3.266	0.514	0.555	0.067	3.110	-0.274	1.864	-0.075	3.641	-0.059	4.676	-0.632	4.409
-0.432	4.873	1.088	3.288	0.692	0.836	0.245	4.178	-0.222	2.080	-0.057	3.777	-0.030	4.803	-0.314	8.054
-0.350	5.574	1.377	4.964	0.697	0.845	0.290	4.458	-0.134	2.503	-0.044	3.874	0.046	5.094	-0.135	10.206
-0.295	6.040	1.385	5.009	0.727	0.907	0.364	4.911	-0.018	3.168	-0.034	3.947	0.092	5.243	0.325	11.528
-0.163	6.994	1.389	5.029	0.791	1.049	0.368	4.937	0.027	3.461	0.244	6.231	0.271	5.595	0.686	8.459
-0.140	7.118	1.414	5.161	0.912	1.382	0.591	6.078	0.117	4.097	0.267	6.403	0.339	5.641	1.073	4.276
-0.131	7.162	1.686	6.163	0.993	1.662	0.629	6.229	0.167	4.473	0.323	6.788	0.347	5.643	1.325	2.495
-0.049	7.443	1.715	6.222	1.029	1.802	0.643	6.279	0.176	4.540	0.354	6.976	0.393	5.643	2.073	0.459
0.103	7.288	1.775	6.312	1.092	2.078	0.665	6.356	0.283	5.385	0.406	7.225	0.640	5.244	2.325	0.258
0.139	7.129	1.787	6.326	1.095	2.090	0.766	6.649	0.418	6.411	0.568	7.429	0.648	5.223	3.047	0.049
0.161	7.006	1.826	6.358	1.213	2.718	0.766	6.649	0.425	6.460	0.624	7.293	0.669	5.161	3.073	0.046
0.170	6.955	2.016	6.246	1.330	3.503	0.930	6.886	0.477	6.808	0.642	7.227	0.791	4.760	4.047	0.005
0.404	5.124	2.076	6.117	1.388	3.961	0.944	6.891	0.565	7.327	0.655	7.176	0.881	4.444	4.073	0.005
0.537	4.027	2.084	6.096	1.391	3.986	0.966	6.893	0.584	7.425	0.707	6.934	0.941	4.231	5.047	0.001
0.559	3.852	2.088	6.086	1.396	4.026	0.989	6.888	0.726	7.969	0.943	5.478	0.970	4.130	6.047	0.000
0.568	3.786	2.127	5.975	1.490	4.873	1.067	6.816	0.778	8.078	0.956	5.399	1.046	3.872		
0.838	2.142	2.385	5.022	1.689	6.955	1.067	6.816	0.790	8.096	0.966	5.341	1.092	3.716		
0.860	2.037	2.389	5.007	1.692	6.988	1.245	6.388	0.816	8.125	1.105	4.606	1.182	3.433		
0.869	1.998	2.414	4.908	1.697	7.040	1.290	6.236	0.866	8.136	1.198	4.219	1.339	2.989		
0.942	1.698	2.525	4.489	1.727	7.375	1.328	6.096	0.982	7.923	1.244	4.055	1.347	2.969		
1.139	1.089	2.602	4.215	1.791	8.042	1.348	6.021	1.091	7.405	1.267	3.979	1.393	2.850		
1.161	1.034	2.686	3.936	1.993	9.656	1.364	5.960	1.117	7.239	1.354	3.709	1.580	2.416		
1.243	0.858	2.715	3.847	2.029	9.819	1.591	4.956	1.167	6.887	1.406	3.556	1.640	2.285		
1.537	0.438	2.787	3.637	2.087	9.994	1.629	4.771	1.176	6.822	1.499	3.273	1.648	2.269		
1.559	0.415	2.826	3.529	2.095	10.009	1.643	4.705	1.283	5.945	1.642	2.789	1.716	2.127		
1.641	0.344	2.903	3.330	2.119	10.043	1.649	4.675	1.418	4.798	1.655	2.742	1.791	1.974		
1.838	0.219	3.084	2.901	2.330	9.651	1.665	4.599	1.477	4.330	1.707	2.553	1.881	1.798		
1.860	0.208	3.088	2.893	2.388	9.360	1.930	3.411	1.489	4.236	1.897	1.863	2.017	1.534		

Appendix 4b. Parameters of the lines fitted to the imaginary shear modulus data for NS2 melt (G0) and Fe-free melts (G1-G7) – continuation...

FITS TO THE IMAGINARY SHEAR MODULUS DATA															
G0		G1		G2		G3		G4		G5		G6		G7	
$\Delta \log_{10}$ τ_M (s)	G_{im} (GPa)	$\Delta \log_{10}$ τ_M (s)	G_{im} (GPa)	$\Delta \log_{10}$ τ_M (s)	G_{im} (GPa)	$\Delta \log_{10}$ τ_M (s)	G_{im} (GPa)	$\Delta \log_{10}$ τ_M (s)	G_{im} (GPa)	$\Delta \log_{10}$ τ_M (s)	G_{im} (GPa)	$\Delta \log_{10}$ τ_M (s)	G_{im} (GPa)	$\Delta \log_{10}$ τ_M (s)	G_{im} (GPa)
1.942	0.172	3.127	2.805	2.391	9.342	1.944	3.359	1.497	4.174	1.943	1.708	2.046	1.478		
2.088	0.123	3.301	2.424	2.396	9.315	1.989	3.195	1.565	3.683	1.956	1.666	2.092	1.387		
2.161	0.104	3.385	2.241	2.420	9.171	2.047	3.000	1.778	2.462	2.036	1.423	2.182	1.213		
2.243	0.086	3.389	2.233	2.689	6.926	2.103	2.831	1.790	2.406	2.105	1.235	2.347	0.912		
2.389	0.062	3.419	2.168	2.692	6.896	2.245	2.477	1.798	2.369	2.198	1.014	2.393	0.834		
2.559	0.042	3.525	1.929	2.727	6.544	2.290	2.383	1.816	2.289	2.337	0.751	2.415	0.800		
2.641	0.034	3.602	1.751	2.818	5.655	2.328	2.309	1.866	2.083	2.354	0.723	2.580	0.569		
2.787	0.025	3.720	1.474	2.887	4.992	2.348	2.272	2.091	1.361	2.406	0.645	2.602	0.543		
2.860	0.021	3.787	1.319	2.993	4.071	2.404	2.172	2.117	1.293	2.499	0.526	2.716	0.424		
2.942	0.017	3.826	1.233	3.029	3.787	2.629	1.799	2.176	1.154	2.655	0.373	2.791	0.358		
3.088	0.012	3.903	1.072	3.087	3.356	2.643	1.776	2.196	1.109	2.707	0.334	2.881	0.293		
3.243	0.009	4.088	0.749	3.119	3.137	2.649	1.766	2.242	1.013	2.735	0.314	2.903	0.279		
3.305	0.008	4.117	0.707	3.188	2.700	2.802	1.521	2.418	0.707	2.897	0.221	3.017	0.215		
3.389	0.006	4.127	0.694	3.388	1.736	2.897	1.373	2.477	0.626	3.036	0.166	3.092	0.181		
3.606	0.004	4.280	0.516	3.391	1.724	2.930	1.322	2.489	0.610	3.105	0.144	3.182	0.148		
3.641	0.003	4.301	0.496	3.420	1.615	2.944	1.301	2.497	0.600	3.198	0.119	3.301	0.113		
3.787	0.003	4.419	0.403	3.586	1.107	3.047	1.149	2.543	0.545	3.337	0.091	3.415	0.087		
3.942	0.002	4.525	0.344	3.689	0.876	3.103	1.069	2.790	0.325	3.406	0.080	3.580	0.059		
4.004	0.002	4.581	0.320	3.692	0.870	3.198	0.939	2.798	0.320	3.499	0.068	3.602	0.056		
4.088	0.001	4.602	0.313	3.818	0.652	3.328	0.780	2.816	0.308	3.735	0.047	3.716	0.043		
4.305	0.001	4.720	0.283	3.887	0.556	3.348	0.758	2.941	0.239	3.864	0.039	3.881	0.030		
4.389	0.001	4.826	0.273	4.087	0.352	3.404	0.700	3.027	0.202	3.897	0.037	3.903	0.028		
4.606	0.000	4.903	0.274	4.119	0.327	3.596	0.548	3.091	0.178	4.036	0.032	4.017	0.022		
4.787	0.000	4.979	0.282	4.188	0.279	3.629	0.529	3.117	0.169	4.165	0.028	4.301	0.012		
5.004	0.000	5.117	0.309	4.388	0.177	3.649	0.518	3.196	0.146	4.198	0.028	4.415	0.010		
5.088	0.000	5.280	0.350	4.420	0.165	3.802	0.458	3.242	0.134	4.337	0.025	4.545	0.008		
5.305	0.000	5.301	0.355	4.586	0.114	3.897	0.436	3.328	0.116	4.563	0.023	4.602	0.007		
5.606	0.000	5.419	0.377	4.727	0.084	4.047	0.418	3.489	0.089	4.735	0.023	4.716	0.006		
6.004	0.000	5.581	0.382	4.818	0.069	4.103	0.414	3.497	0.087	4.864	0.024	4.846	0.006		
6.305	0.000	5.602	0.380	4.887	0.060	4.198	0.412	3.543	0.082	5.036	0.026	4.903	0.006		
		5.720	0.363	5.028	0.047	4.348	0.415	3.725	0.063	5.165	0.029	5.244	0.007		
		5.979	0.315	5.119	0.041	4.404	0.416	3.790	0.058	5.563	0.046	5.301	0.008		
		6.117	0.306	5.188	0.037	4.596	0.419	3.798	0.058	5.864	0.076	5.545	0.012		
		6.150	0.306	5.426	0.033	4.613	0.419	3.941	0.049	5.929	0.086	5.602	0.014		
		6.280	0.319	5.452	0.033	4.802	0.409	4.027	0.045	6.165	0.137	5.846	0.024		
		6.419	0.353	5.586	0.035	4.897	0.396	4.196	0.039	6.230	0.156	6.244	0.058		
		6.451	0.364	5.727	0.041	4.914	0.393	4.242	0.037	6.563	0.316	6.545	0.116		

Appendix 4b. Parameters of the lines fitted to the imaginary shear modulus data for NS2 melt (G0) and Fe-free melts (G1-G7) – continuation...

FITS TO THE IMAGINARY SHEAR MODULUS DATA															
G0		G1		G2		G3		G4		G5		G6		G7	
$\Delta \log_{10}$ τ_M (s)	G_{im} (GPa)	$\Delta \log_{10}$ τ_M (s)	G_{im} (GPa)	$\Delta \log_{10}$ τ_M (s)	G_{im} (GPa)	$\Delta \log_{10}$ τ_M (s)	G_{im} (GPa)	$\Delta \log_{10}$ τ_M (s)	G_{im} (GPa)	$\Delta \log_{10}$ τ_M (s)	G_{im} (GPa)	$\Delta \log_{10}$ τ_M (s)	G_{im} (GPa)	$\Delta \log_{10}$ τ_M (s)	G_{im} (GPa)
		6.581	0.422	5.753	0.043	5.103	0.345	4.328	0.035	6.628	0.363	6.757	0.185		
		6.849	0.624	5.887	0.054	5.198	0.311	4.497	0.032	6.864	0.596	6.846	0.225		
		6.979	0.771	6.028	0.070	5.312	0.267	4.543	0.031	6.929	0.678	7.058	0.344		
		7.150	1.002	6.151	0.091	5.596	0.173	4.725	0.028	7.230	1.129	7.244	0.467		
		7.280	1.172	6.426	0.166	5.613	0.169	4.731	0.028	7.628	1.368	7.456	0.583		
		7.451	1.305	6.452	0.176	5.897	0.127	4.941	0.027	7.929	1.043	7.545	0.610		
		7.849	0.973	6.727	0.325	5.914	0.126	5.027	0.027	8.230	0.649	7.757	0.610		
		8.150	0.556	6.753	0.344	6.312	0.157	5.032	0.027	8.628	0.292	8.058	0.499		
		8.247	0.452	7.028	0.608	6.526	0.218	5.242	0.028	8.929	0.153	8.456	0.268		
		8.451	0.288	7.151	0.761	6.613	0.254	5.328	0.029			8.757	0.142		
		8.548	0.232	7.415	1.083	6.827	0.360	5.430	0.030			9.058	0.072		
		8.849	0.117	7.426	1.094	6.914	0.408	5.725	0.039			9.456	0.029		
		8.946	0.093	7.452	1.118	7.225	0.570	5.731	0.039			9.757	0.015		
		9.150	0.058	7.716	1.236	7.312	0.604	6.027	0.059						
		9.247	0.047	7.727	1.236	7.526	0.633	6.032	0.060						
		9.548	0.023	7.753	1.235	7.613	0.617	6.430	0.123						
		9.946	0.009	8.114	1.008	7.827	0.527	6.643	0.189						
		10.247	0.005	8.151	0.965	8.225	0.303	6.731	0.226						
		10.548	0.002	8.415	0.638	8.526	0.168	6.944	0.344						
		10.615	0.002	8.452	0.595	8.671	0.122	7.032	0.405						
		10.916	0.001	8.716	0.344	8.827	0.086	7.342	0.614						
		10.946	0.001	9.114	0.141	8.972	0.062	7.430	0.646						
		11.247	0.001	9.415	0.071	9.225	0.035	7.643	0.622						
		11.314	0.000	9.625	0.044	9.370	0.025	7.731	0.574						
		11.615	0.000	9.716	0.035	9.526	0.018	7.944	0.422						
		11.916	0.000	9.926	0.022	9.671	0.013	8.342	0.194						
		12.314	0.000	10.114	0.014	9.972	0.006	8.643	0.104						
		12.615	0.000	10.324	0.009	10.370	0.003	8.944	0.057						
		12.916	0.000	10.415	0.007	10.671	0.001	9.342	0.025						
		13.311	0.000	10.625	0.004	10.972	0.001	9.643	0.013						
		13.314	0.000	10.926	0.002	11.370	0.000								
		13.612	0.000	11.324	0.001	11.671	0.000								
		13.615	0.000	11.625	0.000										
		14.010	0.000	11.926	0.000										
		14.311	0.000	12.133	0.000										
		14.612	0.000	12.324	0.000										
		15.010	0.000	12.434	0.000										

Appendix 4b. Parameters of the lines fitted to the imaginary shear modulus data for NS2 melt (G0) and Fe-free melts (G1-G7) – continuation...

FITS TO THE IMAGINARY SHEAR MODULUS DATA															
G0		G1		G2		G3		G4		G5		G6		G7	
$\Delta \log_{10}$ τ_M (s)	G_{im} (GPa)	$\Delta \log_{10}$ τ_M (s)	G_{im} (GPa)	$\Delta \log_{10}$ τ_M (s)	G_{im} (GPa)	$\Delta \log_{10}$ τ_M (s)	G_{im} (GPa)	$\Delta \log_{10}$ τ_M (s)	G_{im} (GPa)	$\Delta \log_{10}$ τ_M (s)	G_{im} (GPa)	$\Delta \log_{10}$ τ_M (s)	G_{im} (GPa)	$\Delta \log_{10}$ τ_M (s)	G_{im} (GPa)
		15.311	0.000	12.625	0.000										
		15.612	0.000	12.832	0.000										
		16.010	0.000	13.133	0.000										
		16.311	0.000	13.434	0.000										
		16.408	0.000	13.832	0.000										
		16.709	0.000	14.133	0.000										
		17.107	0.000	14.434	0.000										
		17.408	0.000	14.832	0.000										
		17.709	0.000	15.133	0.000										
		18.107	0.000												
		18.408	0.000												
		18.709	0.000												
		19.107	0.000												
		19.408	0.000												
		20.002	0.000												
		20.303	0.000												
		20.701	0.000												
		21.002	0.000												
		21.303	0.000												
		21.701	0.000												
		22.002	0.000												
		22.303	0.000												
		22.701	0.000												
		23.002	0.000												
		24.223	0.000												
		24.524	0.000												
		24.922	0.000												
		25.223	0.000												
		25.524	0.000												
		25.922	0.000												
		26.223	0.000												
		26.524	0.000												
		26.922	0.000												
		27.223	0.000												

Appendix 4c. Parameters of the lines fitted to the real shear modulus data for Fe-bearing melts (G8-G14). See also Fig. 69a.

FITS TO THE REAL SHEAR MODULUS DATA													
G8		G9		G10		G11		G12		G13		G14	
$\Delta \log_{10}$ τ_M (s)	G_{real} (GPa)	$\Delta \log_{10}$ τ_M (s)	G_{real} (GPa)	$\Delta \log_{10}$ τ_M (s)	G_{real} (GPa)	$\Delta \log_{10}$ τ_M (s)	G_{real} (GPa)	$\Delta \log_{10}$ τ_M (s)	G_{real} (GPa)	$\Delta \log_{10}$ τ_M (s)	G_{real} (GPa)	$\Delta \log_{10}$ τ_M (s)	G_{real} (GPa)
-2.000	0.006	-2.000	0.003	-2.000	0.001	-2.000	0.000	-2.000	0.068	-2.000	0.004	-2.000	0.002
-1.600	0.013	-1.600	0.007	-1.600	0.002	-1.600	0.001	-1.500	0.185	-1.750	0.007	-1.600	0.007
-1.300	0.018	-1.300	0.011	-1.289	0.004	-1.300	0.004	-1.100	0.322	-1.494	0.013	-1.300	0.022
-1.000	0.024	-1.185	0.012	-1.093	0.008	-1.064	0.011	-0.815	0.467	-1.147	0.037	-0.986	0.085
-0.796	0.029	-0.927	0.017	-0.891	0.018	-0.851	0.030	-0.703	0.543	-1.096	0.045	-0.588	0.487
-0.595	0.034	-0.884	0.018	-0.791	0.028	-0.763	0.045	-0.514	0.717	-0.846	0.110	-0.579	0.506
-0.398	0.040	-0.664	0.026	-0.590	0.066	-0.557	0.115	-0.402	0.863	-0.795	0.133	-0.287	1.660
-0.294	0.045	-0.626	0.029	-0.575	0.071	-0.550	0.119	-0.202	1.270	-0.494	0.381	-0.278	1.717
-0.149	0.055	-0.486	0.041	-0.394	0.158	-0.365	0.276	-0.116	1.543	-0.469	0.413	0.014	4.360
-0.097	0.060	-0.363	0.059	-0.289	0.252	-0.317	0.342	-0.101	1.601	-0.448	0.443	0.037	4.630
-0.073	0.063	-0.228	0.094	-0.274	0.270	-0.256	0.449	0.099	2.685	-0.415	0.492	0.120	5.634
0.104	0.093	-0.185	0.110	-0.093	0.600	-0.249	0.465	0.185	3.405	-0.168	1.076	0.164	6.193
0.152	0.106	-0.124	0.140	-0.036	0.764	-0.064	1.048	0.297	4.622	-0.147	1.151	0.338	8.559
0.204	0.123	0.035	0.263	0.109	1.400	-0.029	1.217	0.439	6.559	-0.114	1.277	0.412	9.608
0.228	0.132	0.073	0.307	0.124	1.487	-0.016	1.283	0.486	7.274	-0.096	1.353	0.421	9.739
0.405	0.239	0.116	0.366	0.209	2.067	0.142	2.447	0.497	7.439	-0.009	1.785	0.465	10.373
0.453	0.285	0.177	0.470	0.265	2.544	0.149	2.520	0.598	8.996	0.154	2.999	0.713	13.849
0.470	0.303	0.336	0.889	0.410	4.144	0.237	3.505	0.740	11.011	0.205	3.507	0.722	13.968
0.602	0.500	0.374	1.033	0.425	4.338	0.272	3.970	0.798	11.751	0.230	3.780	0.736	14.155
0.626	0.547	0.438	1.321	0.525	5.753	0.285	4.144	0.884	12.758	0.241	3.901	0.863	15.724
0.706	0.743	0.514	1.757	0.606	7.050	0.443	6.766	0.899	12.929	0.284	4.427	0.944	16.665
0.771	0.948	0.575	2.196	0.663	8.000	0.450	6.906	1.099	14.988	0.506	7.756	1.014	17.433
0.851	1.270	0.637	2.725	0.711	8.853	0.523	8.314	1.109	15.099	0.531	8.163	1.037	17.681
0.903	1.532	0.739	3.827	0.726	9.123	0.635	10.546	1.137	15.385	0.542	8.337	1.120	18.523
0.927	1.664	0.772	4.246	0.826	10.981	0.670	11.241	1.185	15.879	0.552	8.511	1.164	18.949
1.036	2.399	0.815	4.836	0.907	12.556	0.683	11.484	1.297	17.122	0.585	9.044	1.245	19.698
1.104	2.986	0.876	5.759	0.964	13.641	0.744	12.665	1.411	18.482	0.832	12.667	1.412	21.098
1.152	3.459	1.022	8.200	1.109	16.309	0.751	12.807	1.439	18.829	0.853	12.934	1.421	21.169
1.169	3.642	1.035	8.430	1.110	16.323	0.824	14.157	1.486	19.416	0.904	13.551	1.465	21.508
1.204	4.045	1.073	9.097	1.124	16.562	0.936	16.099	1.497	19.549	0.940	13.963	1.643	22.760
1.228	4.331	1.116	9.838	1.209	17.885	0.971	16.673	1.598	20.767	0.984	14.465	1.713	23.190
1.337	5.833	1.137	10.190	1.224	18.102	0.984	16.872	1.740	22.231	1.154	16.300	1.722	23.244
1.405	6.922	1.177	10.861	1.265	18.655	1.100	18.626	1.798	22.726	1.205	16.853	1.765	23.488
1.453	7.729	1.323	13.053	1.410	20.262	1.142	19.201	1.808	22.812	1.230	17.127	1.863	24.005
1.470	8.028	1.336	13.235	1.411	20.270	1.149	19.301	1.813	22.844	1.241	17.244	1.944	24.394
1.602	10.384	1.374	13.745	1.425	20.401	1.222	20.231	1.884	23.347	1.285	17.748	2.066	24.921
1.625	10.791	1.438	14.549	1.525	21.236	1.237	20.413	2.099	24.461	1.531	20.645	2.120	25.137

Appendix 4c. Parameters of the lines fitted to the real shear modulus data for Fe-bearing melts (G8-G14) – continuation...

FITS TO THE REAL SHEAR MODULUS DATA													
G8		G9		G10		G11		G12		G13		G14	
$\Delta \log_{10}$ τ_M (s)	G_{real} (GPa)	$\Delta \log_{10}$ τ_M (s)	G_{real} (GPa)	$\Delta \log_{10}$ τ_M (s)	G_{real} (GPa)	$\Delta \log_{10}$ τ_M (s)	G_{real} (GPa)	$\Delta \log_{10}$ τ_M (s)	G_{real} (GPa)	$\Delta \log_{10}$ τ_M (s)	G_{real} (GPa)	$\Delta \log_{10}$ τ_M (s)	G_{real} (GPa)
1.626	10.804	1.514	15.442	1.606	21.847	1.272	20.822	2.109	24.508	1.542	20.767	2.164	25.305
1.706	12.198	1.575	16.123	1.663	22.255	1.401	22.182	2.114	24.525	1.552	20.888	2.245	25.600
1.735	12.676	1.629	16.694	1.720	22.679	1.443	22.577	2.137	24.625	1.683	22.264	2.421	26.182
1.771	13.276	1.637	16.779	1.726	22.721	1.450	22.647	2.185	24.818	1.765	22.973	2.464	26.313
1.851	14.532	1.721	17.651	1.809	23.357	1.523	23.291	2.411	25.749	1.832	23.470	2.465	26.316
1.903	15.319	1.739	17.840	1.826	23.492	1.635	24.183	2.439	25.868	1.853	23.609	2.629	26.769
1.926	15.652	1.772	18.181	1.907	24.166	1.670	24.440	2.497	26.118	1.940	24.099	2.643	26.804
1.927	15.663	1.815	18.625	1.964	24.644	1.704	24.678	2.512	26.183	1.984	24.312	2.765	27.072
2.036	17.166	1.876	19.261	2.021	25.139	1.744	24.950	2.550	26.348	2.066	24.644	2.863	27.248
2.104	18.053	1.930	19.815	2.110	25.876	1.799	25.310	2.740	27.085	2.230	25.188	2.930	27.351
2.152	18.645	2.022	20.758	2.124	25.990	1.824	25.468	2.798	27.280	2.241	25.220	2.944	27.370
2.169	18.853	2.035	20.891	2.224	26.736	1.936	26.134	2.808	27.314	2.285	25.354	3.066	27.521
2.228	19.551	2.073	21.272	2.265	27.011	1.971	26.331	2.813	27.328	2.464	25.880	3.164	27.620
2.240	19.693	2.137	21.888	2.358	27.566	2.005	26.516	2.851	27.446	2.531	26.076	3.245	27.692
2.324	20.633	2.177	22.262	2.411	27.835	2.100	27.017	3.109	28.077	2.542	26.106	3.328	27.758
2.337	20.769	2.261	22.987	2.419	27.876	2.142	27.225	3.114	28.085	2.584	26.223	3.464	27.860
2.405	21.497	2.323	23.481	2.425	27.902	2.222	27.609	3.137	28.132	2.683	26.480	3.541	27.919
2.470	22.156	2.328	23.520	2.525	28.320	2.272	27.837	3.249	28.334	2.765	26.667	3.629	27.991
2.541	22.838	2.336	23.582	2.659	28.749	2.336	28.115	3.325	28.458	2.885	26.903	3.643	28.003
2.625	23.569	2.438	24.314	2.663	28.758	2.401	28.386	3.411	28.586	2.940	26.995	3.765	28.116
2.626	23.575	2.562	25.094	2.720	28.901	2.403	28.392	3.439	28.626	2.984	27.066	3.842	28.195
2.735	24.388	2.575	25.171	2.809	29.084	2.443	28.551	3.512	28.727	3.066	27.187	3.930	28.292
2.771	24.627	2.629	25.468	2.826	29.114	2.523	28.851	3.550	28.777	3.241	27.428	3.944	28.308
2.883	25.263	2.721	25.934	2.964	29.319	2.637	29.222	3.627	28.871	3.283	27.487	4.066	28.443
2.926	25.479	2.739	26.021	3.021	29.385	2.670	29.316	3.808	29.061	3.285	27.490	4.328	28.674
2.927	25.482	2.876	26.624	3.025	29.389	2.704	29.404	3.813	29.064	3.446	27.719	4.464	28.746
2.939	25.541	2.920	26.799	3.057	29.422	2.799	29.618	3.851	29.099	3.464	27.745	4.503	28.762
3.036	25.976	2.930	26.839	3.110	29.470	2.824	29.665	4.024	29.237	3.584	27.923	4.541	28.775
3.169	26.558	2.960	26.956	3.224	29.553	2.971	29.876	4.109	29.296	3.683	28.068	4.629	28.800
3.184	26.625	3.022	27.188	3.326	29.608	2.999	29.905	4.114	29.298	3.747	28.158	4.765	28.827
3.240	26.888	3.137	27.596	3.358	29.622	3.005	29.910	4.141	29.316	3.765	28.183	4.804	28.833
3.324	27.305	3.221	27.877	3.411	29.643	3.035	29.938	4.249	29.385	3.885	28.346	4.842	28.838
3.337	27.369	3.261	28.008	3.419	29.646	3.100	29.988	4.325	29.430	3.984	28.473	4.930	28.851
3.470	28.093	3.323	28.204	3.525	29.682	3.222	30.053	4.442	29.498	4.066	28.571	5.202	28.895
3.541	28.484	3.328	28.220	3.659	29.722	3.300	30.082	4.512	29.537	4.145	28.659	5.240	28.904
3.554	28.553	3.438	28.559	3.720	29.742	3.336	30.093	4.550	29.558	4.283	28.795	5.328	28.928
3.582	28.698	3.562	28.916	3.723	29.743	3.401	30.111	4.627	29.598	4.354	28.855	5.503	28.990

Appendix 4c. Parameters of the lines fitted to the real shear modulus data for Fe-bearing melts (G8-G14) – continuation...

FITS TO THE REAL SHEAR MODULUS DATA													
G8		G9		G10		G11		G12		G13		G14	
$\Delta \log_{10}$ τ_M (s)	G_{real} (GPa)	$\Delta \log_{10}$ τ_M (s)	G_{real} (GPa)	$\Delta \log_{10}$ τ_M (s)	G_{real} (GPa)	$\Delta \log_{10}$ τ_M (s)	G_{real} (GPa)	$\Delta \log_{10}$ τ_M (s)	G_{real} (GPa)	$\Delta \log_{10}$ τ_M (s)	G_{real} (GPa)	$\Delta \log_{10}$ τ_M (s)	G_{real} (GPa)
3.625	28.919	3.607	29.035	3.724	29.743	3.403	30.111	4.813	29.686	4.446	28.925	5.521	28.998
3.735	29.412	3.619	29.067	3.809	29.776	3.523	30.138	4.840	29.697	4.464	28.938	5.541	29.006
3.855	29.830	3.629	29.093	4.021	29.908	3.637	30.163	4.851	29.702	4.584	29.014	5.629	29.048
3.883	29.906	3.721	29.314	4.024	29.910	3.695	30.177	4.999	29.760	4.655	29.053	5.804	29.147
3.926	30.014	3.908	29.685	4.025	29.911	3.698	30.178	5.024	29.769	4.747	29.097	5.822	29.158
3.939	30.043	3.920	29.705	4.057	29.941	3.704	30.179	5.141	29.807	4.765	29.105	5.842	29.170
4.036	30.224	3.930	29.723	4.110	29.998	3.799	30.208	5.249	29.836	4.885	29.153	6.202	29.394
4.184	30.405	3.960	29.772	4.326	30.342	3.996	30.309	5.300	29.849	5.053	29.220	6.220	29.404
4.240	30.453	4.022	29.868	4.358	30.408	3.999	30.311	5.325	29.854	5.145	29.262	6.240	29.413
4.253	30.463	4.221	30.140	4.419	30.543	4.005	30.315	5.442	29.878	5.283	29.342	6.503	29.500
4.257	30.466	4.261	30.190	4.422	30.548	4.035	30.339	5.550	29.897	5.311	29.360	6.521	29.504
4.324	30.512	4.306	30.245	4.454	30.622	4.100	30.398	5.627	29.910	5.354	29.391	6.541	29.508
4.541	30.623	4.324	30.267	4.659	31.088	4.300	30.671	5.698	29.921	5.446	29.462	6.804	29.540
4.554	30.629	4.328	30.272	4.720	31.207	4.336	30.735	5.840	29.942	5.584	29.576	6.822	29.542
4.558	30.631	4.562	30.551	4.723	31.211	4.394	30.846	5.904	29.952	5.612	29.599	7.202	29.559
4.582	30.642	4.607	30.602	4.724	31.213	4.403	30.863	5.999	29.966	5.655	29.634	7.220	29.560
4.625	30.662	4.619	30.616	4.755	31.268	4.637	31.344	6.024	29.970	5.747	29.704	7.503	29.568
4.855	30.778	4.625	30.623	5.024	31.584	4.695	31.451	6.141	29.986	6.010	29.871	7.521	29.569
4.883	30.794	4.629	30.628	5.025	31.585	4.698	31.456	6.205	29.994	6.053	29.894	7.822	29.578
4.939	30.828	4.908	30.927	5.057	31.607	4.704	31.465	6.300	30.004	6.145	29.945	8.220	29.592
4.956	30.839	4.920	30.939	5.153	31.658	4.996	31.813	6.325	30.007	6.311	30.038	8.521	29.607
4.993	30.863	4.960	30.979	5.221	31.684	4.999	31.815	6.442	30.017	6.322	30.044		
5.184	30.997	5.023	31.039	5.326	31.712	5.035	31.839	6.603	30.032	6.354	30.062		
5.240	31.041	5.073	31.084	5.358	31.719	5.300	31.943	6.698	30.042	6.446	30.117		
5.253	31.051	5.221	31.201	5.422	31.730	5.336	31.950	6.840	30.060	6.612	30.217		
5.257	31.054	5.261	31.229	5.454	31.734	5.394	31.960	6.860	30.063	6.623	30.223		
5.294	31.084	5.306	31.257	5.522	31.742	5.695	31.990	6.904	30.069	6.655	30.242		
5.554	31.314	5.324	31.268	5.723	31.757	5.698	31.990	6.999	30.086	7.010	30.424		
5.558	31.318	5.374	31.296	5.724	31.757	5.996	32.010	7.141	30.114	7.021	30.429		
5.582	31.340	5.607	31.401	5.755	31.759	5.999	32.010	7.161	30.119	7.053	30.443		
5.692	31.447	5.619	31.405	5.920	31.765	6.394	32.078	7.205	30.129	7.311	30.548		
5.765	31.520	5.625	31.408	6.024	31.769	6.695	32.094	7.300	30.152	7.322	30.553		
5.855	31.611	5.772	31.462	6.025	31.769			7.559	30.227	7.354	30.564		
5.883	31.639	5.856	31.493	6.153	31.772			7.603	30.240	7.392	30.578		
5.956	31.712	5.908	31.512	6.221	31.774			7.698	30.269	7.612	30.651		
5.993	31.748	5.920	31.517	6.422	31.778			7.860	30.317	7.623	30.654		
6.066	31.816	6.023	31.555	6.454	31.779			7.871	30.320	7.693	30.673		

Appendix 4c. Parameters of the lines fitted to the real shear modulus data for Fe-bearing melts (G8-G14) – continuation...

FITS TO THE REAL SHEAR MODULUS DATA													
G8		G9		G10		G11		G12		G13		G14	
$\Delta \log_{10}$ τ_M (s)	G_{real} (GPa)	$\Delta \log_{10}$ τ_M (s)	G_{real} (GPa)	$\Delta \log_{10}$ τ_M (s)	G_{real} (GPa)	$\Delta \log_{10}$ τ_M (s)	G_{real} (GPa)	$\Delta \log_{10}$ τ_M (s)	G_{real} (GPa)	$\Delta \log_{10}$ τ_M (s)	G_{real} (GPa)	$\Delta \log_{10}$ τ_M (s)	G_{real} (GPa)
6.253	31.962	6.073	31.574	6.522	31.780			7.904	30.329	8.010	30.728		
6.257	31.965	6.157	31.606	6.723	31.785			7.999	30.355	8.021	30.729		
6.294	31.987	6.306	31.661	6.755	31.785			8.161	30.396	8.091	30.736		
6.464	32.065	6.324	31.667	6.920	31.789			8.173	30.398	8.311	30.750		
6.554	32.093	6.374	31.685	7.153	31.794			8.205	30.406	8.322	30.750		
6.558	32.094	6.555	31.748	7.221	31.795			8.559	30.470	8.392	30.753		
6.692	32.124	6.607	31.764	7.454	31.800			8.570	30.472	8.525	30.758		
6.765	32.137	6.625	31.770	7.522	31.801			8.603	30.477	8.623	30.761		
6.956	32.167	6.772	31.811	7.920	31.810			8.860	30.516	8.693	30.763		
6.993	32.173	6.856	31.831	8.221	31.817			8.871	30.517	8.826	30.766		
7.066	32.185	7.023	31.865					8.904	30.523	9.021	30.770		
7.257	32.221	7.073	31.874					8.943	30.529	9.091	30.772		
7.294	32.230	7.157	31.889					9.161	30.574	9.223	30.774		
7.464	32.281	7.324	31.920					9.173	30.577	9.322	30.776		
7.692	32.393	7.374	31.929					9.244	30.596	9.392	30.777		
7.765	32.444	7.555	31.968					9.559	30.708	9.525	30.780		
7.993	32.641	7.772	32.029					9.570	30.713	9.693	30.782		
8.066	32.709	7.856	32.059					9.642	30.746	9.727	30.782		
8.464	32.998	8.073	32.158					9.860	30.857	9.826	30.783		
8.765	33.160	8.073	32.158					9.871	30.864	10.028	30.784		
		8.157	32.207					9.943	30.903	10.091	30.784		
		8.157	32.207					10.080	30.976	10.223	30.785		
		8.555	32.282					10.173	31.019	10.392	30.785		
		8.555	32.282					10.244	31.048	10.426	30.785		
		8.856	32.125					10.381	31.090	10.525	30.785		
		8.856	32.125					10.570	31.124	10.727	30.785		
								10.642	31.132	10.826	30.785		
								10.779	31.141	11.005	30.785		
								10.871	31.145	11.028	30.785		
								10.943	31.147	11.223	30.785		
								11.080	31.150	11.306	30.785		
								11.244	31.151	11.426	30.785		
								11.289	31.151	11.525	30.785		
								11.381	31.152	11.704	30.785		
								11.590	31.152	11.727	30.785		
								11.642	31.152	12.005	30.785		
								11.779	31.152	12.028	30.785		

Appendix 4c. Parameters of the lines fitted to the real shear modulus data for Fe-bearing melts (G8-G14) – continuation...

FITS TO THE REAL SHEAR MODULUS DATA													
G8		G9		G10		G11		G12		G13		G14	
$\Delta \log_{10}$ τ_M (s)	G_{real} (GPa)	$\Delta \log_{10}$ τ_M (s)	G_{real} (GPa)	$\Delta \log_{10}$ τ_M (s)	G_{real} (GPa)	$\Delta \log_{10}$ τ_M (s)	G_{real} (GPa)	$\Delta \log_{10}$ τ_M (s)	G_{real} (GPa)	$\Delta \log_{10}$ τ_M (s)	G_{real} (GPa)	$\Delta \log_{10}$ τ_M (s)	G_{real} (GPa)
								11.943	31.152	12.306	30.785		
								11.988	31.152	12.367	30.785		
								12.080	31.152	12.426	30.785		
								12.289	31.153	12.668	30.785		
								12.381	31.153	12.704	30.785		
								12.576	31.153	12.727	30.785		
								12.590	31.153	13.005	30.785		
								12.779	31.153	13.066	30.785		
								12.877	31.153	13.306	30.785		
								12.988	31.153	13.367	30.785		
								13.080	31.153	13.668	30.785		
								13.275	31.153	13.704	30.785		
								13.289	31.153	13.820	30.785		
								13.576	31.153	14.005	30.785		
								13.590	31.153	14.066	30.785		
								13.877	31.153	14.121	30.785		
								13.988	31.153	14.367	30.785		
								14.275	31.153	14.519	30.785		
								14.289	31.153	14.668	30.785		
								14.576	31.153	14.820	30.785		
								14.877	31.153	15.066	30.785		
								15.275	31.153	15.121	30.785		
								15.576	31.153	15.367	30.785		
										15.519	30.785		
										15.820	30.785		
										16.121	30.785		
										16.519	30.785		
										16.820	30.785		

Appendix 4d. Parameters of the lines fitted to the imaginary shear modulus data for Fe-bearing melts (G8-G14). See also Fig. 69b.

FITS TO THE IMAGINARY SHEAR MODULUS DATA													
G8		G9		G10		G11		G12		G13		G14	
$\Delta \log_{10}$ τ_M (s)	G_{im} (GPa)	$\Delta \log_{10}$ τ_M (s)	G_{im} (GPa)	$\Delta \log_{10}$ τ_M (s)	G_{im} (GPa)	$\Delta \log_{10}$ τ_M (s)	G_{im} (GPa)	$\Delta \log_{10}$ τ_M (s)	G_{im} (GPa)	$\Delta \log_{10}$ τ_M (s)	G_{im} (GPa)	$\Delta \log_{10}$ τ_M (s)	G_{im} (GPa)
-0.796	0.140	-2.000	0.033	-2.000	0.033	-2.000	0.060	-2.000	0.050	-2.000	0.040	-2.000	0.073
-0.595	0.176	-1.600	0.059	-1.600	0.083	-1.600	0.147	-1.600	0.112	-1.750	0.072	-1.600	0.182
-0.398	0.247	-1.300	0.100	-1.289	0.165	-1.300	0.286	-1.300	0.201	-1.494	0.129	-1.300	0.363
-0.294	0.303	-1.185	0.123	-1.093	0.255	-1.064	0.479	-1.000	0.359	-1.147	0.286	-0.986	0.744
-0.149	0.409	-0.927	0.192	-0.891	0.398	-0.851	0.748	-0.815	0.516	-1.096	0.322	-0.588	1.792
-0.097	0.457	-0.884	0.207	-0.791	0.497	-0.763	0.890	-0.703	0.646	-0.846	0.571	-0.579	1.826
-0.073	0.481	-0.664	0.308	-0.590	0.781	-0.557	1.295	-0.514	0.953	-0.795	0.642	-0.287	3.195
0.104	0.704	-0.626	0.331	-0.575	0.807	-0.550	1.312	-0.402	1.206	-0.494	1.266	-0.278	3.243
0.152	0.781	-0.486	0.436	-0.394	1.213	-0.365	1.793	-0.202	1.834	-0.469	1.337	0.014	4.718
0.204	0.874	-0.363	0.563	-0.289	1.529	-0.317	1.941	-0.116	2.192	-0.448	1.401	0.037	4.816
0.228	0.919	-0.228	0.751	-0.274	1.581	-0.256	2.153	-0.101	2.263	-0.415	1.506	0.120	5.127
0.405	1.338	-0.185	0.824	-0.093	2.338	-0.249	2.181	0.099	3.327	-0.168	2.540	0.164	5.269
0.453	1.477	-0.124	0.942	-0.036	2.626	-0.064	3.007	0.185	3.857	-0.147	2.651	0.338	5.666
0.470	1.530	0.035	1.335	0.109	3.487	-0.029	3.197	0.297	4.558	-0.114	2.828	0.412	5.742
0.602	1.998	0.073	1.452	0.124	3.585	-0.016	3.266	0.439	5.337	-0.096	2.931	0.421	5.747
0.626	2.093	0.116	1.596	0.209	4.152	0.142	4.247	0.486	5.547	-0.009	3.452	0.465	5.757
0.706	2.441	0.177	1.826	0.265	4.538	0.149	4.297	0.497	5.591	0.154	4.553	0.713	5.396
0.771	2.752	0.336	2.567	0.410	5.498	0.237	4.885	0.598	5.918	0.205	4.906	0.722	5.372
0.851	3.169	0.374	2.780	0.425	5.590	0.272	5.115	0.740	6.125	0.230	5.075	0.736	5.333
0.903	3.462	0.438	3.169	0.525	6.137	0.285	5.194	0.798	6.134	0.241	5.147	0.863	4.944
0.927	3.598	0.514	3.680	0.606	6.497	0.443	6.069	0.884	6.068	0.284	5.431	0.944	4.665
1.036	4.253	0.575	4.126	0.663	6.694	0.450	6.102	0.899	6.046	0.506	6.483	1.014	4.413
1.104	4.684	0.637	4.593	0.711	6.830	0.523	6.366	1.099	5.499	0.531	6.541	1.037	4.327
1.152	4.988	0.739	5.379	0.726	6.865	0.635	6.582	1.109	5.456	0.542	6.562	1.120	4.020
1.169	5.097	0.772	5.625	0.826	7.020	0.670	6.607	1.137	5.343	0.552	6.580	1.164	3.856
1.204	5.320	0.815	5.930	0.907	7.030	0.683	6.612	1.185	5.140	0.585	6.621	1.245	3.558
1.228	5.467	0.876	6.323	0.964	6.970	0.744	6.606	1.297	4.625	0.832	6.337	1.412	2.994
1.337	6.104	1.022	6.954	1.109	6.556	0.751	6.603	1.411	4.117	0.853	6.277	1.421	2.965
1.405	6.447	1.035	6.986	1.110	6.553	0.824	6.539	1.439	3.998	0.904	6.120	1.465	2.831
1.453	6.649	1.073	7.058	1.124	6.495	0.936	6.364	1.486	3.808	0.940	5.999	1.643	2.345
1.470	6.714	1.116	7.097	1.209	6.102	0.971	6.294	1.497	3.767	0.984	5.837	1.713	2.180
1.602	7.051	1.137	7.101	1.224	6.025	0.984	6.268	1.598	3.408	1.154	5.145	1.722	2.159
1.625	7.082	1.177	7.084	1.265	5.811	1.100	5.989	1.740	3.013	1.205	4.929	1.765	2.066
1.626	7.083	1.323	6.788	1.410	5.035	1.142	5.878	1.798	2.881	1.230	4.824	1.863	1.870
1.706	7.137	1.336	6.747	1.411	5.030	1.149	5.857	1.808	2.858	1.241	4.779	1.944	1.723
1.735	7.139	1.374	6.616	1.425	4.957	1.222	5.649	1.813	2.850	1.285	4.593	2.066	1.524
1.771	7.130	1.438	6.364	1.525	4.467	1.237	5.605	1.884	2.710	1.531	3.671	2.120	1.442

Appendix 4d. Parameters of the lines fitted to the imaginary shear modulus data for Fe-bearing melts (G8-G14) – continuation...

FITS TO THE IMAGINARY SHEAR MODULUS DATA													
G8		G9		G10		G11		G12		G13		G14	
$\Delta \log_{10}$ τ_M (s)	G_{im} (GPa)	$\Delta \log_{10}$ τ_M (s)	G_{im} (GPa)	$\Delta \log_{10}$ τ_M (s)	G_{im} (GPa)	$\Delta \log_{10}$ τ_M (s)	G_{im} (GPa)	$\Delta \log_{10}$ τ_M (s)	G_{im} (GPa)	$\Delta \log_{10}$ τ_M (s)	G_{im} (GPa)	$\Delta \log_{10}$ τ_M (s)	G_{im} (GPa)
1.851	7.073	1.514	6.019	1.606	4.108	1.272	5.499	2.099	2.346	1.542	3.636	2.164	1.380
1.903	7.012	1.575	5.714	1.663	3.886	1.401	5.081	2.109	2.329	1.552	3.601	2.245	1.271
1.926	6.981	1.629	5.437	1.720	3.678	1.443	4.933	2.114	2.322	1.683	3.206	2.421	1.075
1.927	6.980	1.637	5.394	1.726	3.659	1.450	4.906	2.137	2.284	1.765	2.992	2.464	1.035
2.036	6.788	1.721	4.952	1.809	3.396	1.523	4.627	2.185	2.209	1.832	2.832	2.465	1.034
2.104	6.635	1.739	4.857	1.826	3.345	1.635	4.156	2.411	1.850	1.853	2.784	2.629	0.905
2.152	6.516	1.772	4.689	1.907	3.119	1.670	4.001	2.439	1.804	1.940	2.605	2.643	0.895
2.169	6.471	1.815	4.478	1.964	2.975	1.704	3.851	2.497	1.707	1.984	2.520	2.765	0.820
2.228	6.305	1.876	4.197	2.021	2.831	1.744	3.671	2.512	1.682	2.066	2.373	2.863	0.764
2.240	6.269	1.930	3.977	2.110	2.620	1.799	3.423	2.550	1.615	2.230	2.105	2.930	0.726
2.324	6.002	2.022	3.658	2.124	2.586	1.824	3.312	2.740	1.284	2.241	2.089	2.944	0.717
2.337	5.959	2.035	3.618	2.224	2.357	1.936	2.836	2.798	1.186	2.285	2.021	3.066	0.641
2.405	5.706	2.073	3.512	2.265	2.265	1.971	2.696	2.808	1.168	2.464	1.751	3.164	0.573
2.470	5.437	2.137	3.360	2.358	2.061	2.005	2.566	2.813	1.162	2.531	1.645	3.245	0.515
2.541	5.104	2.177	3.278	2.411	1.950	2.100	2.220	2.851	1.100	2.542	1.628	3.328	0.457
2.625	4.670	2.261	3.137	2.419	1.932	2.142	2.082	3.109	0.773	2.584	1.559	3.464	0.371
2.626	4.666	2.323	3.047	2.425	1.920	2.222	1.835	3.114	0.769	2.683	1.395	3.541	0.331
2.735	4.061	2.328	3.040	2.525	1.715	2.272	1.695	3.137	0.747	2.765	1.264	3.629	0.292
2.771	3.856	2.336	3.028	2.659	1.449	2.336	1.532	3.249	0.661	2.885	1.084	3.643	0.287
2.883	3.251	2.438	2.877	2.663	1.442	2.401	1.383	3.325	0.616	2.940	1.012	3.765	0.250
2.926	3.032	2.562	2.653	2.720	1.334	2.403	1.380	3.411	0.576	2.984	0.959	3.842	0.235
2.927	3.029	2.575	2.625	2.809	1.178	2.443	1.297	3.439	0.566	3.066	0.874	3.930	0.226
2.939	2.969	2.629	2.508	2.826	1.149	2.523	1.148	3.512	0.541	3.241	0.739	3.944	0.226
3.036	2.541	2.721	2.290	2.964	0.941	2.637	0.973	3.550	0.530	3.283	0.715	4.066	0.228
3.169	2.065	2.739	2.245	3.021	0.866	2.670	0.929	3.627	0.511	3.285	0.713	4.328	0.287
3.184	2.020	2.876	1.917	3.025	0.861	2.704	0.888	3.808	0.476	3.446	0.635	4.464	0.346
3.240	1.863	2.920	1.822	3.057	0.823	2.799	0.787	3.813	0.475	3.464	0.627	4.503	0.366
3.324	1.665	2.930	1.801	3.110	0.764	2.824	0.764	3.851	0.468	3.584	0.571	4.541	0.386
3.337	1.639	2.960	1.740	3.224	0.656	2.971	0.655	4.024	0.430	3.683	0.524	4.629	0.437
3.470	1.399	3.022	1.627	3.326	0.577	2.999	0.639	4.109	0.407	3.747	0.494	4.765	0.513
3.541	1.294	3.137	1.455	3.358	0.556	3.005	0.636	4.114	0.406	3.765	0.486	4.804	0.532
3.554	1.277	3.221	1.359	3.411	0.522	3.035	0.620	4.141	0.397	3.885	0.432	4.842	0.547
3.582	1.241	3.261	1.319	3.419	0.517	3.100	0.590	4.249	0.362	3.984	0.391	4.930	0.572
3.625	1.187	3.323	1.264	3.525	0.459	3.222	0.546	4.325	0.336	4.066	0.362	5.202	0.519
3.735	1.068	3.328	1.259	3.659	0.396	3.300	0.523	4.442	0.297	4.145	0.337	5.240	0.499
3.855	0.958	3.438	1.165	3.720	0.371	3.336	0.513	4.512	0.275	4.283	0.303	5.328	0.445
3.883	0.935	3.562	1.047	3.723	0.370	3.401	0.495	4.550	0.264	4.354	0.290	5.503	0.333

Appendix 4d. Parameters of the lines fitted to the imaginary shear modulus data for Fe-bearing melts (G8-G14) – continuation...

FITS TO THE IMAGINARY SHEAR MODULUS DATA													
G8		G9		G10		G11		G12		G13		G14	
$\Delta \log_{10}$ τ_M (s)	G_{im} (GPa)	$\Delta \log_{10}$ τ_M (s)	G_{im} (GPa)	$\Delta \log_{10}$ τ_M (s)	G_{im} (GPa)	$\Delta \log_{10}$ τ_M (s)	G_{im} (GPa)	$\Delta \log_{10}$ τ_M (s)	G_{im} (GPa)	$\Delta \log_{10}$ τ_M (s)	G_{im} (GPa)	$\Delta \log_{10}$ τ_M (s)	G_{im} (GPa)
3.926	0.902	3.607	1.000	3.724	0.370	3.403	0.494	4.627	0.242	4.446	0.278	5.521	0.322
3.939	0.892	3.619	0.987	3.809	0.338	3.523	0.458	4.813	0.200	4.464	0.276	5.541	0.311
4.036	0.825	3.629	0.975	4.021	0.277	3.637	0.418	4.840	0.195	4.584	0.269	5.629	0.263
4.184	0.735	3.721	0.870	4.024	0.277	3.695	0.396	4.851	0.193	4.655	0.269	5.804	0.185
4.240	0.705	3.908	0.655	4.025	0.276	3.698	0.395	4.999	0.174	4.747	0.271	5.822	0.178
4.253	0.699	3.920	0.643	4.057	0.269	3.704	0.393	5.024	0.172	4.765	0.272	5.842	0.171
4.257	0.697	3.930	0.632	4.110	0.259	3.799	0.357	5.141	0.167	4.885	0.278	6.202	0.084
4.324	0.665	3.960	0.601	4.326	0.229	3.996	0.296	5.249	0.168	5.053	0.289	6.220	0.081
4.541	0.580	4.022	0.542	4.358	0.227	3.999	0.295	5.300	0.170	5.145	0.293	6.240	0.078
4.554	0.575	4.221	0.393	4.419	0.224	4.005	0.294	5.325	0.172	5.283	0.295	6.503	0.049
4.558	0.574	4.261	0.370	4.422	0.224	4.035	0.287	5.442	0.182	5.311	0.295	6.521	0.047
4.582	0.566	4.306	0.348	4.454	0.223	4.100	0.275	5.550	0.194	5.354	0.295	6.541	0.046
4.625	0.553	4.324	0.340	4.659	0.229	4.300	0.261	5.627	0.204	5.446	0.290	6.804	0.031
4.855	0.492	4.328	0.338	4.720	0.236	4.336	0.262	5.698	0.212	5.584	0.276	6.822	0.030
4.883	0.486	4.562	0.264	4.723	0.236	4.394	0.267	5.840	0.226	5.612	0.272	7.202	0.021
4.939	0.474	4.607	0.255	4.724	0.236	4.403	0.267	5.904	0.229	5.655	0.266	7.220	0.020
4.956	0.471	4.619	0.253	4.755	0.240	4.637	0.309	5.999	0.228	5.747	0.251	7.503	0.017
4.993	0.463	4.625	0.252	5.024	0.301	4.695	0.322	6.024	0.226	6.010	0.213	7.521	0.017
5.184	0.427	4.629	0.251	5.025	0.301	4.698	0.323	6.141	0.213	6.053	0.209	7.822	0.015
5.240	0.417	4.908	0.228	5.057	0.311	4.704	0.324	6.205	0.203	6.145	0.203	8.220	0.014
5.253	0.415	4.920	0.228	5.153	0.343	4.996	0.366	6.300	0.185	6.311	0.203	8.521	0.013
5.257	0.414	4.960	0.227	5.221	0.366	4.999	0.366	6.325	0.180	6.322	0.203		
5.294	0.408	5.023	0.227	5.326	0.399	5.035	0.364	6.442	0.158	6.354	0.204		
5.554	0.363	5.073	0.227	5.358	0.408	5.300	0.314	6.603	0.135	6.446	0.210		
5.558	0.362	5.221	0.228	5.422	0.422	5.336	0.305	6.698	0.126	6.612	0.225		
5.582	0.358	5.261	0.229	5.454	0.428	5.394	0.289	6.840	0.119	6.623	0.226		
5.692	0.338	5.306	0.230	5.522	0.435	5.695	0.230	6.860	0.118	6.655	0.230		
5.765	0.324	5.324	0.230	5.723	0.424	5.698	0.230	6.904	0.118	7.010	0.276		
5.855	0.308	5.374	0.231	5.724	0.424	5.996	0.194	6.999	0.118	7.021	0.277		
5.883	0.303	5.607	0.232	5.755	0.418	5.999	0.193	7.141	0.122	7.053	0.281		
5.956	0.290	5.619	0.232	5.920	0.381	6.394	0.124	7.161	0.123	7.311	0.308		
5.993	0.283	5.625	0.232	6.024	0.352	6.695	0.087	7.205	0.124	7.322	0.309		
6.066	0.271	5.772	0.230	6.025	0.352			7.300	0.128	7.354	0.313		
6.253	0.239	5.856	0.228	6.153	0.315			7.559	0.134	7.392	0.316		
6.257	0.239	5.908	0.226	6.221	0.295			7.603	0.134	7.612	0.336		
6.294	0.233	5.920	0.226	6.422	0.241			7.698	0.133	7.623	0.337		
6.464	0.208	6.023	0.221	6.454	0.233			7.860	0.128	7.693	0.341		

Appendix 4d. Parameters of the lines fitted to the imaginary shear modulus data for Fe-bearing melts (G8-G14) – continuation...

FITS TO THE IMAGINARY SHEAR MODULUS DATA													
G8		G9		G10		G11		G12		G13		G14	
$\Delta \log_{10}$ τ_M (s)	G_{im} (GPa)	$\Delta \log_{10}$ τ_M (s)	G_{im} (GPa)	$\Delta \log_{10}$ τ_M (s)	G_{im} (GPa)	$\Delta \log_{10}$ τ_M (s)	G_{im} (GPa)	$\Delta \log_{10}$ τ_M (s)	G_{im} (GPa)	$\Delta \log_{10}$ τ_M (s)	G_{im} (GPa)	$\Delta \log_{10}$ τ_M (s)	G_{im} (GPa)
6.554	0.196	6.073	0.219	6.522	0.218			7.871	0.128	8.010	0.334		
6.558	0.195	6.157	0.214	6.723	0.177			7.904	0.127	8.021	0.333		
6.692	0.178	6.306	0.205	6.755	0.172			7.999	0.124	8.091	0.322		
6.765	0.170	6.324	0.204	6.920	0.148			8.161	0.121	8.311	0.273		
6.956	0.151	6.374	0.200	7.153	0.127			8.173	0.121	8.322	0.271		
6.993	0.148	6.555	0.189	7.221	0.123			8.205	0.121	8.392	0.256		
7.066	0.141	6.607	0.185	7.454	0.114			8.559	0.143	8.525	0.233		
7.257	0.128	6.625	0.184	7.522	0.112			8.570	0.144	8.623	0.222		
7.294	0.125	6.772	0.175	7.920	0.104			8.603	0.148	8.693	0.217		
7.464	0.117	6.856	0.171	8.221	0.098			8.860	0.177	8.826	0.209		
7.692	0.108	7.023	0.163					8.871	0.178	9.021	0.192		
7.765	0.105	7.073	0.161					8.904	0.180	9.091	0.182		
7.993	0.100	7.157	0.159					8.943	0.181	9.223	0.157		
8.066	0.098	7.324	0.154					9.161	0.165	9.322	0.136		
8.464	0.089	7.374	0.153					9.173	0.164	9.392	0.121		
8.765	0.078	7.555	0.149					9.244	0.151	9.525	0.094		
		7.772	0.142					9.559	0.089	9.693	0.066		
		7.856	0.139					9.570	0.087	9.727	0.062		
		8.073	0.131					9.642	0.076	9.826	0.050		
		8.157	0.127					9.860	0.047	10.028	0.031		
		8.555	0.107					9.871	0.046	10.091	0.027		
		8.856	0.087					9.943	0.039	10.223	0.020		
								10.080	0.029	10.392	0.014		
								10.173	0.023	10.426	0.013		
								10.244	0.020	10.525	0.010		
								10.381	0.014	10.727	0.006		
								10.570	0.009	10.826	0.005		
								10.642	0.008	11.005	0.003		
								10.779	0.006	11.028	0.003		
								10.871	0.005	11.223	0.002		
								10.943	0.004	11.306	0.002		
								11.080	0.003	11.426	0.001		
								11.244	0.002	11.525	0.001		
								11.289	0.002	11.704	0.001		
								11.381	0.001	11.727	0.001		
								11.590	0.001	12.005	0.000		
								11.642	0.001	12.028	0.000		

Appendix 4d. Parameters of the lines fitted to the imaginary shear modulus data for Fe-bearing melts (G8-G14) – continuation...

FITS TO THE IMAGINARY SHEAR MODULUS DATA													
G8		G9		G10		G11		G12		G13		G14	
$\Delta \log_{10}$ τ_M (s)	G_{im} (GPa)	$\Delta \log_{10}$ τ_M (s)	G_{im} (GPa)	$\Delta \log_{10}$ τ_M (s)	G_{im} (GPa)	$\Delta \log_{10}$ τ_M (s)	G_{im} (GPa)	$\Delta \log_{10}$ τ_M (s)	G_{im} (GPa)	$\Delta \log_{10}$ τ_M (s)	G_{im} (GPa)	$\Delta \log_{10}$ τ_M (s)	G_{im} (GPa)
								11.779	0.001	12.306	0.000		
								11.943	0.000	12.367	0.000		
								11.988	0.000	12.426	0.000		
								12.080	0.000	12.668	0.000		
								12.289	0.000	12.704	0.000		
								12.381	0.000	12.727	0.000		
								12.576	0.000	13.005	0.000		
								12.590	0.000	13.306	0.000		
								12.779	0.000	13.367	0.000		
								12.877	0.000	13.668	0.000		
								12.988	0.000	13.704	0.000		
								13.080	0.000	13.820	0.000		
								13.275	0.000	14.005	0.000		
								13.289	0.000	14.066	0.000		
								13.576	0.000	14.121	0.000		
								13.590	0.000	14.367	0.000		
								13.877	0.000	14.519	0.000		
								13.988	0.000	14.668	0.000		
								14.275	0.000	14.820	0.000		
								14.289	0.000	15.066	0.000		
								14.576	0.000	15.121	0.000		
								14.877	0.000	15.367	0.000		
								15.275	0.000	15.519	0.000		
								15.576	0.000	15.820	0.000		
										16.121	0.000		
										16.519	0.000		
										16.820	0.000		

Appendix 5a. Parameters of the fits to Eq. 58 for the NS (G0) and Fe-free melts (G1-G7). The G_x values are calculated separately from the imaginary and the real component of the data.

\log_{10} ($\omega\tau_M+x$)	G0		G1		G2		G3	
	G real	G im	G real	G im	G real	G im	G real	G im
-2.0	0.0000	0.0000	0.0019	0.0002	0.1750	0.1246	0.0000	0.0000
-1.5	0.0219	0.0000	0.1349	0.0312	0.1751	0.0056	0.0000	0.0000
-1.0	0.0001	0.0000	0.1625	0.0000	0.1553	0.1134	0.0391	0.0000
-0.5	0.3660	0.0000	0.5722	0.0036	0.0822	0.2377	0.0352	0.0561
0.0	15.3951	14.9655	1.0856	2.2426	0.0725	0.2310	0.0015	0.2968
0.5	9.3074	0.0301	15.0522	10.0915	14.6287	0.2967	8.1990	5.8657
1.0	1.5469	0.0004	6.4520	5.0549	7.3647	4.0287	9.4410	7.5078
1.5	0.9018	0.0000	3.2551	3.6187	5.9618	11.2787	10.6608	9.6254
2.0	0.0018	0.0004	1.7552	0.8130	3.3260	3.9675	3.8472	1.4609
2.5	0.0001	0.0001	1.2422	0.7270	1.4730	3.5155	0.8425	1.5879
3.0	0.0012	0.0000	0.3270	0.0996	0.0010	0.0941	0.0065	0.7968
3.5	0.0010	0.0057	0.2548	0.1563	0.0020	0.4230	0.2604	0.0375
4.0	0.0018	0.0038	0.1844	0.0773	0.0110	0.3699	0.4156	0.2175
4.5	0.0004	0.0004	0.0959	0.0011	0.0051	0.1326	0.4077	0.3276
5.0	0.0081	0.0000	1.8824	0.0000	0.0000	0.0523	0.3669	0.4712
5.5	0.0000	0.0000	0.5231	1.8272	0.0001	0.0044	0.3936	0.0000
6.0	0.0000	0.0001	0.3658	0.4107	0.0185	1.1911	0.3743	0.0000
6.5	0.0000	0.0000	0.0361	0.0110	0.2058	1.7713	0.3075	0.0000
7.0	0.0097	0.0001	0.0230	0.0086	1.0386	0.6120	0.1509	0.3080
7.5	0.0000	0.0002	0.0068	0.0333	0.0004	0.0069	1.2116	0.9406
8.0	0.0001	0.0000	0.0002	0.0283	0.0033	0.0050	0.4487	0.2569
8.5	0.0000	0.0001	0.0096	0.0217	0.0075	0.0053	0.0464	0.0000
9.0	0.0499	0.0000	0.0224	0.0435	0.0018	0.0069	0.0365	0.0000

\log_{10} ($\omega\tau_M+x$)	G4		G5		G6		G7	
	G real	G im	G real	G im	G real	G im	G real	G im
-2.0	0.0000	0.0943	0.0000	0.0331	0.0004	0.0000	0.0000	0.0000
-1.5	0.0001	0.0396	0.0041	0.0170	0.0016	0.0000	0.0000	0.0000
-1.0	0.0487	0.0394	0.0000	0.0142	0.0000	0.0042	0.000	0.0014
-0.5	0.0006	0.0520	0.0000	0.0141	0.0361	0.0000	0.4900	0.0008
0.0	1.5280	0.0834	4.1363	0.0423	4.4974	5.7770	17.7325	16.1418
0.5	5.9260	7.2443	19.7777	14.1438	19.5208	6.0992	16.8805	11.3698
1.0	7.6788	11.4305	4.8209	4.0414	10.4056	2.2264	3.9630	0.1729
1.5	7.9675	2.3323	4.4279	3.7268	4.1285	1.6094	0.9825	0.0003
2.0	1.6608	0.4935	0.6727	0.0106	0.6088	1.2668	1.8693	0.0086
2.5	0.9852	0.0224	0.6900	0.0117	0.7708	0.0000	1.9549	0.0000
3.0	0.8287	0.0214	1.1252	0.0122	1.7880	0.0001	0.0000	0.0005
3.5	0.5856	0.0218	0.0000	0.0122	0.0277	0.0002	0.0000	0.0002
4.0	0.0629	0.0213	0.0052	0.0118	0.0463	0.0010	0.0000	0.0015
4.5	0.0000	0.0182	0.0001	0.0117	0.0658	0.0002	0.0000	0.0004
5.0	0.0395	0.0146	0.0016	0.0115	0.0790	0.0000	0.0000	0.0006
5.5	0.2874	0.0130	0.0092	0.0114	0.0887	0.0041		0.0028
6.0	0.1781	0.0120	0.2608	0.0110	0.2051	0.0060		
6.5	0.2851	0.0096	0.0853	0.0105	0.4789	0.0000		
7.0	0.2216	0.0083	0.5321	0.0100	0.3994	0.0000		
7.5	0.7514	1.2934	0.9496	0.9754	0.9981	0.8812		
8.0	1.0168	0.0095	0.0000	2.7436	0.1060	0.5487		
8.5	0.0854	0.0098	0.0037	0.0101	0.1696	0.0021		
9.0	0.0018	0.0116	0.0001	0.0105	0.0731	0.0005		

Appendix 5b. Parameters of the fits to Eq. 58 for the Fe-bearing melts (G8-G14). The G_x values are calculated separately from the imaginary and the real component of the data.

\log_{10} ($\omega\tau_M+x$)	G8		G9		G10		G11	
	G real	G im	G real	G im	G real	G im	G real	G im
-2.0	0.0000	0.0004	0.0000	0.0096	0.0000	0.0003	0.0000	0.0000
-1.5	0.0000	0.0004	0.0000	0.0009	0.0000	0.0008	0.0000	0.0000
-1.0	0.0000	0.0010	0.0000	0.0030	0.0000	0.1964	0.0000	0.0000
-0.5	0.0000	0.4334	0.0000	0.0028	2.2171	0.0001	0.0000	0.0937
0.0	5.2465	4.4479	0.0000	0.0000	1.4041	0.3566	6.9409	0.8966
0.5	16.1477	8.5137	3.4302	0.0312	15.8547	14.4501	12.2113	12.9970
1.0	3.0832	4.9116	6.9371	10.4640	5.5866	1.3858	4.3732	3.7738
1.5	2.6781	0.3499	9.7484	4.5439	3.5716	1.3829	3.7152	1.4656
2.0	3.5174	1.1559	3.1225	3.3974	4.0870	0.4867	2.7744	1.4317
2.5	0.0000	0.9578	1.8179	1.0503	0.0000	0.3755	0.0000	0.2065
3.0	0.0000	0.0001	1.2603	1.9413	0.0000	0.3531	0.0000	0.0000
3.5	0.0000	0.0000	0.0000	0.0391	0.0000	0.1636	0.0000	0.0000
4.0	0.0000	0.8452	0.0000	0.0280	2.3880	0.0720	0.0000	0.0000
4.5	1.9993	0.0000	0.0000	0.0251	0.0060	0.0096	2.1744	0.9251
5.0	0.0263	0.0001	1.5419	0.0148	0.3084	0.7122	0.1752	0.7976
5.5	0.1986	0.0003	0.0862	1.4871	0.0000	0.0146	0.0000	0.0984
6.0	0.0000	0.0004	0.9836	0.2736	0.0000	0.0012	0.0000	0.0000
6.5	0.0000	0.0006	0.0000	0.0004	0.0000	0.0388	0.0000	0.0000
7.0	0.0000	0.0006	0.0000	0.0159	0.0000	0.0486	0.0000	0.0000
7.5	0.0000	0.0025	0.0001	0.0568	0.0000	0.0267	0.0000	0.0001
8.0	0.0000	0.0220	0.0006	0.0692	0.0002	0.0001	0.0000	0.0015
8.5	0.0000	0.2151	0.0021	0.0634	0.0157	0.0008	0.0000	0.0153
9.0	0.0017	0.0000	0.0150	0.0585	0.0000	0.0000	0.0000	0.0000

\log_{10} ($\omega\tau_M+x$)	G12		G13		G14	
	G real	G im	G real	G im	G real	G im
-2.0	0.1072	0.0095	0.0094	0.0000	0.0013	0.0000
-1.5	0.1304	0.0233	0.0094	0.0001	0.0014	0.0001
-1.0	0.1927	0.0764	0.0093	0.0020	0.0019	0.0001
-0.5	0.3242	0.0631	0.0083	0.0660	0.0044	0.0001
0.0	0.3922	0.0016	0.0938	0.1117	6.7304	4.8103
0.5	9.0289	7.0788	9.1963	9.7856	8.5225	6.5394
1.0	10.6936	6.5564	13.0917	5.1587	5.0040	3.2280
1.5	9.5671	0.9890	1.7607	2.1221	3.7534	1.3111
2.0	1.2907	1.8048	1.1934	1.7142	1.7408	0.9825
2.5	3.0537	1.4779	1.0198	0.8163	1.6519	0.3950
3.0	0.7542	0.0896	1.5969	0.2861	0.3570	0.7156
3.5	0.6931	0.2601	0.9414	0.1834	0.1780	0.0099
4.0	0.2658	0.4572	0.0198	0.1615	0.8879	0.0100
4.5	0.2987	0.1348	0.0202	0.0744	0.0121	0.0102
5.0	0.1812	0.0261	0.0197	0.0930	0.0020	1.1174
5.5	0.0472	0.0805	0.0147	0.0650	0.1904	0.0099
6.0	0.0955	0.3614	0.0086	0.0000	0.5020	0.0097
6.5	0.0069	0.0000	1.0308	0.0145	0.0095	0.0100
7.0	0.0880	0.0497	0.2020	0.4551	0.0109	0.0105
7.5	0.1792	0.1476	0.4399	1.1050	0.0129	0.0100
8.0	0.1481	0.0789	0.0196	0.5373	0.0145	0.0106
8.5	0.0550	0.0002	0.0015	0.0258	0.0194	0.0101
9.0	0.0570	0.3341	0.0008	0.0001	0.0940	0.0101

LEBENS LAUF

Persönliche Daten

Name: **Katarzyna Falenty**
Geburtstag: 22.09.1980
Geburtsort: Wołomin, Polen
Staatsangehörigkeit: polnisch

Schul Ausbildung

09/1987-06/1990 **Grundschule**, Bosewo Stare, gm. Długosiodło, Polen
09/1990-06/1995 **Grundschule** Nummer 4, Obrońców Westerplatte, Wyszaków, Polen
09/1995-06/1999 **Allgemeinbildende Oberschule**, Cyprian Kamil Norwid, (Ausbildungsprofil Biologie-Chemie), Wyszaków, Polen
Reifeprüfung: 09/06/1999

Universitätsausbildung

10/1999-06/2002 **Warschauer Universität**, Fakultät für Geologie, Abteilung für Geochemie, Mineralogie und Petrologie, Warschau, Polen
Abschluss mit Bachelor Titel (BSc – Bachelor of Science)
10/2001-02/2002 **Georg – August - Universität Göttingen**, Deutschland, Socrates-Erasmus Stipendium (das Aktionsprogramm der Europäischen Union für die grenzüberschreitende Zusammenarbeit in verschiedenen Bereichen der allgemeinen Bildung)
10/2002-06/2004 **Warschauer Universität**, Fakultät für Geologie, Abteilung für Geochemie, Mineralogie und Petrologie, Warschau, Polen
Abschluss mit Magister Titel (MSc – Master of Science)
Diplom in Geochemie, Mineralogie und Petrologie

Berufspraxis

11/2004-11/2007 **Wissenschaftliche Mitarbeiterin**
Universität Göttingen, Fakultät für Geowissenschaften und Geographie, Abteilung für Experimentelle und Angewandte Mineralogie, Göttingen, Deutschland
14/11/2007 Ende der Anstellung als Wissenschaftliche Mitarbeiterin

